Development of tools for optogenetic manipulation of intracellular Ca^{2+} release and uptake from/into the sarcoplasmic reticulum

Dissertation

zur Erlangung des Doktorgrades

der Naturwissenschaften

vorgelegt beim Fachbereich Biochemie, Chemie und Pharmazie

der Johann Wolfgang Goethe-Universität

in Frankfurt am Main

Von Frank Georg Becker

aus Bad Brückenau, Bayern

Frankfurt am Main, 2022

(D 30)

Vom Fachbereich Biochemie, Chemie und Pharmazie der

Johann Wolfgang Goethe-Universität als Dissertation angenommen.

Dekan: Prof. Dr. Clemens Glaubitz

Gutachter: Prof. Dr. Alexander Gottschalk

Prof. Dr. Harald Schwalbe

Datum der Disputation: …….

Eidesstattliche Erklärung

Ich erkläre hiermit, dass ich die vorgelegte Dissertation mit dem Titel „Development of tools for optogenetic manipulation of intracellular Ca^{2+} release and uptake from/into the sarcoplasmic reticulum ” selbstständig angefertigt und mich anderer Hilfsmittel als der in der angegebenen Arbeit nicht bedient habe, insbesondere, dass alle Entlehnungen aus anderen Schriften mit Angabe der betreffenden Schrift gekennzeichnet sind.

Ich erkläre hiermit, dass ich mich bisher keiner Doktorprüfung im mathematisch-naturwissenschaftlichen Bereich unterzogen habe.

Declaration

This thesis consists solely of work generated by the doctoral candidate and supervision of his/her advisors.

Except where stated otherwise by reference or acknowledgment, the work presented was generated by myself under the supervision of my advisors during my doctoral studies.

Whenever a figure, table or text is identical to a previous publication, it is stated explicitly in the thesis that copyright permission and/or co-author agreement has been obtained.

Frankfurt am Main, den …….

_____
(Frank Georg Becker)

Contents

Zusammenfassung

Krankheiten wie Herzrhythmusstörungen, CPVT und andere Probleme des menschlichen Herzens sind in großen Teilen immer noch unerforscht. Um auf diesem Gebiet der Forschung einen Beitrag zu leisten, ist es notwendig, dass Werkzeuge zur Kontrolle der räumlichen und zeitlichen Freisetzung und Wiederaufnahme von Ca^{2+} aus dem sarkoplasmatischen/endoplasmatischen Retikulum (SR/ER) entwickelt werden. Die Freisetzung und Aufnahme von Ca^{2+} durch den Ryanodin-Rezeptor (RyR) bzw. die Ca^{2+}-ATPase des sarko-endoplasmatischen Retikulums (SERCA) sind für die Funktion erregbarer Zellen von wesentlicher Bedeutung. Dabei wird die schnelle Ca^{2+}-Freisetzung aus dem SR/ER und die damit verbundene Kontraktion in Muskelzellen in großen Teilen durch RyR moduliert. Jedoch werden auch Krankheiten, die auf einem Kalziumleck beruhen, wie z. B. Herzrhythmusstörungen, Krampfanfälle und kontraktile Dysfunktion, durch RyR verursacht. Die für die Zelle wichtige Ruhe-Ca^{2+}-Konzentration im Zytosol wird durch Ca^{2+}-Freisetzung und Wiederaufnahme in das SR/ER im Gleichgewicht gehalten. Diese Wiederaufnahme wird in erheblichem Maße von SERCA kontrolliert. Der Ryanodin-Rezeptor und SERCA bilden die beiden Hauptakteure des Ca^{2+} Zyklus an der sarko-endoplasmatischen Membran und sind daher ideale Kandidaten für die Erforschung der Ca^{2+} Freisetzung und Wiederaufnahme in das SR/ER.

SERCA ist sowohl bei Nematoden wie *C. elegans* als auch bei Säugetieren für die Entwicklung und die Muskelfunktion wichtig. Dies spiegelt sich vor allem in der Tatsache, dass Mutationen, die zu einem Funktionsverlust führen, zur Letalität führen. Daher gibt es auch hier großen Bedarf an Werkzeugen, die zur Erforschung der genauen Funktion von SERCA beitragen können.

Um dem Ziel der Entwicklung von Werkzeugen zur optogenetischen Stimulation der intrazellulären Ca^{2+}-Freisetzung aus dem SR/ER näher zu kommen, wurde der Modellorganismus *C. elegans* gewählt. Seine Vorteile sind unter anderem das vollständig sequenzierte Genom und das Konnektom des neuronalen Netzes. Darüber hinaus sind die einfache Pflege, die Selbstbefruchtung, die Transparenz und die schnellen Generationszyklen sowie die Tatsache, dass es sich um ein eutelisches Tier handelt, von Vorteil bei der Durchführung optogenetischer Verfahren.

Bisher wurden bereits Instrumente für die lichtinduzierte Ca^{2+}-Freisetzung (LICR) entwickelt. Dabei wurden ChR2-Versionen mit höherer Ca^{2+}-Leitfähigkeit, basierend auf der "CatCh"-Variante erstellt, und die weitere Verbesserung ihrer Leitfähigkeit durch mehrere etablierte Mutationen durchgeführt. Darüber hinaus wurde der Pharynx von *C. elegans* genetisch so angepasst, dass er eine optogenetisch stimulierte muskuläre pumpe simuliert, die den Herzmuskelzellen von Säugetieren ähnelt.

In dieser Arbeit wurde auf Grundlage früherer Veröffentlichungen in einem ersten Schritt versucht, eine verkürzte Version des humanen Ryanodin-Rezeptors zu erstellen. Diese verkürzte Version sollte den mit 2 MDa sehr großen Rezeptor auf ein notwendiges Minimum reduzieren, das hauptsächlich aus dem Transmembranteil von hRyR bestand.
Hierfür wurde der größte Teil des zytoplasmatischen "Kopfes" abgeschnitten. Dieses verkürzte hRyR sollte einfacher zu handhaben sein und besser mit anderen optogenetischen Werkzeugen kombiniert werden können. Einfaches „kürzen“ des Ryanodin Rezeptors aber auch eine modifizierte verkürzte Version, in der der die lange Zentrale Domäne erhalten wurde, konnten jedoch nicht erfolgreich exprimiert werden. Zur gleichen Zeit wurde in parallel dazu geführten Klonierungen dem verkürzten hRyR mit langer Zentraler Domäne C-Terminal ein modifiziertes Channelrhodopsin mit Fluorophor und linker (CatChUP::eYFP::linker Crp1) angehängt. In das verkürzte hRyR mit langer Zentraler Domäne wurden unter anderem auch LOV2 Domänen an verschiedenen insertionsstellen eingefügt. Die Insertion dieser LOV2 Domänen fand meist zwischen α-Helices und β-Faltblättern statt um dort eine möglichst effiziente Konformationsänderung hervorzurufen. Hierbei musste darauf geachtet werden, dass die Insertion der LOV2-Domäne und die Konformationsänderung bei Stimulation, nicht zu einer zu starken Veränderung der Tertiärstruktur und damit einer Einschränkung der Funktionalität führte.
Die Insertion des verkürzten RyRs inklusive des CatChUP Konstrukts führte dazu das durch Injektion keine transgenen Nachkommen von *C. elegans* erzeugt wurden.
Wildtyp und *lite-1* Tiere brachten jedoch nach Injektion von verkürztem hRyR inklusive integriertem LOV2 lebensfähige Nachkommen hervor. Es zeigte sich sowohl für Wildtyp als auch *lite-1* transgene Tiere, dass auch hier das verkürzte hRyR und LOV2 nicht ausreichte um eine eindeutige signifikante Änderung des Schwimmverhaltens oder eine Kontraktion der Körperlänge auszulösen.

In dieser Arbeit wurden sowohl optoUNC-68 (optisch stimulierbares RyR) als auch SERCA/LOV2 in verschiedenen Varianten durch CRISPR/Cas9 und plasmidbasiertes Genome Editing erzeugt, um eine lichtgesteuerte Manipulation der Calziumhomöostase in *C. elegans* zu erzielen. Hier wurde Licht induzierte Ca^{2+} Freisetzung (LICR) durch LOV2-Domänen in einer opto-mechanischen Manipulation von RyR sowie SERCA ausgelöst. Dieser Ansatz wurde durch kürzlich veröffentlichte hochauflösende CryoEM-Strukturbilder ermöglicht. Darüber hinaus wurden alternative Ansätze mit Ca^{2+}-leitfähigkeitsoptimierten Channelrhodopsinvarianten in Körperwandmuskelzellen von *C. elegans* getestet.

Um den Calciumionenfluss über das SR zu manipulieren wurden auch Chrannelrhodopsinvarianten eingesetzt, die darauf untersucht wurden ob sie in der Lage sind Calcium-induzierte Calciumfreisetzung (CICR) auszulösen. Durch Insertion von ChR-XXM in *C. elegans* und anschließende Fluoreszenz Mikroskopie des miteingebrachten GFP, konnte eine Expression in körperwand Muskel Zellen

nachgewiesen werden. Zudem konnte in Kontraktionstests gezeigt werden, dass ChR-XXM sowohl bei mittlere (0.8mW/mm²), als auch bei starker (1.4mW/mm²) Stimulation mit 470nm, Kontraktionen des Tiers von bis zu 16% gegenüber der ursprünglichen Körperlänge auslöst. ChR-XXM wurde somit als hervorragender Kandidat für die Entwicklung eines optogenetischen Werkzeugs identifiziert, da es im Vergleich zu anderen ChR2-Varianten eine deutlich erhöhte Ca^{2+}-Leitfähigkeit aufweist.

Neben ChR-XXM wurde auch $ChRGR_{ER}$ verwendet. ChRGR ist ein Channelrhodopsin-Grün-Empfänger, der sich aus ChR1 und ChR2 zusammensetzt. Es wurde entwickelt und optimiert, um die SR/ER-gerichtete $ChRGR_{ER}$-Version zu schaffen. Es trägt ein ER-Retentionsmotiv des Maus-Ryanodinrezeptors 2 und wurde mit einem Fluorophor gekoppelt. Das Ziel war es, durch Belichtung von $ChRGR_{ER}$ einen Efflux on Ca^{2+} aus dem sarkoplasmatischen Retikulum zu induzieren. Dabei sollte durch die Retention der Channelrhodopsinchimera gewährleistet werden, dass $ChRGR_{ER}$ nur auf der SR/ER Membran verbleibt. Der Ca^{2+} Efflux würde dabei die CICR an den intrinsischen auf der SR/ER Membran gelegenen Ryanodinrezeptoren auslösen. Es stellte sich heraus, dass keiner der Stämme, denen das $ChRGR_{ER}$-Plasmid injiziert wurde eine Veränderung während oder nach der Photostimulation zeigte. Dies deutet darauf hin, dass eine Ca^{2+}-Freisetzung nicht ausgelöst wurde oder der Ca^{2+}-Efflux aus dem SR/ER nicht stark genug war, um eine messbare Veränderung der Körperlänge oder des Schwimmverhaltens zu verursachen.

Ein weiteres Konzept zur Schaffung eines lichtaktivierten Werkzeugs war die Ca^{2+}-Freisetzung aus dem SR/ER zu manipulieren und das Werkzeug auf die sarkoplasmatische Membran von *C. elegans* zu beschränken. Hierfür wurde zum einen das Retentionsmotif der Transmembrandomäne TM5 und TM6 des intrinsischen Ryanodinrezeptors von *C. elegans* verwendet. Dabei deuteten durch Photostimulation der transgenen Tiere gesammelte Daten darauf hin, dass PsCatCh::YFP::UNC-68 TM5+6 ein nützliches Werkzeug für die optogenetische Beeinflussung der intrazellulären Ca^{2+}-Freisetzung aus dem SR/ER sein könnte, da es in den Muskelzellen der Körperwand exprimiert wird und komplexe koordinierte Schwimmbewegungen beeinflusst. Dieser Effekt ist jedoch nur sichtbar, solange *C. elegans* eine koordinierte Bewegung ausführen muss, wie es der Fall in Schwimmverhaltenstest ist. Das zweite Konzept, dass sich dem Retentionsmotif der TMH I+II des Inositol-1,4,5-Trisphosphat-Rezeptors bediente, zeigte keine eindeutigen Ergebnisse die eine Expression und eine Retention von PsCatCh::YFP::UNC-68 TM5+6 in transgenen Tieren nachweisen konnte. Eindeutige Ergebnisse bei Schwimmverhaltens- und Kontraktionsstests konnten ebenfalls nicht beobachtet werden.

Aufgrund der Ergebnisse, die die transgenen Tiere lieferten, in denen die LOV2 Domänen im verkürzten humanen Ryanodin-Rezeptor exprimiert wurden, wurde parallel dazu der Versuch unternommen, die LOV2 Domänen direkt in den natürlichen RyR von *C. elegans* einzufügen. Auf diese Weise konnte

jeglicher Einfluss, der durch artfremde Adaptation des Rezeptors an die eigenen Lebensumstände während der Evolution stattgefunden hatte, ausgeschlossen werden. Die Verwendung von CRISPR/Cas9 zum Einfügen von AsLOV2-Domänen (L404-L546) in verschiedene Insertionsstellen von RyR ermöglichte es, einen transgenen Stamm von *C. elegans* zu erzeugen, der während 0,3 mW/mm² Photostimulation zur Elongation angeregt werden konnte. Dadurch konnte aufgezeigt werden, dass RyR durch konformationelle Änderungen der LOV2 Domäne und der dadurch resultierenden Störung der Porenregion, durch photostimulation zeitlich und räumlich manipuliert werden kann.

CRISPR/Cas9 wurde ebenfalls dazu verwendet Stämme zu erzeugen, in dem CatChUP::EYFP::CRP-1 N-Terminal vor Exon 1.1 des UNC-68 integriert wurde (GOA01). Um die Möglichkeit auszuschließen, dass durch alternatives splicing die Expression von CatChUP::EYFP::CRP-1 unter Exon 1.1 nicht erfolgt, wurde ein zweiter Stamm generiert. Dieser trägt CatChUP::EYFP::CRP-1 sowohl vor dem Exon 1.1 als auch 1.2 (GOA14) und garantiert somit eine Expression des Inserts in jeder der 16 möglichen Isoformen des Ryanodin-Rezeptors. GOA14 wurde zusätzlich mit einem transgenen Stamm gekreuzt, der C1V1 ET/ET im Pharynx exprimiert. Theoretisch sollten auf diese Weise optoUNC-68 mit 470nm am SR/ER und C1V1 ET/ET mit 570nm an der Zellmembran optisch aktiviert werden. Eine Stimulation mit 1Hz-Pulsen von 590nm könnte C1V1 ET/ET aktivieren, dadurch wäre ein Pacing des Pharynx möglich was eine Simulation des menschlichen Herzens simulieren könnte. Durch die Belichtung mit 470nm sollte die Ca^{2+}-Freisetzung erhöht werden. Dies würde ablaufen während der intrinsische Ca^{2+}-Zyklus das zytosolische Ca^{2+} reduziert und den nächsten Pumpzyklus des Pharynx ermöglicht. Da dies durch die künstlich hervorgerufene Ca^{2+}-Freisetzung nicht ordnungsgemäß geschehen sollte, ist mit einer arrhythmischen Situation zu rechnen, ähnlich einer CPVT.
In Pharynx Pumping Tests wurde der Stamm GOA01 durch 470nm Blaulicht mit einem pacing von 1Hz stimuliert. Dabei wurde weder eine signifikante Auswirkung auf die Frequenz noch auf die Regelmäßigkeit der Pumpzyklen eindeutig nachgewiesen.
Es muss daher davon ausgegangen werden, dass die Expression von CatChUP::EYFP::CRP-1 RyR entweder gar nicht oder in zu geringen Mengen stattgefunden hat.

Auch der Stamm GOA14 C1V1 ET/ET wurde in Pharynx Pumping Tests stimuliert. Eine signifikante Änderung des Pharynxpumpens unter sowohl 470nm als auch 590nm Stimulation wurde bei Frequenzen von 1-4Hz nicht detektiert. Es konnte damit nicht bestätigt werden, dass das Doppelsystem aus optoUNC-68 und C1V1 in dieser Form gleichzeitig einen Schrittmacher und Arrhythmie erzeugenden Effekt auslösen kann.

SERCA ist an der SR/ER-Membran lokalisiert und fungiert als Ca^{2+}-Translokator und somit als RyR-Antagonist, der quantitativ die meisten Ca^{2+}-Ionen in das SR transportiert. SERCA ist damit ein idealer Kandidat für die Schaffung einer modifizierten Version, die die Wiederaufnahme von Ca^{2+} aus dem

Zytosol in das SR unter Blaulichtaktivierung beeinflussen kann. Die CRISPR/Cas9-Methode wurde daher auch hier verwendet, um LOV2-Domänen in SERCA einzufügen. Besonders kritisch war dabei die Auswahl geeigneter Insertionsstellen. Informationen über relevante Konformationsänderungen und den katalytischen Zyklus wurden aus den atomaren Strukturen vergangener Publikationen abgeleitet. Auch hier wurden Schleifen zwischen α-Helices oder β-Strängen ausgewählt, in denen die LOV2-Domäne die Funktion der Pumpe beeinflussen kann, sobald sie eine lichtinduzierte Konformationsänderungen erfährt. Um auszuschließen, dass die Insertion einer LOV2-Domäne sterische Konflikte während des katalytischen Zyklus mit anderen SERCA-Domänen hervorruft, mussten spezifische molekulare Stellen identifiziert werden. Diese wurden relativ peripher zum Rest des Proteins in der ATP-bindenden "N"-Domäne gefunden. Sie umfasst mehrere Verbindungsschleifen und β-Faltblätter und faltet sich bei Konformationsänderungen von den anderen Domänen weg. Es wurden vier Schleifen zwischen β-Strängen ausgewählt, die ~10 Å voneinander entfernt sind, was der Distanz des N- und C-Terminus der LOV2-Domäne entspricht. Aufgrund lichtinduzierter Konformationsänderungen und damit einhergehender Störungen dieser β-Strang-Domänen ist es wahrscheinlich, dass funktionelle Probleme in SERCA auftreten, da die N-Domäne während des Translokationszyklus wesentlich an der ATP-Bindung und Phosphorylierung beteiligt ist. In Anbetracht der Tatsache, dass eine vollständige Deletion von SERCA letal ist, würde das alleinige Überleben eines Stammes sofort beweisen, dass die Einfügung von LOV2 an sich die Funktionalität von SERCA nicht übermäßig beeinträchtigt. Diese Annahme wurde dadurch belegt, dass die Manipulation durch CRISPR/CAS9 bei zwei Stämmen (GOA07 und GOA09) zur Letalität führte.

In Kontraktionstests mit transgenen Tieren konnte gezeigt werden, dass eine durch Photostimulation ausgelöste Konformationsänderung der LOV2 Domänen zum Stopp oder Beeinträchtigung der Ca^{2+} Ionen Translokation durch SERCA aus dem Cytosol in das SR/ER führt. Dies hatte im Gegensatz zu LOV2 in RyR eine Kontraktion der Körperlänge von *C. elegans* zur Folge.

Die hier aufgeführten Daten weisen darauf hin, dass der intrazelluläre Ca^{2+} Zyklus zwischen SR/ER und Cytosol durch das Einbringen optogenetischer Tools erfolgreich manipuliert werden kann. Es stellte sich auch heraus das die Manipulation/Beeinträchtigung einzelner Komponenten dieses Ca^{2+} Zyklus, wie z.B. RyR, oder SERCA, meist unzureichend ist, um eine eindeutige Reaktion zu erzielen. Die gleichzeitige Manipulation der beiden Hauptakteure RyR und SERCA ist wahrscheinlich der beste Weg, um einen weiteren Schritt zur Schaffung optogenetischer Werkzeuge für die lichtstimulierte Kontrolle der Ca^{2+}-Freisetzung und Wiederaufnahme aus dem SR/ER zu machen.

Abstract

Diseases such as cardiac arrhythmias, CPVT and other issues of the human heart still remain largely unexplored. To contribute to this field of research, it is necessary to create tools to control the spatial and temporal release and reuptake of Ca^{2+} from the sarcoplasmic/endoplasmic reticulum (SR/ER). Ca^{2+} release and uptake by the ryanodine receptor (RyR) and Sarcoplasmic/endoplasmic reticulum calcium ATPase (SERCA), respectively, are essential for the function of excitable cells. In this process, the rapid Ca^{2+} release from the SR/ER and the associated contraction in muscle cells is modulated by RyR. However, diseases due to calcium leakage, such as cardiac arrhythmias, seizures and contractile dysfunction, are also caused by RyR. The resting Ca^{2+} concentration in the cytosol, which is important for the cell, is kept in balance by Ca^{2+} release and reuptake into the SR/ER. This reuptake is controlled quite considerably by SERCA. SERCA is important for development and muscle function in both nematodes such as *C. elegans* and mammals, though there is also a great need for tools that can help study precise function.

To advance towards the goal of developing tools for optogenetic stimulation of intracellular Ca^{2+} release from the SR/ER, the model organism *C. elegans* was chosen. Its advantages are the fully sequenced genome and the neural network connectome. In addition, the ease of maintenance, self-fertilisation, transparency and rapid generation cycles, as well as the fact that it is a eutelic animal, are advantages for the application of the optogenetic approach.

So far, tools for light-induced Ca^{2+} release (LICR) have already been developed, involving the creation of ChR2 versions with higher Ca^{2+} conductivity based on the "CatCh" variant and further improving their conductivity through several established mutations. In addition, the pharynx of *C. elegans* was modified to produce an optogenetically stimulated muscle pump that resembles mammalian cardiac muscle cells. In this work, both optoUNC-68 (optically excitable RyR) and SERCA/LOV2 were generated in different variants by CRISPR/Cas9 and plasmid-based genome editing to achieve light-driven manipulation of calcium homeostasis in *C. elegans*. Here, LICR was triggered by LOV2 domains in an opto-mechanical manipulation of RyR as well as SERCA. This approach was made possible by recently published high-resolution cryoEM structural images. In addition, alternative approaches using Ca^{2+} conductance-optimised channelrhodopsin variants were tested in *C. elegans* body wall muscle cells.

By inserting ChR-XXM into *C. elegans* and subsequent fluorescence microscopy of the co-introduced GFP, an expression in body wall muscle cells could be detected. Furthermore, in contraction assays, ChR-XXM was demonstrated to induce contractions of the animals of up to 16% compared to the original body length in both medium (0.8mW/mm²) and high (1.4mW/mm²) stimulation at 470nm. ChR-XXM was thus identified as an excellent candidate for the development of an optogenetic tool, as it exhibits significantly increased Ca^{2+} conductivity compared to other ChR2 variants.

The use of CRISPR/Cas9 to insert AsLOV2 domains (L404-L546) into different insertion sites of RyR allowed the generation of a transgenic strain of *C. elegans* that could be stimulated to elongate during 0.3mW/mm² photostimulation. This demonstrated that RyR can be manipulated by photostimulation, spatiotemporally through conformational changes in the LOV2 domain and the resulting disruption of the pore region.

The CRISPR/Cas9 method was also used to insert LOV2 domains into SERCA. Here it could be demonstrated that a conformational change of the LOV2 domains induced by photostimulation leads to a stop or impairment of Ca^{2+} ion translocation by SERCA from the cytosol into the SR/ER. In contrast to LOV2 in RyR, this resulted in a contraction of *C. elegans* body length.

The data presented here indicate that the intracellular Ca^{2+} cycle involving the SR/ER and cytosol can be successfully manipulated by the introduction of optogenetic tools. It turned out that the manipulation/impairment of individual components of this system, such as RyR or SERCA, is usually insufficient to achieve a clear response. Therefore, simultaneous manipulation of the two main actors RyR and SERCA is arguably the best way to take another step towards creating optogenetic tools for light-stimulated manipulation of Ca^{2+} release and reuptake from the SR/ER.

1. Introduction

As an important signalling molecule and building material, calcium is an essential ion that is used in many metabolic pathways. It is used ubiquitously in every cell (Bootman and Berridge 1995), and life on earth in its known form would be inconceivable without it. Calcium serves as a scaffolding material in bones and teeth (Murshed 2018), as a messenger substance, as an essential ion in the structure of proteins, etc., and is involved in the transmission of impulses in nerve cells, in blood clotting (Lovelock J. E. and Porterfield 1952), and in heart rhythm (Liao et al. 1994). As an essential intracellular signalling molecule (Endo 2006), calcium has been linked to the regulation of several important physiological processes, including the activity of the gut microbiome (Song et al. 2019), enzymatic activity, the circadian clock, the regulation of obesity, nervous system excitability and muscle contraction (Simpson et al. 1995; Kon and Fukada 2015; Gagliano et al. 2020). The calcium content of the blood is mainly regulated by two hormones, the parathyroid hormone and calcitonin (Akerström et al. 2005). Much effort is being put into uncovering and influencing how exactly calcium interacts with the body, whether through pharmaceutical or genetic research methods.

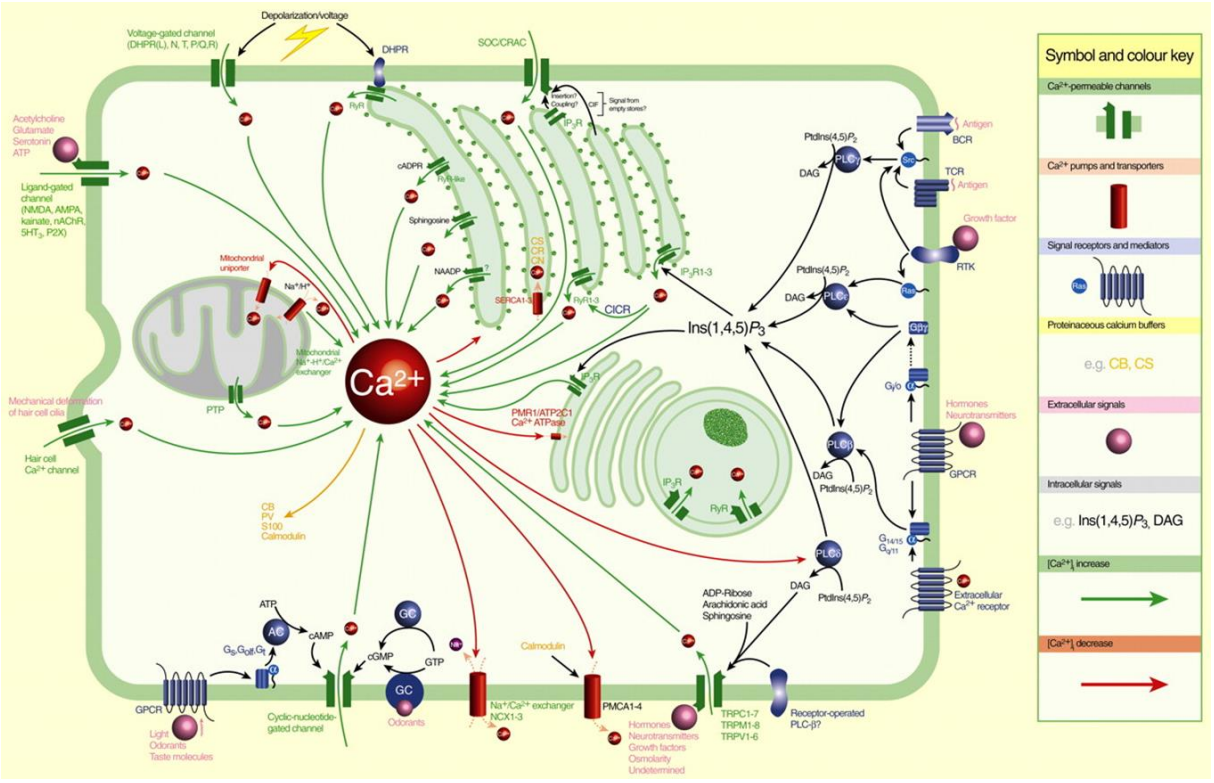

Figure 1: Overview of the intracellular calcium signalling. Adapted from Nowycky et al. 2002.

Optogenetics offers a toolbox with a wide range of light-responsive proteins, both of artificial and natural origin, that are used here to control the spatio-temporal Ca^{2+} flux of the sarco-/endoplasmic reticulum (SR/ER). With adequate optogenetic tools excitable cells such as neurons, muscles and some endocrine cells (Mollard and Schlegel 1996) could be stimulated by light and the associated release of calcium from the SR/ER, or the suppressed reuptake of calcium could be controlled. In this case, the focus lies on the development of tools for optogenetic manipulation of intracellular Ca^{2+} release and reuptake from the SR/ER and by that on the associated contraction or relaxation of the muscle.

Modern society of the first world countries is increasingly plagued by diseases that originate in unhealthy diets and too little physical activity. This results in an increasing number of cardiovascular diseases such as heart disease (*Figure 2* and *3*) and musculoskeletal disorders such as digital neuritis, ruptured/herniated disc or DeQuervain's syndrome.

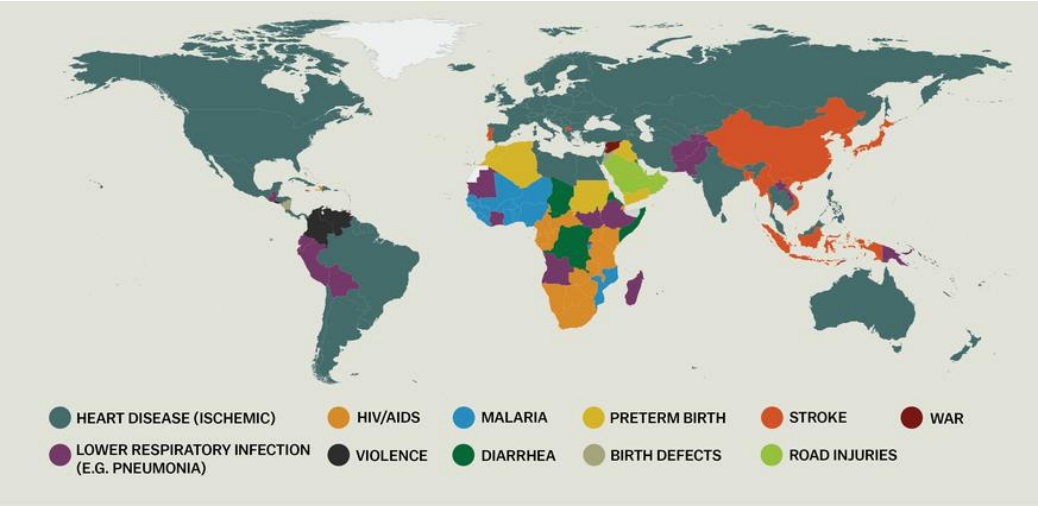

Figure 2: Leading causes of lost years of life in 2013. Global burden of disease study & the Lancet, 2014. Matthews 2015; Global, regional, and national age–sex specific all-cause and cause-specific mortality for 240 causes of death, 1990–2013: a systematic analysis for the Global Burden of Disease Study 2013-2015.

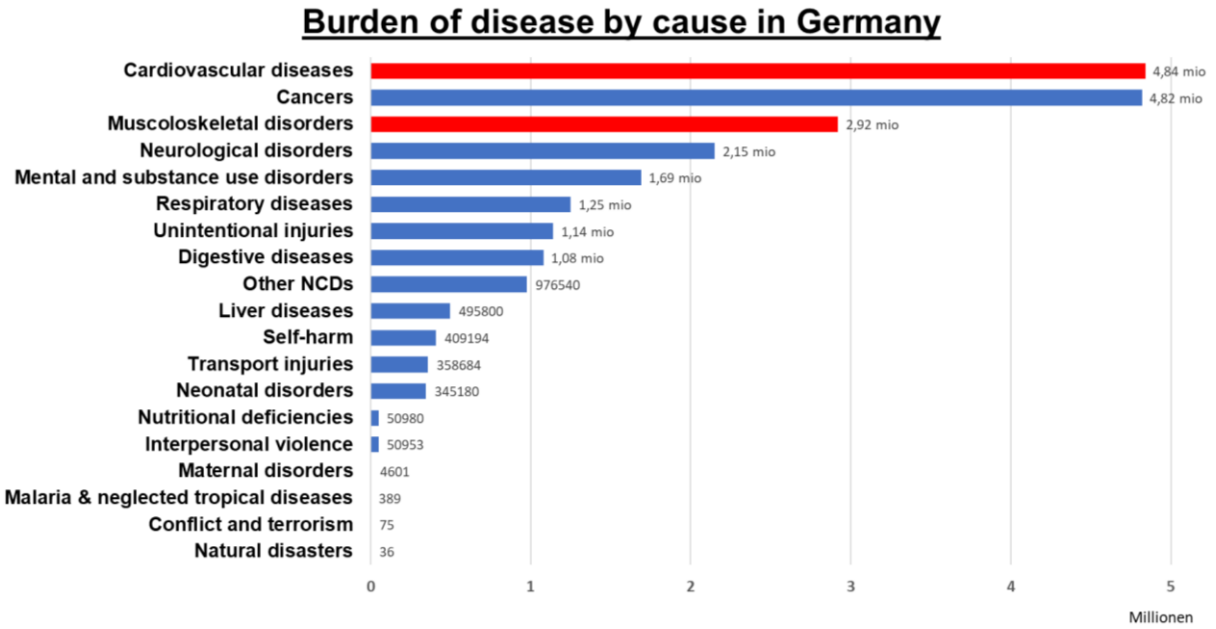

Figure 3: Total burden of disease in Germany 2017, measured in Disability-Adjusted Life Years (DALYs) by sub-category of disease or injury. DALYs measure the total burden of disease – both from years of life lost due to premature death and years lived with a disability. One DALY equals one lost year of healthy life. Figure adapted from IHME, Global Burden of Disease OurWorldInData.org/burden-of-disease.

Few of the diseases listed above are fully understood, and for most of them there is still a long way of research ahead to fully solve these problems. Although many of these diseases can already be effectively treated and their consequences minimised, this is a growing problem for the world's population (*Figure 3*).

In Germany, cardiovascular diseases such as coronary heart disease, myocardial infarction, Marvan syndrome and rheumatic heart disease, to name but a few, are the most common cause of death, as illustrated in *Figure 3*. Reasons for these rising problems are next to high cholesterol and high salt

consumption (Bruckert et al. 2020; Kloss et al. 2015), also a genetic predisposition (Scheuner 2001). For instance, cardiac arrhythmias and arterial diseases that lead to heart attack or strokes. One cause of cardiac diseases such as arrhythmias or catecholaminergic polymorphic ventricular tachycardia (CPVT), is the leakage of Ca^{2+} from the lumen of the endoplasmic reticulum (ER) Ca^{2+} stores. This is usually caused by missense mutations in the ryanodine receptor 2 (RyR2) channels and also by defects in the ER luminal Ca^{2+} storage protein calsequestrin-2 (Venetucci et al. 2012; Marsman et al. 2014; Sedej et al. 2010). The Ryanodine receptors are the mediators of Ca^{2+}-induced Ca^{2+} release (CICR) and are expressed in most muscle cells in the sarcoplasmic reticulum (SR). To investigate the subcellular mechanism and consequences of the RyR2-Ca^{2+} leak, we aim to develop optogenetic tools to induce a specific, spatiotemporal and acute leak of Ca^{2+} from the RyR or stop the reuptake of Ca^{2+} by manipulating SERCA.

1.1. *C. elegans* as model organism

Since Caenorhabditis elegans was introduced as a model system by Sydney Brenner (Nigon and Félix 2018; Brenner 2001), it has been closely linked to microscopy by the fact that the worm, its eggs and the larvae are transparent. In recent decades, this has led to important advances in the understanding of biology and still does. The development of new methods and technologies is therefore an essential part in the endeavour to gain further insights into the fields of optogenetics (Bergs et al. 2018), neuronal networks (Gottschalk 2020), disease research (Fischer et al. 2017), ageing (Olsen et al. 2006), developmental biology (Gilbert 2000) and many more.

Under natural conditions *C. elegans* is a 1.1 mm long, free-living androdioecious nematode (Stewart and Phillips 2002). In adulthood, it consists of 959 cells as hermaphrodite and 1031 cells as male, and thus belongs to the eutelic animals (Sulston and Horvitz 1977; Kimble and Hirsh 1979). The ability to grow thousands of animals on a single petri dish seeded with a lawn of *Escherichia coli* as a food source (W. Wood 1988) is an important capability, and astoundingly, the 300-350 eggs produced by a single hermaphrodite are even greater than the offspring produced by a T4 phage, upon lysis of its *E. coli* host (Golec et al. 2014). There is even the potential to generate up to 1400 eggs when males fertilize

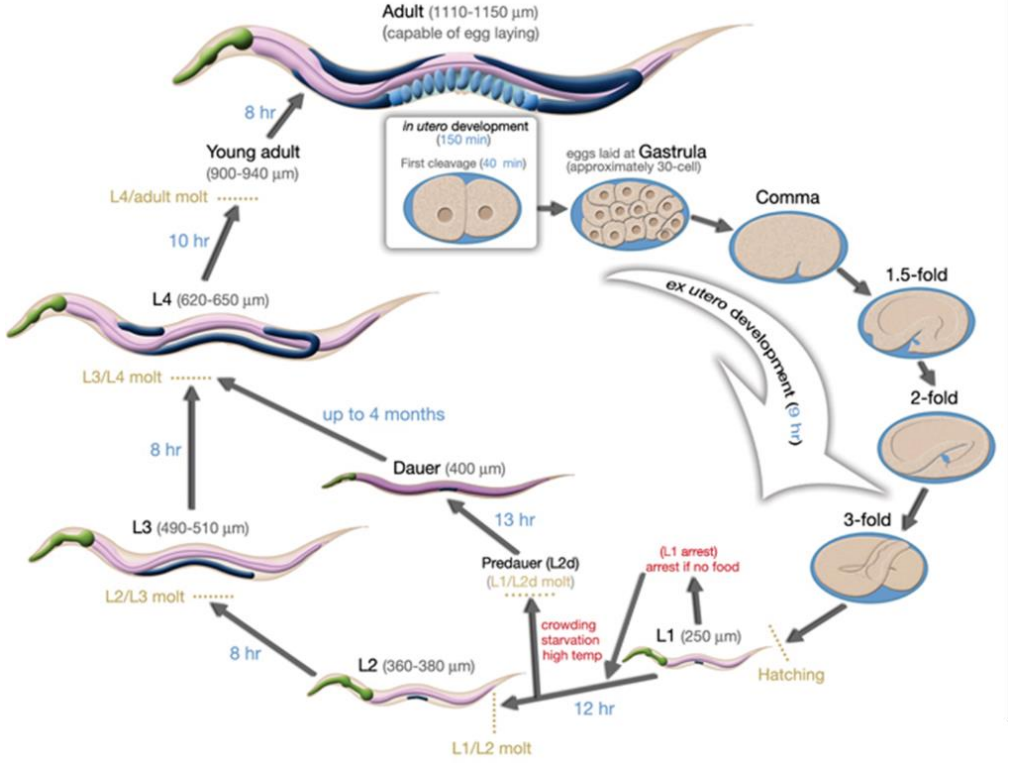

Figure 4: Adult male and life cycle of hermaphroditic *C. elegans*. A) Adult male. Scale bar 0,1mm. B) Enlarged unilobed distal gonad of the male animal. C) adult male tail, ventral view. Cloaca is marked by arrow and fan by *arrowhead*. Rays 1-9 are labelled with asterisks. D) Life cycle of *C. elegans* from fertilization to adulthood at 22°C. Image adapted from (Altun and Hall 2009c).

a hermaphrodite (Kimble, J. and S. Ward 1988). From egg to adult, the worm needs 2.5 days (Figure 4 D) in laboratory conditions. In the common wild-type laboratory strain, males are generated with a probability of 0.2% (Chasnov and Chow 2002; Teotónio et al. 2006). After hatching, the worm passes through four larval stages L1-L4 and each of it ends with the sleep-like lethargus, an inactive period that occurs before each of the four moults (Raizen et al. 2008; Cassada and Russell 1975). Under unfavourable environmental conditions, such as crowding, scarcity of food, drought (Erkut et al. 2013), etc., which are perceived by the chemosensory systems, the animals may enter the dauer stage. In this stage, they can be arrested immediately after hatching (L1), until conditions change again and the

progression of development can be resumed (Johnson et al. 1984). It is also possible to enter the dauer stage during L2. Wherein, upon high population density, pheromones, temperature or lack of food, can induce an alternative L2d stage (Golden and Riddle 1984). Depending on the continuance of these parameters, L2d animals either develop into normal L3, or remain in dauer larval stage, in which they can survive for several months. To do this, they reduce locomotion, metabolism and stop all food intake, whereby the mouth of dauer larvae is closed by the cuticle, until they find favourable conditions again. As soon as this happens they can revert to a normal L4 stage and eventually develop to an adult worm (Riddle 1997a; Patrick J. Hu 2018).

Differences of physique and function of the gonads can be seen between both sexes. The hermaphroditic germline produces both eggs and sperm, the latter being formed during the L4 stage. Gonads, which do not form until the adult stage, are then responsible for egg production and fertilisation by male sperm or self-fertilisation (L'Hernault 2006). The gonads form the oviduct, which consists of two symmetrical lobes connected to the uterus and the spermatheca. After fertilisation by spermatozoa from the spermatheca, the eggs are released from the vulva, which is located ventrally in the middle of the body (Sulston et al. 1983; Sulston and Horvitz 1977). The male gonad on the contrary, consists of one tube connected to the cloaca on the posterior tail ending (Sulston et al. 1980). The copulatory apparatus is established in the tail and comprises several structures that include the fan, sensory rays, hook and post-cloacal sensilla (Lints and Hall 2004). Moreover, the male bears 79 additional neurons that are necessary for the complex mating behaviour (Lints, R. and Hall, D.H. 2009).

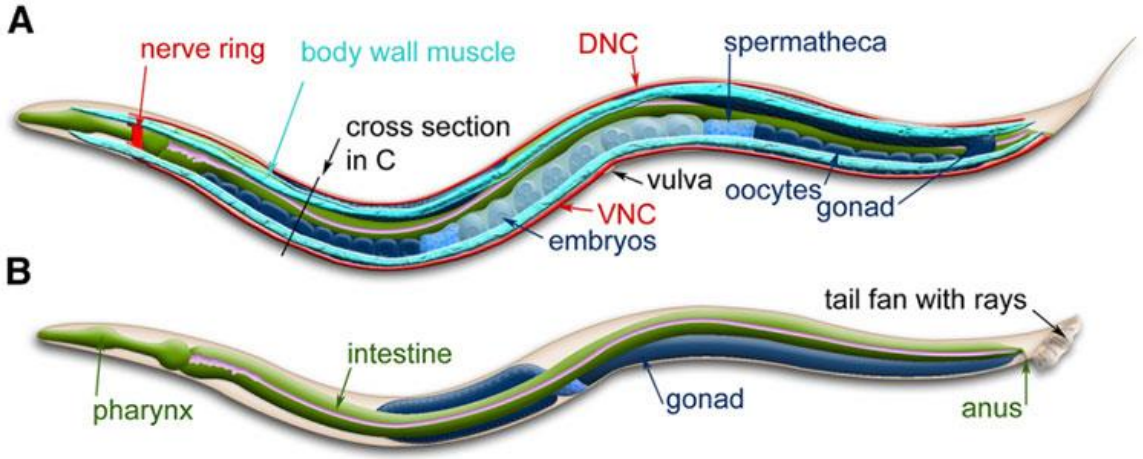

Figure 5: Major anatomical features of *C. elegans* anatomy. A) Hermaphroditic animal. B) Male animal. Lateral view. Adapted from (Corsi et al. 2015)

The hypodermis forms a tubular body with underlying musculature that includes its reproductive and digestive systems. Although it has most of the important differentiated tissue types such as muscles, nerves, intestine, hypodermis and gonads, an adult animal consists of less than 1000 non-gonadal nuclei (Sulston and Horvitz 1977).

The fully mapped neuronal network of *C. elegans* comprises 302 neurons (White et al. 1986) and is capable of processing the complex information of sensory input, computation of appropriate behaviours, and even formation of simple types of memory (Ardiel and Rankin 2010). Neurons can be classified into subtypes based on their location, function and span of the neuron axons, e.g. motor neurons, sensory neurons and intermediate neurons (Badhwar and Bagler 2015). While the main ganglia, which comprise certain sensory and interneurons, are found at the anterior and posterior ends, motor neurons are mainly distributed over the ventral nerve cord (White et al. 1976). Some of these ventral cord neurons form a dorsal nerve cord by extending their processes circumferentially. In addition, certain head neurons also extend their processes posteriorly along the dorsal nerve cord. The animal responds to external signals received from sensory neurons. By sending signals to the effector

organs via the motor neurons which form neuromuscular junctions on their axonal ends and receive input from command interneurons and other motor neurons on their dendritic processes (Stetina et al. 2005). Both the dorsal and the ventral nerve cord control locomotion of the animal.

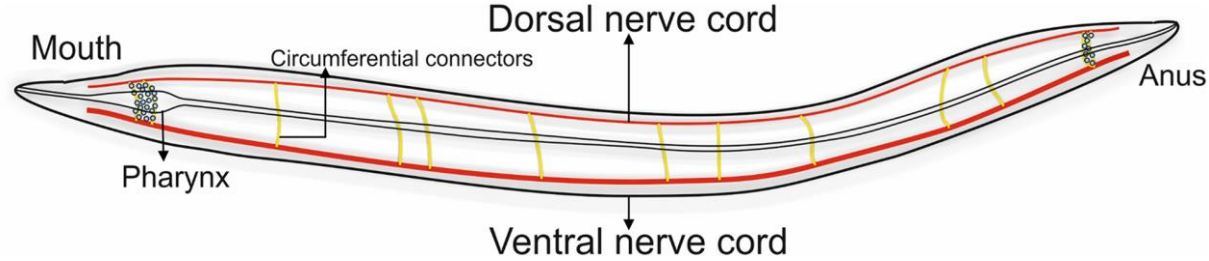

Figure 6: Graphic of *C. elegans* nervous system. The gastrointestinal tract lies in the middle of the body. Circumferential ring neurons (yellow) and pharyngeal neurons are responsible for communication of dorsal and ventral nerve cord (red). Figure adapted from (Badhwar and Bagler 2015).

The endodermal germ layer includes the alimentary system, that is necessary for the breakdown of food and the absorption of nutrients and mineral uptake (Dimov and Maduro 2019). Starting at the tip of the head with the mouth (buccal cavity), the nematode digestive system comprises only a simple pharynx (oesophagus), intestine and hindgut including rectum. Like the oesophagus, the pharynx is self-contained and consists of 58 cells. These contain their own neurons, muscles and epithelium (Mango 2009; Sulston et al. 1983). The grinder, a cuticular structure, is located at the posterior end of the pharynx. Three sets of muscles, including two muscles that create a ring around the ventral posterior of the intestine, regulate the control of the anus (White 1986). Through this structure, the attachment of the intestine to the pharynx and hindgut and the ventral posterior muscles are the only fixed connections from the intestine to the body (Altun and Hall 2009a; Altun and Hall 2009c).

Due to its fully sequenced genome (Hillier et al. 2005), its well-defined small nervous system (White 1986), its transparency and its high and fast reproducibility, it is excellently suited for optogenetics. In cholinergic neurons or body wall muscles, tools can be tested that affect membrane potential. Effects of this manipulation are determined by muscle contraction or relaxation either by measuring membrane currents by elctrophysiology or the macroscopic body length of the animal, which is distinguished by the simultaneous contraction or relaxation of all muscles.

1.2. Muscles as primary target of the project

In *C. elegans*, the sarcoplasmic reticulum surrounds the myofilament lattice and is composed of a network of vesicular membranous organelles. These vesicles are flattened and lie adjacent to the apical plasma membrane, on the hypodermal side, beneath the lattice and extend around dense bodies (DBs), where they are localized randomly (Robert H. Waterston 1988). Plasma membrane and SR vesicles are separated by a gap of 12-14nm. A sarcomere is a single unit of myofilament lattice between two DBs and is formed by two adjacent half I-bands and an A-band in the middle (*Figure 7*). In the nematode, the T-tubule system has no equivalent, probably as a result of the direct attachment of the SR to the plasma membrane negating its utility (Robert H. Waterston 1988).

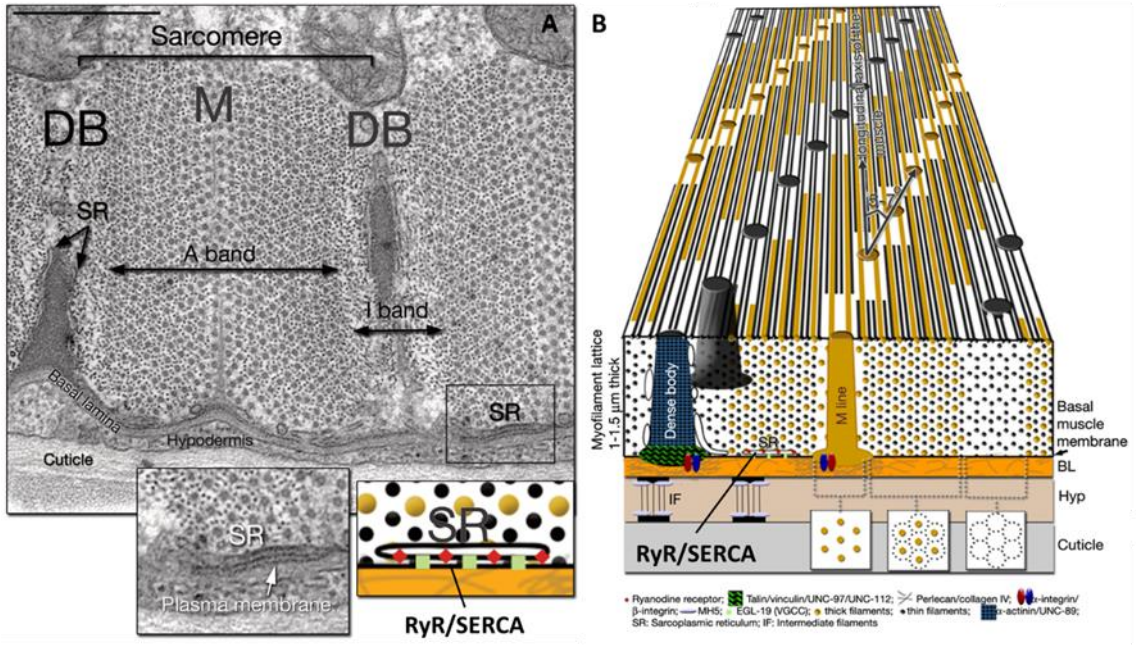

Figure 7: Cross section of the contractile apparatus in a body wall muscle and organization of the myofilament lattice including localisation of RyR and SERCA. A). The filaments of the lattice are oriented longitudinally and perpendicular to the surface. A dense body (DB) is the anchor of the thin (actin) filaments, M line-homologs anchor the thick (myosin) filaments. SR: Sarcoplasmic reticulum. Sarcomere: 1µm, scalebar: 0.5 µm. B*)* Illustration of a cross section of the myofilament lattice. The sheet of filaments lies inside the muscle membrane, separated from the hypodermis by a 20nm basal lamina (BL). RyR and SERCA localised on the sarcoplasmic reticulum (SR). Cuticle lies outside the hypodermis (Hyp). Striations created by the thin and thick filaments build an angle of 5-7° to the longitudinal axes of the filaments and the muscle cell. Yellow lines: Thick filaments; black lines: thin filaments; black dots: DB; brown dots: M lines. Image modified and adapted from (Altun and Hall 2009b).

The ryanodine receptor (RYR), is encoded in *C. elegans* by the *unc-68* gene (Maryon et al. 1996; Hamada et al. 2002). RyR is expressed, for instance, in the muscles of the terminal bulb of the pharynx, the vulva and uterine muscles, the body wall muscle cells, the anal sphincters and depressors, and the diagonal muscles of the male tail (EB Maryon 1998). The initiation of the first twitch movements in somatic muscle is consistent with UNC-68 expression (Altun and Hall 2009b). UNC-68 is localised in SR vesicles within body wall muscles, predominantly between the rows of dense bodies in the A-band region (EB Maryon 1998). The fact that *unc-68* null mutants are still able to propagate weak coordinated contraction waves, demonstrates that UNC-68 has a function in enhancing motility. Though it is not indispensable for excitation-contraction coupling (EC), as it is in vertebrate muscle. It is hypothesised that upon excitatory, cholinergic, neurotransmission to the NMJs, action potentials are triggered in the muscle arms by the opening of nicotinic AChR, ligand-gated ion channels, which then converge and spread to the contractile compartment of the muscle (Richmond and Jorgensen 1999; Jospin et al. 2002; Schafer 2002). The action potentials are postulated to depend on voltage-activated

Ca^{2+} currents across the muscle plasma membrane via L-type channels, as there are no voltage-activated Na^{+} channels in *C. elegans* (Altun and Hall 2009b). The activation of Ca^{2+} channels is similar to the dihydropyridine receptor (DHPR), encoded by *egl-19*. It is hypothesised that this allows sufficient Ca^{2+} influx from the orifice and propagate through the extracellular space across the plasma membrane to trigger CICR. This directly initiates the opening of UNC-68 and thus the Ca^{2+} increase in the cytosol, through EGL-19 and enhanced by UNC-68, leading to a contraction in the body wall muscles, where the sarcomeres are located in close vicinity to the plasma membrane (Lee et al. 1997; EB Maryon 1998; Jospin et al. 2002).

Neuromuscular junctions (NMJs) of *C. elegans* are formed by arms that grow from the muscle cell into the direction of the motor neuron (Stretton, 1976; Sulston and Horvitz, 1977; Sulston et al., 1983; White et al., 1986; Dixon and Roy, 2005; Dixon et al., 2006). To connect to the neuron, these muscle arms have simple structures consisting of a bifurcated terminus and stalk. NMJs are formed en passant by the innervating neurons onto these muscle arms, similar to chemical synapses between neurons (White et al., 1986). To become accessible to muscle arms in synaptic regions, each motor neuron process of a process bundle, moves to the outside of the bundle sporadically.

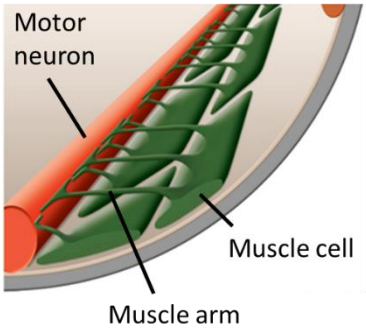

Figure 8: Body wall muscle development. In the adult, each muscle cell contains three to six arms (dark green arms) connected to the motor neuron (red). Image modified and adapted from (Altun and Hall 2009b).

Muscle cells are an essential component of the nematode that are relatively easy to access and manipulate. By using well-studied and characterised promoters, such as myo-2 and myo-3 (Fire et al. 1990; Fire and Waterston 1989), protein expression in pharyngeal and body wall muscle cells, respectively, can be controlled. In this way the effect of this gene manipulation can be easily analysed by behavioural assays and contraction measurements of the worm. This renders muscle cells as one of the excitable cells containing an SR, an ideal candidate to develop tools for optogenetic manipulation of intracellular Ca^{2+}release and uptake.

1.2.1. The Sarcoplasmic reticulum - main intracellular storage of Ca^{2+} ions

The sarcoplasmic reticulum is found in muscle cells, where it represents a membranous structure analogous to the endoplasmic reticulum, only in the muscle cells, and therefore more specialised in certain aspects. Due to the fact that calcium ion levels outside the cell are ~10000 times higher than within the cytosol, it is necessary to maintain this imbalance relatively constant, which is one role of the SR (Bronner 2001). This in turn means that small changes such as depolarisation by an action potential and the associated Ca^{2+} influx can result in a large change. The SR traverses through the muscle cells with a network of tubes, in vertebrate skeletal and cardiac muscle cells so-called transverse tubules (T-tubules). These extend into the interior of the muscle cell as an extension of the cell membrane. T-tubules do not arise in invertebrates such as *C. elegans*. Since the Ca^{2+} concentration in the cytosol is lower than in the SR, calcium uptake into the SR must be ensured by so-called sarco-(endo) plasmatic reticulum Ca^{2+} ATPases. These membrane-bound ion pumps consume ATP when transporting two Ca^{2+} ions into the SR (Periasamy and Kalyanasundaram 2007). Storage of calcium in the SR is ensured by the buffer calsequestrin, capable of binding ~50 Ca^{2+} and thus reducing the amount of dissolved Ca^{2+} (Beard et al. 2004). Calsequestrin is mainly residing within the junctional

SR/luminal space (Kobayashi et al. 2000). Ca^{2+} ion release from the SR is mediated by the ryanodine receptor upon binding of cytosolic Ca^{2+}, which can be increased by an action potential.

1.2.2. Structure and shape of the body wall muscles in *C. elegans*

In the nematode, the myofilament lattice of the contractile unit is attached to the basal lamina and muscle cell membrane by dense bodies and M-lines. These extend from the cytoplasm to the plasma membrane and are regularly arranged, highly ordered structures. In addition, dense bodies also share components with the muscle-muscle attachment plaques (Francis and Waterston 1985). M-lines and dense bodies on the plasma membrane are mechanically linked to the outside cuticle through hypodermal fibrous organelles and basal lamina components (Francis and Waterston 1991; Robert H. Waterston 1988; Riddle 1997b; Hresko et al. 1999; Hahn and Labouesse 2001; Cox and Hardin 2004).

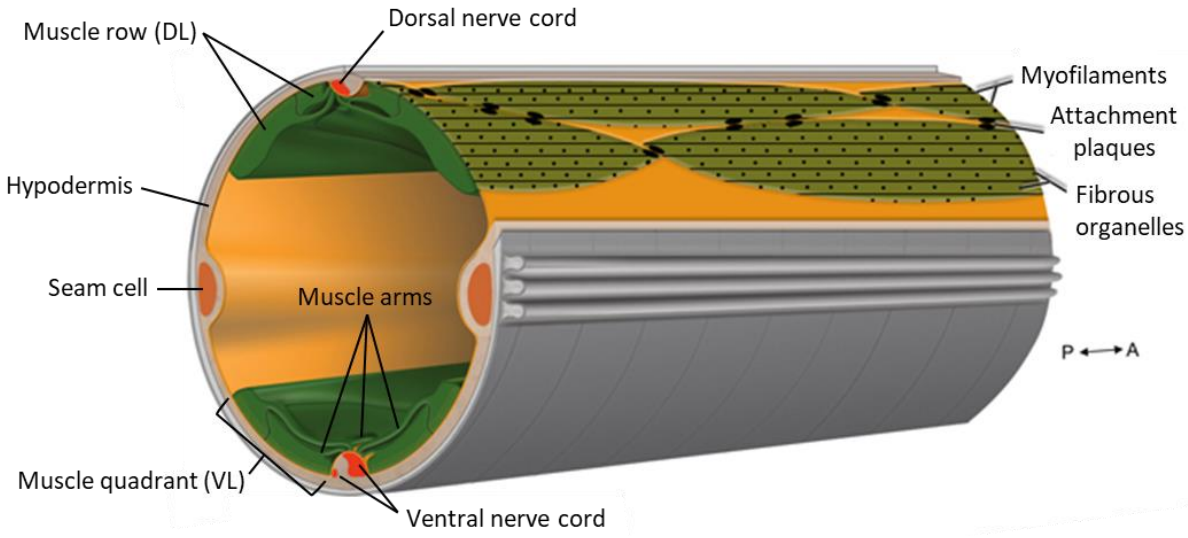

Figure 9: Body wall muscle structure. Graphical section through the body with the cuticle (grey) and the hypodermis (beige) peeled off from the dorsal left quadrant to expose fibrous organelles (small dots), attachment plaques (large oval dots), and the underlying muscle (green). Basal lamina (orange layer). Cross section of the body indicating muscle arms of the body wall muscles, arranged in four quadrants with two rows of muscle cells in each quadrant. Each body muscle cell is innervated by extending several muscle arms that reach the nearest nerve cord. Basal lamina separates the muscle from the nerve cords and the hypodermis. Hypodermis separates muscle from cuticle. Image adapted from (Altun and Hall 2009c).

1.2.3. The nematode pharynx and its relation to human cardiac biology

The pharynx is the feeding organ of *C. elegans* which is a rhythmically active muscle pump (Avery and You 2012) that has similarities but also differences to the vertebrate heart (Mango 2007). It consists of 20 muscle cells and accessory cells. These are connected by gap junctions, as in the heart, and form an elongated structure with anterior and terminal bulbs and an axial lumen (

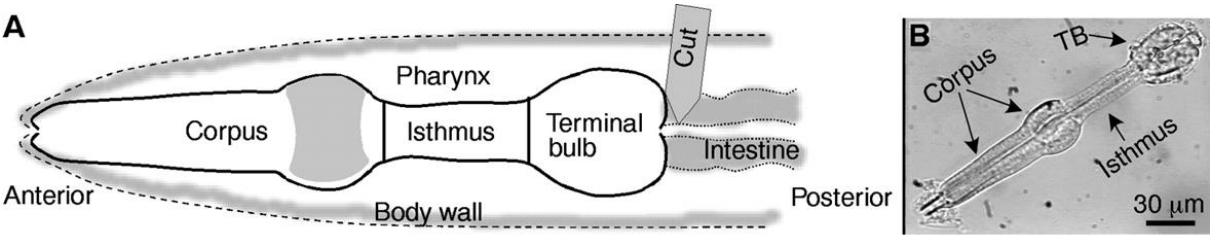

*Figure **10***). The genesis of the pharynx from the ectoderm and that of the heart from the mesoderm,

however, indicate a convergent development of the two organs (Mango 2007).The pharynx has an autonomic nervous system of 20 neurons. It is almost completely isolated from the remaining nervous system and is primarily required for rapid pumping and modulation of pharyngeal activity in the presence or absence of bacterial food (Avery and Horvitz 1987; Avery and Horvitzt 1989; Franks et al. 2006). Bacteria are imbibed and moved through the procorpus and anterior bulb to be collected in the anterior isthmus. The frequency at which the pharynx pumps can reach 4Hz in the presence of bacteria (Horvitz et al. 1982). Food is mechanically lysed after it has been transported to the terminal bulb by isthmus peristalsis (Fang-Yen et al. 2009). As long as there are no coordinated neural inputs, pharyngeal contractions can continue, as in the heart, but only in the presence of acetylcholine. The pharyngeal action potential has been found to be very similar to the human cardiac action potential due to its plateau, as well as ion channels that facilitate the controlled pharyngeal action. EAT-2 nicotinic acetylcholine receptors (McKay et al. 2004), are required for rapid pumping and replace voltage-gated sodium channels. T-type and L-type VGCCs encoded by *cca-1* and *egl-19* shape the rise and plateau phases of pharyngeal action potentials (Shtonda and Avery 2005). Glutamate-gated chloride channels control repolarisation, but voltage-gated K^+ channels, encoded by *exp-2* carry it out (Davis et al. 1999). Although homology is low, EXP-2 is functionally similar to UNC-103 K^+-channels and the mammalian HERG channels. Since mutations in the UNC-68 ryanodine receptor expressed by pharyngeal muscles and the SR Ca^{2+} storage protein CSQ-1, which is similar to human CASQ-2, can occur and affect the electrical and physiological properties of pharyngeal pumping, they can therefore also serve as a model system for homologous mutations in humans (Hamada et al. 2002; EB Maryon 1998; JH Cho 1999).

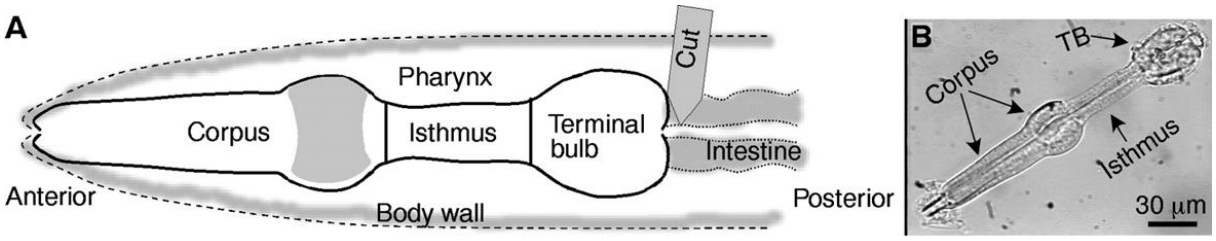

Figure 10: Head and pharynx of *C. elegans*. (A) Schematic of the *C. elegans* pharynx as it is positioned in the worm's head. D) Skinned and digested pharynx, depicts Corpus, Isthmus and Terminal bulb (TB). Adapted from (Shtonda and Avery 2005).

1.2.3.1. The pharynx as an arrythmia model

The heart is a muscle that needs to be well regulated to ensure that the organs of the body are supplied with oxygen and nutrients from the blood. This is done through many regulatory mechanisms that require to be balanced. If these systems disequilibrate, they can cause a variety of diseases and conditions, starting with hypertension and cardiomyopathy to heart failure. A simple model system, which is reasonably similar to the human heart, but amenable to manipulation, would facilitate research into the causes of these diseases and advance the knowledge in this field (Fischer et al. 2017). Three observations suggest that the pharynx and heart represent convergent evolution. The mammalian heart is a mesodermal organ. The pharynx, on the other hand, appears to be of ectodermal origin, being topologically connected to the epidermis and lined with cuticle, like the epidermis (Albertson and Thomson 1976). The myoepithelial muscle of the pharynx, having apical domains separated from the basolateral surfaces by adherens junctions, are in contact with a basal lamina (Portereiko and Mango 2001; Albertson and Thomson 1976). Lastly, the electrical conductance of the heart and pharynx differ in that, in the heart the action potential is initiated by a fast Na^+ spike. This role is taken over by the nicotinic acetylcholine receptors (*eat-2*), building Na^+ channels. These are

expressed by the pharyngeal muscle cells (Towers et al. 2005; D. Raizen et al. 1995; McKay et al. 2004). Cardiac hERG and EXP-2, two potassium channels of the heart and pharynx, respectively, terminate the action potential, however, both are only remotely related (Shtonda and Avery 2005; Davis et al. 1999).

Besides the differences, however, there are also commonalities between the vertebrate heart and the *C. elegans* pharynx, that imply an orthology. The heart and pharynx are tubes constructed by binucleate muscle cells that continuously pump material along their lumen throughout life (Kellerman

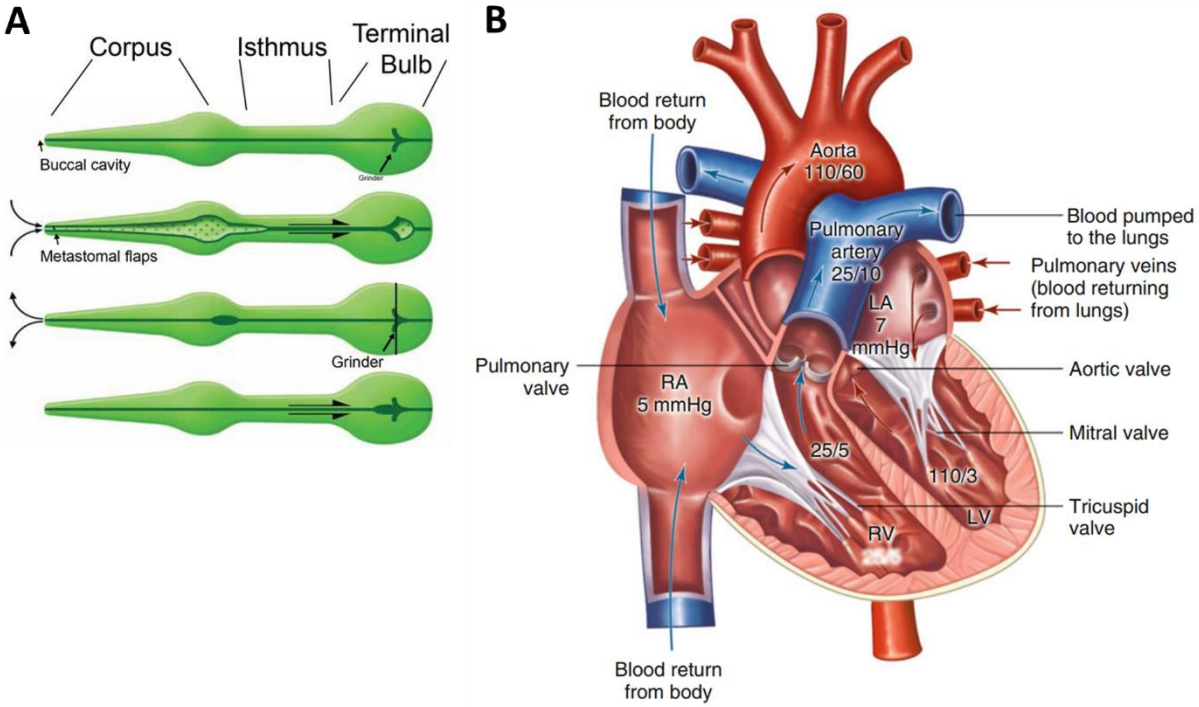

Figure 11: Comparison of fluid flow of *C. elegans* pharynx and human heart A) Functional units of the pharynx: corpus, isthmus, and posterior bulb. Major steps of feeding (top to bottom): ingestion by the corpus, fluid expulsion, and isthmus peristalsis to deliver food to the grinder. B) Blood flow and intracardiac pressures in a normal heart. RA right atrium, RV right ventricle, LA left atrium, LV left ventricle. Figures adapted from A) (Cook et al. 2019) and B)Adapted from Rickert-Sperling et al. 2016.

1992; Albertson and Thomson 1976). Furthermore, in both organs, gap junctions connect adjacent muscle cells to each other, synchronising contractions without relying on neuronal input (Bernstein and Morley 2006; Avery and Horvitzt 1989; Trojanowski and Fang-Yen 2015; Starich et al. 1996; Starich et al. 2003). L-type voltage-gated calcium channels and LQT potassium channels, which share similarities, are also found in the heart and pharynx (Raizen and Avery 1994; Salkoff et al. 2005; Avery and Horvitzt 1989). Neurotransmitters that couple to GPCRs modulate contraction speed, including serotonin and acetylcholine (Penela et al. 2006; Steger and Avery 2004; Hobson et al. 2003). Another argument that can be raised is that the organs rely on Nkx2.5 in the zebrafish heart and *ceh-22* in the pharynx, both NKX transcription factors, during their genesis, and when expressed under the control of the *ceh-22* promoter, Nkx2.5 can rescue *ceh-22* mutants (Haun et al. 1998). When Nkx2.5 is expressed in *C. elegans* body wall muscles, it can activate the CEH-22 target gene *myo-2* (P. Okkema and A. Fire 1994; P. Okkema et al. 1997; J. Chen and M. Fishman 1996).

Taken together, the differences and similarities suggest that convergent rather than homologous evolution has taken place in two muscular pumps confronted with the same biological tasks. Differences such as the regular pumping of the heart, controlled by the sympathetic and parasympathetic nervous systems, and the pharyngeal pumping, which depends on the food supply, can be compensated by an artificial pacemaker system (Fischer 2015; Fischer et al. 2017; Schüler et al. 2016).

1.3. The Calcium cycle – Influx and efflux of Ca^{2+} from the SR/ER

Ca^{2+}-dynamic regulation in striated muscle cells is governed by the sarcoplasmic reticulum, a network of tubules and cisternae closely associated with the contractile apparatus. This endomembrane network regulates Ca^{2+} release and reuptake, among other things, and thus controls excitation-contraction coupling in striated muscles (Lefebvre et al. 2016).
In this work, the aim was to develop methods to control SR/ER and its calcium flux optogenetically, therefore the focus is on muscle cells that harbour a sarcoplasmic reticulum (SR). These electrically excitable cells, that contain smooth ER similar to the SR, include neurons and muscle cells in *C. elegans*, as well as glandular cells such as the insulin-releasing β-cells of the pancreas (Shyr et al. 2019), some plant cells (Wayne 1993) and fertilised eggs (Miyazaki et al. 1974).

1.3.1. The Ryanodine receptor - major Ca^{2+} release channel of the SR

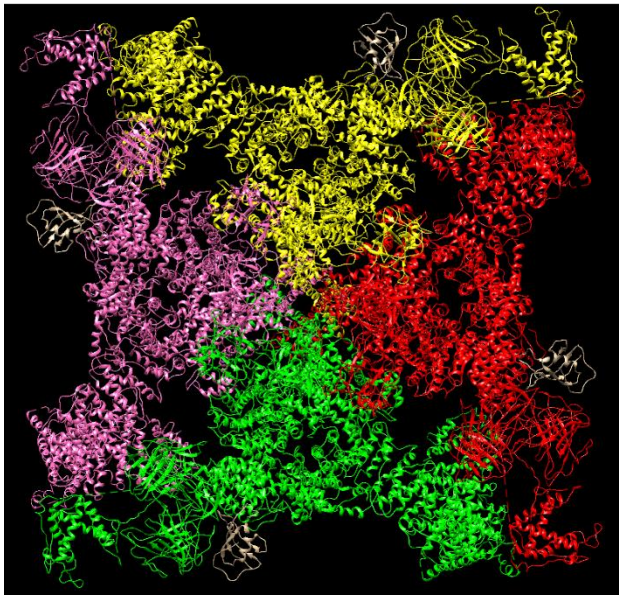

Figure 12: Top view of the ryanodine receptor 2 (RyR2). Each of the four protomers is individually coloured. Software: PyMol

Focusing on optogenetic manipulation of intracellular Ca^{2+} release from the SR/ER, the ryanodine receptor (RyR) plays a pivotal role in this thesis. As a secondary messenger, intracellular Ca^{2+} is essential for signal transduction and indispensable for cellular processes such as excitation-contraction coupling (EC-coupling) and the function of excitable cells (Zalk et al. 2007). The main source of intracellular Ca^{2+}, is the SR in striated muscle and the ER in other cell types. There are two major release channels on the SR-membrane, the ryanodine receptors (Otsu et al. 1990), and the inositol-1,4,5-triphosphate receptors (IP_3Rs) (Nixon et al. 1994). In vertebrates, RyRs exist in three isoforms (RyR1-3), that form homotetrameric channels and are named after the plant alkaloid ryanodine. Due to its high affinity and specificity, it binds to the RyRs and exhibits preferential interactions with the open state of the channel. This allows the functional state of the channel to be determined (Imagawa et al. 1987; A. Chu et al. 1990; Inui et al. 1987; Lai et al. 1988). In *C. elegans*, the *unc-68* locus, located on chromosome V, encodes a single RyR gene, with the UNC-68 protein sharing 63% homology and 45% sequence identity with human cardiac RyR2 (Fischer et al. 2017). Expression of UNC-68 (4967 amino acids), leads to the formation of the 2.26 mega Dalton

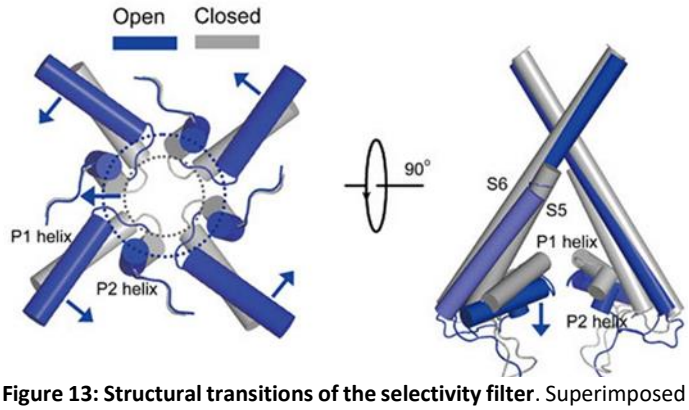

Figure 13: Structural transitions of the selectivity filter. Superimposed presentation of the selectivity filter region of the closed- and open-state RyR1 structures. Left: luminal view. Right: side view. Arrows indicate the movements of P1 and P2 in the open-state, relative to the closed-state. Substantial expansion of the pore in the open-state, relative to the closed-state, is marked. Adapted from (Wei et al. 2016).

tetrameric ion channel, that can be found in body wall muscles, neurons, the posterior isthmus and in terminal bulb muscle cells of the pharynx (EB Maryon 1998). RyRs are members of the six-transmembrane ion channel superfamily. These comprise a transmembrane region with a pore-forming domain containing outer S6, inner S5 helices, and a 4-helix bundle of S1-S4which is similar to the voltage-sensitive domains in voltage-gated channels (Zalk et al. 2015; Zalk and Marks 2017). The massive cytosolic head, largely constructed of an α-helical scaffold, is interspersed with a series of globular domains (van Petegem 2016). In vertebrates, RyRs are modulated directly or indirectly by the dihydropyridine receptor (DHPR, or CaV1.1/1.2) and by various molecules, proteins and ions:

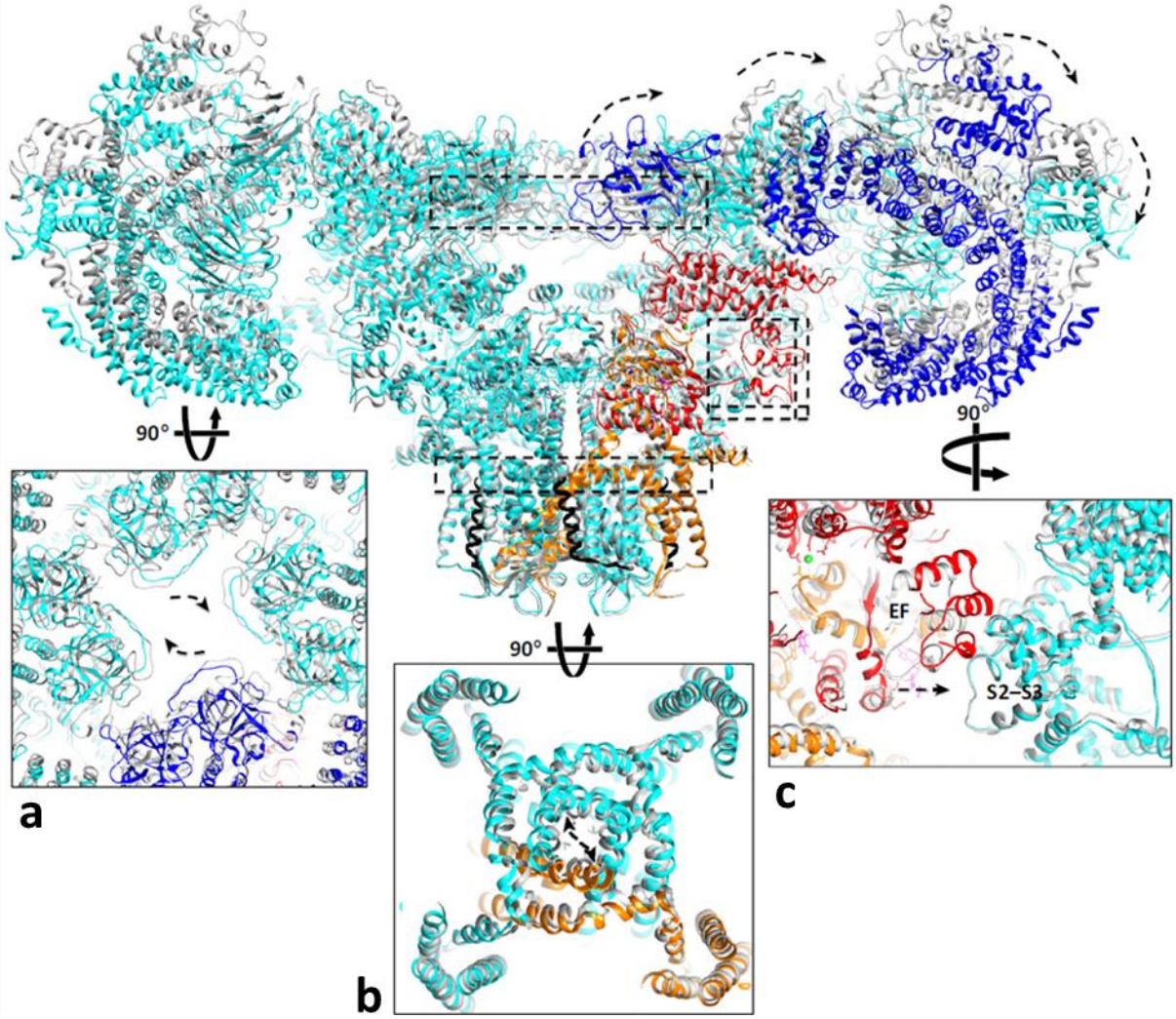

Figure 14: Moving parts of ryanodine receptor 1. Upon Ca^{2+} and ATP binding, the widened channel pore opening can be observed (b), which is associated with exorotation of the cytoplasmic envelope and translation of the cytoplasmic vestibule of the N-terminal domain (NTD) in a clockwise direction b) Translation of the EF-hand pair towards S2-S3 helical bundle. c) Insets of broken rectangles: enlarged view the structure. Broken arrows: apparent direction of movement from closed to open state. Adapted from (Zalk and Marks 2017).

Ca^{2+}/calmodulin-dependent protein kinase II (CaMKII), calmodulin (CaM), calsequestrin (CSQ), protein kinase A (PKA), FK506-binding proteins (FKBP12 and 12.6), triadin, junctin, Mg^{2+} and especially Ca^{2+} (Timerman et al. 1996; Tanabe et al. 1990; Tripathy et al. 1995; Smith et al. 1986; Ikemoto et al. 1991; Sabbadini et al. 1992; Wang and Best 1992; Brillantes et al. 1994; Chen and MacLennan DH. 1994; Yang et al. 1994; Ma et al. 1995; Rodney et al. 2000; Nakai et al. 1998; Porter Moore et al. 1999; Mayrleitner et al. 1995). Of these, junctin and triadin, both of which associate with RyR2 and form a macromolecular Ca-signalling complex (Terentyev et al. 2005), are the only ones not found in *C. elegans*. Instead, the C-terminal region of CSQ-1 with its positive charges, possibly binds directly with

the intraluminal loops of RyR by electrostatic interactions (Cho et al. 2007), Upon an action potential, Ca^{2+} release from the SR is triggered by calcium-induced calcium release (Tanimoto et al. 2017; Catterall 2011), whereupon cytoplasmic Ca^{2+}, provided by the L-type voltage-dependent Ca^{2+} channel EGL-19 (Jospin et al. 2002), initiates muscle contraction. Ca^{2+} ions are subsequently pumped back into the SR by the SERCA, resulting in muscle relaxation (Nakai et al. 1998; Fill and Copello 2002). This Ca^{2+} release is caused by the conformational change in the RyR.

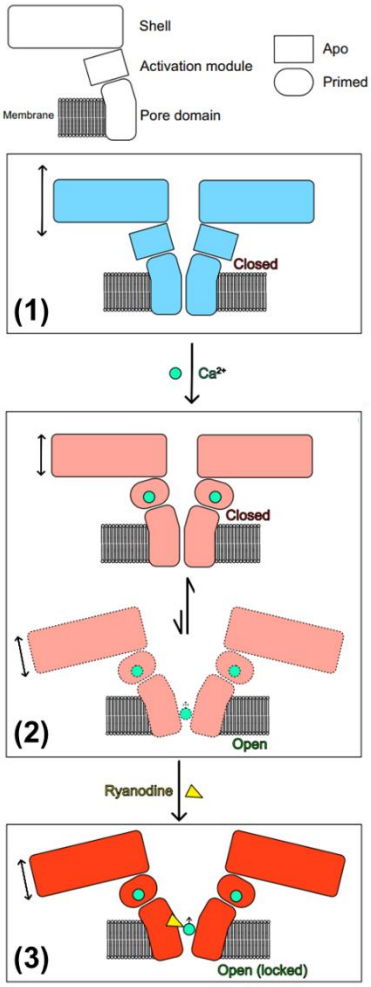

Figure 15: Course of opening of the RyR. (1) Closed state. (2) Opening of the channel upon Ca2+ binding to the Ca2+ binding site. (3) Open blocked state caused by binding of Ryanodine. Square activation module: Apo state; rounded activation module: primed state. Adapted from (Des Georges et al. 2016)

Previous studies have shown that RyR has a lower-affinity C^{2+}-dependent inhibition site at high Ca^{2+} concentrations and a moderate-affinity Ca^{2+}-dependent activation binding site at concentrations in the µM range (Bezprozvanny et al. 1991). The putative Ca^{2+} activation site is located near caffeine and ATP binding sites, two activators of RyR and also directly adjacent to an E4032 interface where mutation leads to Ca^{2+}-dependent activation of the channel. E4032 interacts with the C-terminal domain (CTD) in the Ca^{2+} bound state, stabilising a conformation that allows Ca^{2+} binding (Des Georges et al. 2016), but it has also been suggested that E4032 forms part of the activating Ca^{2+} binding site (Fessenden et al. 2001). However this is not the case in Ca^{2+} bound structures (Des Georges et al. 2016). In RyRs and IP_3Rs, all Ca^{2+} coordinating residues are conserved. In RyR, the three activating ligands, Ca^{2+}, ATP and caffeine, can bind to the CTD, resulting in a rearrangement of the channel core that primes RyR for opening. At low concentrations Ryanodine, a plant alkaloid, locks the channel in a reduced conductance state. When a high concentration is reached, it locks the pore in an open state by binding in the TM conduction pathway (Nagasaki and Fleischer 1988). Wherein the opening transitions within the pore-forming domain correspond to those of members of the 6-TM ion channel family, with the inner helix S6 bending around a conserved glycine hinge. This generates enough space for a hydrated Ca^{2+} to permeate, upon expansion of the pore around a hydrophobic constriction point. A direct connection exists with the voltage-sensing like domain (VSL) and the S6 extension. The inner helix extends towards a zinc-finger motif that interacts with an upstream "U-motif", allowing movement of the elongated S6 helix coupled to the U-motif or allowing movement of the VSL that is tightly coupled to the pore domain (van Petegem 2016; Wei et al. 2016). Motions in the TM region must be the outcome of conformational changes in the cytosolic cap, as the activating Ca^{2+} binding site is located elsewhere. The central domain connects the movements to the U-motif and thus to the TM region. The region of the cap containing the N-terminal domains moves outwards and upwards, exactly around the 4-fold symmetry axis (Samsó et al. 2009; Kimlicka et al. 2013). Four different closed states (C1-C4) are described, with the cap movement decreasing from C4 to C1. The C3 state seems to be closest to the open channel, but still some differences remain (Bai et al. 2016).

The termination of Ca^{2+} release and the associated closing of the pore in RyR has not yet been conclusively clarified. Theories are based on the assumption that a random closure, a so-called

stochastic attrition, takes place, or that RyR becomes inactive after a Ca^{2+} spark (Sham et al. 1998), or that it simply remains open until the SR Ca^{2+} is exhausted (Fill and Gillespie 2018).

The human RyR, as the most important intracellular Ca^{2+} release channel, plays an important role in various diseases due to its complexity and interactions with various associated proteins, molecules and ions. These include, for example, malignant hyperthermia (MH) (Denborough 1998), central core disease (RyR1), arrhythmogenic right ventricular dysplasia (ARVD), catecholaminergic polymorphic ventricular tachycardia (CPVT), both caused by RyR2 (Lanner et al. 2010), and RyR2 is implicated in muscle pathologies such as skeletal muscle fatigue and cardiac arrhythmias (SE Lehnart 2008; Durham et al. 2008; Bellinger et al. 2009; Bellinger et al. 2008). The brain is also affected by Alzheimer's disease, with RyRs (1, 2 and 3) playing a key role in learning and memory performances (Oulès et al. 2012). Hence, focussing on RyR can improve the further understanding of channelopathies and RyR-mediated Ca^{2+} homeostasis can be used as a target for new therapeutic approaches.

1.3.2. SERCA the major Ca^{2+} uptake pump of the SR

The Sarco-Endoplasmic Reticulum Calcium ATPase (SERCA) replenishes the SR by actively removing Ca^{2+} from the cytoplasm and is thereby the main controller in regulating cytosolic Ca^{2+} concentration and homeostasis (Wu et al. 1995). In contrast to RyR, SERCAs are essential for the relaxation of the myocytes after contraction by ensuring a rapid re-sequestration of Ca^{2+} ions into the SR (Zwaal et al. 2001). In the invertebrate nematode *C. elegans*, SERCA and its isoforms a, b and c (K11D9.2a; b; c), are encoded by the gene *sca-1* on chromosome III (The *C. elegans* Sequencing Consortium 1998; Kishore and Arnaboldi 2021). Invertebrate and mammalian SERCAs share a high homology (70% identity, 80% similarity) (Hoon Cho et al. 2000). Additionally, the ATP binding domains share 59% amino acid identity, the anchor domain 67% and the phosphorylation domains share 81% AA identity. The putative cytosolic interaction site for phospholamban (PLB), as it can be found in vertebrate SERCA1 and SERCA2, is absent in *C. elegans* SERCA (CeSERCA) and other invertebrate SERCAs (Verboomen et al. 1992; Young et al. 1989). Typically, only one SERCA gene, which is orthologous to the vertebrate SERCA2, can be found in invertebrates (Vandecaetsbeek et al. 2011). The ATP-binding regions of the SERCA pumps are localised on the cytoplasmic face of the ER, in the nuclear outer membrane-endoplasmic reticulum membrane network and the nuclear envelope (Wu and Bers 2006). They can likely be found in all cell types and are particularly important in neuronal cells, body wall muscles, pharyngeal and vulval muscles and excretory cells (Zwaal et al. 2001). Human orthologs of this gene are implicated in diseases like the Brody myopathy (Voermans et al. 2012), Morbus Darier (Hovnanian 2007) and cardiac arrythmias (Erkasap 2007). SERCA is also associated with neuropathological conditions, such as

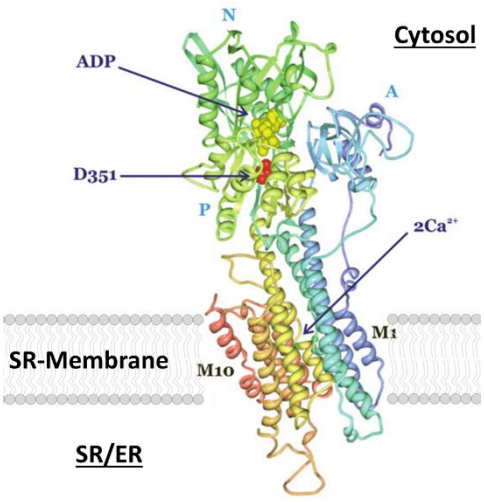

Figure 16: Crystal structure of SERCA localised in the SR-membrane. the ADP-and Ca^{2+}-bound state is shown. D351 (in red) is the residue phosphorylated during the movement of Ca^{2+} ions into the ER or SR. The three cytoplasmic domains, phosphorylation (P), nucleotide binding (N) and actuator (A) are labelled. ADP is shown in yellow and Ca^{2+} ions in green. Modified and adapted from (Watson 2015).

schizophrenia, bipolar disorder, Parkinson's disease and like RyR, also in Alzheimer's disease (Britzolaki et al. 2020; Green et al. 2008a; Dahl 2017).

When undergoing a catalytic cycle, SERCA uses ATP hydrolysis as energy source to transport 2 Ca^{2+} ions from the cytosol into the SR lumen. In turn, 2 protons are exported from the SR lumen to the cytosol (Yu et al. 1993; Zafar et al. 2008). During this cycle, SERCA operates in a high- Ca^{2+} affinity state (E1) or a low- Ca^{2+} affinity state (E2), the two main structural states *(Figure 17*). The E1 state starts the catalytic cycle in which the transmembrane transport sites are exposed to the cytosol. During E1, one ATP is bound into the nucleotide-binding domain and two Ca^{2+} ions are bound from the cytosol transmembrane into the transport sites. The coupling of ATP hydrolysis and Ca^{2+} transport is facilitated by the ATP-bound E1-Ca^{2+} complex, which induces a structural rearrangement of the pump. Formation of the E1-P-ADP-2 Ca^{2+} SERCA intermediate, is facilitated by ATP hydrolysis (Toyoshima and Mizutani 2004). In the catalytic cycle, this step induces a structural transition to the phosphorylated E2P-2 Ca^{2+} state. Dissociation and release of 2 Ca^{2+} ions from the SERCA into the SR/ER lumen is induced by the E2P-2 Ca^{2+} state due to its low Ca^{2+} affinity. The release of Ca^{2+} ions from SERCA results in the diffusion of two luminal protons into the transport sites, stabilising the phosphorylated, low-Ca^{2+} affinity E2-P state (Hauser and Barth 2007; Toyoshima and Cornelius 2013; Musgaard et al. 2011; Obara et al. 2005). To occupy the apo E2 state of the pump (Toyoshima 2009; Bublitz et al. 2010; Toyoshima and Mizutani 2004), dephosphorylation of SERCA follows (Toyoshima and Nomura 2002; Olesen et al. 2004), after which two protons are spontaneously released into the cytosol from the transport sites (Inesi et al. 2008; Andersson et al. 2008; Hauser and Barth 2007). The structural transition from E2 to E1, which is required to adopt the E1 state for the next Ca^{2+} pump cycle, is thus accelerated (Toyoshima 2009; Bublitz et al. 2010).

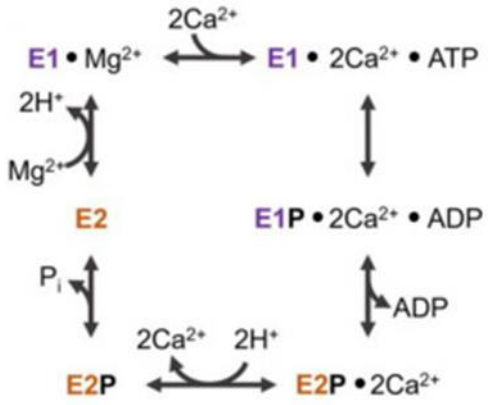

Figure 17: Schematic representation of the Post-Albers pumping cycle of SERCA. Adapted from (Aguayo-Ortiz and Espinoza-Fonseca 2020)

Control of the full intracellular Ca^{2+} cycle, involving the release and reuptake of Ca^{2+} ions from the SR, is the final goal of this project. To achieve this, it is necessary to control the ryanodine receptor and the associated Ca^{2+} ion release from the SR. Conversely, it is also essential to control the reuptake of Ca^{2+} into the SR by the SERCA.

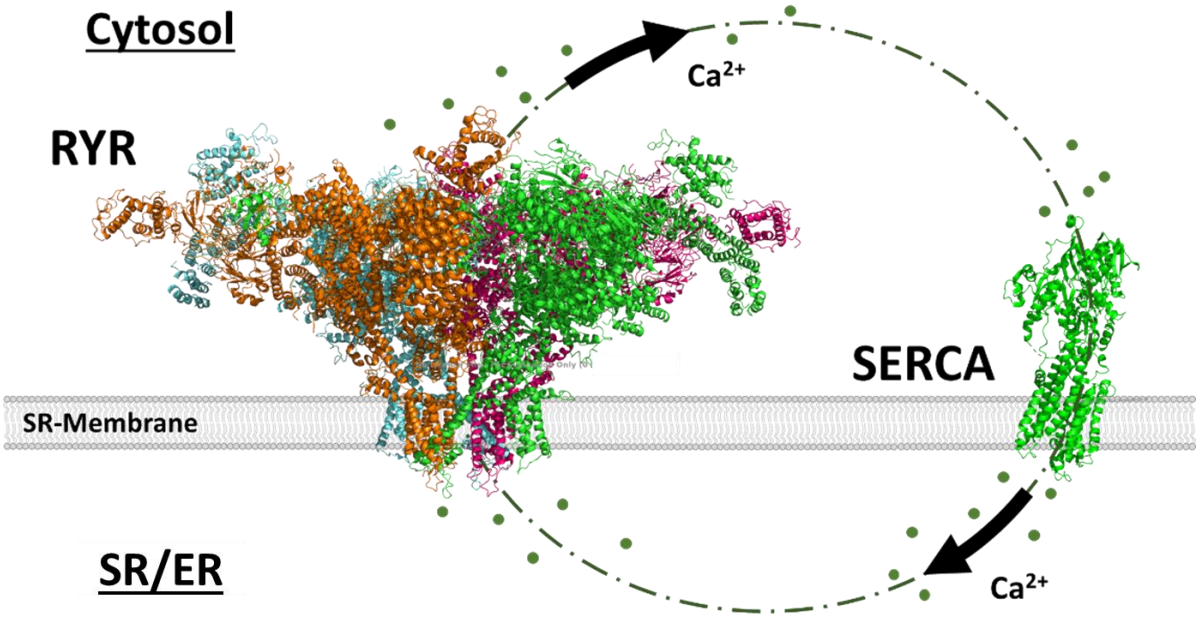

Figure 18: Full intracellular Ca^{2+} cycle between SR/ER and cytosol. To control the full cycle of Ca^{2+} efflux and influx from the SR, it is critical to control both the RyR and the SERCA. RyR: ryanodine receptor, SERCA: sarco/endoplasmic reticulum Ca^{2+}-ATPase, SR: sarcoplasmic reticulum.

Why not include the excitable neuronal cells in the SR manipulation? Similar to muscle cells, neuronal cells are also excitable, containing an SR of which the Ca^{2+} flux could be controlled. Here, however, the focus is on the muscle cells, as their mammalian pendant, in particular the heart, can also operate without neurological stimulation (Moorman et al. 1997). The focus of this work is not on neurons, as they are already the subject of plenty of other research. However, it should be noted that the use of CRISPR affects all cells that express RyR and SERCA, including neurons. It must be expected that any effect that occurs during the behavioural assays may also be partially due to neuronal effects. If such effects are observed, they would have to be investigated in subsequent research. Human muscles, especially the heart, are affected by a variety of diseases that need to be investigated, for which special tools are required. *C. elegans* will serve as a model organism for this purpose, allowing the development of such novel tools more straightforwardly than vertebrate models.

1.4. Optogenetic tools

Since its beginnings in 2005, optogenetics provided a plethora of tools that enable largely non-invasive control of cellular processes using light-senstive proteins and light application. Various of these tools can be used for the objectives to be achieved in this thesis. Essentially, this work is composed of the optogenetic stimulation of intracellular Ca^{2+} release from and uptake into the sarcoplasmic reticulum, by manipulating intrinsic (the worm's innate natural ion transporters like CeRyR, ceSERCA) and extrinsic (genetically introduced hRyR2, $ChRGR_{ER}$, ChR2) ion transporters. When targeted to specific muscles or neurons, optogenetic tools, i.e. genetically encoded molecules, enable spatio-temporal control of these cells (Boyden et al. 2005; Boyden 2011). The tools used here, which were inserted using CRISPR/Cas9, are an exception. For these, it must be assumed that optical stimulation can cause reactions in the muscle cells as well as in the neurons, which could impair the precision of the spatiotemporal control.

With the discovery of the light-driven proton pump bacteriorhodopsin in haloarchaea, in the 1970s, a new field of cellular and molecular biology could evolve (Sharma et al. 2006). This finding led to the discovery of further rhodopsin paralogs in this archaeal phylum and, more importantly, to homologues in many disparate bacteria and eukaryotes. These include the green algae type 1 rhodopsins in *Chlamydomonas reinhardtii* (Sineshchekov et al. 2002; Nagel et al. 2002; Suzuki et al. 2003), the alveolate *Pyrocystis lunula* (Okamoto and Hastings 2003), the cryptomonads *Guillardia theta* and *Cryptomonas* (Sineshchekov et al. 2005) and many fungal species from Ascomycota and Basidiomycota (Brown 2004). One of the most important results was the characterization of Channelrhodopsin-2 (ChR2). The photoactivity of this light-gated ion channel, that is composed of a covalently linked dimer (Deisseroth and Hegemann 2017; Kato et al. 2012), was first observed in Human embryonic kidney (HEK) cells and in *Xenopus laevis* oocytes. It was found that heterologously expressed ChR2 causes a plasma membrane depolarization upon blue light illumination, on a millisecond timescale, as long as all-trans retinal is covalently linked (Nagel et al. 2003a).

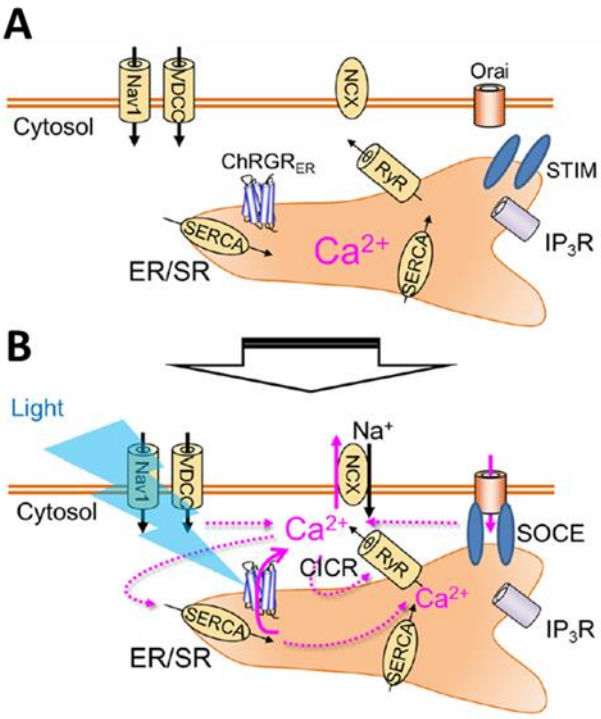

Figure 19: Optogenetics of $ChRGR_{ER}$, RyR, IP_3R and SERCA on the SR/ER-membrane. Light absorption by $ChRGR_{ER}$ induces the release of Ca^{2+} from the intracellular store, activating multiple Ca^{2+} signalling cascades, like calcium-induced calcium release (CICR) or store-operated calcium entry (SOCE). Nav1: voltage-dependent sodium channel 1 (not present in *C. elegans*); VDCC, voltage-dependent calcium channel; NCX: Na+-Ca^{2+} exchanger; RyR: ryanodine receptor; IP3R: IP3 receptor; SERCA, sarco/endoplasmic reticulum Ca^{2+}-ATPase. Figure adapted from Asano et al. 2018.

Besides *C. elegans*, optogenetic tools have been used to study behaviour in other organisms such as zebrafish *Danio rerio*, *Drosophila melanogaster*, rodents and even non-human primates (Arenkiel et al. 2007; Douglass et al. 2008; Han 2012; Zhang et al. 2007). Optogenetic tools were also assessed with a view to possible future clinical applications to restore hearing impairment, visual disorders and in the treatment of neuronal conditions such as Parkinson's disease (Bi et al. 2006; Gradinaru et al. 2009; Shimano et al. 2013).

The advent of optogenetics through the characterisation of the two genes channelrhodopsin-1 (ChR1) and ChR2 in *Chlamydomonas reinhardtii* (Nagel et al. 2002; Nagel et al. 2003b; Sineshchekov et al. 2002; Suzuki et al. 2003), was followed by the first in vivo application in body wall muscle (BWM) cells and mechanosensory neurons of *C. elegans* (Nagel et al. 2005).
Possible applications in this work include the use of intrinsic Ca^{2+} balance maintaining ion transporters such as the ryanodine receptor or SERCA and the transformation of these by integrating the LOV2 domain or a ChR variant to generate photosensitive tools. Furthermore, ion channels such as hRyR, which are similar to the intrinsic *C. elegans* channels or parts thereof, such as the TM helices, can be coupled with ChRs or LOV2.

1.4.1. Manipulation of Ca^{2+} dynamics in the SR/ER by opsin-based tools

Opsin based tools in optogenetics are predominantly derived from the microbial photoreceptor proteins of the type-I rhodopsins. The most commonly used light-gated ion channels belong to the Channelrhodopsin family. Besides the ion channels of the microbial photoreceptors, the ion pumps are mainly comprised of archaeal rhodopsins, bacteriorhodopsins and halorhodopsins (Sharma et al. 2006). Type I rhodopsins are highly conserved and all of them share seven transmembrane helices, of which the 7th TM helix (at a conserved lysine) is covalently linked to retinal. The rhodopsins type-I and type-II of microbial and animal origin, share the seven-transmembrane protein structure, yet they have no detectable sequence homologies (Nagel et al.2003). ChR2 and its derivatives used in this work are part of this family and require the co-factor all-trans-retinal (ATR) for photosensitivity (Nagel et al. 2003b). The structural change of the chromophore is triggered by isomerisation upon photon absorption. In microbial opsins, this structural change leads to conduction of ions and a change in membrane potential. ATR is naturally generated by vertebrate cells themselves and is present in sufficient quantities to maintain opsin function. Invertebrates, including *C. elegans,* lack endogenous ATR. To ensure the function of ChR, this can be provided to the organism by simple supplementation of the bacterial diet (Nagel et al. 2005). Invertebrates and vertebrates naturally utilise the animal type II rhodopsins, where these light-activated proteins function as GPCRs that initiate signal cascades, regulating plasma membrane de- or hyperpolarization, or intracellular signalling pathways that do not affect membrane potential (Zuker 1996; Hardie and Raghu 2001). Of these opsins, the 11-cis-retinal isomer is used for photon absorption.

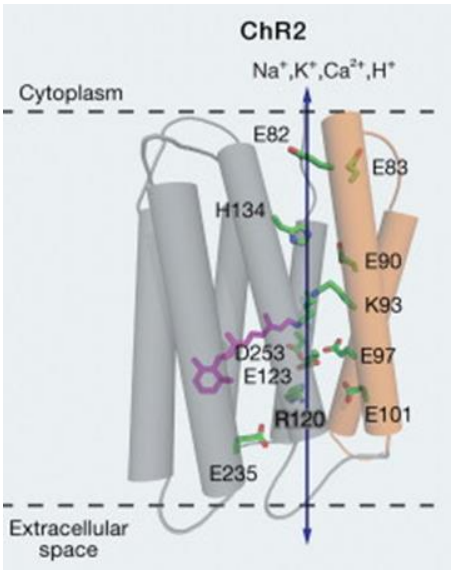

Figure 20: Structure of ChR displaying the 7-TM helices. The sequence of the illustrated residues may create a polar environment for water molecules and cation permeation. (Zhang et al. 2011)

However, the cellular reaction occurs with slower kinetics compared to type-I opsins (Zhang et al. 2011). As a light sensitive channel, photo-activated ChRs can depolarise the plasma membrane by conducting a flux of cations. These comprise monovalent ions such as H^+, Na^+ and K^+, as well as divalent Ca^{2+} and Mg^{2+} ions (Nagel et al. 2002; Nagel et al. 2003a).

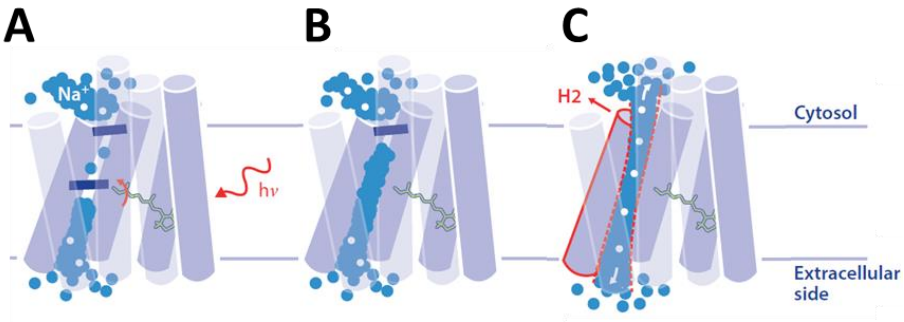

Figure 21: Light induced ChR2 pore formation. A) Retinal isomerisation upon photon absorption. B) Disruption of hydrogen bond and deprotonation opens the inner gate. C) H_2 moves outward and a disconnection of hydrogen bonds at the inner gate leads to pore formation. Blue spheres: water molecules, white spheres: Na^+ ions, dark blue bars: closed gates in the protein. Adapted from (Schneider et al. 2015)

The photocycle of ChR2 involves six excited states, including the intermediates identified by infrared difference spectroscopy and UV/VIS spectroscopy. Starting with the dark state D470, a protonated Schiff base is converted into the early intermediate P500, upon light-induced isomerisation of the retinal. A transient Schiff base deprotonation triggered by thermal relaxation leads to P390 after 25µs. Subsequent reprotonation of the protein creates the conductive state P520 after 1.5ms, whereby P390 and P520 are in a pH-dependent equilibrium. The dark state is restored via P480a and P480b, which are also in a pH-dependent equilibrium. Changes in the hydrogen bonding of Glu90, determine the structure and decay of these species. After 40s, a major backbone rearrangement in P480b recovers the dark state, which can optionally be restored by green light absorption of P520 (green arrow *Figure 22*). A shortcut of the photocycle can be caused by the conversion of the photoreactive P480b through blue light absorption. In this case, the dark state is skipped (blue arrow) and the early P500 intermediate is formed (Ritter et al. 2008).

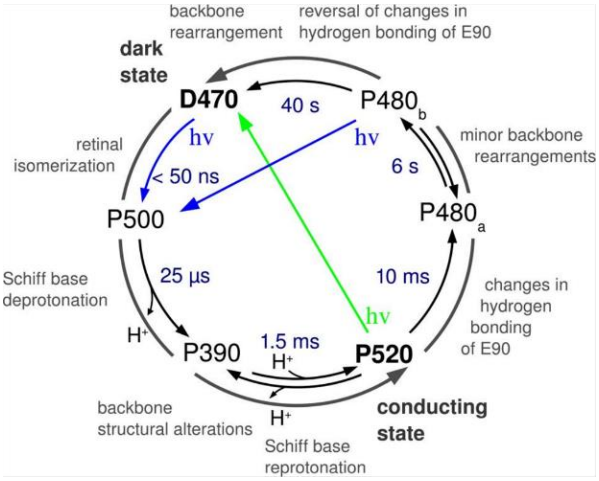

Figure 22: Photocycle model of ChR2. τ values (blue) of WT are indicated for pH 6. Blue light activates the cycle and can accelerate the photocycle. Absorption of green light can lead to faster channel closing. Adapted from (Ritter et al. 2008).

1.4.1.1. Enhancement of the expression of ChR and prolongation of its open state lifetime by the "XXM" mutation (ChR2(D156H))

Next to the intrinsic channels/receptors RyR, SERCA and IP_3R, other variants of ChR were promising candidates to take a further step towards managing a direct stimulation of cation release from the SR/ER by light. One of these is ChR2-XXM (XXM), the ChR2 D156H mutant, a recently optimised ChR version, for extra high expression and medium long open state, created by Scholz et al. The use of this ChR variant was an attempt to explore if this variant of the light sensitive cation conducting channel is significantly conductive for Ca^{2+}, and if its opening in the SR membrane thereby induces a local Ca^{2+} spark that would activate the RyR. Different approaches could be taken to achieve this. One was to start using a ChR variant, test if it works in *C. elegans* by conducting enough Ca^{2+} to maybe induce a RyR opening and whether it can be restricted to the SR membrane. Otherwise implementation of this channel in the plasma membrane would cause other problems/conditions. Furthermore, it has been demonstrated that expression of ChRs in muscle under a myo-3 promoter leads to a depolarisation and thus to muscle contraction, but without directly manipulating the Ca^{2+} flux of the SR/ER (Bruegmann et al. 2015; Nagel et al. 2005). Advantages of the XXM compared to ChR2 are as the name indicates an extra high expression and medium open state (Scholz et al. 2017). Moreover it exhibits a two-fold increased K^+ selectivity over H^+ together with a four-fold increased Na^+ selectivity over H^+. Most important is a four times higher Ca^{2+} permeability compared to wild-type ChR2 (Duan et al. 2019). In addition, the mutation of the conserved aspartate of TM helix 4 had an impact on the expression, kinetics and photocurrents (*Figure 23*). These were characterised by ~30-fold increased steady-state photocurrents, compared to ChR2. This might be a result of the increased single channel conductance, higher plasma membrane expression or a higher light-sensitivity, that was caused by a much-prolonged closing kinetic of the channel (Duan et al. 2019).

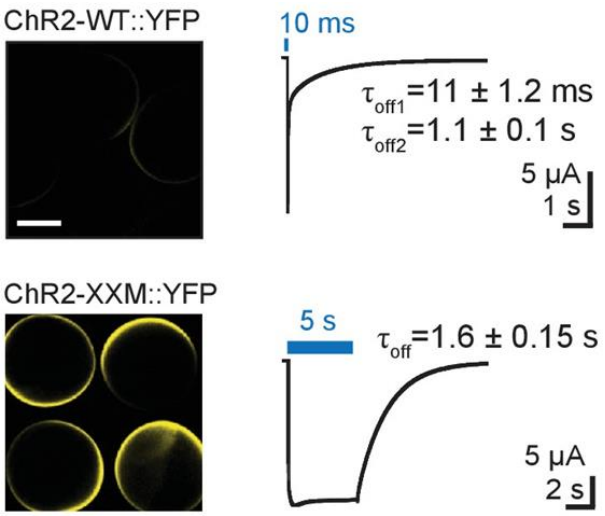

Figure 23: Expression of ChR2-WT::YFP and ChR2-XXM::YFP in Xenopus oocytes and photocurrents. Right side: 10ms exposure: rapid biphasic photocurrent decay. 5s photostimulation: the longer time constant τoff dominates. Adapted from (Scholz et al. 2017)

Other ChR variants have been unable to induce sufficient Ca^{2+} efflux from the SR to provoke muscle contraction due to the low Ca^{2+} conductance of the protein. Retention of the SR is crucial here but not an easy task (Damijonaitis 2011), and an improved ChR could help to master this challenge.

1.4.1.2. The chimera ChRGR$_{ER}$-the channelrhodopsin green receiver on the ER

Another candidate is an artificially engineered chimera named ChRGR ("channelrhodopsin-green receiver")(Asano et al. 2015). ChRGR was built for this purpose on the basis that ChR1 generates a photocurrent that has several advantages over ChR2, e.g. rapid ON and OFF kinetics and small desensitisation (Nagel et al. 2002; Nagel et al. 2003a; Hegemann et al. 2005; Ishizuka et al. 2006; Wang et al. 2009). On the other hand, the retarded membrane expression and other unresolved reasons cause a small amplitude (Wang et al. 2009). To overcome these problems, the sixth TM helix domain was exchanged for its counterpart in ChR2. By that, ChRGR exhibits smaller desensitization and faster ON and OFF kinetics, both being smaller and faster than in ChR1 and ChR2, respectively (Wen et al. 2010). Furthermore, to manipulate the Ca^{2+} release from intracellular Ca^{2+} stores with high spatiotemporal precision, ChRGR was specifically targeted to the SR/ER. It was therefore equipped with an ER-retention motif of the mouse RyR2 (NM_023868), encoded in the cDNA sequence of Gln4765-Ile4866. By that the ER restricted channel rhodopsin green receiver ChRGR$_{ER}$ was created (Asano et al. 2018). Under an illumination of 450-475nm the light triggered ChRGR$_{ER}$, which has a higher Ca^{2+} conductivity than ChR1 or ChR2. It should also be able to release the necessary amount of Ca^{2+} ions from the SR into the cytosol to induce the opening of RyR and thus CICR.

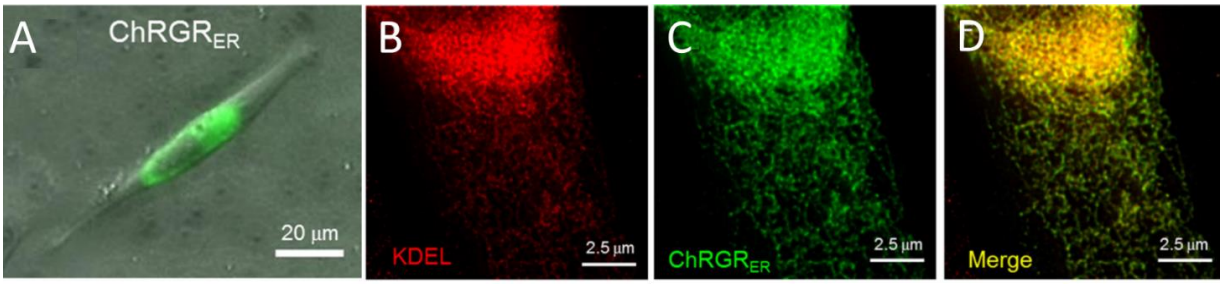

Figure 24: Cellular expression of ChRGR$_{ER}$. A) Image of Venus fluorescence in a C2C12 cell expressing ChRGR$_{ER}$. B) Immunostaining of ER-marker KDEL (red). C) C2C12 immunostained for Venus (green), in ChRGR$_{ER}$ expressing C1C12. D) Merged image of super-resolution microscopy (STED) B) and C). Image adapted from (Asano et al. 2018).

This chimera, bearing an integrated ER-retention motif, will be used as a ready-made tool to manipulate the Ca^{2+} efflux from the SR. What remains to be tested and verified here is whether a mouse SR retention sequence also functions in the nematode *C. elegans* and can completely retain ChRGR$_{ER}$ in the SR. The decisive factor here is, if incorporation into the plasma membrane is prevented, which could superimpose a direct manipulation of the SR Ca^{2+} flux.

1.4.1.4. PsChR a promising candidate for a light induced Ca^{2+} flux on the SR

The channelrhodopsin variant "PsChR" built from the phototaxis receptor of the algae *Platymonas (Tetraselmis) subcordiformis* is a 7 TM domain channelrhodopsin with its maximum sensitivity at 445nm and it is one of the most blue-shifted ChRs. It exhibits a ~3-fold higher unitary conductance, greater relative permeability to Na^+ ions and faster recovery from excitation. With all these advantages combined, compared to CrChR2, PsChR is a potentially useful optogenetical tool, to approach a light-controlled Ca^{2+} flux from the SR (Sineshchekov et al. 2013; Govorunova et al. 2013). Some adaptations, together with its increased conductivity even at low expression, made it an ideal candidate for this project.

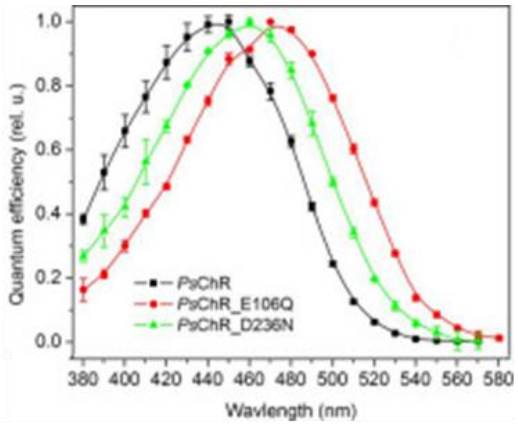

Figure 25: Spectra of channel currents generated by PsChR (wild-type and mutants) at pH 7.4. X-axis: Wavelength (nm), Y-axis: Quantum efficiency (rel. u.). Adapted and modified from (Govorunova et al. 2013).

1.4.1.5. Inositol 1,4,5-trisphosphate receptor (IP_3R receptor)

In almost every cell type in the body, at least one or more of the three different Inositol (1,4,5)-Trisphosphate Receptors (IP_3R) are expressed. IP_3Rs are Ca^{2+} channels that release Ca^{2+} from the ER in response to a variety of neurotransmitters, growth factors and hormones (Berridge 2009; Mikoshiba 2007). Both, RyR and IP_3R are part of the major family of intracellular Ca^{2+} channels and both are mainly, but not exclusively, expressed in the ER or SR (Taylor et al. 1999; Dellis et al. 2006). Several basic biological processes being activated or regulated by Ca^{2+} signalling necessitate IP_3R function, including gene transcription (Lewis 2001), fertilization (Malcuit et al. 2006), secretion (Petersen and Tepikin 2008) and, most interestingly, smooth muscle contraction (Sanderson et al. 2008). Structurally, IP_3R and RyR exist as homo tetrameric assembly of subunits (Xiao et al. 2002; Taylor et al. 1999). Studies showed that the membrane-bound C-terminal domain of the IP_3R leads to ER retention of fusion proteins (Sayers et al. 1997), they also revealed that this function can be attributed to the first two TMDs (transmembrane domains) of the receptor (Parker et al. 2004; Pantazaka and Taylor 2009; Meur et al. 2007). This led to the approach of using the transmembrane helices (TMH) TMH I and TMH II of the receptor as SR retention signal.

1.4.1.6. The Ryanodine receptor as light triggered tool

Utilizing the Ryanodine receptor to manipulate the Ca^{2+} dynamics of the SR coincides in many aspects with the interconnection of DHPR and RyR in vertebrates. Since RyR2 does not carry a low-affinity Ca^{2+} binding site, compared to RyR1, which would argue for a relation to UNC-68 (Fischer et al. 2017), the hypothesized structure of DHPR-RyR would be coclustered into punctate foci as observed by GFP-tagging (Grabner et al. 1998) or immunolabeling (Flucher et al. 1994; Jorgensen et al. 1989), as seen in *Figure 26*.

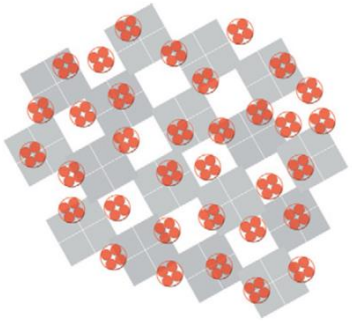

Figure 26: Clusters of DHPR-RyR in cardiac muscle membranes. cDHPRs are marked in red, RyR2 in grey. The cDHPRs are arbitrarily distributed with respect to the RyR2. Adapted from Grabner and Dayal 2010.

When connecting RyR to a light activatable channel, there are two possible ways that can cause an opening of RyR. One would be CICR, the other the conformational changes of the light driven domain (LOV or ChR). For example, the DHPR-RyR interaction, in which a rapid Ca^{2} influx through the cDHPR triggers the release of Ca^{2+} from the SR by opening Ca^{2+}-sensitive RyR2 of cardiac muscles. Skeletal muscles, on the other hand, would be activated by the direct physical contact of skDHPR and RyR1, and the depolarisation-induced conformational change induces the opening of RyR1 (Grabner and Dayal 2010).

1.4.2. Light-Oxygen-Voltage-sensing Domain (LOV) introduction

Photoactivatable fusion proteins hold great potential to create photoswitches. The flavin-binding photosensor, known as light-sensitive light oxygen voltage sensing domain 2 (LOV2) of the oat plant *Avena sativa*, will be used in this work to convert the ryanodine receptor and SERCA into a photoactivatable fusion protein. To achieve this goal, LOV2 will be integrated into the ryanodine receptor, to directly manipulate the Ca^{2+} release from the SR. For this purpose, the LOV2 DNA was directly cloned into the cDNA of truncated hRyR2, and the plasmid was injected into *C. elegans*. The other option, to integrate LOV2 into the *C. elegans* intrinsic SERCA and RyR, was carried out using the CRISPR/Cas9 method.

NPH1 from *Arapidopsis thaliana*, a photoreceptor for phototropism was found to be a photoreceptor serine/threonine kinase after initial cloning and sequencing, and was renamed phototropin (Huala et al. 1997). Each NPH1 binds a flavin-mononucleotide (FMN) cofactor in each of the two N-terminal LOV domains (Christie et al. 1999). Absorption of blue light by LOV-domains regulates the autophosphorylation activity of the C-terminal serine/threonine kinase domain (Christie et al. 1998). Furthermore, phototropins regulate several aspects of plant photomorphogenesis, such as chloroplast translocation as well as leaf and stomatal opening (Briggs 2007). Genes encoding LOV domains coupled to other effector domains in addition to kinases were soon discovered in fungi (Ballario et al. 1998; Froehlich et al. 2002; Heintzen et al. 2001; Idnurm and Heitman 2005; Schwerdtfeger and Linden 2001), plants (Nelson et al. 2000; Somers et al. 2000) and stramenopilic algae (Takahashi et al. 2007). The same cysteinyl C4(a) photochemistry was also found to regulate a range of developmental phenomena and circadian processes. In bacterial genomes LOV-domains have also been detected (Crosson and Moffat 2002; Losi et al. 2002), where they regulate processes such as cell envelope physiology (Purcell et al. 2007), general stress response (Akbar et al. 2001; Avila-Pérez et al. 2006) and virulence (Swartz et al. 2007) through different signalling output domains (Briggs 2007; Crosson et al. 2003; Losi 2004).

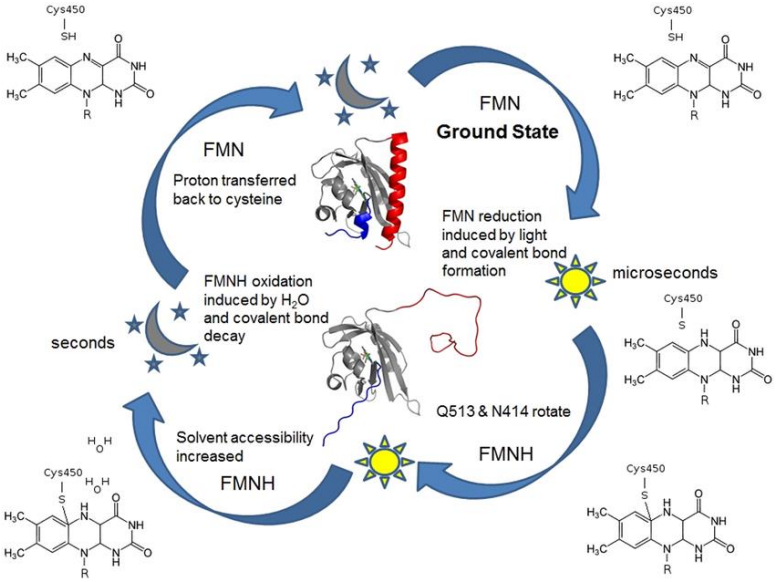

Figure 27: AsLOV2 photocycle chemistry. Photon absorption causes the FMN to be excited into a singlet and then a triplet state. The N5 of FMN becomes a strong nucleophile and takes the proton from the adjacent C450 to form a covalent bond with the FMN C4a atom. Reduction of the FMNH state is impeded by the fact that water cannot immediately enter the binding pocket of the chromophore and catalyse the retransfer of the proton to the cysteine until a conformational change involving residues N414 and Q513 occurs. The protein returns to the dark state due to the broken covalent bond. Adapted from (Zayner and Sosnick 2014)

The close proximity of the N- and C-terminal helices of approximately 10 Å was one of the important characteristics in the selection of a suitable light-sensitive protein. The biological output signal of the

LOV2 domain is generated by the FMN chromophore, which upon illumination forms a covalent bond with cysteine, thus leading to the release of the carboxy-terminal Jα-helix (Zayner et al. 2012). This energy, generated by partial unfolding upon photostimulation (Halavaty and Moffat 2007; Yao et al. 2008), could in turn introduce a steric disorder in the beta sheet, which it might transmit to the scaffold of RyR and SERCA.

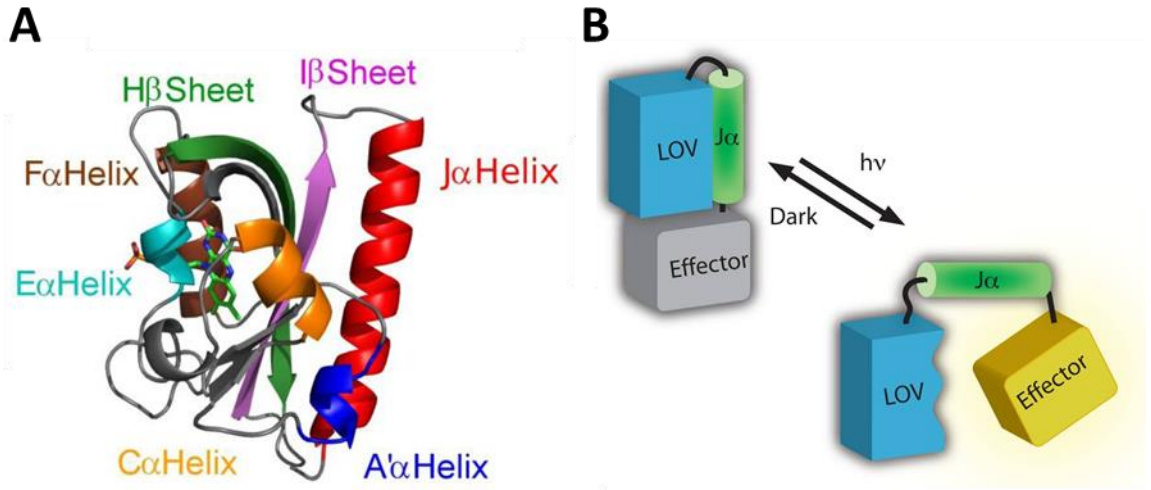

Figure 28: AsLOV2 structure and signalling. A) LOV2 structure-forming helices and beta sheets are colour-coded: A'α Helix (blue), Cα Helix (yellow), Jα Helix (red), Eα Helix (turquoise), Fα Helix (brown), Hβ Sheet (green) and Iβ Sheet (violet). FMN depicted in the centre (light green). Adapted from (Zayner et al. 2012). B) In phototropin-type signalling, cysteinyl-flavin adduct formation induces conformational change in the LOV2 domain (blue) that results in disruption of the interaction with the Jα helix (green). Illumination of a LOV domain (blue) can induce conformational changes in an extended Jα helix (green). Adapted from (Herrou and Crosson 2011).

1.4.2.1. Opto-mechanical gating of RyR by the LOV-domain

Insertion of the LOV2 domain of *A. sativa* into the human ryanodine receptor, had to be targeted to the appropriate positions to maximally affect the allosteric channel gating upon light-induced conformational changes, with minimal structural disruption of RyR. This was similar to the approach of the Hahn lab, where the LOV2 domain was inserted into loops between two β-strands (Dagliyan et al. 2016). For a light-induced conformational change of the protein, sterically accessible β-loops should support the insertion of the LOV2 domain. For this purpose, the steric tension of the N- and C-termini (Halavaty and Moffat 2007; Dagliyan et al. 2019), which are ~10Å apart from each other in the LOV2 domain, should be transferable to the β-loop to induce a conformational change in the affected protein (Bubeck et al. 2018; Dagliyan et al. 2016). Hence, the sequences that will be replaced by LOV2 in hRyR2, should not be spaced more than 10 Å, in order to pass on the disorientation of the terminal helices under irradiation. Through novel cryoEM structural analyses of the open and closed states and the consideration of a primed state of RyR1 (Des Georges et al. 2016; Peng et al. 2016), the following four positions of hRyR2 were selected:

OptoRyR$_{Pore}$(1): replaces SGKDVID sequence near high affinity Ca^{2+} binding site
OptoRyR$_{Pore}$ (2): replaces GSAKR sequence between β1 and β2 near the U-motif
OptoRyR$_{Pore}$ (3): replaces luminal TSSVVEGKELPTRSSSENAKVTSLDSSSHRIIA sequence between β-strands in the voltage sensor
OptoRyR$_{Pore}$ (4): replaces cytosolic voltage sensor domain sequence GEFYG

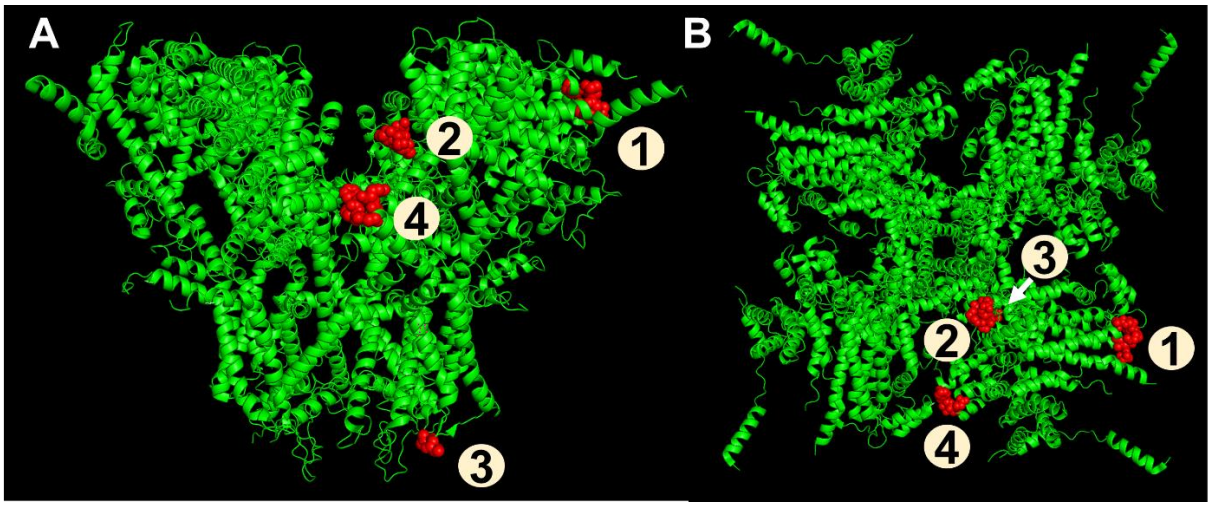

Figure 29: Insertion sites of LOV2 in hRyR2 pore. A) Top view of hRyR2pore (green) and location of LOV2 domain insertion sites 1-4 (red). B) Top view of hRyR2pore and insertion sites.

1.5. Analysis of behaviour and the use for verification of genetic manipulation

When considering using the movement behaviour of *C. elegans* to study genetic manipulations, it is important to be aware of some distinctive characteristics of the worms. In this work the behavioural analysis will cover feeding (pharyngeal pumping), contraction (change in bodylength) and swimming behaviour. Analysing the pharyngeal pumping will be done, either by counting the pumps of the isthmus in the pharynx or by using the Nemametrix system, that utilises an EPG to determine the number of pumps. Pharyngeal pumping is used, as it can be considered an optogenetic arrhythmia model (Fischer et al. 2017; Schüler et al. 2016). When the worm is suspended in a liquid, it swims with an undulating motion similar to its crawling motion on a solid substrate (A.H.J. Burr and A. Forest Robinson 2004; J. Gray and H. W. Lissmann 1964; Korta et al. 2007; Tsechpenakis et al. 2008). After transferring *C. elegans* from solid medium into liquid, continuous swimming will be observed for approximately 93min until it abruptly stops for 7s (Ghosh and Emmons 2008).
It is possible to use locomotion, in this case swimming behaviour and contraction of the whole worm, to analyse the effects of optogenetic manipulation (Gottschalk 2020). *C. elegans* will be genetically modified in muscle cells using the promoter myo-3, myo-2 or CRISPR techniques to integrate the photoactivatable tools directly to or in the SERCA and the RyR in muscle cells. Only muscle cells would express CatChUP::RyR in this case, this construct would accordingly only be incorporated into the SR membrane, as only here is RyR naturally present in the muscle. In a swimming assay, wild-type animals would thrash at a frequency of 120 body bends per min (bbpm). A transgenic strain expressing CatChUP::RyR would be stimulated by light while swimming, causing RyR channels to open and Ca^{2+} to pass from the SR into the cytosol of the cell. As soon as this happens, however, while no coordinated signal has been triggered by the nervous system, a change in swimming behaviour should occur in the form of an uncoordinated halt, slowdown, acceleration or stop. This would be revealed by analyses of swimming frequency and statistical evaluation. The same would apply to contraction assays, but here analyses would be based solely on the body length of the worm.
Feeding-induced behaviour will be considered in this thesis only in the analysis of pharyngeal pumping, and only in the sense that in some cases serotonin is used as a pump-inducing agent since it also induces pharyngeal pumping in natural feeding (Song and Avery 2012).

1.6. Objectives

Main objective of this work is the development of tools for optogenetic manipulation of intracellular Ca^{2+} release and reuptake from the SR/ER. In order to biophysically detect and accurately analyse the underlying subcellular mechanisms and implications of Ca^{2+} leakage, in a site-specific manner, it is crucial to induce an acute, spatiotemporally limited and molecularly specific Ca^{2+} leak. Optimally, this would be achieved in a non-invasive and reversible way. Such a tool to influence the SR/ER- Ca^{2+} cycle would eventually allow addressing urgent biomedical questions as well as putative disease mechanisms, i.e. to determine exactly the amount of muscle cells with ER Ca^{2+} leak, sufficient to induce significant pathologies. Hence, aim of this work is therefore to extend this toolbox with new optogenetic SR/ER-Ca^{2+} manipulation tools to contribute to basic research, especially in the field of cardiac arrhythmias and epilepsies. This comprises two different aims. First, the manipulation of Ca^{2+} release from the SR/ER. To achieve this objective, it is first necessary to have a suitable model for investigating the Ca^{2+} flux. Therefore, the ryanodine receptor will be chosen, due to its major task of releasing Ca^{2+} from the SR upon CICR. To do this, RyR has to be transformed into a light sensitive channel, that would allow to control the spatio-temporal Ca^{2+} release from the SR. For that, the light-sensitive proteins ChR and LOV2 were chosen.

On the other hand, light-sensitive ChRs will be inserted directly into the SR membrane to control Ca^{2+} efflux directly by activating these channels by light (LICR). This local Ca^{2+} spark would then induce CICR via the RyR. To accomplish this task, SR retention needs to be ensured. This is going to be attempted with sequences derived from UNC-68, transmembrane helices from IP_3R and *M. musculus* RyR retention sequences. *C. elegans* has long been a well-established model organism and genetic methods are relatively easy to apply and control. Humans are the ultimate target of this research and since hRyR cDNA is the only one available, it will be used if extrinsic ryanodine receptor is to be implemented.

The second goal is, the reuptake of Ca^{2+} from the cytosol into the SR. To control the full circle of Ca^{2+} release from and reuptake into the SR/ER, SERCA, a major player in the translocation of Ca^{2+} into the SR/ER, becomes another logical target of research. Hence, SERCA will be converted into a light-sensitive tool using the LOV2-domain from *Avena sativa* to block the uptake of Ca^{2+} ions into the SR/ER by blue light irradiation. LOV2 will be inserted at sites where maximum effect would be achieved by contact to the SERCA scaffold without compromising the structure to the point of functional impairment.

Successful transformation of *C. elegans* would then be validated by fluorescence imaging and confocal microscopy. Depending on the tool, a fluorophore would be integrated directly into the construct, or a co-marker would be injected. For swimming assays, a setup will be used that allows the screening of entire petri dishes including several hundred *C. elegans* worms. The system used for contraction, on the other hand, precisely measures the length of a single animal. Also designed for single animal measurements is the Nemametrix system, which is used for the examination of the pharyngeal pumps. Behavioural tests such as swimming and contraction assays would be performed by using data analysis software that would need to be adapted to the setup and requirements of the experiment. This software would then process the videos of the experiment to evaluate the thrashing frequency in swimming assays and the relative contraction of body length in contraction assays. The Nemametrix system works and evaluates the frequency of the pharynx pumps with its own software. With this selection of tools and methods, it should be possible to ontogenetically influence the Ca^{2+} flow into and out of the SR/ER and draw conclusions about the resulting muscular effects and behaviours.

2. Material and Methods

2.1. Materials

2.1.1. Chemical substances

Table 2.1.: Chemical substances

Substance	Manufacturer
Acetic acid	Carl Roth
Agar	AppliChem
Agarose	Invitrogen
Aldicarb	Merck
All-*trans* retinal	Merck
Ampicillin sodium salt	AppliChem
Bovine serum albumin (BSA)	New England Biolabs (NEB)
Calcium chloride	Carl Roth
Desoxy nucleotide triphosphate (dNTP)	Invitrogen
Dimethyl sulfoxide (DMSO)	Carl Roth
Dopamine hydrochloride	Merck
Ethylene-diamine-tetra-acetic acid (EDTA)	Carl Roth
Ethanol 96 %	Carl Roth
Ethanol 99 % (AR grade)	AppliChem
Ethidium bromide 5 %	Carl Roth
GeneRuler 100bp DNA Ladder	Fermentas
GeneRuler 1 kb Plus DNA Ladder	Fermentas
Halocarbon oil	Halocarbon
Histamine	Merck
Isopropanol	Carl Roth
Kanamycin	Carl Roth
Kobe Agar	Carl Roth
Magnesium chloride	Carl Roth
Magnesium sulfate	Carl Roth
Nitrogen	Linde

Nystatin	Merck
Oligonucleotides	Eurofins MWG
Phenol chloroform isoamyl alcohol (50:49:1)	Carl Roth
Potassium acetate	Carl Roth
Potassium citrate	Carl Roth
Potassium chloride	Carl Roth
Dipotassium phosphate	Carl Roth
Monopotassium phosphate	Carl Roth
Polyethylen glycol (PEG) 6000 g/mol	Carl Roth
Polystyrene beads (0.1 µm)	POLYCIENCES
Sodium acetate	Carl Roth
Sodium azide	Carl Roth
Sodium chloride	Carl Roth
Sodium hydroxide	Carl Roth
Sodium hypochlorite 12 %	Carl Roth
Disodium phosphate	Carl Roth
Streptomycin	AppliChem
Tris-(hydroxymethyl)-aminomethane (TRIS)	Carl Roth
Triton X-100	Carl Roth
Tryptone/Peptone from Casein	Carl Roth
Yeast extract	Carl Roth

2.1.2. Buffers and Media

Media and buffer components were diluted in ddH_2O, if not noted otherwise. If necessary, the pH was adjusted, and media or buffer were autoclaved.

Table 2.2.: Buffers and media

Buffer/medium	Ingredients/Supplier
8 P medium	2% (w/v) Tryptone/Peptone 0.3% (w/v) Sodium chloride 2.5% (w/v) Agar 1 mM Calcium chloride 1 mM Magnesium sulfate 25 mM Potassium phosphate buffer 0.0005% (w/v) Cholesterol (in ethanol)
Antarctic phosphatase (AP) buffer (10x)	NEB
Bleach solution	0.5 M Sodium hydroxide 3.6% (w/v) Sodium hypochlorite
Bleach solution for embryo isolation	0.5 M Sodium hydroxide 20% (v/v) Clorox
DNA loading dye, purple (6x)	2.5% Ficoll-400 10 mM EDTA 3.3 MM Tris-HCl (pH 8)
dNTP Mix	100 mM dATP 100 mM dCTP 100 mM dGTP 100 mM dTTP
Injection buffer (10x)	20% (w/v) PEG 200 mM Potassium phosphate 0.33 mM Calcium chloride 0.33 mM Magnesium sulfate
Lysogeny broth (LB) medium	0.5% (w/v) Yeast extract 1% (w/v) Tryptone/Peptone 1% Sodium chloride Optional 1.5% (w/v) Agar Optional after autoclaved: 100 µg/µL Ampicillin 200 µg/µL Streptomycin
M9 buffer	1 mM Magnesium sulfate 20 mM Monopotassium phosphate 40 mM Disodium phosphate 85 mM Sodium chloride
NEB CutSmart buffer (10x)	NEB

NEBuffer 1.1 (10x) NEBuffer 2.1 (10x) NEBuffer 3.1 (10x)	NEB NEB NEB
Nematode growth medium (NGM)	0.25% (w/v) Tryptone/Peptone 0.3% (w/v) Sodium chloride 1.7% (w/v) Agar 1 mM Calcium chloride 1 mM Magnesium sulfate 25 mM Potassium phosphate buffer 0.0005 % (w/v) Cholesterol (in ethanol) 0.001 % (w/v) Nystatin (in ethanol)
Phusion HF buffer (5x)	NEB
Potassium phosphate buffer (1 M, pH 7.5)	1 M Monopotassium phosphate 1 M Dipotassium phosphate
Single egg/worm lysis buffer (SEWLB)	2.5 mM Magnesium chloride 10 mM Tris-HCl (pH 8.3) 50 mM Potassium chloride 0.05% (w/v) Gelatin 0.45% (v/v) Tween-20
S buffer (pH 6)	6.5 mM Monopotassium phosphate 43.5 mM Dipotassium phosphate 100 mM Sodium chloride
T4 DNA ligase buffer (10x)	NEB
ThermoPol buffer (10x)	NEB
TRIS acetate EDTA (TAE) buffer (50x, pH 8.5)	40 mM TRIS/Acetic acid 2 mM EDTA

2.1.3. Enzymes

All used restriction enzymes were obtained from Thermo Fisher or NEB and applied according to the manufacturer's protocol and recommendation.

Table 2.3.: Enzymes

Enzyme	Supplier
Antarctic phosphatase	NEB
Phusion DNA Polymerase	NEB
Proteinase K	Thermo Fisher Scientific
Restriction enzymes	NEB
Shrimp Alkaline Phosphatase	NEB
T4 DNA Ligase	NEB
Taq DNA Polymerase	NEB

Enzymes used during this work are: AarI, AatII, AccI, AciI, AfeI, AflII, AgeI, AhdI, ApaI, AscI, AvaI, AvaII, AvrII, BamHI, BccI, BciVI, BclI, BfaI, BglI, BmgBI, BmtI, BpmI, Bpu1102I, BsaAI, BsaBI, BsaI, BseRI, BsgI, BsiWI, BslI, BsmI, Bsp1286I, BspEI, BspHI, BspMI, BssHII, Bst1107I, BstBI, BstXI, BstZ17I, Bsu36I, DdeI, DpnI, DraI, DraIII, EagI, EcoNI, EcoRI, EcoRV, FatI, HincII, HindIII, HpaI, KasI, KpnI, MscI, MseI, MspI, NaeI, NarI, NgoMIV, NheI, NotI, NspI, PacI, PciI, PmeI, PmlI, PpuMI, PsiI, PspXI, PstI, RsrII, SacI, SacII, SalI, SbfI, SexAI, SfoI, SmaI, SnaBI, SpeI, SphI, SspI, XbaI, XcmI, XhoI, XmaI.

2.1.4. Kits

Kits were used and applied according to manufacturer's protocol.

Table 2.4.: Kits

Kit	Manufacturer	Application
Gel/PCR DNA Fragments Extraction Kit	Geneaid	Gel extraction
NucleoBond Xtra Midi	Macherey-Nagel	Plasmid DNA purification
ROTI®Prep PCR Purification	Carl Roth	PCR product purification
ROTI®Prep Plasmid Mini	Carl Roth	Plasmid DNA purification
NucleoBond PC 100	Macherey-Nagel	Plasmid DNA purification
NucleoSpin Plasmid Kit	Macherey-Nagel	Plasmid DNA purification
QIAquick Gel Extraction Kit	Qiagen	Gel extraction
QIAquick PCR Purification Kit	Qiagen	PCR product purification
TOPO® TA Cloning® Kit	Thermo Fisher	DNA-cloning

2.1.5. Equipment and devices

Table 2.5.: Equipment and devices

Name	Type	Supplier
Autoclave	Line FVS 5075 ELVC	Fedgari Tuttnauer
Bunsen burner	Tipe 1010	Usebeck
Cameras	AxioCam MRm DC290 Zoom CCD EOS 500D EOS 750D Falcon 4M30, 4 MP ORCA-Flash2.8 ORCA-Flash4.0 PowerShotG9 PowerShotG10	Carl Zeiss Kodak Canon Canon DALSA Hamamatsu Hamamatsu Canon Canon
Camera lens	Rodagon Lens, 60 mm, f/4.0	Rodenstock
Centrifuges	Biofuge Pico 17 Centrifuge 5810R Centrifuge 5415R Mikro 200R	Heraeus Heraeus Eppendorf Hettich
ddH_2O equipment	Milli-Q Plus	Millipore
Electrophoresis chamber	Varia 1	Carl Roth
Filter sets	F31-044 (eCFP) F37-525 (eGFP) F39-472 (ChR2) F41-007 (mCherry) F41-028 (YFP)	AHF Analysetechnik AHF Analysetechnik AHF Analysetechnik AHF Analysetechnik AHF Analysetechnik
Gel documentation system	Felix 6040	Bio Step
Heating block	Rotilabo- Block Heater H 250	Carl Roth
High Power LED	KSL 70 (470 nm) KSL 70 (590 nm) Blue 3W 30lm 10° 3.1V	Rapp Optoelectronic Rapp Optoelectronic ledxon GmbH
Incubation shaker	Ectron (37°C)	INFORS HT
Incubator	DF8528 Slim Vip (-80°C) FSK 3600 Index 20B (20°C) Vinothek (15°C)	Skadi Liebherr Liebherr
Lamps	HBO 50 Mercury-vapor HBO 100 Mercury-vapor UVT-20 M/W	Osram Osram Herolab
Magnetic stirrer	Stuart CB162	Bibby Scientific

Micromanipulator	MMJ	Märzhäuser
Micropipette puller	Modell P97	Sutter
Microscopes	Axiovert 40 CFL Axiovert Observer Z1 Axiovert 200 Axiovert 35 Phase Contrast Microscope Axio Scope.A1 Leica MZ 16F SMZ 645 Zeiss Cell Observer SD Spinning Disc Confocal microscope	Carl Zeiss Carl Zeiss Carl Zeiss Carl Zeiss Carl Zeiss Leica Nikon Carl Zeiss
Microwave oven	Generic	MikroMaxx
Optical power meter	PM100 PM100A S120UV S130A	Thor Labs Thor Labs Thor Labs Thor Labs
pH meter	Cyberscan pH 510	Eutech
Photometer	NanoDrop ND-1000	Thermo Scientific Jenway
Pipette	0.5 µL, 1 µL, 100 µL, 1000 µL	Eppendorf
Pipette controller	Pipetus Accu	Hirschmann
Multiple dispenser	Mulitpette	Eppendorf
Power meter	PM100D	Thorlabs
Shutter	Shutter	Shutter Instrument Company
Shutter control system	Lambda SC	Shutter Instrument Company
Stereo microscope	SMZ 645	Nikon
Thermal cycler	MyCycler Personal Thermal Cycler	Bio-Rad
UV lightbox	BioView	BioView
UV transilluminator	Sunshine instruments	Sunshine instruments
Vortex shaker	Vortex Genie 2	Scientific Industries
Weighing machine	Analysewaage 770	Kern

2.1.6. Consumables

Table 2.6.: Consumables

Description	Type	Manufacturer
Centrifuge tube	15 mL and 50 mL	Greiner Bio-One
Cover slip	Squared cover slip 22x22 mm	Carl Roth
Disposable tips	1 µL, 100 µL, 1000 µL	Carl Roth
Glass capillary	1B 100 F-4	World Precision Instruments
Glass pipettes	5 mL, 10 mL and 25 mL	Brand
Microcentrifuge tube	200 µL Row of 8x 200 µL 1.5 mL and 2 mL	Sarstedt neoLab Carl Roth
Microcentrifuge plate	96x 200 µL	Carl Roth
Microscope slide	Microscope slide 76x26 mm	Carl Roth
Objective immersion oil	Immersol 518F	Carl Zeiss
Petri dish	60/15 mm, 100/20 mm and 150/20 mm	Greiner Bio One
Protective gloves	LABSOLUTE Latex and nitrile	Th. Geyer
Parafilm	Parafilm M	VWR

2.1.7. Plasmids

Plasmid named as pFBX were created during this work.

Table 2.7.: Plasmids

Name	Description	Source
pFB02	*pmyo-3::hRyR2 short*	This work
pFB03	*pmyo-3::mNEON:(Gly4-Ser)8::hRyR2 short*	This work
pFB04	*pmyo-3::mNEON::hRyR2 short CDL*	This work
pFB05	*pmyo-3::mNEON::hRyR2 short CDL::LOV2(1)*	This work
pFB06	*pmyo-3::mNEON::hRyR2 short CDL::LOV2(2)*	This work
pFB07	*pmyo-3::mNEON::hRyR2 short CDL::LOV2(3)*	This work
pFB08	*pmyo-3::mNEON::hRyR2 short CDL::LOV2(4)*	This work
pFB09	*pmyo-3::mNEON*	This work
pFB10	*pmyo-3::CatChUP::EYFP::CRP1::hRyR2short CDL*	This work

pFB11	*pmyo-3::ChR-XXM::mVenus*	This work
pFB12	*pmyo-3::ChR-XXM::eYFP::ITR-1 TM I+II*	This work
pFB13	*pmyo-3::ChRGR(ER)::mCherry*	This work
pFB14	*pmyo-3::mVenus*	This work
pFB15	*pmyo-3::ChRGR(ER)::mVenus*	This work
$ChRGR_{ER}$	*pCAGGS::$ChRGR_{(ER)}$::Venus*	Provided by Toshifumi Asano/Toru Ishizuka
ChR-XXM	*pGEM::ChR-XXM::eYFP*	Provided by Shiqiang Gao
PsCatch ITR-1 TM I+II	*pmyo-3::PsCatCh::eYFP::ITR-1 TM I+II*	Provided by Alexander Gottschalk/Shiqiang Gao/ Arunas Damionaitis
PsCatch UNC-68 TM5+6	*pmyo-3::PsCatCh::eYFP::UNC-68 TM5+6*	Provided by Alexander Gottschalk/Shiqiang Gao/Arunas Damionaitis
CatChUP::EYFP::CRP-1	*pCMV::CatChUP::eYFP::linkerCRP1::hRyR2*	Provided by Alexander Gottschalk/Phillip Sasse

2.1.7.1. Reducing the ryanodine receptor 2 to a minimum pore version

To assess whether a truncated hRyR2 could operate as a rescue in UNC-68 defective animals, the construct pmyo-3::hRyR2short (RyR_{pore}) was created by restriction digestion and ligation. The vector pDD96.52 and the plasmid pFB01 were cut with the enzymes XhoI and EcoRI, followed by ligation using T4 DNA ligase. The new plasmid pFB02, as seen below, was injected in *unc-68* deletion mutants and wild-type animals. The stable strain ZX2273 and ZX2274 could be generated and were tested in a swimming assay in a 96-Well plate.

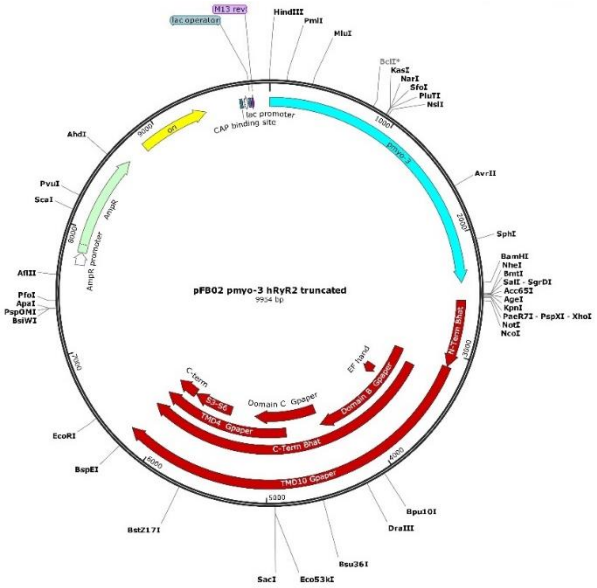

Figure 30: Plasmid map of pFB02 (pmyo3::hRyR2 short (RyR_{pore}) shows the remaining domains of the truncated version of hRyR2 . Created with SnapGene Viewer.

A modified version of RyR_{pore} was created with a longer central domain. This was done because some of the missing parts of the N-terminal domain could be required to achieve a functional or at least partially functional expression. The plasmid pmyo-3::hRyR2short CDL was created by amplifying pFB02 by PCR and inserting the restriction site NotI. Afterwards the new pFB02 was cut with Bpu10I and NotI. The long central domain was excised from pcmv::hRyR2 likewise, with Bpu10I and NotI. Fragments were ligated to the plasmid pFB04 by T4 DNA ligase.

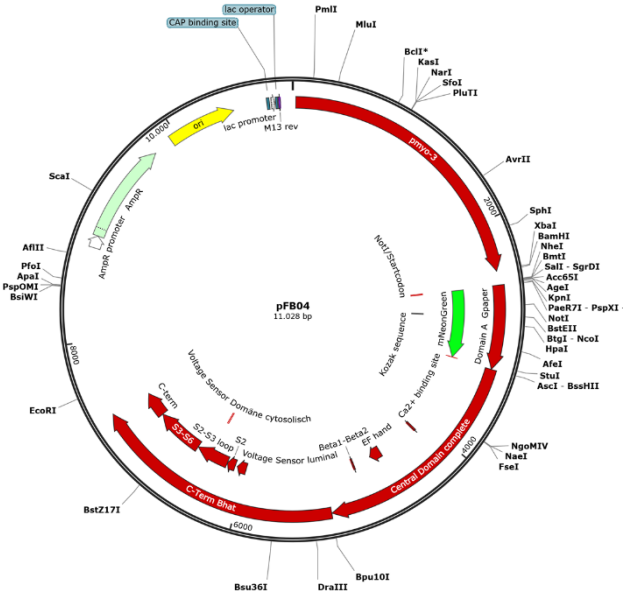

Figure 31: Plasmid map of pFB04 (pmyo3::mNEON::hRyR2 short CDL) depicts the remaining domains of RyR_{pore} with a long central domain. Created with SnapGene Viewer.

2.1.7.3. Insertion of LOV2 domains into truncated hRyR2

The basis for the integration of the LOV2 domain was the plasmid pFB04 and the plasmid mCherry-PI(WT)-Vav2(DPZ) (Dagliyan et al. 2016), that contained the LOV2 sequence L404-L546:

```
lattler ieknfvitdp rlpdnpiifa sdsflqltey sreeilgrnc rflqgpetdr atvrkirdai
dnqtevtvql inytksgkkf wnlfhlqpmr dqkgdvqyfi gvqldgtehv rdaaeregvm likktaenid
eaakel
```

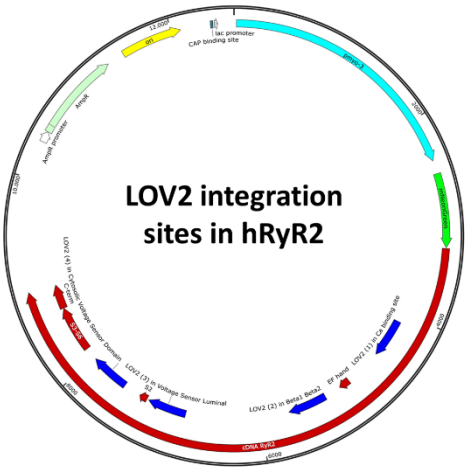

The final plasmids pFB05, pFB06, pFB07 and pFB08 (E. List of Tables) were created by PCR of LOV2 and addition of Gibson overlaps by primers. $hRyR2_{pore}$ CDL cassettes were generated comprising the long central domain of the ryanodine receptor and the LOV2 domain, including different positions (Figure 24) of LOV2(1), LOV2 (2), LOV2 (3), LOV2 (4), as described in 1.4.2.1. Opto-mechanical gating of RyR by the LOV-domainThese CDL LOV2 cassettes were integrated into pFB04 by Gibson assembly.

Figure 32: Plasmid chart of hRyR2 cDNA, including the four integration sites of the LOV2 domain marked in blue.

2.1.8. Oligonucleotides

Oligonucleotides created during this work were named oFBX. All oligonucleotides were ordered at Eurofins or Microsynth Seqlab.

Table 2.8.: Oligonucleotides

Name	Sequence	Description
oFB1	CAGGAGATGCTGGCTAACAC	*pcmv::hRyR2* sequencing, forward
oFB5	ACACTCTCCGACAGGGAAG	*pcmv::hRyR2* amplification, nested, forward
oFB6	GAGCAGAGGAGCAGCTATC	*pcmv::hRyR2* amplification, nested, reverse
oFB7	GGCCGCTCTAGAACTAGTGG	*pmyo-3::hRyR2 short* sequencing, forward
oFB8	CTGCAGAAGGATATGGTGGTC	*pmyo-3::hRyR2 short* sequencing, forward
oFB9	CTCAGATCTCGGAGTCGGAC	*pmyo-3::hRyR2 short* sequencing, forward
oFB10	AAAGCCGAGGGAGAAGATGG	*pmyo-3::hRyR2 short* sequencing, forward
oFB11	GGCAGCTCTGGACTTCAGTG	*pmyo-3::hRyR2 short* sequencing, forward
oFB12	TAGAGGTGATTGGGTCTGAG	*pmyo-3::hRyR2 short* sequencing, reverse
oFB13	ATGTCCGGACCAGCGACACATG	*pmyo-3::mNEON* amplification, forward
oFB14	CACCTCGTTCTCGTAGCAGAACACG	*pmyo-3::mNEON* amplification, reverse
oFB15	ATTTAGCTGGTCTTCATACTGTTTCC	*pmyo-3::hRyR2 short* amplification, reverse
oFB16	TAAACTCAGACCCAATCACCTC	*pmyo-3::hRyR2 short* amplification, forward
oFB17	AGTATGAAGACCAGCTAAATGCGCGCGGAGGTGGAGGGAGTGGC	*pmyo-3::hRyR2 short* sequencing, gibson overlap, forward
oFB18	AGCGGGGGAGGAGGGTCATACGTAATGTCCGGACCAGCGACACA	*pmyo-3::hRyR2 short* sequencing, gibson overlap, reverse
oFB19	AGTCACGTTTCCACCCTCTTC	*unc-68(r1162)* genotyping, forward
oFB20	ACTGCGGCTTCAGCTATTCAC	*unc-68(r1162)* genotyping, forward
oFB21	TGAGTTGCAAGAACCGGAACAG	*unc-68(r1162)* genotyping, reverse
oFB22	AGTATGAAGACCAGCTAAATGCGCGCGGAGGTGGAGGTTCAGGTG	*pmyo-3::hRyR2 short* amplification, gibson overlap, forward
oFB23	GTGTCGCTGGTCCGGACATTACGTATGATCCTCCACCTCCAGATCC	*pmyo-3::hRyR2 short* amplification, gibson overlap, reverse
oFB24	CACCTGAACCTCCACCTCCGCGCGCATTTAGCTGGTCTTCATACTG	*pmyo-3::hRyR2 short* amplification, gibson overlap, forward
oFB25	GGATCTGGAGGTGGAGGATCATACGTAATGTCCGGACCAGCGACAC	*pmyo-3::hRyR2 short* amplification, gibson overlap, reverse
oFB26	GCTACGAGAACGAGGTGTAATGATAAACTCAGACCCAATCACCTC	*pmyo-3::hRyR2 short* amplification, gibson overlap, forward
oFB27	GAGGTGATTGGGTCTGAGTTTATCATTACACCTCGTTCTCGTAGC	*pmyo-3::hRyR2 short* amplification, gibson overlap, reverse
oFB28	CCCAGTACATCATCGGGAATGACTTTGC	*unc-68(r1162)* genotyping, forward
oFB29	CCATGTGTCCGTCCATTTCAGATCACTC	*unc-68(r1162)* genotyping, reverse
oFB30	CATATACTCCGTCCGTCTCCCACGTTGG	*unc-68(r1162)* genotyping, reverse
oFB31	AAGCTTGGGCTGCAGGTCGGCTATAATAAGTTC	*pmyo-3::hRyR2 short* amplification, forward
oFB32	TAGCTGGTCTTCATACTGTTTCCGGAAGCAATCCC	*pmyo-3::hRyR2 short* amplification, reverse
oFB33	CGCTAACAACTTGGAAATGAAATAAGCTTGGGCTGCAGGTCGGC	*pmyo-3::hRyR2 short* amplification, gibson overlap, forward

oFB34	GCCGACCTGCAGCCCAAGCTTATTTCATTTCCAAGTTGTTAGCG	*pmyo-3::hRyR2 short* amplification, gibson overlap, reverse
oFB35	ATTTCATTTCCAAGTTGTTAGCG	*pDD96.52* linearize, reverse
oFB36	CACCTGAACCTCCACCTCCGCGCGCATTTAGCTGGTCTTCATACTGTTTCCGGAAGCAATCCCCTGCTGGG	*pmyo-3::hRyR2 short* amplification, gibson overlap, reverse
oFB37	CGCTAACAACTTGGAAATGAAATAAGCTTGGGCTGCAGGTCGGCTATAATAAGTTCTTGAATAAAATAATTTTCCCG	*pmyo-3::hRyR2 short* amplification, gibson overlap, forward
oFB38	GAGGACACGCTAACTAAGATGAGGTCATCTCCAACTCG	*pmyo-3::hRyR2* short amplification, gibson overlap, reverse
oFB39	GGTCCTTGCACTGGGAATCAACAGAGTTTGGCAC	*pmyo-3::mNEON:(Gly4-Ser)8::hRyR2 short* linearise, forward
oFB40	TACGTAGTGAGCAAGGGCGAGGAGGATAACATGGCCTCTCTCCCAGCGACACATGAGTTACACATCTTTGGC	*pmyo-3::mNEON* amplification, forward
oFB41	AGAGGTGATTGGGTCTGAGTTTACCTGCAGGCTTGTACAGCTCGTCCATGCCCATCACATCGG	*pmyo-3::mNEON* amplification, reverse
oFB42	GGTTCAGGTGGAGGTGGATCTGGAGGTGGAGGATCATACGTAGTGAGCAAGGGCGAGGAGGATAACATGG	*pmyo-2::mCherry* amplification, forward
oFB43	CACTGGTCAAGAAACGTACGTACG	*punc-68::unc-68::mKate::ßHK-ATPase::ChR2(L132C,H134R,T159C)* sequencing, forward
oFB44	AATCAAGGAGGCCGACAAAGAGAC	*punc-68::unc-68::mKate::ßHK-ATPase::ChR2(L132C,H134R,T159C)* sequencing, forward
oFB45	ATGGATTATGGAGGCGCCCTGAG	*punc-68::unc-68::mKate::ßHK-ATPase::ChR2(L132C,H134R,T159C)* sequencing, forward
oFB46	CCATGTTATCCTCCTCGCCCTTGCTCACTACGTATGATCCTCCACCTCCAGATCCACCTCCACCTGAACC	*(Gly4-Ser)-linker* amplification, gibson overlap, reverse
oFB47	CCGATGTGATGGGCATGGACGAGCTGTACAAGCCTGCAGGTAAACTCAGACCCAATCACCTCT	*(Gly4-Ser)-linker* amplification, gibson overlap, forward
oFB48	TTGTACCTGAGCGCAAACAGGGCCGACCTGACCGTCAGAATG	*pcmv::hRyR2 central domain* amplification, reverse
oFB49	AATCTGGCGGCCGCATGCCAAGGCATCGGGCTGTCAATCTCTTTC	*pcmv::hRyR2 central domain* amplification, forward
oFB50	CGACGGTACCGGTCAGATATCACTCGAGCGGCCGCATGGTGAGCAAGGGCGAGGAGGATAACATG	*pmyo-3::hRyR2 short* amplification, gibson overlap, forward
oFB51	ATGTTATCCTCCTCGCCCTTGCTCACCATGCGGCCGCTCGAGTGATATCTGACCGGTACCGTCG	*pmyo-3::hRyR2 short* amplification, gibson overlap, reverse
oFB52	GATGTGATGGGCATGGACGAGCTGTACAAGGCGCGCGGAGGTGGAGGTTCAGGTGGAGGTGGATCTGG	*(Gly4-Ser)-linker* amplification, gibson overlap, forward

oFB53	TCCAGATCCACCTCCACCTGAACCTCCACC TCCGCGCGCCTTGTACAGCTCGTCCATGCC CATCACATC	*(Gly4-Ser)-linker* amplification, gibson overlap, reverse
oFB54	AGGTGGAGGTGGATCTGGAGGTGGAGGA TCATACGTACCAAGGCATCGGGCTGTCAAT CTCTTTCTTC	*(Gly4-Ser)-linker* amplification, gibson overlap, forward
oFB55	TGAAGAAAGAGATTGACAGCCCGATGCCT TGGTACGTATGATCCTCCACCTCCAGATCC ACCTCCACC	*(Gly4-Ser)-linker* amplification, gibson overlap, reverse
oFB56	AGGACTTCAGGCAGAAAGTG	*mCherry-PI(WT)-Vav2(DPZ)* sequencing, reverse
oFB57	TCGCGTCCGATAGTTTCTTG	*mCherry-PI(WT)-Vav2(DPZ)* sequencing, forward
oFB58	CAGGAATCAATTAGTGACTTTTATTGGTAT TACTTGGCTACTACACTTGAACGTATTGAG AAGAAC	*mCherry-PI(WT)-Vav2(DPZ) to hRyR2 central domain* amplification, gibson overlap, forward
oFB59	TTCTTCTCAATACGTTCAAGTGTAGTAGCC AAGTAATACCAATAAAAGTCACTAATTGAT TCCTG	*mCherry-PI(WT)-Vav2(DPZ) to hRyR2 central domain* amplification, gibson overlap, reverse
oFB60	TTCAGAGCCTGGCCGGCCTGATGCAGTCA TGTAGTGTCC	*hRyR2 central domain* to *mCherry-PI(WT)-Vav2(DPZ)* amplification, gibson overlap, forward
oFB61	AATATTGATGAGGCGGCAAAAGAACTTGA ACAAGGACAACGGAATTTCTCCAAAGCTA TCC	*hRyR2 central domain* to *mCherry-PI(WT)-Vav2(DPZ)* amplification, gibson overlap, forward
oFB62	TGGATAGCTTTGGAGAAATTCCGTTGTCCT TGTTCAAGTTCTTTTGCCGCCTCATCAATAT TTTC	*hRyR2 central domain* to *mCherry-PI(WT)-Vav2(DPZ)* amplification, gibson overlap, reverse
oFB63	TCCAGCCCTTTCTGGGCCGCATCGAAATCA TGTTGGCTACTACACTTGAACGTATTGAGA AGAAC	*hRyR2 central domain* to *mCherry-PI(WT)-Vav2(DPZ)* amplification, gibson overlap, forward
oFB64	AGTTCTTCTCAATACGTTCAAGTGTAGTAG CCAACATGATTTCGATGCGGCCCAGAAAG GGCTGG	*hRyR2 central domain* to *mCherry-PI(WT)-Vav2(DPZ)* amplification, gibson overlap, reverse
oFB65	ACTGCAGAAAATATTGATGAGGCGGCAAA AGAACTTATCGAGAGGGTCTATTTTGAAAT CAGTGAGTCCAGC	*mCherry-PI(WT)-Vav2(DPZ)* to *hRyR2 short* amplification, gibson overlap, forward
oFB66	TCGGCTGGACTCACTGATTTCAAAATAGAC CCTCTCGATAAGTTCTTTTGCCGCCTCATCA ATATTTTCTGCAG	*mCherry-PI(WT)-Vav2(DPZ)* to *hRyR2 short* amplification, gibson overlap, reverse
oFB67	ATCAATTTCATCTTGCTCTTTTATAAGGTCT CCTTGGCTACTACACTTGAACGTATTGAGA AGAACTTTG	*hRyR2 central domain* to *mCherry-PI(WT)-Vav2(DPZ)* amplification, gibson overlap, forward
oFB68	ACAAAGTTCTTCTCAATACGTTCAAGTGTA GTAGCCAAGGAGACCTTATAAAAGAGCAA GATGAAATTGATAG	*hRyR2 central domain* to *mCherry-PI(WT)-Vav2(DPZ)* amplification, gibson overlap, reverse
oFB69	CTTTCGGACATCTTTGGCCTGGATCTGAAG	*hRyR2 central domain* to *mCherry-PI(WT)-Vav2(DPZ)* amplification, gibson overlap, forward
oFB70	ACTGCAGAAAATATTGATGAGGCGGCAAA AGAACTTGTTCACTATGTACTAGAGGAGA GCAGCGGCTACATG	*mCherry-PI(WT)-Vav2(DPZ)* to *hRyR2 short* amplification, gibson overlap, forward
oFB71	ATGTAGCCGCTGCTCTCCTCTAGTACATAG TGAACAAGTTCTTTTGCCGCCTCATCAATA TTTTCTGCAG	*mCherry-PI(WT)-Vav2(DPZ)* to *hRyR2 short* amplification, gibson overlap, reverse

oFB72	ACAAATTTGTTAAAAGAAAGGTTATGGATAAATATTTGGCTACTACACTTGAACGTATTGAGAAGAACTTTG	*hRyR2 central domain* to *mCherry-PI(WT)-Vav2(DPZ)* amplification, gibson overlap, forward
oFB73	ACAAAGTTCTTCTCAATACGTTCAAGTGTAGTAGCCAAATATTTATCCATAACCTTTCTTTTAACAAATTTGTC	*hRyR2 central domain* to *mCherry-PI(WT)-Vav2(DPZ)* amplification, gibson overlap, reverse
oFB74	ACTGCAGAAAATATTGATGAGGCGGCAAAAGAACTTCGAGACAGAATCAGTGAATTACTTGGCATGGACAAG	*mCherry-PI(WT)-Vav2(DPZ)* to *hRyR2 central domain* amplification, gibson overlap, forward
oFB75	TGCCTTGTCCATGCCAAGTAATTCACTGATTCTGTCTCGAAGTTCTTTTGCCGCCTCATCAATATTTTCTGCAG	*mCherry-PI(WT)-Vav2(DPZ)* to *hRyR2 central domain* amplification, gibson overlap, reverse
oFB76	AAACCCACGACCACTAGATCC	*pmyo-3::mNEON:(Gly4-Ser)8::hRyR2 short* sequencing, forward
oFB77	TGAAGAACCAGCCGATGTACG	*pmyo-3::mNEON:(Gly4-Ser)8::hRyR2 short* sequencing, forward
oFB78	GTGGGAACTCCACAGTACAG	*pmyo-3::mNEON:(Gly4-Ser)8::hRyR2 short* sequencing, reverse
oFB79	TACCGATGTGATGGGCATGGACGAGCTGTACAAGGCGCGCCCAAGGCATCGGGCTGTCAATCTCTTTCTTC	*pmyo-3::mNEON* amplification, gibson overlap, forward
oFB80	TGAAGAAAGAGATTGACAGCCCGATGCCTTGGGCGCGCCTTGTACAGCTCGTCCATGCCCATCACATCGG	*pmyo-3::mNEON* amplification, gibson overlap, reverse
oFB81	TTCGCATAAGGGTCAAGATATTGTACCTGAGCGCAAACAGGGCCGACCTGACCGTCAGAATGG	*pcmv::hRyR2* amplification, reverse
oFB82	GTTGACATTAGCGGCCGCGTAATGGTGAGCAAGGGCGAGG	*pmyo-3::mNEON* amplification, forward
oFB83	AGGGAGTGAATTCTTAGCGTCACTTGTACAGCTCGTCCATGC	*pmyo-3::mNEON* amplification, reverse
oFB84	AGGCGTTTTGCGCTGCTTCGCGATCGGAAGCTTGGGCTGCAGGTCGGCTATAATAAG	*pmyo-3* Bsp68I amplification, forward
oFB85	AGCGATGACTAATACGTAGATCTCTAGATGGATCTAGTGGTCGTGGGTTTGATGGCTCCCTGCC	*pmyo-3* Bsp68I amplification, forward
oFB86	TTGGAGGTCGCTGAGTAGTG	*pmyo-3* sequencing, forward
oFB87	CTTCGCTCCGCTGACTTTAG	*pmyo-3* sequencing, forward
oFB88	CTCACCACGCTTTACCATTG	*pmyo-3* sequencing, forward
oFB89	CCGTGAGTCAAACCGCTATC	*pmyo-3* sequencing, forward
oFB90	CCTGCTATTGTCTTCCCAATCC	*pmyo-3::CatChUP::EYFP::CRP1::hRyR2short CDL* sequencing, reverse
oFB91	TGGCATCCCTTGGTCAGATTC	*pmyo-3::CatChUP::EYFP::CRP1::hRyR2short CDL* sequencing, forward
oFB92	TTGCTGCGTGCTGGCTACTATG	*pmyo-3::CatChUP::EYFP::CRP1::hRyR2short CDL* sequencing, forward
oFB93	GATATCACTCGAGGAGCTCCCGAGATCTTCAGCGCTCAATGGATTATGGAGGCGCCCTGAGTGCCGTTGGGCGCGAGCTGCTATTTG	*pmyo-3* to *CatChUP::EYFP::CRP1::hRyR2short CDL* amplification, overlap, forward

oFB94	ATAGCAGCTCGCGCCCAACGGCACTCAGG GCGCCTCCATAATCCATTGAGCGCTGAAG ATCTCGGGAGCTCCTCGAGTGATATCTG	*pmyo-3* to *CatChUP::EYFP::CRP1::hRyR2short CDL* amplification, overlap, reverse
oFB95	GCAGGGGATTGCTTCCGGAAACAGTATGA AGACCAGCTAAATTAATTAAGGGCCTCGT GATACGCCTATTTTTATAGGTTAATGTC	*CatChUP::EYFP::CRP1::hRyR2short CDL* to *pmyo-3* amplification, overlap, forward
oFB96	GACATTAACCTATAAAAATAGGCGTATCAC GAGGCCCTTAATTAATTTAGCTGGTCTTCA TACTGTTTCCGGAAGCAATCCCC	*CatChUP::EYFP::CRP1::hRyR2short CDL* to *pmyo-3* amplification, overlap, reverse
oFB97	CCTTTGCCTTTGATGGCTTCAAGGCCCAGC GGTGGCATCAGGGCAATGAACACTATGGG CGCTCTTGGCAAGCAGGCGATGTC	*CatChUP::EYFP::CRP1::hRyR2short CDL* to *hRyR2short CDL* amplification, overlap, forward
oFB98	GCCTGCTTGCCAAGAGCGCCCATAGTGTTC ATTGCCCTGATGCCACCGCTGGGCCTTGAA GCCATCAAAGGCAAAGGCACGTTC	*CatChUP::EYFP::CRP1::hRyR2short CDL* to *hRyR2short CDL* amplification, overlap, reverse
oFB99	GACTGGCCTGGAGAGTGTTAAAAGTGCAC TCAGAGCTTTTCTGGACAACGCTGCAGAG GATCTGGAGAAGACCATGGAAAACCTC	*hRyR2 short CDL* to *hRyR2short CDL* amplification, overlap, forward
oFB100	GAGGTTTTCCATGGTCTTCTCCAGATCCTCT GCAGCGTTGTCCAGAAAAGCTCTGAGTGC ACTTTTAACACTCTCCAGGCCAGTC	*hRyR2 short CDL* to *hRyR2short CDL* amplification, overlap, reverse
oFB101	AGCTAAATGCGGCCTTAAGGGCC	*hRyR2 short CDL* to *pmyo-3* amplification, overlap, forward
oFB102	TCGGCCATTTCTACGAATGCTGAGC	*hRyR2 short CDL* to *pmyo-3* amplification, overlap, reverse
oFB103	TCGTAGAAATGGCCGATGGGGGC	*hRyR2 short CDL* to *hRyR2short CDL* amplification, overlap, forward
oFB104	GAGAGTGTGATAGTGAAATTTCAGCAATT	*hRyR2 short CDL* to *hRyR2short CDL* amplification, overlap, reverse
oFB105	TCACTATCACACTCTCCGGCTCT	*hRyR2 short CDL* to *hRyR2short CDL* amplification, overlap, forward
oFB106	GCTGAGGTTTCACTTTATTTATTATAGGCT GG	*hRyR2 short CDL* to *hRyR2short CDL* amplification, overlap, reverse
oFB107	AAAGTGAAACCTCAGCTCTTGAAAAC	*hRyR2 short CDL* to *hRyR2short CDL* amplification, overlap, forward
oFB108	AAGGCCGCATTTAGCTGGTCTTCATACT	*hRyR2 short CDL* to *pmyo-3* amplification, overlap, reverse
oFB109	CGAGGCGCGCCGTACCGAGCTCGAATTCA CTG	*hRyR2 short CDL* to pUC19L amplification, overlap, reverse
oFB110	CTCGGCGCGCCGGCATGCAAGCTTGGC	*hRyR2 short CDL* to pUC19L amplification, overlap, forward
oFB111	TGAGGCGCGCCGTACCGAGCTCGAATTCA CTG	*hRyR2 short CDL* to pUC19L amplification, overlap, reverse
oFB112	AGCGGCGCGCCGGCATGCAAGCTTGGC	*hRyR2 short CDL* to pUC19L amplification, overlap, forward
oFB113	TTTGGCGCGCCGTACCGAGCTCGAATTCAC TG	*hRyR2 short CDL* to pUC19L amplification, overlap, reverse
oFB114	CTTGGCGCGCCGGCATGCAAGCTTGGC	*hRyR2 short CDL* to pUC19L amplification, overlap, forward
oFB115	GATATCTGACCGGTACCGTGGTTCCACTAG TTCTAGAGC	*CatChUP::EYFP::linkerCrp1::hRyR2* amplification, reverse

oFB116	CCCACTGCTTACTGGCTTATCGAAATTAATACGACTCAC	*CatChUP::EYFP::linkerCrp1::hRyR2* amplification, forward
oFB117	TTGATCATAGTCGACCTGGTGAGCAAGGGC	*ChRGR(ER)* to *mCherry* amplification, gibson overlap, forward
oFB118	CGGGAGCTCCTCGAGTTACTTGTACAGCTC	*ChRGR(ER)* to *mCherry* amplification, gibson overlap, reverse
oFB119	GGACCCTTGGCTAGCATGGCTCGGAGACCTTG	*pmyo-3* to *ChRGR(ER)* amplification, gibson overlap, forward
oFB120	CCTTGCTCACCAGGTCGACTATGATCAAACCTTG	*pmyo-3* to *ChRGR(ER)* amplification, gibson overlap, reverse
oFB121	ACCATGATTACGCCAAGCTG	*pmyo-3* sequencing, forward
oFB122	TGGGCGCTAGTGAAGAATTG	*pmyo-3* sequencing, reverse
oFB123	GCGTGAAAGAACGTGTTAGC	*pmyo-3::mNEON:(Gly4-Ser)8::hRyR2 short* sequencing, reverse
oFB124	CACGTCCACAGACTGGTAAG	*CatChUP::EYFP::CRP1::hRyR2* sequencing, reverse
oFB125	CCCAGCAGGAGACGAGTATG	*unc-54 UTR* sequencing, forward
oFB126	TCCGCTTACAGACAAGCTGTG	*unc-54 UTR* sequencing, reverse
oFB127	GGCATGGACGAGCTGTACAAG	*unc-54 UTR* sequencing, forward
oFB128	GTCGCCCGATAACGGTTAATAC	*pmyo-3::PsCatCh::YFP::CeRyR* sequencing, forward
oFB129	GCAGAAGAACGGCATCAAGG	*pmyo-3::PsCatCh::YFP::CeRyR* sequencing, forward
oFB130	TGGCCGACAAGCAGAAGAAC	*pmyo-3::PsCatCh::YFP::IP3* sequencing, forward
oFB131	ATAAGCTTGGGCTGCAGGTC	*pmyo-3::CatChUP::EYFP::CRP1::hRyR2short CDL* linearizing, forward
oFB132	AGGCATGGGTGTTGTCTCTTG	*pmyo-3::CatChUP::EYFP::CRP1::hRyR2short CDL* linearizing, reverse
oFB133	TGATGGCCTTCATCTCTGGTC	*pmyo-3::CatChUP::EYFP::CRP1::hRyR2short CDL* linearizing, forward
oFB134	GCTGCTCTTTCTCGTGAAGAC	*pmyo-3::CatChUP::EYFP::CRP1::hRyR2short CDL* linearizing, reverse
oFB135	GGAGTTCTTGTCAGGCATAGG	*pmyo-3::CatChUP::EYFP::CRP1::hRyR2short CDL* linearizing, forward
oFB136	CGGCCGACTAGTAGGAAACAG	*pmyo-3::CatChUP::EYFP::CRP1::hRyR2short CDL* linearizing, reverse
oFB137	AAAACCGGTTTTTAGAGGTGATTGG	*pmyo-3::CatChUP::EYFP::CRP1::hRyR2short CDL* linearizing, forward
oFB138	cttgGAGAGGCAGACGATGTCTCCC	*CatChUP::EYFP::CRP1::hRyR2short CDL* to *CeRyR* amplification, CRISPR, forward
oFB139	AAACGGGAGACATCGTCTGCCTCTC	*CatChUP::EYFP::CRP1::hRyR2short CDL* to *CeRyR* amplification, CRISPR, reverse
oFB140	TTGATCATAGTCGACGTGAGCAAGGGCGAG	*pmyo-3::mVenus* amplification, forward
oFB141	TCAGTTGGAATTCTCACTTGTACAGCTCGTCC	*pmyo-3::mVenus* amplification, reverse
oFB142	TGATGGCAACGTATGGGTCAAC	*pmyo-3* sequencing, forward
oFB143	AGATACCAGGTCTTCAGCGCTCAGCATTC	*pmyo-3* to *CatChUP::EYFP::CRP1::hRyR2* amplification, overlap, forward
oFB144	GAGCTCCTCGAGTGATATCTGACCGGTAC	*pmyo-3* to *CatChUP::EYFP::CRP1::hRyR2* amplification, overlap, reverse
oFB145	AGAATCACTCGAGGGTGAGCAAGGGCGAG	*mVenus* amplification, overlap, forward

oFB146	CGACCGGCGCTCAGTTGGAATTCTTACTTG	*mVenus* amplification, overlap, reverse
oFB147	CGACGGCCAGTGAATTGTAATACGAC	*ChR-XXM* to *mVenus* amplification, overlap, forward
oFB148	AGAACTAGTCCTCGAGTGAACATTGATGTC TATTTG	*ChR-XXM* to *mVenus* amplification, overlap, reverse
oFB149	AGCGGTACCATGAACGGAACAGAAGGTC	*ChR-XXM* to *mVenus* amplification, overlap, forward
oFB150	AGTCGGTACCATGCGCGAGCTGCTATTTG	*ChR-XXM* to *mVenus* amplification, overlap, forward
oFB151	CGACGTCCTCGAGTATACCGCGCCAGCCTC	*ChR-XXM* to *mVenus* amplification, overlap, reverse
oFB159	ACGACGGCCAGTCGCCGGCACTAGTCAC CGGAGAGTTTAATTAGAAACCACAATTCCT C	*pDD287* amplification, CRISPR, forward
oFB160	TTTTAAACTTACCTCCTAGGTCGACCGTTGT CGATCGTCGATCTGATAATGTTCGGTCG	*pDD287* amplification, CRISPR, reverse
oFB161	TATACGAAGTTATTTTCAGACTAGTATGGA TTATGGAGGCGCCCTGAGTGCCGTTGGG	*CatChUP::EYFP::CRP1* amplification, CRISPR, forward
oFB162	CGCCTCCTCCCTGCTCCTCCTTGTCGGCGG TTCCACTAGTTCTAGAGCGGCCGCTCGAC	*CatChUP::EYFP::CRP1* amplification, CRISPR, reverse
oFB163	GACAACGATGGCCGACAAGGgttttagagcta gaaatagcaagt	pDD162 amplification, PAM site, forward
oFB164	GTCGAGCGGCCGCTCTAGAACTAGTGGAA CCGCCGACAAGGAGGAGCAGGGAGGAGG CG	*CatChUP::EYFP::CRP1* amplification, overlap, CRISPR, forward
oFB165	ACAGGAAACAGCTATGACCATGTTATCGA TATCCCGCAAACACTGTAACGACAGTTTGC	*pDD287* amplification, CRISPR, reverse
oFB166	TCCGCCGTCATTCACCTAT	*CatChUP::EYFP::CRP1::CeRyR* amplification, CRISPR, forward
oFB167	TGCGAATCGCGCACTTACA	*CatChUP::EYFP::CRP1::CeRyR* amplification, CRISPR, reverse
oFB168	CAGCGTGAAAGAACGTGTT	CRISPR strain GOA01 sequencing, reverse
oFB169	TCTCACCTGCCCGGTCATT	CRISPR strain GOA01 sequencing, forward
oFB170	CTCTGGCCTTCCTCGTACTTA	CRISPR strain GOA01 sequencing, reverse
oFB171	AAGAAATGCGGCGTGTGT	CRISPR strain GOA01 sequencing, forward
oFB172	GAACATTCTCACAGCTCAGC	CRISPR strain GOA04 sequencing, forward
oFB173	AGCGAGCAAGTCTACCAG	CRISPR strain GOA04 sequencing, reverse
oFB174	AATGGCTGAGACCGAGAATG	CRISPR strain GOA06 sequencing, forward
oFB175	TGGATTTACGATCACGGGAG	CRISPR strain GOA06 sequencing, reverse
oFB178	AGGTTTCGAGCCCGCATATT	CRISPR strain GOA05 sequencing, forward
oFB179	TCCATCTTGGTGTCACTATCCC	CRISPR strain GOA05 sequencing, reverse
oFB180	CTCTTTCACTTGCAGCCTAT	CRISPR strain GOA05 sequencing, forward
oFB181	CAGCCGATCTCCGTCTTGTG	CRISPR strain GOA08 sequencing, reverse
oFB182	ACGGATTCCAGCGTGGTTAC	CRISPR strain GOA08 sequencing, reverse
oFB183	CTGGCAATCTTGGGTCAGTA	CRISPR strain GOA08 sequencing, reverse
oFB184	TACGAGAAAGTCGGAGAAGC	CRISPR strain GOA08 sequencing, forward
oFB185	GAAGTTGAAGGATTTGACCACA	CRISPR strain GOA03 sequencing, forward
oFB186	TAGTTGTAACCGCTCTTGAATG	CRISPR strain GOA03 sequencing, reverse
oFB187	CTGTTATTTGCGTTGCTGTT	CRISPR strain GOA07 sequencing, forward

oFB188	TTTCCAGTGGTATCCTCGTT	CRISPR strain GOA07 sequencing, reverse
oFB189	ACTTTCAAGCGTGAGAAGGA	CRISPR strain GOA11 sequencing, forward
oFB190	GGTGATGAAGTTCAGCGACT	CRISPR strain GOA11 sequencing, forward
oFB191	CTGCAGGTTTCTACAAGGTC	CRISPR strain GOA11 sequencing, forward
oFB192	ATCTCGGACATGCTCAGTTC	CRISPR strain GOA11 sequencing, reverse
oFB193	CGGTATACTCGAGGAGCAAGGGCGAGGAGC	*ChR-XXM::eYFP* to *ITR-1 TM I+II* amplification, overlap, forward
oFB194	CCGCTTACAGACAAGCTGTGACCGTCTC	*ChR-XXM::eYFP* to *ITR-1 TM I+II* amplification, overlap, reverse
oFB195	TACGAGAAAGTCGGAGAAGC	CRISPR strain GOA09 sequencing, forward
oFB196	CAGTGGTATCCTCGTTCTCT	CRISPR strain GOA09 sequencing, reverse
oFB197	CACGGGAGACGAAGAGC	*lite-1* genotyping, forward
oFB198	GCCTTAGAACATTGACGC	*lite-1* genotyping, forward
oFB199	GTCTACTCCTTCCGTGCTA	CRISPR strain GOA14 sequencing, forward
oFB200	TACAAGACCCGTGCTGAG	CRISPR strain GOA14 sequencing, reverse
oFB201	ACGGACACAAGTTCTCTGTT	CRISPR strain GOA14 sequencing, forward
oFB202	TCTGATGTTTTTGGATACCG	CRISPR strain GOA14 sequencing, reverse

2.1.9. Strains generated during this work

Strain	Genotype	Source
ZX2272	fkb-2(ok3007) I.	This work
ZX2273	N2 zxEX1092[pmyo-3::hRyR2short; pmyo-2::mCherry]	This work
ZX2274	unc-68 (r1162) V zxEX1092[pmyo-3::hRyR2short; pmyo-2::mCherry]	This work
ZX2275	N2 zxEX1093[pmyo-3::hRyR2short::(Gly4-Ser)8::mNEON; pmyo-2::mCherry]	This work
ZX2276	unc-68 (r1162) V zxEX1093[pmyo-3::hRyR2short::(Gly4-Ser)8::mNEON; pmyo-2::mCherry]	This work
ZX2444	N2 zxEX1113 [pmyo-3::hRyR2 short CDL::LOV2(1); pmyo-2::mCherry]	This work
ZX2445	N2 zxEX1114 [pmyo-3::hRyR2 short CDL::LOV2(2); pmyo-2::mCherry]	This work
ZX2446	N2 zxEX1115 [pmyo-3::hRyR2 short CDL::LOV2(3); pmyo-2::mCherry]	This work
ZX2447	N2 zxEX1185 [pmyo-3::mNEON;pmyo-2::mCherry]	This work
ZX2448	lite-1 (ce314) X zxEX1113 [pmyo-3::hRyR2 short CDL::LOV2(1); pmyo-2::mCherry]	This work
ZX2449	lite-1 (ce314) X zxEX1114 [pmyo-3::hRyR2 short CDL::LOV2(2); pmyo-2::mCherry]	This work
ZX2450	lite-1 (ce314) X zxEX1115 [pmyo-3::hRyR2 short CDL::LOV2(3); pmyo-2::mCherry]	This work
ZX2451	lite-1 (ce314) X zxEX1147 [pmyo-3::hRyR2 short CDL::LOV2(4); pmyo-2::mCherry]	This work
ZX2452	lite-1 (ce314) X zxEX1183 [pmyo-3::PsCatCh::YFP::CeRyR; pmyo-2:mCherry]	This work
ZX2453	lite-1 (ce314) X zxEX1184 [pmyo-3::PsCatCh::YFP::IP3; pmyo-2:mCherry]	This work
ZX2454	N2 zxEX1186 [pmyo-3::hRyR2shortCDL::mNEON;pmyo-2::mCherry]	This work
ZX2503	N2 zxEX1147 [pmyo-3::hRyR2 short CDL::LOV2(4); pmyo-2::mCherry]	This work

ZX2538	lite-1 (ce314) X zxEX1194 [pmyo-3::PsCatCh::YFP::CeRyR; pmyo-2:mCherry]	This work
ZX2539	lite-1 (ce314) X zxEX1195 [pmyo-3::PsCatCh::YFP::IP3; pmyo-2:mCherry]	This work
ZX2540	unc-68 (r1162) V zxEX1187[pmyo-3::hRyR2short::(Gly4-Ser)8::mNEON; pmyo-2::mCherry]	This work
ZX2541	unc-68 (r1162) V zxEX1188[pmyo-3::hRyR2short::CDL; pmyo-2::CFP]	This work
ZX2542	lite-1 (ce314) X zxEX1189 [pmyo-3::PsCatCh::YFP::CeRyR; pmyo-2:mCherry]	This work
ZX2543	lite-1 (ce314) X zxEX1190 [pmyo-3::PsCatCh::YFP::IP3; pmyo-2:mCherry]	This work
ZX2544	lite-1 (ce314) X zxEX1191 [pmyo-3::ChRGR::mCherry; pmyo-2::CFP]	This work
ZX2545	lite-1 (ce314) X zxEX1192 [pmyo-3::ChRGR::mCherry; pmyo-2::CFP]	This work
ZX2546	lite-1 (ce314) X zxEX1193 [pmyo-3::ChRGR::mVenus; pmyo-2::mCherry]	This work
ZX2575	lite-1 (ce314) X zxEX1196 [pmyo-3::XXM4::mVenus; pmyo-2::mCherry]	This work
ZX2592	N2 CatChUP::YFP::unc-68	SunyBiotech
ZX2593	N2 unc-68::LOV2 (1)	SunyBiotech
ZX2594	N2 unc-68::LOV2 (2)	SunyBiotech
ZX2595	N2 unc-68::LOV2 (3)	SunyBiotech
ZX2596	N2 unc-68::LOV2 (4)	SunyBiotech
ZX2597	N2 sca-1::LOV2 (1)	SunyBiotech
ZX2598	N2 sca-1::LOV2 (2)	SunyBiotech
ZX2599	N2 sca-1::LOV2 (3)	SunyBiotech
ZX2600	N2 sca-1::LOV2 (4)	SunyBiotech
ZX2631	N2 unc-68::LOV2 (1) , ZX2593 including Balancer +/nT1[qIs51] (IV;V)	SunyBiotech
ZX2632	lite-1 (ce314) X CatChUP::YFP::unc-68	SunyBiotech
ZX2633	lite-1 (ce314) X sca-1 LOV2 (3)	SunyBiotech
ZX2634	lite-1 (ce314) X CatChUP::YFP::unc-68; zx1663 N2 zxIs78 [pmyo-2::C1V1 ETET; pmyo3::mCherry]	This work
ZX2635	N2 Exon1.1 CatChUP::YFP::unc-68, Exon1.2 CatChUP::YFP::unc-68	This work
ZX2636	N2 Exon1.1 CatChUP::YFP::unc-68, Exon1.2 CatChUP::YFP::unc-68	This work
ZX2686	lite-1 (ce314) X unc-68 LOV2 (2)	This work

2.1.10. Software

Table 2.9.: Software

Name	Version	Developer
Arduino	1.8	Arduino Team Experimental protocols written by Wagner Steuer Costa
Argus X1	3	Biostep
Axio Vision	4.5	Carl Zeiss
Canvas	9	ACD Systems
Citavi	6	Swiss Academic Software
Clone Manager	9	Sci Ed Central
Clustal Omega		EMBL-EBI

FIJI	Updates 2016-2020	Fiji contributors
Graph PadPrism 8	8.0.2	GraphPad Software, Inc.
ImageJ	1.47v	Wayne Rasband
Inkscape	0.48.4 r9939	The Inkscape Team
KNIME Desktop	2.12	KNIME.com Evaluation programmes by Wagner Steuer Costa
LSM Image Browser	4.2	Carl Zeiss
Micro-Manager	1.4	Open Imaging
Microsoft Office	12.0.6607.1000	Microsoft
NEBioCalculator™	V1.8.1	NEB
NemaAcquire	2.1	Nemametrix
NemAnalysis	0.2	Nemametrix
Notepad++	6.5.5	Notepad++ team
Origin	9.1	OriginLab
PyMOL Molecular Graphics System	2.0	Schrödinger, LLC.
R	3.2.1	R Core Team
SnapGene Viewer	5.0.8	SnapGene
VirtualDub	1.10.4	Avery Lee
ZEN lite 2012	1.1.1.0 blue edition	Carl Zeiss

2.2. Methods

2.2.1. Molecular and Microbiological methods

This section includes the methods used for cloning and analysing of deoxyribonucleic acid (DNA).

2.2.1.1. Extraction of genomic DNA from C. elegans

Genomic DNA extraction was done by following the adapted protocol from WormBook (Ahringer 2006). Ten animals of one strain were pooled into a tube containing 2.5 µl single worm lysis buffer (SEWLB) including 2% (v/v, 10mg ml^{-1}) Proteinase K. Following a freeze fracture of the cuticle of the animals by freezing for at least 20 min at -80°C and incubation for 1 h at 60°C to activate the Proteinase K. For the inactivation of the enzyme the sample was incubated for 15 min at 95°C. To confirm the genotype of a strain, for each strain minimum twelve animals were tested, by the procedure as described above.

2.2.1.2. Polymerase Chain Reaction

Amplifying DNA exponentially *in vitro* is called polymerase chain reaction (PCR). For this method Primers are needed, these are oligonucleotides that are flanking the regions of interest. During this work different polymerases were used, depending on the length of the product, the quality of the desired result and the cost per reaction. Genotyping was done either with Taq, for deletion or insertion mutants, or Phusion polymerase if failure or single point mutants had to be sequenced. Cloning based on PCR products was performed with Phusion polymerase.

In Table 2.10 the basic content of a PCR reaction is depicted. Reaction volume was adapted depending on the required conditions. The volume of analytical PCRs was scaled between 25 µl and 50 µl per reaction tube. Volumes higher than 50 µl were equally distributed across several tubes.

Table 2.10.: Basic PCR reaction mix

Substance	Volume [µl]
DNA Template (10 ng μl^{-1})	1
DNA Polymerase	0.5
Polymerase Buffer	10
Forward primer (10 pM)	0.5
Reverse primer (10 pM)	0.5
dNTP	2
ddH_2O	add to 50

The PCR mix was processed in a thermal cycler with a program, that was adjusted to the length of the PCR product and the DNA polymerase that is used. PCRs with Taq polymerase were performed according to Table 2.11. For long PCR products and DNA that is used for cloning, Phusion polymerase was used according to Table 2.12.

PCR reaction condition using Taq polymerase:

Table 2.11.: PCR with Taq polymerase

Process	Temperatur [°C]	Time[s]	Cycles
Initial denaturation	95	300	
Denaturation	95	20	
Primer Annealing	Primer specific	30	35
Primer extension	68	Product dependent	
Final extension	68	600	
Hold	4	For ever	

PCR reaction condition using Phusion polymerase:

Table 2.12.: PCR with Phusion polymerase

Process	Temperatur [°C]	Time[s]	Cycles
Initial denaturation	98	30	
Denaturation	98	10	
Primer Annealing	Primer specific	150	35
Primer extension	72	Product dependent	
Final extension	72	600	
Hold	4	For ever	

2.2.1.3. Primer design

The primers used in this work were designed with the program Clone Manager 9, or Benchling online tool for plasmid and primer design (Benchling 2020). Primer intended for genomic PCR were validated with Primer-BLAST, an online tool provided by NCBI (Primer designing tool 2021) that uses the Primer3 algorithm to find binding sites of the primers in a database defined by the user. Here the specificity of the primer pair was checked evaluated against Eschericha coli (E. coli) and *C. elegans* genome. The primers were ordered at Eurofins Genomics GmbH (Ebersberg, Germany) and Microsynth (Göttingen, Germany).

2.2.1.4. Colony PCR

To quickly screen many transformant bacteria after a transformation with a plasmid of interest, a colony PCR was applied. Therefore, transformant bacteria colonies were picked with a sterile pipette tip and either solved in 20µl ddH_2O and then used 2µl in the reaction mix, or the tip was briefly dipped into the PCR reaction mix. This reaction mix was used to perform a PCR. The remaining bacteria on the tip were streaked out on a fresh LB-agar plate, including a proper antibiotic for selection of colonies. The PCR positive colonies were used to propagate the DNA of interest.

2.2.1.5. Gel electrophoresis

The DNA gel electrophoresis is a method to analyse and purify DNA fragments and to measure the length in base pairs (bp). It is used for analytical and preparative separation of DNA fragments. Due to the phosphate residues in the backbone, the DNA is a negatively charged molecule, that can be separated in an electric field from the negative cathode to the positive anode (Aaij and Borst 1972; Ahringer 2006). In 1x TAE buffer 1-2% agarose (w/v) was dissolved and heated until the solution was totally cleared. For small DNA fragments the content of agarose was increased. After cooling down to approximately 50°C it was poured into a chamber and a grid was put in the gel to create pockets. The size of the pockets is depending on the amount of the DNA sample. DNA and 6x loading dye were mixed proportionally and the sample was loaded into the pockets of the gel. The loading dye was added for visual tracking, pull down DNA in the pocket and inhibition of metal-dependent enzymes. As a reference for DNA length, an additional pocket was loaded with 5-10 µl “GeneRuler 1 kb DNA ladder” from Fermentas. Electrophoresis was performed in 1x TAE buffer at 120-140 V, 5 V/cm to 8 V/cm gel length, for 30-45 min. After electrophoresis the gel was stained with Ethidium Bromide (EtBR) in a 0.1% (v/v) ddH_2O solution for 10 min. Visualization of DNA was done under the exposure of 590 nm UV light and images were recorded with a Canon EOS 500 and the program Argus X1 V.3.

2.2.1.6. Gel extraction

Extraction of DNA fragments after gel electrophoresis (see 2.2.1.5.) was performed under a minimum of UV irradiation. The fragments of interest were excised with a scalpel, with a minimum of agarose gel around. After transferring into an Eppendorf tube, the gel was weighed, and DNA extraction was performed according to the manual of the QIAquick Gel Extraction Kit from Quiagen. Modifications of the protocol were increased binding time of DNA to the column and incubation time of DNA elution.

2.2.1.7. PCR product purification

Purification of PCR product was done with the Kits QIAquick PCR Purification Kit and ROTI®Prep PCR Purification, according to the manufacturer’s manuals. To enhance the amount of extracted DNA

elution was prolonged up to 10 min at 50°C. Amounts of water were adjusted according to the expected amount of PCR product, also the last centrifugation step was repeated at maximum speed.

2.2.1.8. DNA restriction digest

Restriction digest of DNA allows to cut DNA at specific recognition sites. Restriction enzymes bind to these specific sites and cut the DNA by generating "sticky" or "blunt" ends. These linear DNA fragments can be used for DNA ligation, PCR, sequencing or other applications. Digests in this work were planned and performed according to supplier recommendation. Double digests were planned with the online tools NEBcloner (NEBcloner 2020) and NEBcutter V2.0 (NEBcutter V2.0 2020). If sequential digestion was necessary, due to low activity or non-compatible enzyme condition, a purification step was performed in between.

2.2.1.9. DNA sequencing

All sequencing assignments were purchased from Eurofins MWF GmbH or Microsynth Seqlab. Samples were prepared according to each company's recommendation. Purified PCR DNA of up to 3 kb, or plasmid DNA products, of up to 25 kb were solved in ddH_2O. Concentrations were in the range of 80 ng/µl to 120 ng/µl. Samples were premixed with 2 µl respectively 3µl appropriate primers.

2.2.1.10. DNA fragment ligation

Ligation of the DNA fragments was performed as described in the following table. The reaction mix was prepared in a microcentrifuge tube on ice, using a molar ratio of 1:3 vector to insert. Gently flicking the tube or briefly pipetting up and down mixed the reaction sufficiently. Sticky ends were incubated for 10min at room temperature or at 16°C overnight. Blunt ends were incubated for at least 2h at room temperature or 16°C overnight. Incubation was followed by heat inactivation at 65°C for 10min and subsequent transfer to ice until 1-5µl was used for transformation with *E. coli* competent cells.

Table 13.: T4 Ligation reaction mix

Component	Quantity
T4 DNA Ligase	1µl
T4 DNA Ligase Buffer (10X)	2µl
Vector DNA (0.02pmol)	50ng
Insert DNA (0.06pmol)	37.5ng
ddH_2O	add to 20µl

2.2.1.11. Phenol-Chloroform-Isoamyl alcohol Extraction

Phenol-chlorofom-isoamyl alcohol (PCA) extraction is a method used to separate DNA and RNA from proteins from salts. It is based on the solubilities of different molecules. First 0.5 volumes of a phenol:chloroform:isoamyl alcohol mixture with the proportions 25:24:1 were added to the DNA or RNA containing solution. The mixture was emulsified for 1 min on a vortexer, followed by a centrifugation step for 5 min at 16000 x g, at room temperature. This step separates the DNA containing water Phase on top, from the protein containing dense organic phase on the bottom. The top phase was separated and 2.5 volumes of 0.12 mM sodium acetate in ethanol were added followed by freezing at -80°C for 30 min. The next step is a centrifugation for 1 h at 4°C and 16000 x g, to pelletize the DNA. The supernatant was disposed, and the pellet was washed with 500µl 70% ethanol. After

centrifugation for 1 h at 20°C and 16000 x g the supernatant was removed, and the purified DNA was dried at RT for 1 h. Finally, the pellet was solved in ddH_2O and the concentration was measured.

2.2.1.12. Transformation of competent E. coli

Competent *E. coli* cells were used for heat shock transformation. For this, the cells were thawed on ice and ~5ng (2µl) of the ligation mix was cooled on ice in microcentrifuge tubes. To 50µl of competent cells, 2µl of DNA was added and gently mixed by flicking the tube 3 times or pipetting up and down. Shaking or vortexing should be avoided, also in the following steps. Incubation on ice for 30min was followed by heat shock at 42°C for 30s (depending on manufacturer and cell type). This was followed by the addition of 950µl SOC medium or LB medium. The tube was placed in a shaker at 37°C for 60min with vigorous shaking or rotation of approximately 250rpm. During incubation, selection plates were pre-warmed with the appropriate antibiotic corresponding to the resistance gene. 50-100µl of the transformed cell mixture was spread on the plates and incubated overnight at 37°C. After picking the colonies, the plates could be stored at 4°C for a few days.

2.2.1.13. Electroporation Protocol

The electroporation protocol will vary depending on the strain, so this protocol may need to be optimized. For control electroporation dilute pUC19 to 10 pg/µl with Milli-Q water. The electroporator needs to be set to 1.7-2.5kV (optimize for every strain), 200Ω and 25µF. SOC for recovery period needs to be placed in 37°C water bath and the LB-antibiotic plates have to be pre warmed to 37°C. Thaw cells on ice for 10min or use freshly made cells. Place an appropriate number of microcentrifuge tubes and 1mm electroporation cuvettes on ice. Before transferring 25µl of cells to the microcentrifuge tubes, flick the cells a few times to mix them. Then add 1µl of a 10pg/µl DNA solution (ddH_2O) to the cells. Transfer the mixture of DNA and cells into a cold cuvette and tap it on the table 2 times to get rid of bubbles. Ensure the outside of the cuvette is dry and place it into the electroporation module. Push start and subsequently add 975µl 37°C warm SOC. Mix by pipetting up and down one time and transfer it to a 15ml falcon tube. After an incubation for 1h at 37°C you prepare appropriate dilution, for 10pg DNA you dilute: 10µl cells into 990µl SOC and plate 100µl for a 1000-fold dilution,

100µl cells into 900µl SOC and plate 100µl for a 100-fold dilution.

Transfer the cells to a pre-warmed LB-antibiotics plate and incubate overnight at 37°C.

2.2.2. Microscopy methods

This chapter describes microscopic imaging techniques used for qualitative and quantitative analysis of fluorescent proteins in *C. elegans* during this work.

2.2.2.1. DIC microscopy

Imaging of *C. elegans* was performed using an Axiovert 200 (Zeiss) with a 10x (Zeiss A-Plan 10x / 0.25) or a 100x oil immersion objective (Zeiss C-Plan 100x / 1.3 oil). It was equipped with an AxioCam MRm (Zeiss) camera and the AxioVisionAC 4.5 software. Alternatively, a Canon PowerShot G9 camera was attached instead of an ocular, controlled by custom software and a custom signal generator consisting of an Arduino UNO REV3.

2.2.2.2. Stereo microscopy

Handling and maintenance of *C. elegans* not relying on fluorescence-based selection was performed using the Nikon SMZ 645 stereomicroscope. Swimming experiments were performed on the stereomicroscope with a 96-well plate. For video recording, the stereomicroscope was equipped with a Canon Power shot G9, which replaced an ocular.

2.2.2.3. Qualitative analysis of fluorescence

Handling of fluorescent protein expressing *C. elegans* was done by using qualitative fluorescence microscopy. Level of transmission efficiency, mosaicism and expression of extrachromosomal or integrated DNA was estimated by the strength of the fluorophore, which could be observed in a Leica Mz 16F microscope. In the microscope filter sets for cyan fluorescent proteins (CFP), green fluorescent proteins (GFP) and red fluorescent (RFP) were mounted to analyse transgenic lines of *C. elegans*.

2.2.2.4. Quantitative analysis of fluorescence

For quantitative imaging, worms were paralysed either on a 10% agar pad (w/v in ddH2O) with polystyrene beads or on a 2.5% agar pad (w/v in ddH2O) with 10 µl 50mM sodium azide (NaN3) in M9 buffer on a microscope slide. These methods prevented *C. elegans* from moving during imaging, however, polystyrene beads could not fully immobilise the animals and were therefore only used when muscle activity was desired. The microscopes, objectives and cameras used in this work were the Axio Observer Z1 (Zeiss) with a 10x Zeiss A-Plan 10x / 0.25 or a 100x oil immersion Zeiss C-Plan 100x / 1.3 oil objective together with a ORCA-Flash2.8 (Hamamatsu) or an ORCA-Flash4.0 (Hamamatsu); a Axiovert 200 (Zeiss) with a 10x Zeiss A-Plan 10x / 0.25 or a 100x oil immersion Zeiss C-Plan 100x / 1.3 oil objective together with an AxioCam MRm (Zeiss)camera and AxioVisionAC 4.5 software and the Zeiss Cell Observer SD with a 100x oil immersion (alpha Plan-Apochromoat 100x/1.46 Oil DIC (UV)) objective equipped with a Laser 488nm and two Rolera EM-C2 cameras.

2.2.3. *C. elegans* handling

2.2.3.1. Generating male C. elegans

As it is necessary for crossing of *C. elegans* to have males, the rate of males per generation had to be increased artificially. The proportion of 0.1-0.2% males in a natural population (Maures et al. 2014), can be raised drastically with this protocol, using the fact that more males are generated if hermaphrodites are stressed for example by being exposed to alcohol or heat, which increases the X-non-disjunction (Lints and Hall 2004). Here the used method is based on heat induced male generation. Five to ten plates, each with 5 L4 hermaphrodites are incubated for 4-6 hours at 31°C. Plates were taken out after 4 h, 4.5 h, 5 h, 5.5 h, and 6 h and returned to 20°C. The F1 generation can be screened as soon as males can be differentiated from hermaphrodites. To get a ratio of 50:50 by mating males with hermaphrodites, L4 animals are transferred to fresh unseeded NGM plates in a ratio of 1 hermaphrodite to 3 males. The next generation should be composed of approximately 50% male worms. To maintain a relatively high percentage of males, the most effective way is to pick new plates in a ratio of 1:3 every week and keep the plates at 15°C.

2.2.3.2. Backcrossing

This backcrossing strategy is suited for autosomal mutations. In the first step heterozygous animals are kept on a plate until L4 progeny appears. Six of these L4 progeny are picked to individual plates and each is mated with 6-12 wild-type males. Genotyping of the hermaphrodite mothers is performed two days after the mating was set up, by PCR. Matings that did not carry the mutation of interest are discarded after genotyping. The next step is to pick 6-10 L4 male cross progeny from a successful mating and two L4 wild-type hermaphrodites and transfer them to fresh plates. Mating animals are moved to new plates for two days. If the three days old plates are checked and you have 50% males among the progeny, the mating can be considered as successful and sixteen of these L4 progeny are transferred to fresh plates. Two days after picking, the animals have produced enough progeny and the mothers can be used for genotyping by PCR. Plates that did not show positive crossing can be discarded. Successful genotyped animals have been backcrossed now (autosomes have been backcrossed two times, the X chromosome one time). For further backcrossing directly repeat the steps until sufficient backcrossing has been done. After several rounds of backcrossing, let a mutant self-fertilize and lay eggs. Single 16 animals of the progeny to individual plates and genotype the mother for homozygosity after they laid eggs for two days. The successful mutant strain will be frozen for long-term storage.

2.2.3.3. Crossing and obtaining homozygotes

The strategy to cross *C. elegans* is based on the protocol of Green et al., 2008 (Green et al. 2008b). To cross strains of *C. elegans*, the first step is to generate male animals of one strain, as described in 2.2.3.1. Generating male C. elegans Then six L4 hermaphrodite worms of the first strain and six males of the second strain are transferred to one fresh unseeded plate. Here no additional OP50 is needed, as there is enough on the pick to feed them, furthermore the animals will mainly stay on the small area with food which increases the probability of mating. The plate is being incubated at RT for one day. Following each of the six F0 hermaphrodites is singled to a separate petri dish. These singled animals grow for three days until the F1 generation can be screened for approximately 50% males. Do not breed for more than 3 days, it is important that there is no crossing of the F1 generation. Four hermaphrodites of each successful crossing are singled to fresh seeded NGM plates, and they are grown until the next generation reaches adulthood. Again 4 individuals of the F2 generation are singled to fresh seeded NGM plates and grown to adulthood. After one day the mother can be used for screening, if the test is positive for homozygosity the progeny can be considered as homozygous. Alternatively, the last step is to screen F3 worms, by PCR or fluorescent marker if used.

2.2.3.4. DNA micro injection

Injecting micro DNA is one of the standard techniques to generate transgenic animals (Hope 2005), that carry an extrachromosomal DNA array in *C. elegans*. A DNA mixture (Table *14*) injected in the gonads of late L4 to young hermaphrodites, can lead to transgenic animals. These show either expression present in every cell or a mosaic expression in some cells of the body (Stinchcomb et al. 1985). It is also possible that no array is inherited to the next generation, therefore it is essential to maintain the transgenic strain. To easily do that a co-marker will be co-injected with the plasmid of interest, to express a visible fluorophore, that can be seen under the microscope.

2.2.3.4.1. DNA injection mix

Substances as described in *Table 14* were mixed to a final concentration of ≥100ng/µl and 30µl in volume. The mix was then centrifuged for 10min at 15000g, only the upper 15µl were used for micro injections.

Table 14: Injection mix substances

Substance	Volume / concentration
DNA of interest	0.1ng/µl to 100ng/µl
Co-Marker plasmid	1ng/µl to 10ng/µl
Fill DNA	add to 100ng/µl
Injection buffer	3µl
ddH_2O	Add to 30µl

2.2.3.4.2. Injection

Micro injection was basically done as described by (Mello et al. 1991). The injection mix prepared in 2.2.3.4.1. DNA injection mixwas transferred with long thin pipette tips into glass needles, as close to the tip as possible. Needles were made in a puller beforehand. To avoid bubbles the needles were flicked gently. Additionally, a cover slip was mounted on a microscope slide, the slide was covered on top with a dry agar pad (2% agar (w/v) in ddH_2O). Small scratches were made on the pad to break the tip of the glass needle and a droplet of halocarbon oil was applied, to prevent the animals from desiccation. As soon as the injection mix in the tip of the glass needle lost all air bubbles, it can be mounted in the micro injection manipulator, holding the air pressure outlet. Agar pad and microscope slide were then placed in the Zeiss Axiovert 40 CFL and aligned to the visual centre. Prior to injection the needle had to be broken, this step is quite critical, because a thin tip is necessary to do the least possible damage to the injected animal, but also the flow of injection mix has to be ensured. To break it properly, air pressure was applied to the needle and the tip has to be moved gently towards the edge of the agar or the scratches made beforehand, until it brakes on the right position. One up to ten animals could be placed on the pad in the halocarbon oil with an eyelash pick. After injection of DNA into both or one gonad, the animals were transferred into a small drop of M9, to wash off remaining oil and then to seeded NGM plates. These were kept at 20°C for 3d to 7d, depending on the *C. elegans* strain. As soon as progeny is big enough, screening can be done by looking for the co-marker.

2.2.3.5. CRISPR/Cas9

To edit the genome of *C. elegans,* and to integrate DNA one method used in this work was the clustered regularly interspersed short palindromic repeats (CRISPR)–Cas9 system. The protocol used for genome editing was based on the method of (Dickinson et al. 2015).

First identify a 100-200 bp region where you want the Cas9 target site to be, usually it is a 200 bp window in the middle of the target site. Then Submit this genomic sequence to a CRISPR design tool and check the genome for specificity on e-crisp.org. Target sites should be chosen with a specificity score >95. If there are multiple candidate sites with high specificity, select the site closest to the desired insertion site. ideally, the insertion site is within the guide sequence and within 10 bp of the PAM so that the insertion disrupts the target site. To insert the 5'N20-NGG-3' returned by the design tool into the Cas9-sgRNA construct (pDD162, Addgene #47549), the Q5 Site-Directed Mutagenesis Kit can be used. It is important that the PAM (NGG motif) is not included in the primers for the Cas-sgRNA construct, it must only be present in the target DNA. Then the correct insertion can be verified by sequence analysis. Use PCR to generate the homology arms and insert them in place of the ccdB negative selection markers flanked by restriction sites. For Gibson assembly, these primers will amplify

the homology arms and add sequence overlaps to the ends of each arm. Your primers must also introduce silent mutations if the FP::SEC insertion does not disrupt the Cas9 target site to prevent Cas9 from cutting the repair template. Following this, 50-60 L4 worms of a suitable strain of *C. elegans* are injected with the mixture of homologous repair template, Cas9-sgRNA and co-injection markers. Three animals per plate are then transferred to freshly seeded plates, in addition a negative control can be produced for drug selection. Allow the worms to lay eggs for 2-3 days at 25°C. On day 3, add 500µl, 250µg/ml hygromycin to the plates, allow to dry and return to 25°C. On day 6 or 7, the plates are checked for healthy animals that have survived the hygromycin treatment and meet the selection criteria such as Rol phenotype and lack of red fluorescence. 5-10 animals were then singled to new plates without hygromycin. After 9-10 days, the plates are checked for homozygous knock-in animals. Plates should contain100% Rol animals of L4 and adults. Selectable markers can be removed by heat-shocking visible fluorescent heterozygous animals and identification of animals that excised the marker based on the phenotype of the injected strain with additional fluorescence.

2.2.3.6. Genotyping

Injection of extrachromosomal arrays, crossing strains or using the CRISPR method to directly integrate DNA into genome, has to be verified. In order to do that genotyping was done by picking a single worm, or a batch of 10, into 2.5µl SEWLB buffer supplemented with Proteinase K, in a PCR-tube. The mix was then frozen at -80°C for at least 30min. After that it was lysed at 60°C for 1h and Proteinase K was inactivated at 95°C for 15min. Suitable primer pairs were chosen to create a template that can be distinguished from the wild-type allele on an agarose gel after PCR. Optional a Duplex PCR can be performed, using three primers in one PCR, which will produce products of different length for mutant and wild-type, or a mix for heterozygous animals (Ahringer 2006). Single point mutations or small changed sequences that could not be distinguished by restriction enzyme digest, were sent to Eurofins or Microsynth Seqlab for sequencing.

2.2.3.7. Integration of extrachromosomal arrays by UV irradiation

Due to the fact that extrachromosomal arrays are not transmitted to all descendants, it is necessary to integrate these arrays into the genome in perpetuity. To do that, the here used method is using UV irradiation. 100 L4 animals were transferred to 100mm unseeded NGM petri dishes one day before. UV irradiation was done in a Stratagene UV crosslinker (Stratalinker), therefore the lid was removed, and the plates were exposed to two pulses of 33.3mJ UV-light, interrupted by a 30s break. Subsequently animals were transferred in batches of 5 to seeded NGM plates. These were cultivated at 20°C until starvation, and then chunked to seeded 140mm plates. After 3d at 20°C 600-800 animals were singled to seeded petri dishes and cultivated at 20°C. Here the first selection was done, by only transferring non-mosaic, transgenic animals. As soon as the F2 generation reached adulthood, the plates were screened for 100% transgenic animals, using the co-injected selection marker. Furthermore, plates with morphologic or behavioural unobtrusive worms were favoured. Integrated animals were back-crossed 4 times with the strain used for injection to repair potential UV damages of the genome.

2.2.3.8. Decontamination of C. elegans

In case of a contamination like yeast or mould in a *C. elegans* culture, several gravid adult animals were transferred to a fresh seeded NGM petri dish. By pipetting 50µl of 1:1 sodium hydroxide (NaOH) : 5% sodium hypochloride (NaClO) (v/v) on the animals, bacteria and other contamination was removed. Adult animals are decomposed but eggs survive, because a bleach resistant cuticle protects them. New

hatching larvae are then contamination free and the new colony can be scored after 3d to 5d days for successful decontamination.

2.2.4. Analysis of *C. elegans* behaviour

To account the intrinsic variability of a *C. elegans* population the experiments in this work were repeated at least twice on different days and during different times of day.

2.2.4.1. Analysis of swimming behaviour

Swimming behaviour was analysed in 96 well plates, with flat bottoms. Well bottoms were filled with 60-100µl NGM to prevent the worms from sticking to the plastic surface. After cooling, 100µl M9 buffer were added and up to 10 animals were transferred to the well by a hair pick, to avoid bacteria contamination. Animals were kept in the dark for at least 10min to accommodate to the new environment. Videos were acquired a Canon G9 camera under red (650nm ± 50nm) transmission light of an Axiovert 200 (Zeiss) microscope. Blue light illumination was done with an HBO 50 lamp (Zeiss, 470nm ± 20nm), or a 470nm LED light source (KSL 70, Rapp OptoElectronic). Intensity was adapted to the individual strains. Data evaluation was done by counting body bends, which are defined as a complete sinusoidal movement of a worm. Time intervals of darkness and illumination were counted separately, swimming cycles were calculated as body bends per min (bbpm). To not disregard the episodic nature of *C. elegans* swimming behaviour, periods of no movement were also ascribed to an animal (Ghosh and Emmons 2008). Mean, SEM and n-number were determined, and statistical evaluation was done by students t-test or ANOVA.

2.2.4.2. Multi Worm Tracker

Behavioural assays of whole populations of *C. elegans* were carried out using the Multi Worm Tracker (MWT). The MWT allows video capturing of thrashing assays in 30mm petri dishes and crawling assays in 60mm petri dishes. Preparation for thrashing assays consisted of separating the transgenic *C. elegans* animals into a standard NGM petri dish the day before an experiment, using a fluorescence microscope. This was to avoid non-transgenic animals and to ensure there was no pre-activation of light sensitive receptors or channels, that could alter behaviour. Before measurement starts, approximately 30 animals were transferred to a 30 mm petri dish with an NGM layer on the bottom, to prevent the animals from sticking to the bottom. For thrashing assays, a thin layer of 800-900 µl M9 buffer was added (not too thick to prevent swimming up and down). After adding M9 buffer the animals were kept in the dark for at least 10min, to adapt to swimming. In the software LabView, time of the Video, timing, length and frequency of light pulses were set. The video was captured in darkness except for the red background light with 660nm red light, not exceeding 1.65µW/mm², for the DALSA, Falcon 4M30, 4MP (2352 x 1728), 31fps, 10bit, equipped with a camera lens from Rodenstock, 60mm, f/4.0 Rodagon Lens.

2.2.4.3. Contraction assays

Body length determination of *C. elegans*, before during and after light stimulation, was done under an Axiovert 35 Phase Contrast Microscope (Zeiss), using a band pass filter BS605 675nm ± 50nm for transmission light. Activation of channelrhodopsin was done using a 470nm ± 40nm filter. The microscope was equipped with a mechanical shutter, controlled by an Arduino, additionally a Canon G9 was connected to the Arduino to synchronize video recording and light stimulation. Single animals

were transferred to the centre of an unseeded NGM plate. After adapting to the new environment in darkness, the plates were fixed in the stage. Video acquisition was started on the Arduino. while Animals were kept in the centre of the video by manual adjustment of the stage, while the illumination protocol was run by the Arduino automatically. Videos were transformed to black and white videos and data analysis was done with a Konstanz Information Miner (KNIME), workflow written by Wagner Steuer Costa (Steuer Costa 2016). Relative body length contraction was determined by averaging worm length before stimulus as reference level compared to periods with and after illumination. All depicted graphs of contraction assays show averaged normalized relative body length.

2.2.4.4. Pharynx pumping assays

In order to measure the electrophysiological effects of the modified RyR, the rate of pharyngeal pumping was measured by using the Nemametrix system. This system is composed of a chip in which the frequency of the pharyngeal pumps is counted by measuring the electrical potentials of the pharynx muscles.

For the preparation of pumping assays transgenic animals were transferred to NGM petri dishes, seeded with OP50 including 0.2% ATR, and incubated overnight at RT. Before they could be used in the Nemametrix system 50-100 animals were transferred into 500µl M9 buffer in an Eppendorf vial and washed 2-3 times with M9 and centrifuged at 1000-1500g for 2 min to put the worms to the ground. After washing the animals, they were either incubated in Serotonin if necessary or directly soaked into the Nemametrix ScreenChip. In the ScreenChip the worms were soaked in between two electrodes that measure the electrical potentials of the pharynx. With the program NemAcquire the Electropharyngeograms of the animals were recorded. After that the data could be analysed to get the final data of how many pumps per second (Hz) the animals did. Pharynx pumping was tested with different protocols:

1. Stimulation with 1Hz 50ms at 590nm 780µW/mm² for 1min
2. Stimulation with 1Hz 50ms at 515nm 710µW/mm² for 1min
3. Stimulation with 4Hz 50ms at 590nm 710µW/mm² for 1min
4. Stimulation with 1Hz 50ms at 470nm 1.41mW/mm² for 1min
5. No stimulation as control

The final intension of the pharynx measurements was to establish a strain that could be paced with green light (zx1963 N2 zxIs78 [pmyo-2::C1V1 ETET; pmyo3::mCherry]). This strain was crossed into the strain GOA14 to combine the possibility of controlling the blue light activated RyR (CatChUP::eYFP::RyR) and control the green light activated C1V1 ET/ET variant at 590nm (Erbguth et al. 2012). Therefor a blue and yellow LED light source (470nm, KSL 70 and 590nm KSL054, Rapp OptoElectronic, Hamburg, Germany) were used. The protocol then was designed as follows: Permanent illumination with 590nm yellow light to pace the pharynx by activating C1V1 with 4 Hz (possible pacing from 0-5Hz). Simultaneously illumination with 470nm blue light would then activate the Channelrhodopsin connected to RyR with 2 Hz. Expectation would be that a 4 Hz pumping pharynx would show alteration (e.g. delay or stop), of the 4 Hz pacing as long as the blue light pulses open the RyR in the SR-membrane.

2.2.4.5. Statistical analysis

In the analysis of *C. elegans* behavioural assays, data were obtained and pooled from at least three experiments involving animals from different generations of the same genotype. These were reared on different days under the same conditions and measured under identical experimental settings. The

total number of animals analysed is given as n. Statistical normal distribution was verified with the chi squared test. Data are presented as mean or median ± SEM and statistical significance is indicated as p-value after one-way/two-way ANOVA including Bonferroni correction. Alternatively, paired and unpaired Student's t-test with Welch's correction was applied depending on whether the same animals were measured under the same conditions. Significant differences are represented as * $p<0.05$, ** $P<0.01$ and *** $P<0.001$.

3. Results

To achieve the goal of light-inducible calcium release from the SR/ER, via the ryanodine receptor, several strategies were investigated:

1. Fusion of a Ca^{2+}-conducting version of ChR2 to the C-terminus of UNC-68. For this purpose, a fosmid containing the *unc-68* gene of *C. elegans* was engineered by bacterial recombination. This was then to be expressed in a genomic null mutant background to a) test the functionality of the modified UNC-68 protein by rescue experiments and b) see if light stimulation could provoke increased muscle activity.
2. A similar approach was followed by our collaboration partner Philipp Sasse using the mammalian RyR2 and the N-terminal fusion of ChR2 with a long linker sequence. Since this construct revealed light-induced Ca^{2+} transients in HEK293 cells, we aimed to test whether the same construct can be functionally expressed in *C. elegans*. Here, too, the rescue of the *unc-68* mutant and the light-induced stimulation were to be tested.
3. Expecting that the very large hRyR2 cDNA construct would be very difficult to handle, a truncated version, previously described as a functional Ca^{2+}-triggered channel, was also to be tested.
4. The shorter construct was designed to test a different approach, namely insertion of LOV2 domains at strategic sites to enable light-evoked structural disturbance that may lead to channel opening.
5. The same approach would be used for the endogenous *unc-68* locus to insert LOV2 domains using the CRISPR/Cas9 technique.
6. Ca^{2+}-conductive variants of ChR2 should be targeted to the SR/ER membrane to assess the possibility of light-induced Ca^{2+} release (LICR) from the SR/ER.

3.1. Substituting *unc-68* with an engineered photo-sensitive version encoded on a fosmid

A first attempt to rescue a *unc-68* deletion in *C. elegans* with transgenic constructs encoding (modified) *unc-68* was made using an adapted fosmid, generated by Dr. Satoshi Tsunoda and Dr. Elisabeth Fischer. Swimming assays were performed with the deletion mutant strain *unc-68 (r1162) V* (from now on only *unc-68*). These animals do not express a working ryanodine receptor, thus making them suitable candidates for rescue experiments. They appear smaller and flaccid compared to equally aged wild-type animals. Furthermore, the *unc-68* deletion leads to very slow movement and defective pharyngeal pumping (Maryon et al. 1998). The animals are not capable to cover large distances, yet they exhibit nearly normal muscle ultrastructure (Maryon et al. 1996).

Here, DNA injection can lead to expression of naturally occurring and inserted full length RyR protomers. In case wt UNC-68 and the *punc-68::unc-68::mKate::ß-H/K-ATPase::ChR2(L132C;H134R; T159C)* encoded by the fosmid are expressed in one animal, hyprid channels could be formed. The possible configurations of assembly of the hybrid tetrameric structure of the RyR channel are illustrated in *Figure 33*. Both, protomers of CeRyR and *punc68::unc-68::mKate::ß-H/K-ATPase::ChR2 (L132C; H134R;T159C)* could be assembled into a tetrameric channel, with possible content of *punc-68::unc-68::mKate::ß-H/K-ATPase::ChR2 (L132C;H134R;T159C)* protomers ranging from 1/4 to 4/4.

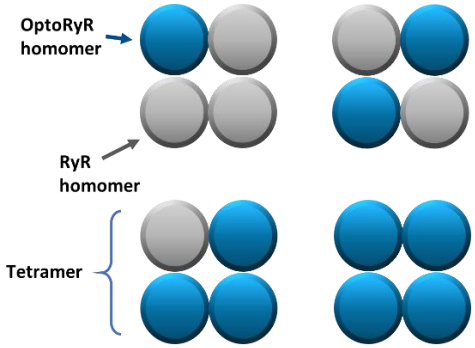

Figure 33: Top view of the chimeric RyR channels. Potential assembly of the different chimeric RyR channels when optoUNC-68 and WT-RyR of C. elegans are simultaneously expressed.

I first analysed animals carrying a fosmid containing the entire genomic locus of *unc-68*. In these the C-terminus was modified by bacterial recombineering, to encode, in-frame, the fluorophore mKate, the ß-subunit of the H^+/K^+-ATPase to ensure the correct orientation of the modified ChR2 variant and ChR2(L132C;H134A;T159C) (termed "CatCh-up"). The fosmid *punc-68::unc-68::mKate::ß-H/K-ATPase::ChR2(L132C;H134R;T159C)* was injected by Dr. Elisabeth Fischer at a concentration of 1ng/µl.

For the detection of locomotion defects, a first and straight forward experiment is counting the body thrashes that the animals perform in a swimming assay. As *C. elegans* exhibits swimming locomotion in liquid media and this test is very sensitive for detecting defects in locomotion, this assay can be performed to reveal subtle differences better than an assay for crawling on a solid surface (Li and Kim 2008). Animals of different strains were submerged in liquid buffer and analysed. The following box plots represent the effect of the injected plasmid, that was tested in a thrashing assay during a period of 60s without stimulus, followed by 60s of illumination of 0.5mW/mm² 470nm light and a recovery period of 60s without stimulus. *Figure 34* and 35 depict the strains ZX1966 *unc-68(r1162)V; lite-1(ce314),zxEx797[punc-68::unc-68::mKate::ß-H/K-ATPase::ChR2 (L132C;H134R; T159C)* (1ng); *pmyo-3::GFP],* and the control *unc-68 (r1162)V; lite-1 (ce314)* and the deletion mutant *unc-68(r1162)*. Each of them was supplemented with ATR overnight at RT or without ATR before the measurement.

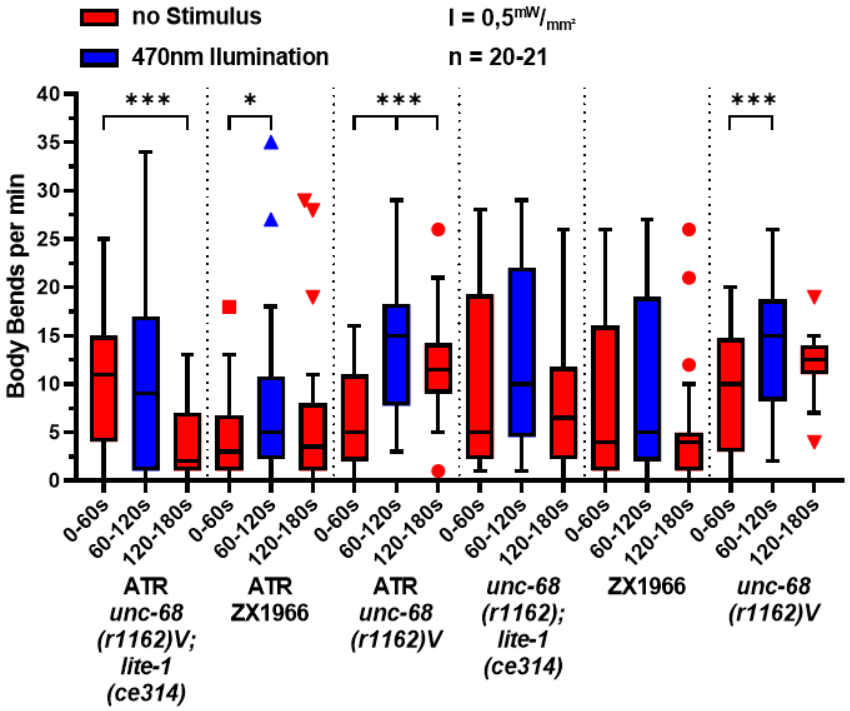

Figure 34: The rescue plasmid enhances thrashing rate in deletion mutants. Thrashing assay of *unc-68 (r1162)V; lite-1 (ce314)* and ZX1966 shows body bends per min before during and after blue light illumination. Red: 60s no stimulus, blue: 60s 470nm 0.5mW/mm². Animals were fed overnight on agar plates with ATR 0.2% in OP50 and without ATR. Comparison of ATR *unc-68 (r1162)V; lite-1 (ce314)* and ATR ZX1966 shows a significant difference during 0-60s no stimulus. Box plot, two-way ANOVA with Bonferroni correction, ***: $p \leq 0.001$, **: $p \leq 0.01$, *: $p \leq 0.05$. Median, IQR, Tukey-whiskers plus outliers.

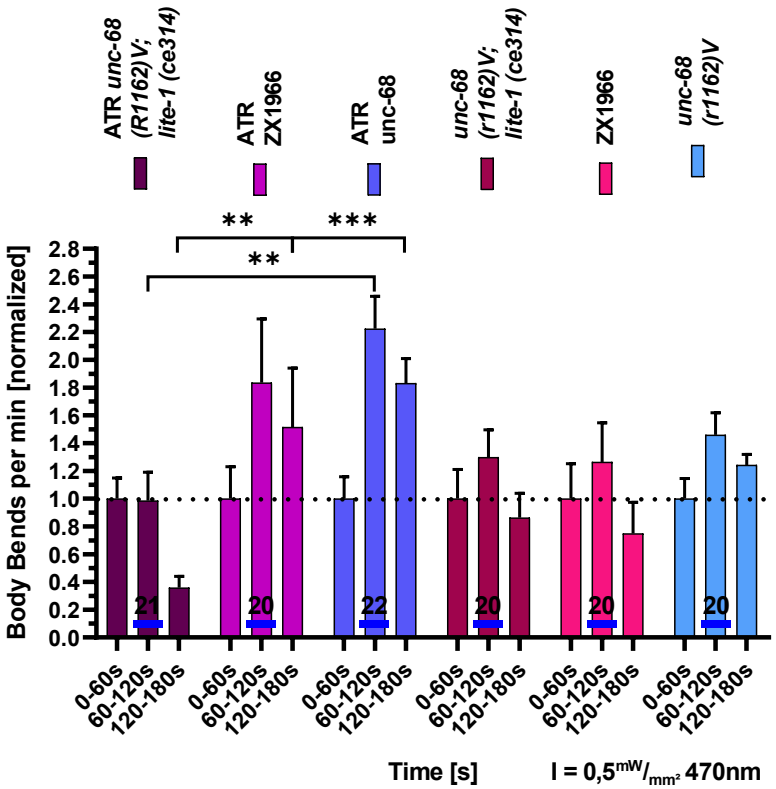

Figure 35: Light stimulation increased thrashing rate of ATR supplemented transgenic animals, in relation to no stimulation. Swimming cycles per minute for each strain and condition. Comparison of time frame 120-180s of both, ATR ZX 1966 and ATR *unc-68* with ATR *unc-68 (r1162)V; lite-1 (ce314).* Stimulation protocol: 60s no stimulation, 60s 470nm 0.5mW/mm² stimulation and 60s no stimulation. Photostimulation denoted by blue bar, n numbers for each strain are given over the X-axis. Transgenic strains were analysed by two-way ANOVA, with Bonferroni correction to the corresponding time frame of the respective control, ***: $p \leq 0.001$, **: $p \leq 0.01$, *: $p \leq 0.05$.

Statistical significance is evident from the results of the comparison of 0-60s to 60-120s and 0-60s to 120-180s within the strain, by two-way ANOVA . It revealed a significant change in body bends per min (bbpm) for the strain *unc-68 (r1162)V; lite-1 (ce314)* with ATR during the time frames 0-60 s/120-180s (*Figure 34*). Additionally, the ATR supplemented strain ZX1966 had a significant difference, when 0-60s and 60-120s are compared (*Figure 34*). Though, there is also significance for the control without ATR supplementation in the time frame 0-60s/60-120s, with the p-value 0.05, indicating a response to blue-light exposure.

The normalized data (*Figure 35*) of ATR fed *unc-68 (r1162)V* and ZX1966 animals illustrates the relative strong increase of thrashes during and after photostimulation but no significant change of swimming cycles of *unc-68 (r1162)V; lite-1 (ce314)* animals. The significantly changed bbpm after photo stimulation of ZX1966 and *unc-68 (r1162)V; lite-1 (ce314)* underline that the strain ZX1966, with a deleted RyR in *lite-1* background, is affected by blue light illumination, and even more after termination of photo stimulation. Control animals without ATR supplementation are not changing behaviour significantly during and after blue light exposure.

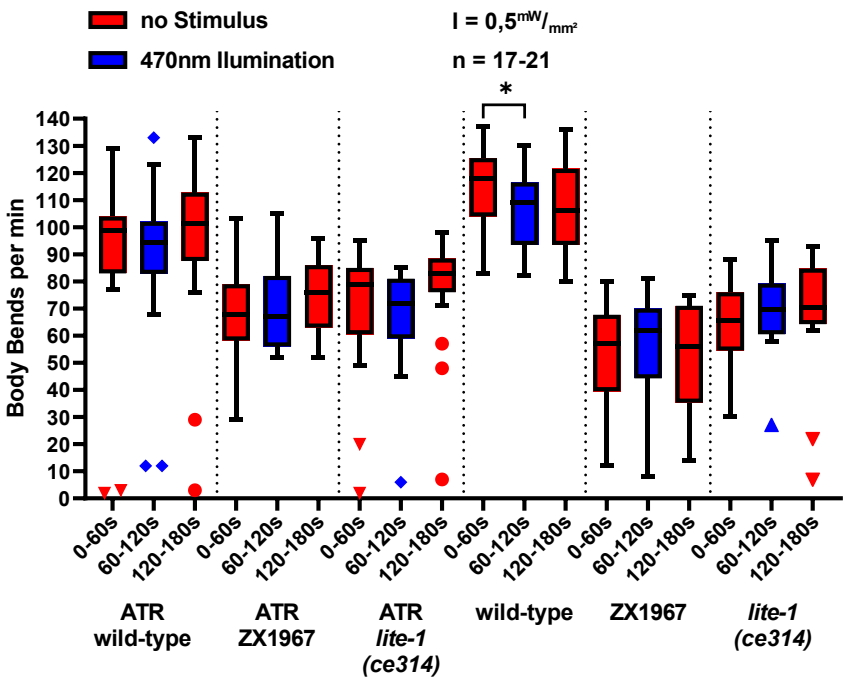

Figure 36: ZX1967 displays similar swimming behaviour as *lite-1 (ce314)*. Wild-type animals without ATR supplementation are reducing thrashing rate significantly during stimulation. Red: 60s no stimulus, blue: 60s 470nm 0.5mW/mm². Animals were fed overnight on agar plates with ATR 0.2% in OP50 and without ATR. Median, IQR, Tukey-whiskers plus outliers.

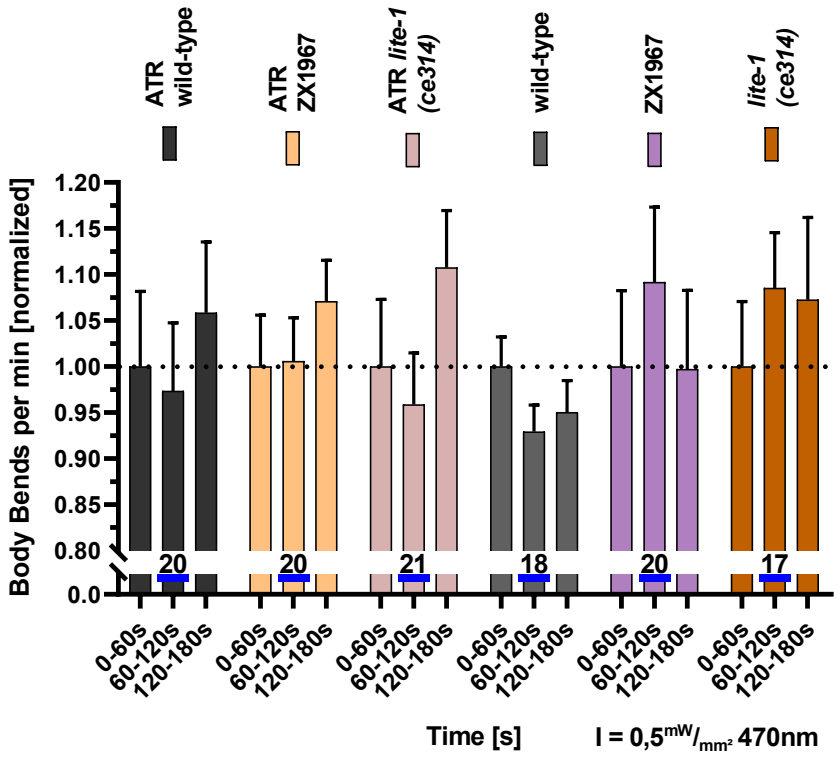

Figure 37: The rescue plasmid has no notable effect in *lite-1* background. When comparing the respective time intervals of ATR-fed animals, no unsuspected differences could be found, the same applies to the non-supplemented animals. Red: 60s no stimulus, blue: 60s 470nm 0.5mW/mm². Animals were fed overnight on agar plates with ATR 0.2% in OP50 and without ATR. Median, IQR, Tukey-whiskers plus outliers.

In *Figure 37* the results of the strains ZX1967 *lite-1(ce314), zxEx797[punc-68:.unc-68::mKate:: ß-H/K-ATPase::ChR2(L132C;H134R;T159C)* (1 ng); *pmyo-3::GFP*] and the control strain *lite-1 (ce314)* (from now on only *lite-1*) can be seen. Light protocol and statistics were performed as described above. Significances were calculated with ANOVA for the strain ZX1967 and the control *lite-1* after light stimulus in the time frame 120-180s. Comparison of the time frames 0-60s to 60-120s and 0-60s to 120-180s using a paired two tailed t-test revealed no substantial change in thrashing rate for animals with ATR or without supplementation.

To rule out that the response to blue light exposure is merely a natural reaction of *C. elegans* to changing light conditions, animals of the control strains wild-type and *unc-68* deletion mutants were also examined under the same light settings. As depicted in *Figure 36* and *Figure 37*, wild-type animals exhibited decreased swimming cycles (114 ± 3.66bbpm to 107 ± 3.29), when no stimulus time frame is compared to blue light stimulus. Thrashes of the deletion mutant animals in *Figure 34* (*unc-68 (r1162)V*) are, 0-60s: 6.5 ± 1.03; 60-120s: 14.5 ± 1.52; 120-180s: 11.9 ± 1.15. There was also a substantial raise in thrashes (bbpm: 0-60s: 9.7 ± 1.41; 60-120s: 14.2 ± 1.54; 12.1 ± 0.75) for the time frame 0-60s/60-120s, for animals without ATR supplementation. It is important to note that while wild-type responds to blue light with a reduction in swimming cycles, the deletion mutant does the opposite with an almost doubled swimming rate, which can be seen best in *Figure 35*.

Figure 34 reveals that some animals of strain ZX1966 with ATR supplementation were thrashing at a drastically higher frequency than control *unc-68 (r1162)V; lite-1 (ce314)* animals, both during and after blue light exposure. This might indicate that folding and assembly of the protein encoded by the fosmid *punc-68::unc-68::mKate::ß-H/K-ATPase::ChR2(L132C;H134R;T159C)* worked out better than in other animals or it was expressed stronger in some animals (Evans 2021). The fact that the fosmid exhibits no rescue suggests that the ChR2 may cause interference at the C-terminus. Unfortunately, it could not be shown whether the fosmid alone is capable of rescue without ChR2, so the exact problem cannot be named. A possible reason for the lack of rescue could be the relatively small injection amount of 1ng.
The fact that the fosmid *punc-68::unc-68::mKate::ß-H/K-ATPase::ChR2 (L132C;H134R;T159C)*, worked out, albeit to a lesser extent than expected, led to the approach outlined in the next chapter, the introduction of human RyR into *C. elegans*. Furthermore, it was argued that the cDNA as a plasmid might be more manageable than the fosmid. In addition, it was demonstrated in HEK cell lines that N-terminal fusion works (Sasse Lab).

3.2. Investigating whether functional expression of human ryanodine receptor 2 is possible in *C. elegans*

Each subunit of the homotetramer of RyR2, comprises ~5000 amino acids, thus forming a 560kDa Structure. The groups of Bhat et al. and Zhao et al. found that one-fifth of the C-terminus builds the channel conducting pore, while ~4000 AA constitute the "head" of RyR in the cytosol (Franzini-Armstrong and Protasi 1997; Meissner 1994; Coronado et al. 1994). A truncated version, comprising only the SR-membrane bound C-terminal sequences demonstrated sensitivity to ryanodine, a regulation by Ca^{2+} and single channel conductance comparable to the full-length RyR. This suggested, even before a full-length high-resolution structure was available (Des Georges et al. 2016; Peng et al. 2016; Zalk and Marks 2017), that the ~1000 AA C-terminus harbours the ionic pathway, the Ca^{2+} binding site and the ryanodine binding sites, that are necessary for a working channel (Bhat et al. 1997; Zhao et al. 1999; Chen et al. 1998). Recent studies found that the first Ca^{2+}-binding site can be found in the C-terminal domain (AA4957-5037) and the cytosolic membrane leaflet in the core solenoid (AA 3667-4174) (Des Georges et al. 2016). With this information in mind, a truncated version of RyR (RyR_{Pore}) will be generated in this thesis.

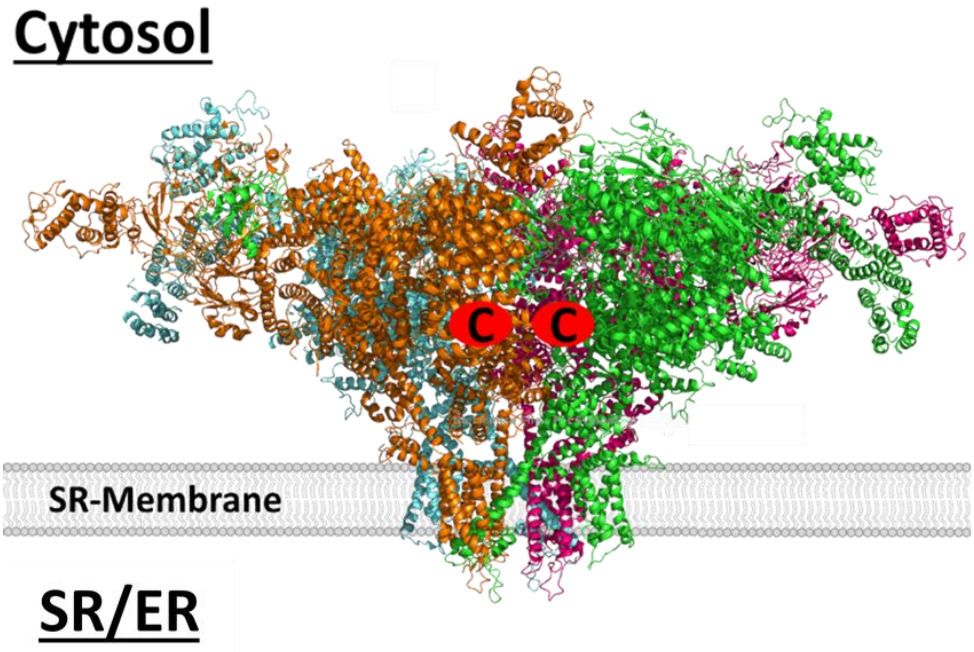

Figure 38: Ryanodine receptor in the SR/ER membrane. *The red circles indicate the position of the* C-termini in the centre of the RyR head, in the middle of the ion pore. Structure of RyR2 (6JHN)(Chi et al. 2019), image generated with PyMol.

The same principle that applies to the RyR_{Pore} construct is also applied here, with the difference that an N-terminal fusion of the CatChUP construct (consisting of Linker EYFP and CatChUP), will be realised with the complete ryanodine receptor. This should avoid steric hindrance as the N-terminus is located at the top of the pore in the cytosolic head. The functionality of this construct would rely on the presence of a mechanical coupling through the linker with CatChUP. The other opening mechanism would be based on RyR2 as the facilitator of CICR, mediated by the cytosolic EF-hands (Zalk et al. 2015).

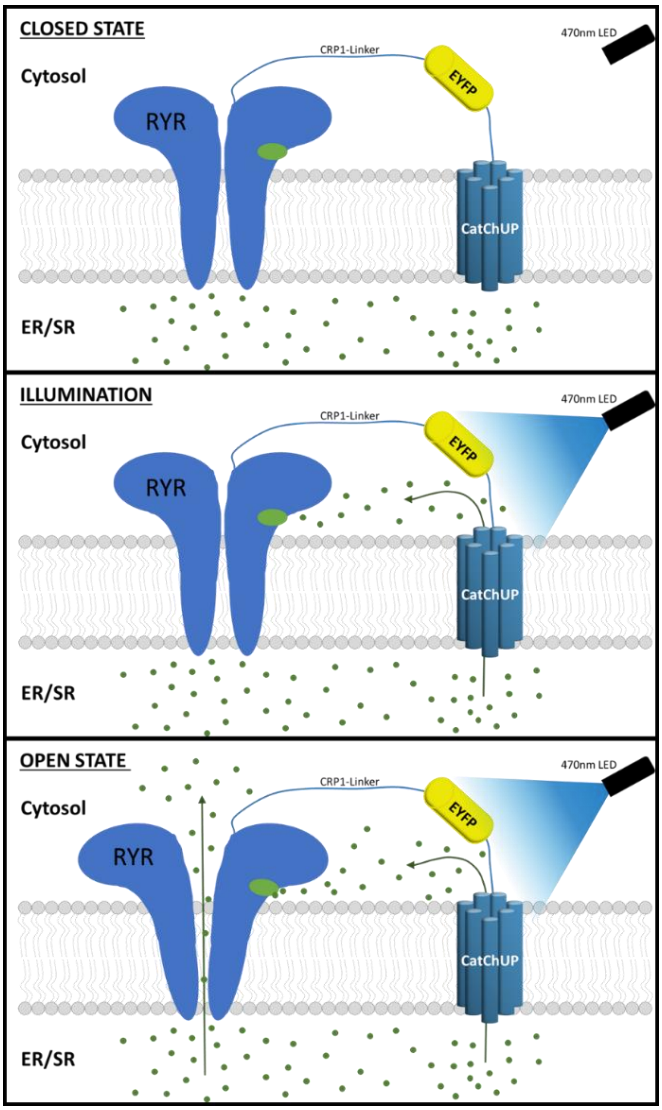

Figure 39: Schematic of the different states of RyR in the SR/ER membrane. Open and closed state under 470nm blue light illumination. Top: Closed state: CatChUP is not photoactivated by blue-light. No Ca^{2+} ions are binding to Ca^{2+}-binding sites (green oval) of the RyR. Middle: Illumination: Blue-light illumination causes Ca^{2+} efflux from the SR into the cytosol, thereby Ca^{2+} can bind to the Ca^{2+}-binding sites. Bottom: Open state: Bound Ca^{2+}-binding sites lead to a conformational change which leads to the opening of the RyR channel. An open RyR releases all Ca^{2+} ions from the SR into the cytosol, which subsequently leads to a cascade of other RyRs, if not already activated by the local Ca^{2+} efflux of CatChUP. The strong raise of Ca concentration results in an action potential.

Homology of the UNC-68 protein in *C. elegans* and cardiac RyR2 in *H. sapiens* is 63%, the sequence identity is 45% (Fischer et al. 2017). With that in mind, and the information obtained in 3.1. I attempted to express the cDNA of human ryanodine receptor 2, provided by the Andrew R. Marks Laboratory, in *C. elegans* by using the body wall muscles (BWM) promoter pmyo-3.

3.2.1. Expression of a truncated version of hRyR2 in *C. elegans muscle cells*

The extraordinary size of the RyR makes it a challenging protein to manage, when it comes to molecular and microbiological manipulations. With a molecular mass of 2.3 MDa it is one of the largest known ion channels. When this work began, it was not known, whether the C-terminus was located on the ER-lumenal or cytosolic side. Based on the results of Bhat et al., who could show that a truncated version of RyR already has Ca^{2+} activatable pore functions on the lipid bilayer membranes , a first attempt was made to find out if a shortened version of hRyR2 would work in *C. elegans* (Bhat et al. 1997).

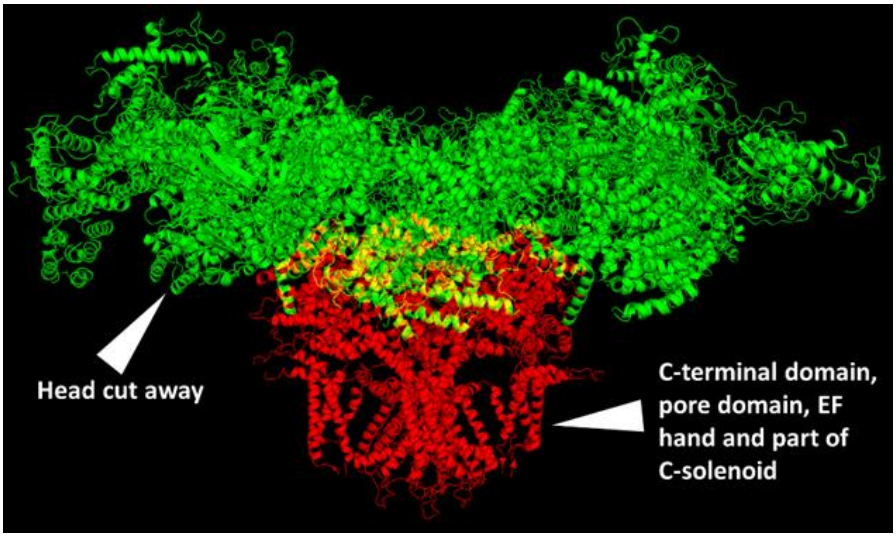

Figure 40: Human Ryanodine receptor 2. Red: C-terminal domain, pore domain, EF-hand and part of the C-solenoid. Localized in the SR membrane. Green: Head of RyR2, localized in the cytosol. Structure of RyR2 (6JHN)(Chi et al. 2019), image generated with PyMol.

In a truncated version hRyR2 comprises the amino acids (AA) 1-188 and 3925-4967. 188 AA of the N-terminus were retained. The C-terminal domain, the pore domain, the EF-hand and part of the C-solenoid form the main channel in the SR-membrane. Bhat et al. 1997 demonstrated these transmembrane domains as a very important part of the RyR pore function, and sufficient to ensure a functional channel activity in Chinese hamster ovary cells. With that in mind the C-terminus of RyR_{Pore} was linked to CatChUP via a flexible G_4S-linker and YFP to create the $OptoRyR_{Pore}$. C-terminal fusion of CatChUP and RyR_{Pore} was only promising, if the pore was not affected by steric hindrance or other obstruction caused by the interaction of the linker and the head.

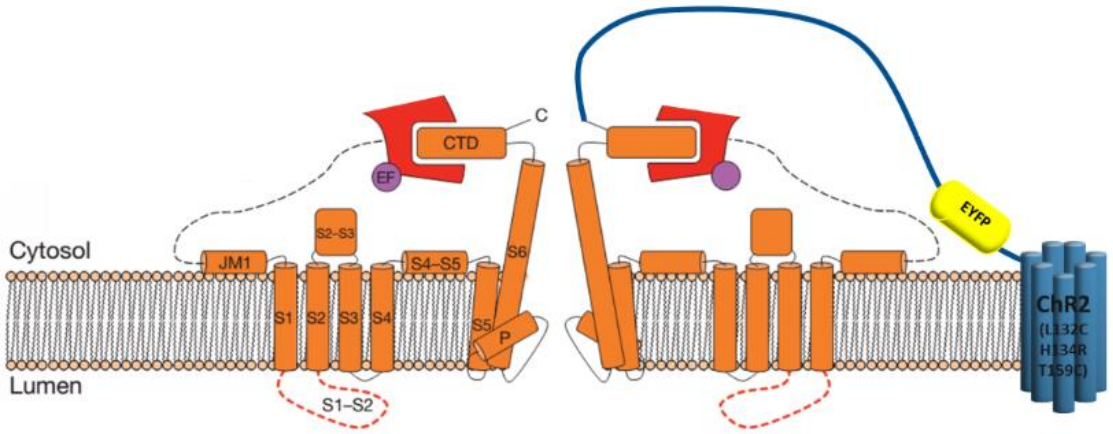

Figure 41: Schematic of OptoRyRPore. The remaining pore of RyR after truncation and linking to CatChUP, EYFP and G4Slinker C-terminally. Adapted from (Zalk et al. 2015).

3.2.1.1. Potential effects of RyR_{pore} on locomotion were examined in thrashing assays

RyR_{pore} was equipped with a linker to connect the fluorophore mNEON to it, in order to detect a SR-membrane retention of the construct pmyo-3::hRyR2short::Gly-Ser-linker::mNEON (RyR_{pore}).

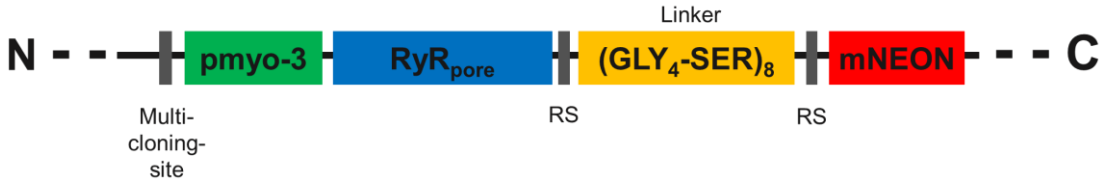

Figure 42: Simplified construct map of pFB03 (pmyo3::hRyR2 short::Gly-Ser::mNEON) illustrates RyR_{pore} including a C-terminal fused linker and fluorophore.

Figure 43 depicts the results of swimming assays performed with the strain *unc-68 (r1162)* and the lines 1-8 *unc-68 (r1162) [pmyo-3::hRyR2short::Gly-Ser-linker::mNEON(1.5ng/µl); pmyo-2:: mCherry (1.5ng/µl)]*, after injection. Very low background light for the camera was used for 60s video capturing. Mean: 9.2; 5.6; 15.7; 4.8; 5.3; 7.1; 8.2; 7.6; 9.4. Median: 7; 6; 15.5; 2.5; 4; 8; 7.5; 4.5; 9. One-way ANOVA with Bonferroni correction, calculated no significant differences between *unc-68 (r1162)* control and the lines 1-8. Line 2 animals were thrashing the most. When *unc-68 (r1162)* animals are compared we see a raise of mean from 9.2bbpm ± 1.29 to 15.7bbpm ± 3.47 and median from 7 to 15.5bbpm. Unfortunately, the statistics are not significant, to prove that we have a significant alteration of movement of the UNC-68 deletion here. Analysis of the transgenic animals under the microscope for mNEON fluorescence, could not provide indications for associated expression of RyR_{pore}. Furthermore, it should be pointed out, that strain ZX2274 (data not shown), did not show any significant difference of movement, even without any additional linker and fluorophore. Taken together, the data of strains with injected RyR_{pore}, do not provide evidence, that hRyR2 could alter the UNC-68 deletion in this way.

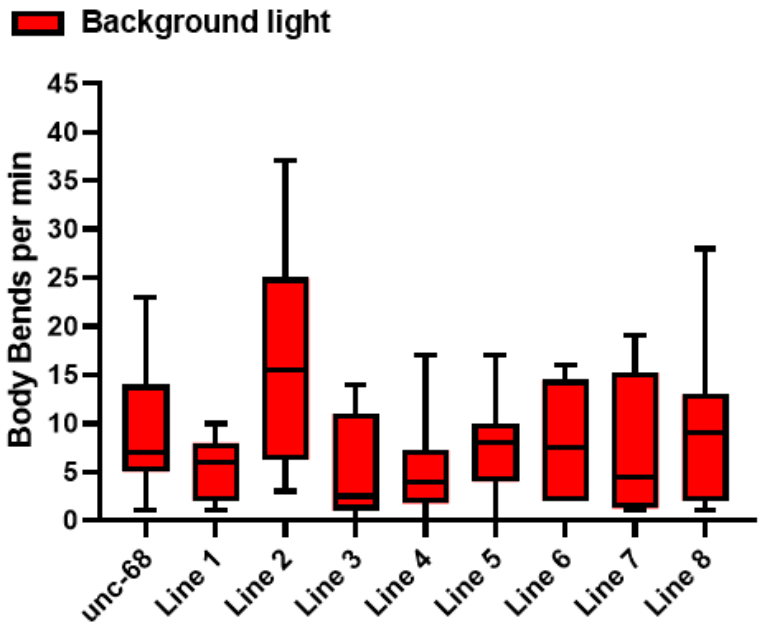

Figure 43: Basal thrashing rate of transgenic rescue strains. A) *unc-68* and RyR_{pore} [*pmyo-3::hRyR2short::Gly-Ser-linker::mNEON; pmyo-2::mCherry]* injected strains. n: 23, 8, 10, 10, 10, 11, 6, 8, 11. Box plot, median, whiskers: 2.5 to 97.5.

3.2.1.2. The effect of RyR_{pore} CDL on the swimming cycles

The results of the preliminary experiments revealed no significant change with a truncated hRyR2 version compared to the deletion mutants. The new version RyR_{pore} CDL was created with a longer central domain. This was done because we speculated, some of the missing parts of the N-terminal domain could be required to achieve a functional or at least partially functional expression and/or assembly of the hRyR2 tetramer. To investigate this, the plasmid pFB04 (pmyo-3::mNEON::hRyR2short CDL) was created.

This plasmid (*Figure 45*) served as the basis for the insertion of the LOV2 domains at various sites (LOV2 1-4) see the following chapters.

Figure 44: Simplified plasmid chart of pFB04 pmyo3::mNEON::RyRpore CDL illustrates RyR_{pore} including a long central domain and including a N-terminal fused fluorophore.

3.3. Attempting to achieve photo-triggering of the truncated hRyR2 through the LOV2 domain

The truncated hRyR2 did not alter the behaviour of deletion mutant animals. Either, it is not functional in the truncated form, or the human RyR2 is not functional in the *C. elegans* background, e.g. due to different membrane composition. Expression could not be verified by fluorescence imaging. However, it may lie below the detection level. Nevertheless, it seemed possible that a pore-forming tetramer could be present, that could not be triggered by Ca^{2+} ions, but may be activated by conformational changes. Channelrhodopsins, while offering a good possibility to create light activatable tools at the plasmamembrane, would not work with the truncated hRyR2, as it could only act via the Ca^{2+} conductance out of the SR lumen. However, ChRs are not the only option to transform a channel, transporter or enzymes into a light triggered instrument. Optogenetic tools can also be triggered by conformational changes, e.g. by inducing structural perturbations. Here, I tried to use the LOV2 domain to evoke a conformational change in the human ryanodine receptor upon blue light stimulation. This approach would also alleviate the need for ATR supplementation. In this way, a hRyR2 "optoRyR", activated by blue light, is supposed to evoke a reaction that either increases or reduces the length of body wall muscles or the number of swimming cycles of *C. elegans*.

3.3.1. Integration of LOV2 domain into $RyR2_{pore}$ CDL

The basis for the integration of the LOV2 domain into the RyR_{pore} CDL were the reports of Dagliyan et al. 2019; Dagliyan et al. 2016. Their work demonstrated that inserting a LOV2 domain into a host protein at strategic locations, e.g. in a β-hairpin or a loop between adjacent α-helices, can induce light-dependent disorder in the host protein without disturbance of its structure in the dark state. The choice of integration sites of the LOV2 domain into a target protein was determined by first identifying the potential loop sites using high resolution 3D structural images. Care must be taken to ensure a certain stability of the target protein. Domain insertions are most effective in structures that contain a tight, short, surface-exposed loop connecting interacting structural units (Dagliyan et al. 2019). In this project, the focus was on finding sites that provide enough space for LOV2 not to disturb the hRyR structure too much or lead to steric hindrances. Yet, they should be close enough to cause a change in the spatial structure of RyR upon light activation of LOV2. It had to be ensured that the distance between the beta-sheets or alpha-helices was about 10-15 Angström (Halavaty and Moffat 2007; Dagliyan et al. 2019), as this is the distance between the LOV2 C- and N-termini. Here, the conformational change of LOV2 should lead to an increase in the gating probability of RyR_{pore}. The plasmid shown schematically in *Figure 45* was generated according to these specifications, creating the versions LOV2 (1-4):

- LOV2 (1): replaces SGKDVID sequence near high affinity Ca^{2+} binding site
- LOV2 (2): replaces GSAKR sequence between β1 and β2 near the U-motif
- LOV2 (3): replaces luminal TSSVVEGKELPTRSSSENAKVTSLDSSSHRIIA sequence between β-strands in the voltage sensor
- LOV2 (4): replaces cytosolic voltage sensor domain sequence GEFYG

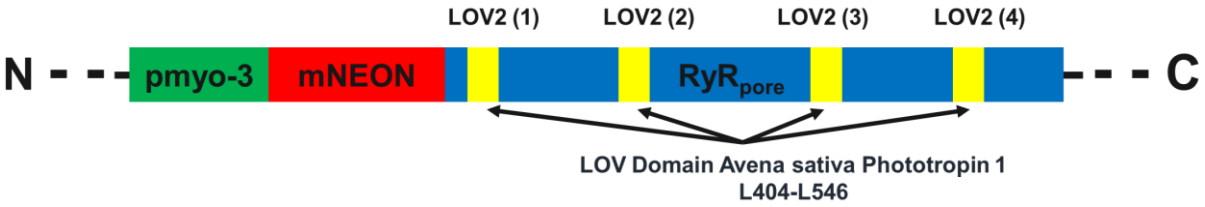

Figure 45: Schematic location of the LOV-RyR$_{pore}$ construct, including integration sites LOV2-domain in the RyR$_{pore}$. Promoter (green), fluorophore (red), RyR$_{pore}$ CDL (blue), integration sites of LOV2-domain L404-L546 (yellow).

3.3.2. Examination of possible light dependent effects on optoRyR$_{pore}$-LOV2 inserted strains

Exposure of *C. elegans* to blue light must be considered critically and requires a careful approach, as the worms react very sensitively to blue light which evokes light avoidance behaviour or reversals. The first attempts to find a light-dependent effect of optoRyR$_{pore}$-LOV2 ("opto" refers to strains including a light sensitive protein) were carried out with wild-type animals, exposed to different light intensities, to determine the threshold at which they respond to blue light. Subsequent assays would repeat the protocol in *lite-1* background. The swimming assay started with 30s background light, followed by 30s 470nm 0.16mW/mm². This, and another (0.19 mW/mm²) low intensity was chosen to find the one at which wild-type animals do not yet react to the blue light illumination. As depicted in *Figure 46*, this led to no significant response, as shown. By statistical tests in bbpm (A) and normalized thrashes (B), neither for wild-type nor for animals expressing any of the LOV2 inserted optoRyR$_{pore}$ animals. However, it is striking that all transgenic strains clearly exhibit fewer thrashes even in the non-stimulated state (0-30s), which can be attributed to the influence of the plasmid. An exposure of 470nm 0.16mW/mm² is not sufficient to elicit a significant light response in wild-type animals. The result of the slightly higher illumination (*Figure 47*) was, that wild-type animals reacted to the blue light illumination by decreasing thrashes by 15%, best seen in B). LOV2 containing strains, on the other hand, did not react as intensely. A fluorescent signal of the construct of the transgenic strains could not be detected by fluorescence microscopy, except for the co-marker.

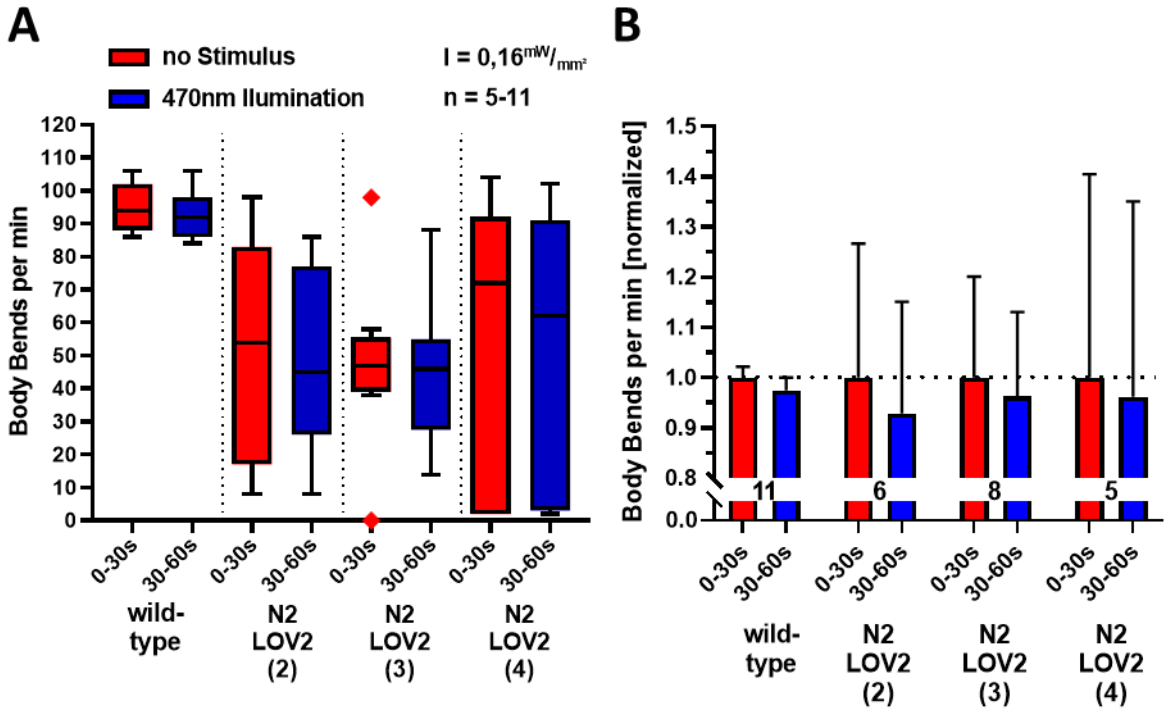

Figure 46: Low blue light intensity does not provoke light dependent changes of swimming behaviour. A) Depicted are bbpm of the strains wild-type, N2 LOV2 (2), N2 LOV2 (3), and N2 LOV2 (4), before and during blue light illumination. B) Normalized data of A) displays a relatively high SEM of optoRyR$_{pore}$-LOV2 inserted strains. Red: 30s no stimulus, blue: 30s 470nm 0.16mW/mm². Box plot, median, IQR, Tukey-whiskers plus outliers. Normalized data of A) with SEM

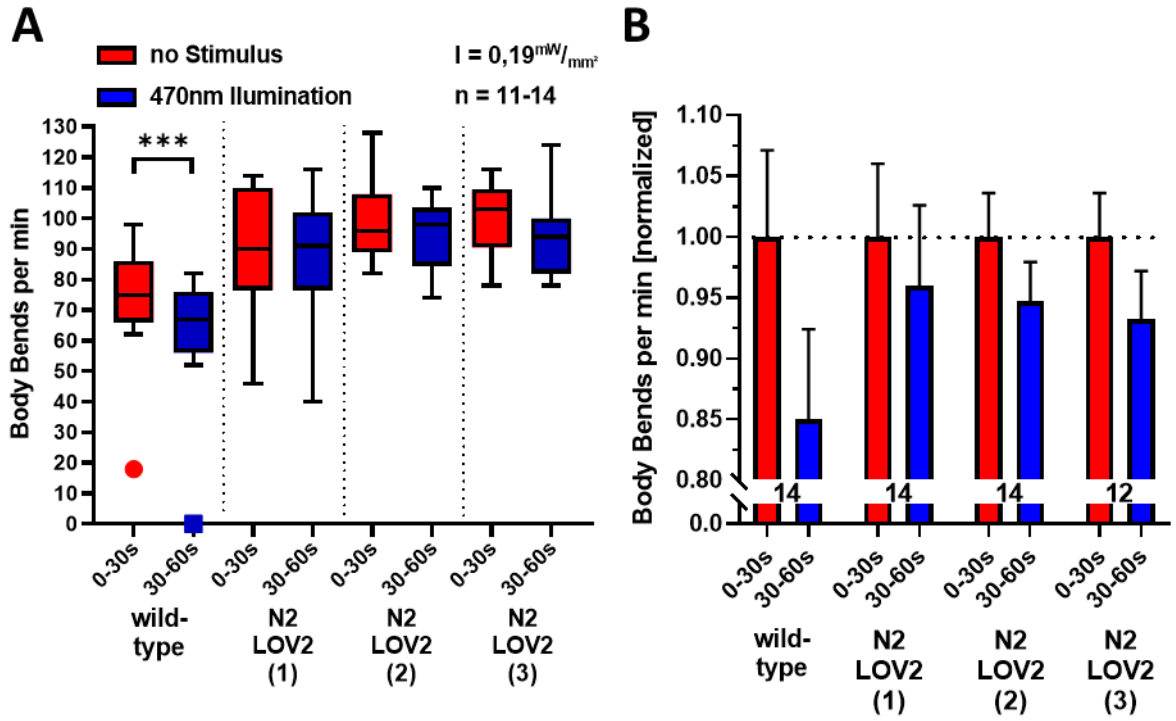

Figure 47: Wild-type animals start to respond to blue light stimulation at 0.19mW/mm². Thrashing assay of wild-type and N2 LOV2 (1), N2 LOV2 (2), N2 LOV2 (3), shows body bends per min before and during blue light illumination. Red: 30s no stimulus, blue: 30s 470nm 0.19mW/mm². A) Wild-type animals significantly decrease the thrashing rate as long as blue light is shining. Box plot, two-tailed paired t-test, ***: $p \leq 0.001$, **: $p \leq 0.01$, *: $p \leq 0.05$. Median, IQR, Tukey-whiskers plus outliers. B) optoRyR$_{pore}$-LOV2 inserted strains do not respond notably to photostimulation. Normalized data of A) with SEM.

3.3.3. Excluding light avoidance behaviour with in the *lite-1* background

Light perception of *C. elegans* is conferred to large extent by the protein LITE-1. Inducing a light avoidance behaviour through UV- and blue light exposure (Gong et al. 2016), leads to a change in speed and direction of movement (Edwards et al. 2008). To exclude a possible light avoidance reaction the plasmids pFB05-08 were also injected into strain *lite-1 (r1162)* and tested under the same conditions. The results of *lite-1* animals in *Figure 48* are similar in tendency, when compared to wild-type results. The apparent trend of the strains to reduce thrashes, could not be confirmed by the normalised values in B), comparing the change from pre-stimulation to stimulation (*lite-1*: -10.3%, lite-1 LOV2(1): -1.2%, lite-1 LOV2(2): 2%, lite-1 LOV2(3): -2.8% and lite-1 LOV2(4): -7%). A two-way ANOVA is only significant for *lite-1*, wherein the mean dropped from 67bbpm ± 2.7 to 60.1bbpm ± 2.9. An intensity of 0.19mW/mm² could not evoke light dependent reaction in lite-1 LOV2 animals.

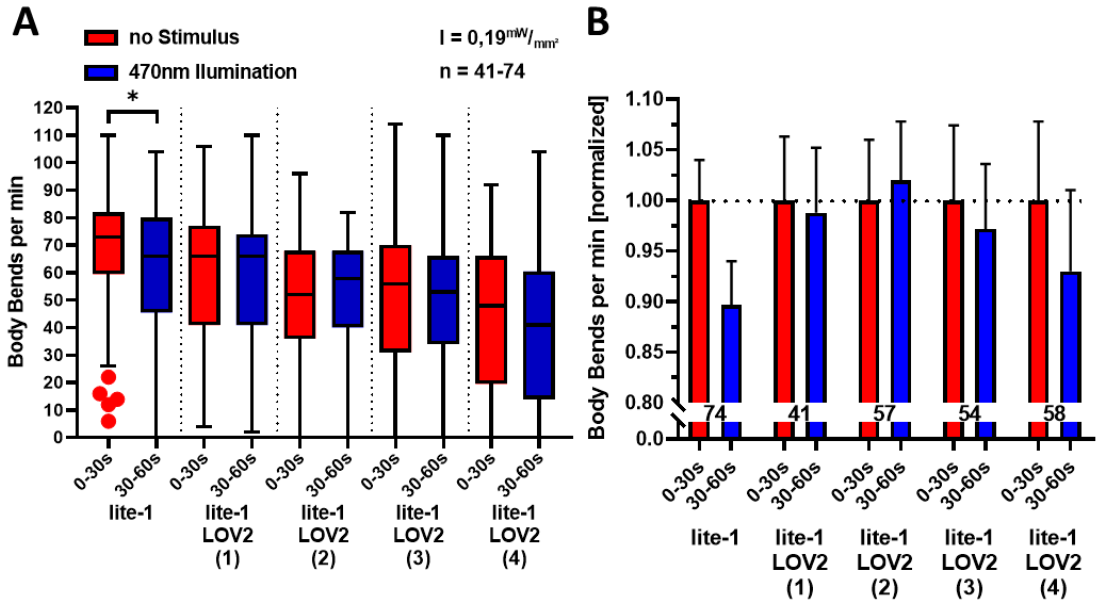

Figure 48: *lite-1* animals exhibit a light dependent change of swimming behaviour under 0.19mW/mm² illumination. A) Two-tailed paired t-test of *lite-1* animals reveals a significant difference when comparing before and during light stimulus. B) The analysis of optoRyR$_{pore}$-LOV2 inserted strains versus the control *lite-1* did not indicate a clear difference. Box plot, two-tailed paired t-test, ***: p ≤ 0.001, **: p ≤ 0.01, *: p ≤ 0.05. Median, IQR, Tukey-whiskers plus outliers.

Next, we further increased the light intensity to determine if the LOV2 insertions needed a higher light intensity to be activated and provoke effects. The light depending response of *lite-1* animals to 0.19mW/mm² creates the expectation that a more than doubled intensity of 0.42mW/mm² would also evoke a significant reduction in thrashes. This would also extend to the optoRyR$_{pore}$-LOV2 strains, but here we have none in any of the tested strains. A reason for this could be the shortened no illumination period, albeit no stimulus should not change the behaviour of *C. elegans* regardless how long the video is. Exceptions for that are fatigue- and rest-phases of the animals over very long periods of time. Illumination with 0.42mW/mm² did not lead to an increased response in swimming behaviour of animals injected with the plasmid optoRyR$_{pore}$-LOV2. One problem encountered, could be that the discrepancy between single animals of optoRyR$_{pore}$-LOV2 strains is quite high, compared to *lite-1*.

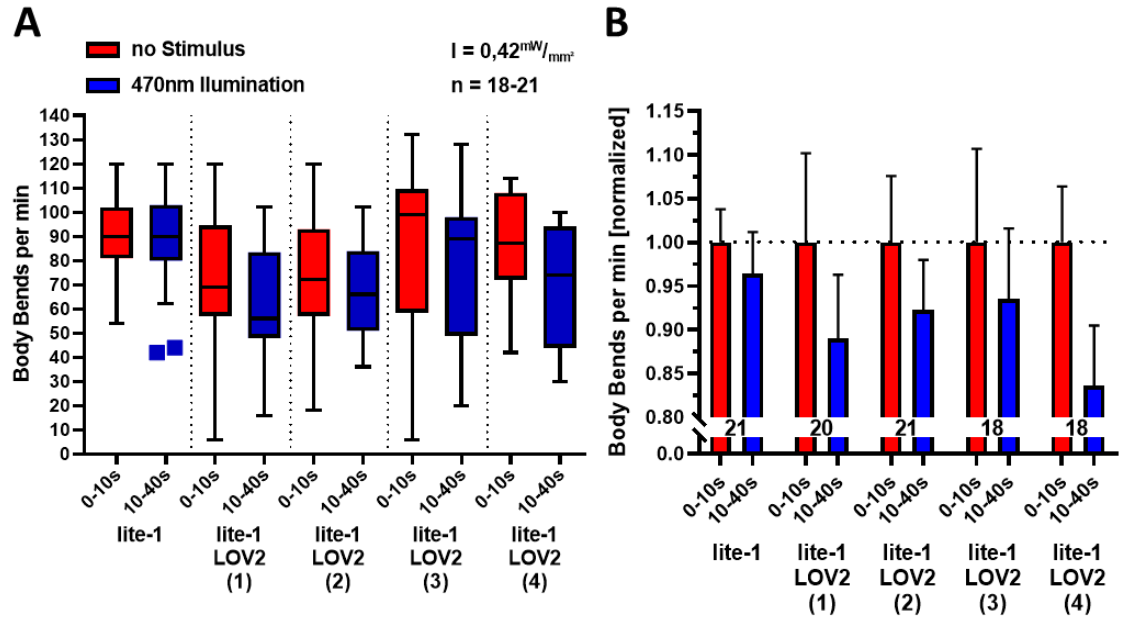

Figure 49: A further increase in light intensity could cause a decline of thrashes, in all strains when light stimulation was applied. A) Thrashing assay of *lite-1* and lite-1 LOV2 (1), lite-1 LOV2 (2), lite-1 LOV2 (3), lite-1 LOV2 (4), reveals the lowered thrashing rate during stimulation of all strains. B) Normalized data illustrate the reduction during blue light stimulation. Red: 10s no stimulus, blue: 30s 470nm 0.42mW/mm². Box plot, median, IQR, Tukey-whiskers plus outliers.

The highest, technically determined, tested light intensity was 0.53mW/mm², in the strains *lite-1* and lite-1 LOV2(4). The mean of lite-1 LOV2(4) did not change, although median decreased by 15.4%, which may indicate that some animals were responsive to blue light illumination. Based on the data of N2 LOV2(1-4) and lite-1 LOV2(1-4) animals, no definitive evidence was found that the construct of optoRyR$_{pore}$ including a LOV2 domain in (1) near a high affinity Ca^{2+} binding site, (2) replacing a β1 and β2 sheet near the U-motif, (3) replacing a luminal sequence between β-strands in the voltage sensor and (4) the replacement of a cytosolic voltage sensor domain, was expressed and assembled correctly in *C. elegans* and altered the thrashing rate of swimming behaviour.

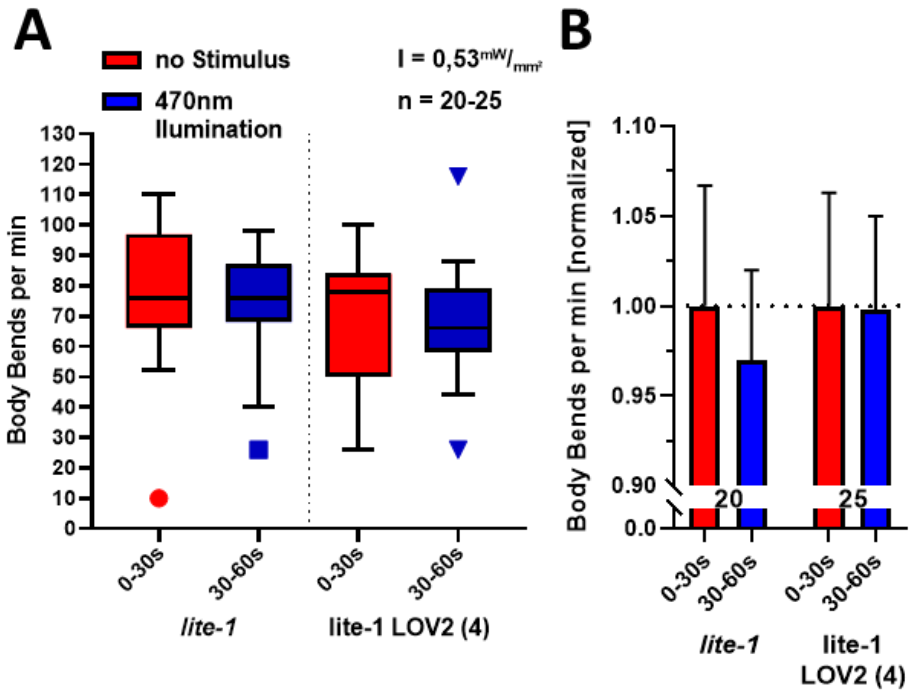

Figure 50: The highest intensity could not provoke a clear change of swimming behaviour. Thrashing assay of *lite-1* and lite-1 LOV2 (4), did not alter after initiation of stimulation. Red: 30s no stimulus, blue: 30s 470nm 0.53mW/mm². Box plot, median, IQR, Tukey-whiskers plus outliers.

3.3.4. Influence of reduced photostimulation intensity on the body length of optoRyR$_{pore}$-LOV2 inserted strains

Analysing the swimming behaviour is a sensitive test, yet it is possible that small changes in muscle contraction could be triggered by blue light illumination. To quantify contractions of the body wall muscles, we use the contraction assay. This assay differs from counting body bends per min in so far, that a higher magnification is used when measuring the body length of a single animal, and thus a small aberration can be detected. Whether optoRyR$_{pore}$-LOV2 led to a light triggered contraction or elongation of body wall muscles, can be analysed with the software KNIME and a customized evaluation protocol (Steuer Costa 2016).

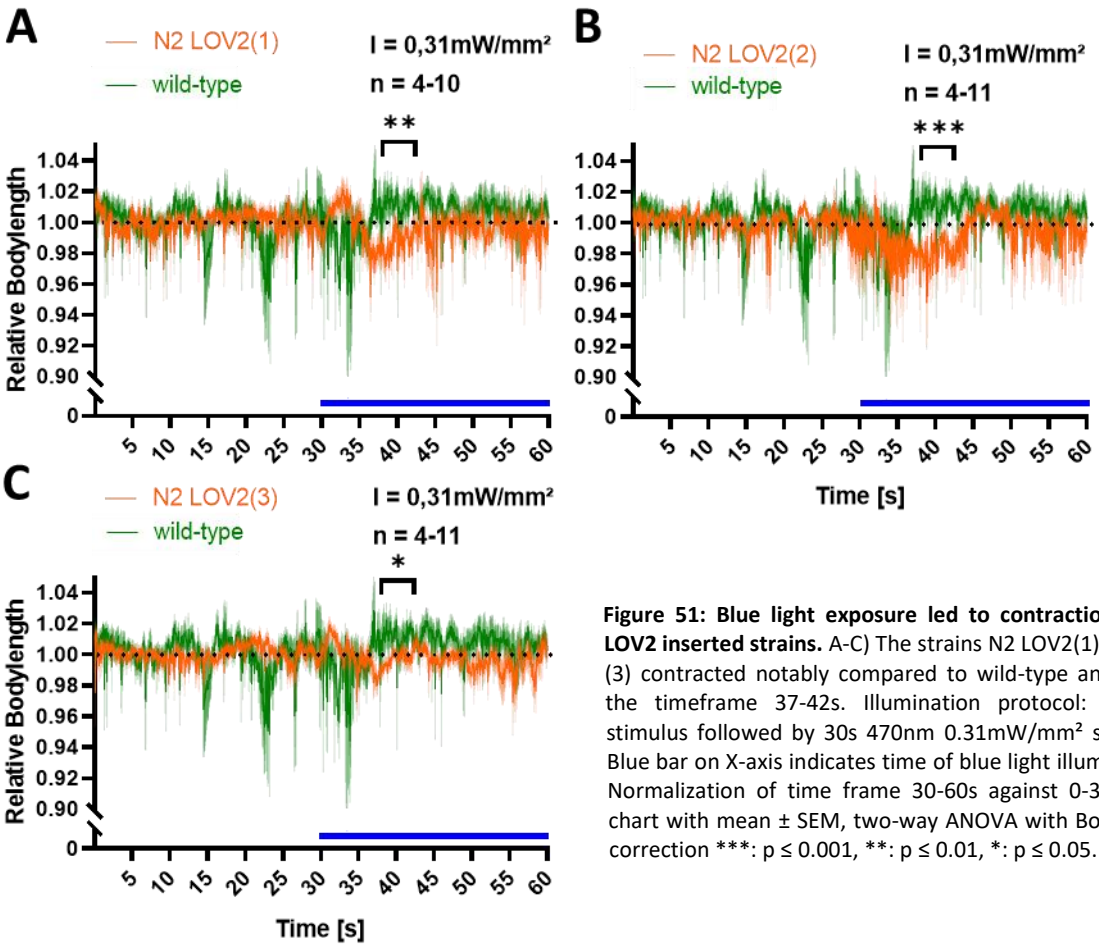

Figure 51: Blue light exposure led to contraction of all LOV2 inserted strains. A-C) The strains N2 LOV2(1), (2) and (3) contracted notably compared to wild-type animals in the timeframe 37-42s. Illumination protocol: 30s no stimulus followed by 30s 470nm 0.31mW/mm² stimulus. Blue bar on X-axis indicates time of blue light illumination. Normalization of time frame 30-60s against 0-30s. Line chart with mean ± SEM, two-way ANOVA with Bonferroni correction ***: $p \leq 0.001$, **: $p \leq 0.01$, *: $p \leq 0.05$.

Strains tested were N2 LOV2(1), N2 LOV2(2), N2 LOV2(3) (orange) including control wild-type (green) as depicted in *Figure 51*. By the time the experiments were performed, these were the only stable strains that carried a LOV2 insert. Marked significances were calculated by two-way ANOVA. Time frame 37-42s gives a significant contraction in relative body length for N2 LOV2(1), N2 LOV2(2), N2 LOV2(3) and wild-type. The strains contracted by 1.59%, 2.29% and 1.1%, compared to wildtype animals. The contraction persists only for 5s, before wild-type and transgene animals equalise again. With the onset of 470nm illumination at 30s, N2 LOV2(1) and N2 LOV2(2) animals, answer to blue light with an elongation of approximately 2%, followed by a contraction after 4s stimulus. The animals recover after 10 to 16s though not to baseline value. Wild-type, on the other hand, reacts in the opposite way, contracting immediately after the blue light stimulus and elongating after 6s.

Concluding from the results, it can be said that there is a slight contraction in the transgenic strains, however, this is very weak and only exhibits a significant difference due to the elongation of the wild-type control, which is contrary to the norm.

Here it can be speculated that not all body wall muscle cells expressed the inserted construct, hence the worm can adapt by recruiting more muscles that compensate and keep on moving. Since even in the more light sensitive wild-type animals, compared to *lite-1*, no conclusive results were obtained, lite-1 LOV2 strains were not measured any longer.

3.4. Targeting endogenous full-length UNC-68 (ceRyR) with an N-terminal, Ca^{2+}-conductive ChR2 variant (CatChUP)

Generation of an optogenetically triggered ryanodine receptor in *C. elegans* required a variant of the ryanodine receptor functional in *C. elegans*, and an optogenetic tool / approach to trigger the RyR, here termed. A truncated human RyR2 cDNA (see 3.2.1. Expression of a truncated version of hRyR2 in *C. elegans muscle cells*) was used, as it was available on a plasmid, yet this construct did not result in any behavioural rescue of *unc-68* mutants. It was therefore unclear whether a light-controlled version of this construct would work. Hence, I reiterated an earlier approach in the Gottschalk lab, described above (3.1.), using the *unc-68* gene for C-terminal modification with CatChUP (a Ca^{2+}-permeable variant of ChR2). This approach had been established by our collaborator Philipp Sasse (University of Bonn) based on human RyR2. CatChUP is based on the light-sensitive Ca^{2+} permeable channelrhodopsin-2 variant CatCh (Kleinlogel et al. 2011). Albeit, CatCh was optimized by mutation to CatChUP (ChR2 (L132C; H134R; T159C)), to increase photo sensitivity, retinal stability and (Ca^{2+})conductivity (Bergs et al. 2018). CryoEM structures of RyR1 and RyR2, revealed that the C-terminal helices are functionally linked to the central domain, which probably prevented our earlier approach from working (Efremov et al. 2015; Des Georges et al. 2016; Peng et al. 2016; Yan et al. 2015; Zalk et al. 2015). A more promising linkage to CatChUP, also in *C. elegans*, might therefore be the N-terminus of UNC-68.

Following that, "OptoUNC-68" was created in the genome of *C. elegans* by integrating the CatChUP::EYFP::CRP-1 into the *unc-68* locus, in which the CRP-1 as a rod-like protein connects CatChUP to the UNC-68 N-terminus distal to the plasma membrane. Transgene strains listed in *Table 16* were generated by SunyBiotech, using CRISPR/Cas9. The *unc-68* gene has two alternative first exons and two promoters, and it is unclear in which tissues these isoforms are expressed. Hence, the subsequent insertion at both sites in the trunk was achieved in strain "GOA14", which carries CatChUP::EYFP::CRP-1 in front of exon 1.1 and 1.2. By that expression in all possible isoforms of UNC-68, which is essential as remaining *unc-68* isoforms can at least partly compensate for most phenotypes (Marques et al. 2020). "GOA01" contains CatChUP::EYFP::CRP-1 only in front of exon 1.1.

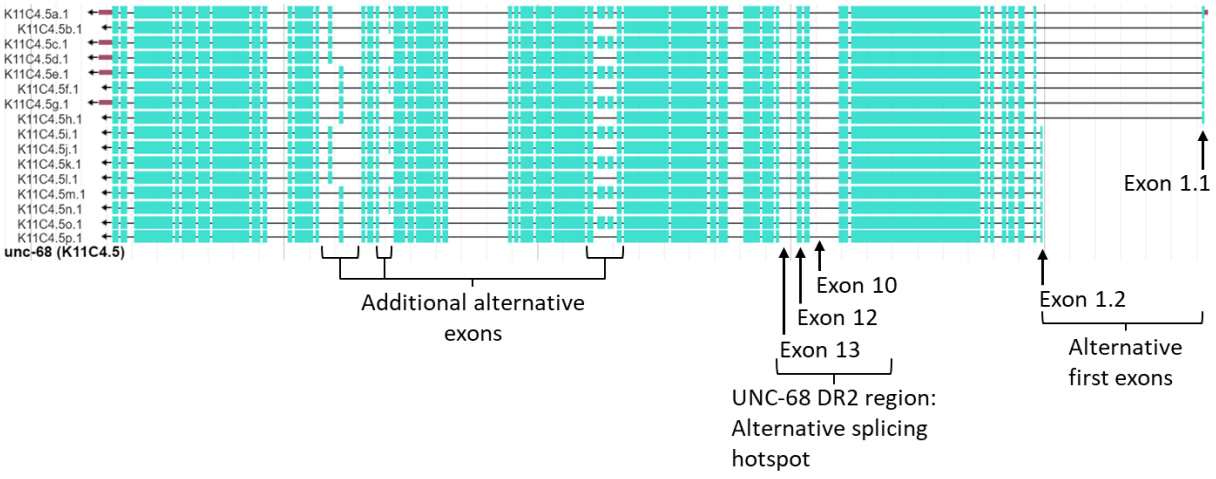

Figure 52: Localization of alternative exons in the current *unc-68* gene model. Wormbase ID WBGene00006801 (Dec 2020).

Table 15: Abbreviation, ZX number of the Gottschalk lab, description integration site of LOV2 domain and SunyBiotech denotation are listed.

Abbr.	ZX	description	Integration site
GOA01	ZX2592	CatChUP::EYFP::unc-68	CatChUP::EYFP::CRP-1 integrated after start codon of *unc-68* exon 1.1
lite-1 GOA01	ZX2632	CatChUP::EYFP::unc-68, crossed into *lite-1(ce314)*	1 integrated after start codon of *unc-68* exon 1.1
GOA14	ZX2635	exon1.1 CatChUP::EYFP::unc-68, exon1.2 CatChUP::EYFP::unc-68	1 integrated after start codon of *unc-68* exon 1.1 and exon 1.2, different codon usage
GOA14 C1V1	ZX2636	GOA14 crossed into strain ZX1663 N2 zxIs78 [pmyo-2::C1V1 ETET; pmyo3::mCherry]	CatChUP::EYFP::CRP-1 integrated after start codon of *unc-68* exon 1.1 and exon 1.2, different codon usage

Additionally, the strain GOA01 was crossed into *lite-1(ce314)* to prevent light avoidance of the worms during photostimulation, and the strain GOA14 was crossed into ZX1663, for possible two colour photostimulated pharynx pumping assays.

3.4.1. Analysing effects of CatChUP::EYFP::CRP-1 inserted downstream the start codon of *unc-68* exon 1.1

3.4.1.1 Assessing the expression of OptoUNC-68 in the nematode C. elegans

To verify expression of the integrated CatChUP::EYFP::CRP-1 (OptoUNC-68) linked to the intrinsic ryanodine receptor, confocal images were acquired in *Figure 53*, and GOA01 fluorescence was compared with wild-type animals in *Figure 54.* Confocal images of the head region illustrate, that small fluorescent grains are evident where body wall muscles are located and in the muscles of the terminal bulb of the pharynx (white arrow heads in *Figure 53* B). However, the comparatively very strong fluorescence of the gut and viscera, make a clear interpretation, of whether there is genuine CatChUP expression in the BWMs and pharynx, debatable. To clarify this ambiguity, pictures were taken with a more light-sensitive camera. For an accurate comparison of GOA01 and wild-type, the acquisition parameters such as objective, exposure, gain, minimum and maximum displayed value remained identical. Comparison of the head fluorescence in A) and D), and the midsegment of the body in B) and E), did not reveal any distinctive difference in fluorescence between wild-type and GOA01. A clear difference was only evident in the tails of C) and F), with GOA01 showing a substantial stronger fluorescence than wild-type animals in F). Nevertheless, this fluorescence was limited to the intestines and was not visible in BWMs or at the sphincter. A clear statement of the correct expression and folding of OptoUNC-68 could thus not be made.

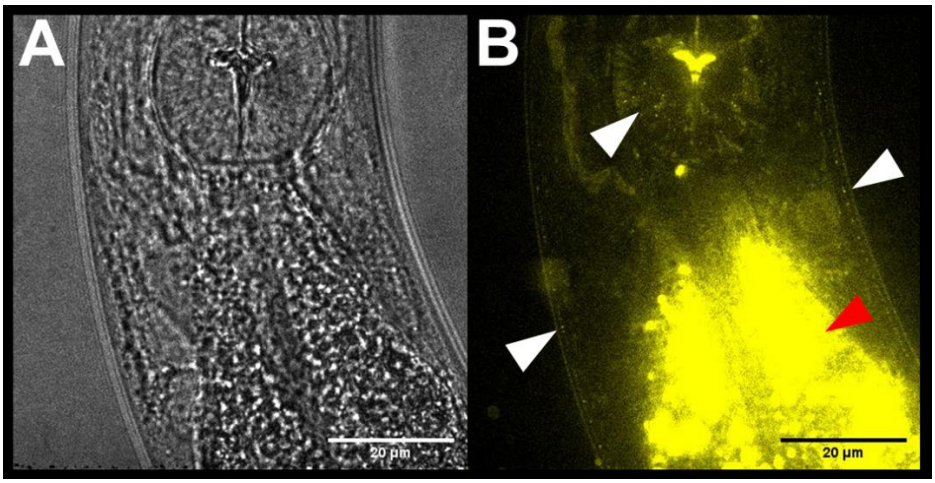

Figure 53: Possible expression of GOA01 in BWM and pharynx. White arrow heads indicate OptoRyR expressed in the SR membrane of body wall muscles and pharynx. A) DIC image of Terminal bulb and intestines. B) Fluorescence of small grains in the BWMs, Terminal bulb (white arrow heads) and autofluorescence in the gut and intestines, marked by red arrow head. Confocal images, scale bar 20nm.

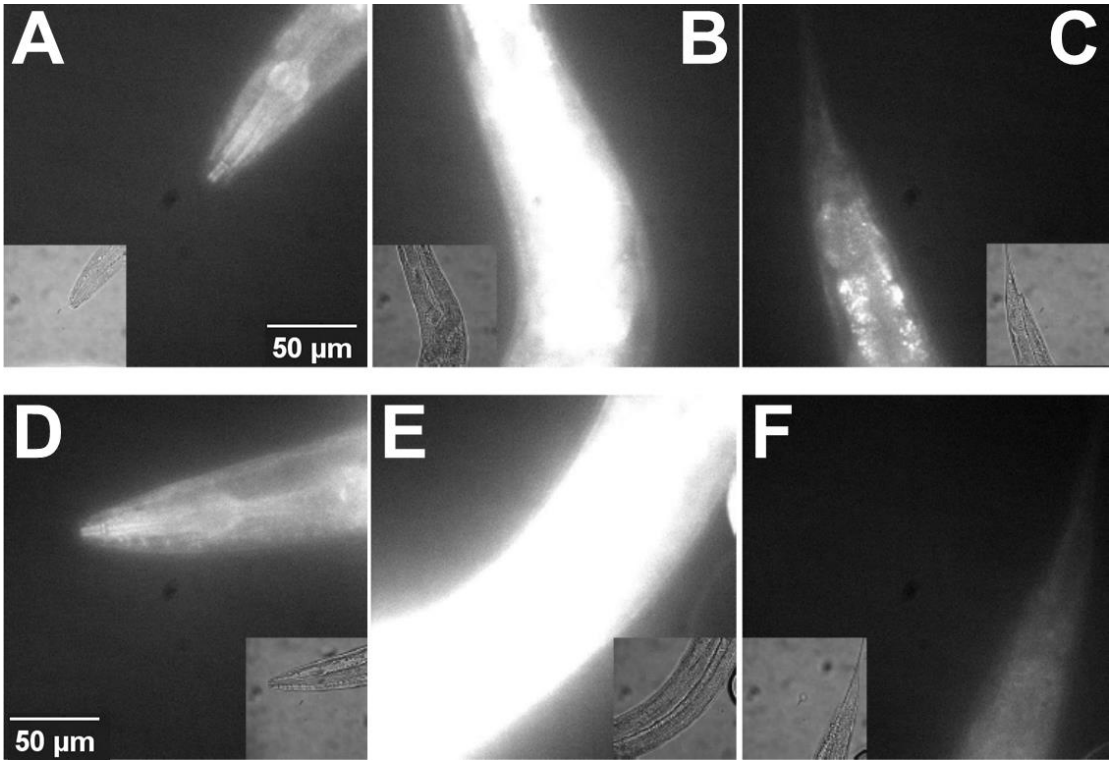

Figure 54: Comparing the fluorescence of transgenic and wild-type animals. A-C) Fluorescence of strain GOA01. D-F) Wild-type control. Inlays depict DIC images of the respective fluorescence image. Scale bars, 50µm, every picture was taken with the same magnification.

3.4.1.2. Swimming behaviour and the effect of short-term and long-term stimulation

Expectation of the GOA01 strain with the OptoUNC-68 integrated at exon 1.1, was a response to blue light after prolonged strong exposure. The thought behind it was, that an extended stimulation would activate more channelrhodopsins, thus increasing the likelihood of an activated RyR.

Graph B) of *Figure 55* illustrates significant time periods of normalized swimming cycles of GOA01 and ATR GOA01. Maximal swimming cycles were reduced in GOA01 from 69.7 ± 1.72bbpm before the onset

of the light pulse to 58.5 ± 2.88bbpm after 270s, equivalent to a slowdown of -16.2%, followed by a recovery to a maximum -5.1% before photostimulation ended. When GOA01 was reared with ATR, an opposing answer to illumination occurred. There was an increase in thrashes from 61.5 ± 1.07bbpm before light to 66 ± 2.56bbpm in the time frame 360-390s, giving an increase of 7.1%. Altogether, the strongest variations could be observed until time frame 360-390s. The entire assay was abridged to 5min blue light pulse instead of 10min, as most of the behavioural changes took place in the first half of the assay, and the vast amount of data generated by the camera could be reduced by 50%.

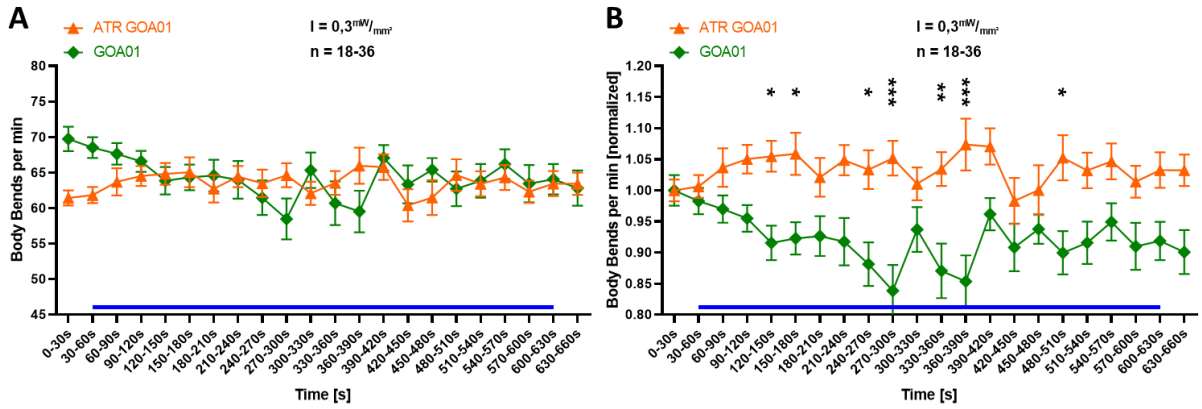

Figure 55: Long term illumination does not reveal exceptional swimming behaviour after prolonged blue light stimulus. A) Absolut thrashing rate of ATR reared animals is similar to GOA01 after 2min. B) Normalized data indicates, that contrary to GOA01 animals, ATR fed animals tend to elongate during photostimulation. Stimulation protocol: 30s no stimulation, 10min 470nm 0.3mW/mm² stimulation and 30s no stimulation. Blue bar on X-axis indicates time of blue light illumination. Animals were fed overnight on agar plates with ATR 0.2% in OP50. Graph with mean ± SEM, unpaired two-tailed t-test, with Welch's correction and two-way ANOVA with Bonferroni correction ***: $p \leq 0.001$, **: $p \leq 0.01$, *: $p \leq 0.05$.

Assays were continued with an adapted light protocol: 30s no stimulus – 5min 0.3 / 0.8mW/mm² 470nm – 30s no stimulus. *Figure 56* displays the swimming cycles per min in A) and C), and the normalized data of these. Statistics in A) and C) was done by comparing the basal thrashing rate (0-30s) of a strain to the first half of photostimulation (30-180s), second half (180-330s) and the recovery period (330-360s). In B) and D) the same time intervals of ATR reared animals, were compared with their respective control strain. The results of 0.3mW/mm² intensity in A) and B) illustrate a distinct discrepancy of -9.3% between the basal thrashing rate (Mean ± SEM: 84.2 ± 2.38bbpm) and the recovery phase (Mean ± SEM: 76.3 ± 2.47bbpm) for animals lacking ATR, with this being not the strongest reduction, they reduce thrashes by -11.5% during stimulation, but not considered as significant as it is included in the first half of photostimulation. Considering the contrary response of ATR GOA01 animals, a raise of thrashes by 4.4% (Mean ± SEM: 75.2 ± 2.15bbpm) from basal thrashes to time interval 300-330s, the comparison of normalized control and ATR data reveals a notable higher thrashing rate during and after the light pulse. As soon as the intensity of the light pulse is enhanced to 0.8mW/mm² (C and D), both strains exhibit a stronger decrease of swimming cycles, a light avoiding behaviour, than under low light intensity. ATR GOA01 animals dropped by -17% in time frame 30-60s, and GOA01 dropping by -11.6%. This makes the change of behaviour before (0-30s) and during (30-180s) photostimulation significant (C). Though, this could not be subsidized by the comparison of normalized data in D). Besides a recovery after that during photostimulation, no additional effect could be observed.

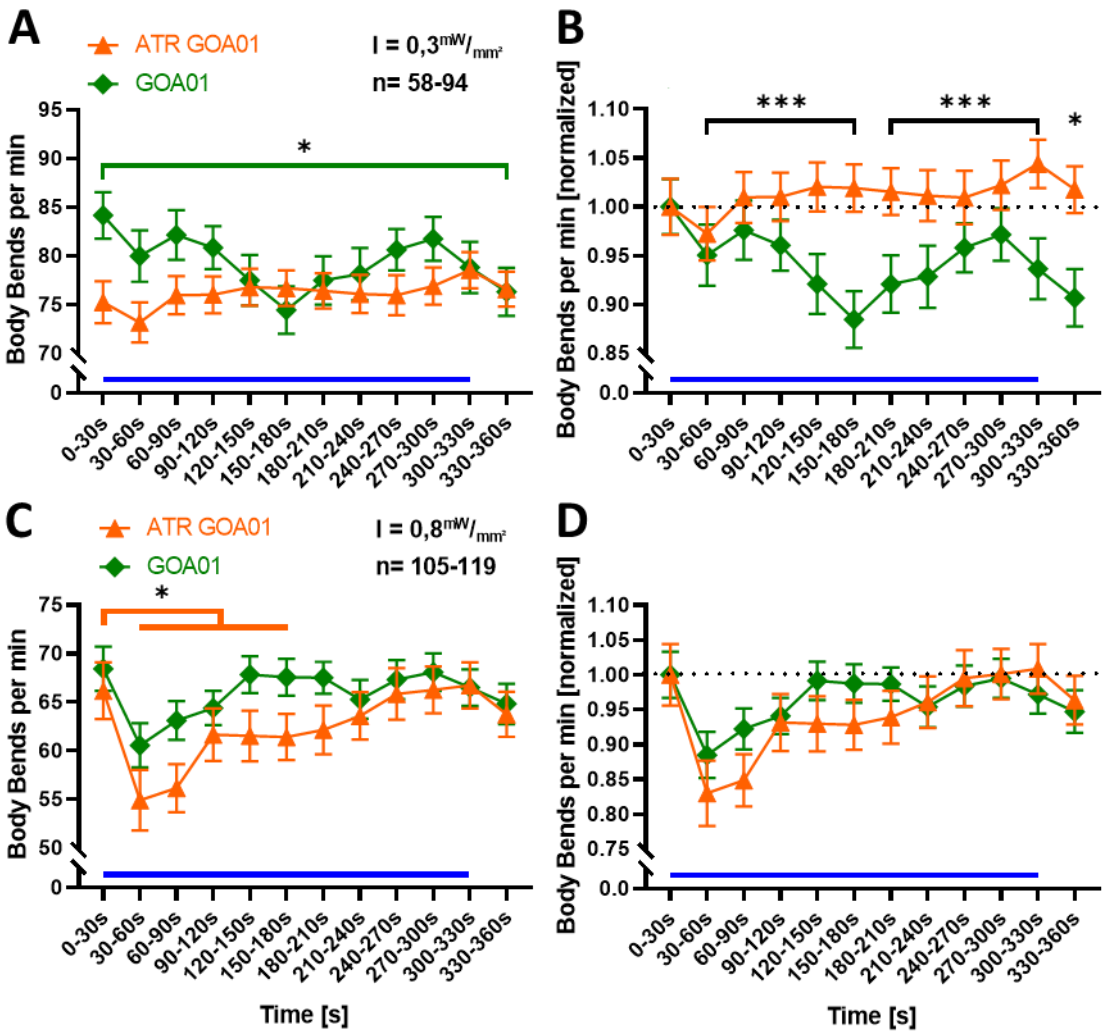

Figure 56: Low light induced effects, are stronger in ATR lacking animals, and high intensity reveals a stronger effect on ATR reared animals A) GOA01 animals exhibited diminished thrashing rate during and after low light stimulation. B) Normalized data of GOA01 and ATR GOA01 reveals significant disparities of thrashes during and after stimulus. C) Higher illumination leads to a stronger decrease of thrashes than low light. D) No mismatch was found in the normalized data of 0.8mW/mm² stimulated animals. Stimulation protocol: 30s no stimulation, 5min 470nm 0.3mW/mm² respectively 0.8mW/mm² stimulation and 30s no stimulation. Blue bar on X-axis indicates time of blue light illumination. Animals were fed overnight on agar plates with ATR 0.2% in OP50. Graph with mean ± SEM, unpaired two-tailed t-test, with Welch's correction and two-way ANOVA with Bonferroni correction ***: $p \leq 0.001$, **: $p \leq 0.01$, *: $p \leq 0.05$.

Comparing normalized data of 0.3mW/mm² 10min long-term illumination (*Figure 56*) to 5min illumination, a coincident change in swimming cycles can be seen in the period of 60-300s, in which GOA01 animals (green) are diminishing body bends. Tendentially the animals are reducing and increasing bbpm in similar repeating time periods, during the same intensity of light stimulus. This could be interpreted as short "walking" phases for recovery during a long-distance race.

3.4.1.3. lite-1 background leads to enhanced light response in GOA01

Crossing the strain GOA01 into the *lite-1* background had the intention to avoid the typical light response of wild-type animals. Results of a 10min blue light stimulation confirm this for lite-1 GOA01, by dropping swimming cycles -11.4% from 111.2 ± 3.33bbpm to 98.5 ± 4.27bbpm during photostimulus. Interestingly lite-1 GOA01 supplemented with ATR drops even more by reducing thrashes 19.6%. Furthermore, both strains are not recovering after the stimulus has ended but decrease thrashes even more. Besides, it has to be mentioned that basal thrashing rate of *lite-1*

defective animals is around 80bbpm (Gong et al. 2016). As we can see here, lite-1 GOA01 thrashes at the beginning with 113.7 ± 3.9bbpm which is an increase of 41%.

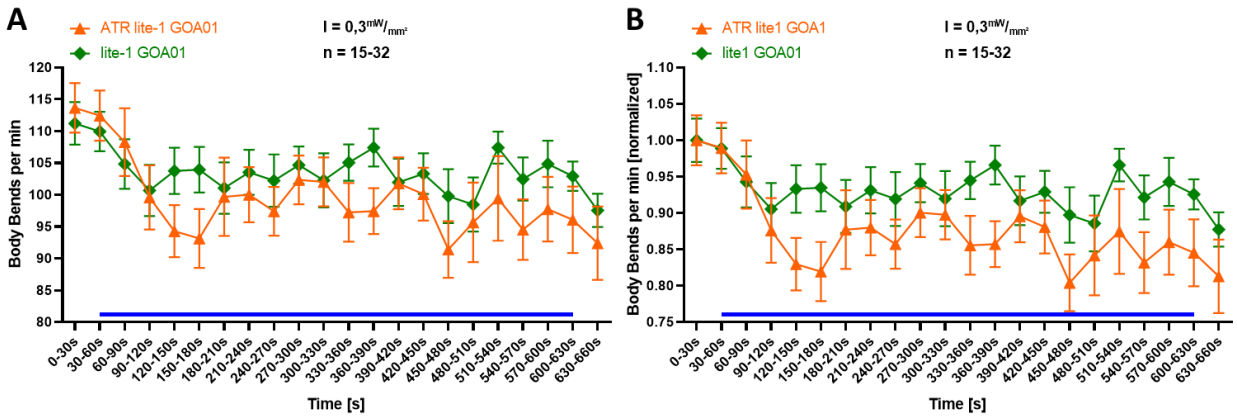

Figure 57: Long term illumination of lite-1 GOA01 displays a reduction of swimming cycles during photostimulation, and a further drop of thrashes after light pulse. Stimulation protocol: 30s no stimulation, 5min 470nm 0.3mW/mm² stimulation and 30s no stimulation. Blue bar on X-axis indicates time of blue light illumination. Animals were fed overnight on agar plates with ATR 0.2% in OP50.

When swimming assays were repeated with a reduced illumination period of 5min, the data changed in that, lite-1 GOA01 animals now exhibit a stronger reduction during light stimulation, with -8.9%. In comparison, ATR lite-1 GOA01 decreased -4% from (*Figure 58* A, B).

As expected, the relative reduction of thrashes in lite-1 GOA01 is more pronounced, when light intensity is enhanced to 0.8mW/mm². Maximal reduction while light pulse is -8.3% in lite-1 GOA01, and in ATR lite-1 GOA01 it is -11.3%. Correlating 0.3mW/mm² and 0.8mW/mm² points out, the minimum in 0.3mW/mm² is -8.9%. Normalised data in B) and D) illustrates opposing behaviour of the strains, as lite-1 GOA01 had its strongest reduction under low photostimulation and ATR lite-1 GOA01 during 0.8mW/mm² blue light pulse. This could be interpreted as an ATR dependent response, that only becomes apparent when a certain threshold value is exceeded. The large unexpected difference in basal thrashing rate between lite-1 GOA01 (*Figure 57*) and GOA01 (*Figure 56*) is about 40bbpm. Here we can just speculate whether this was caused by some kind of compensation during the crossing of the *lite-1 (ce314)* strain with GOA01.

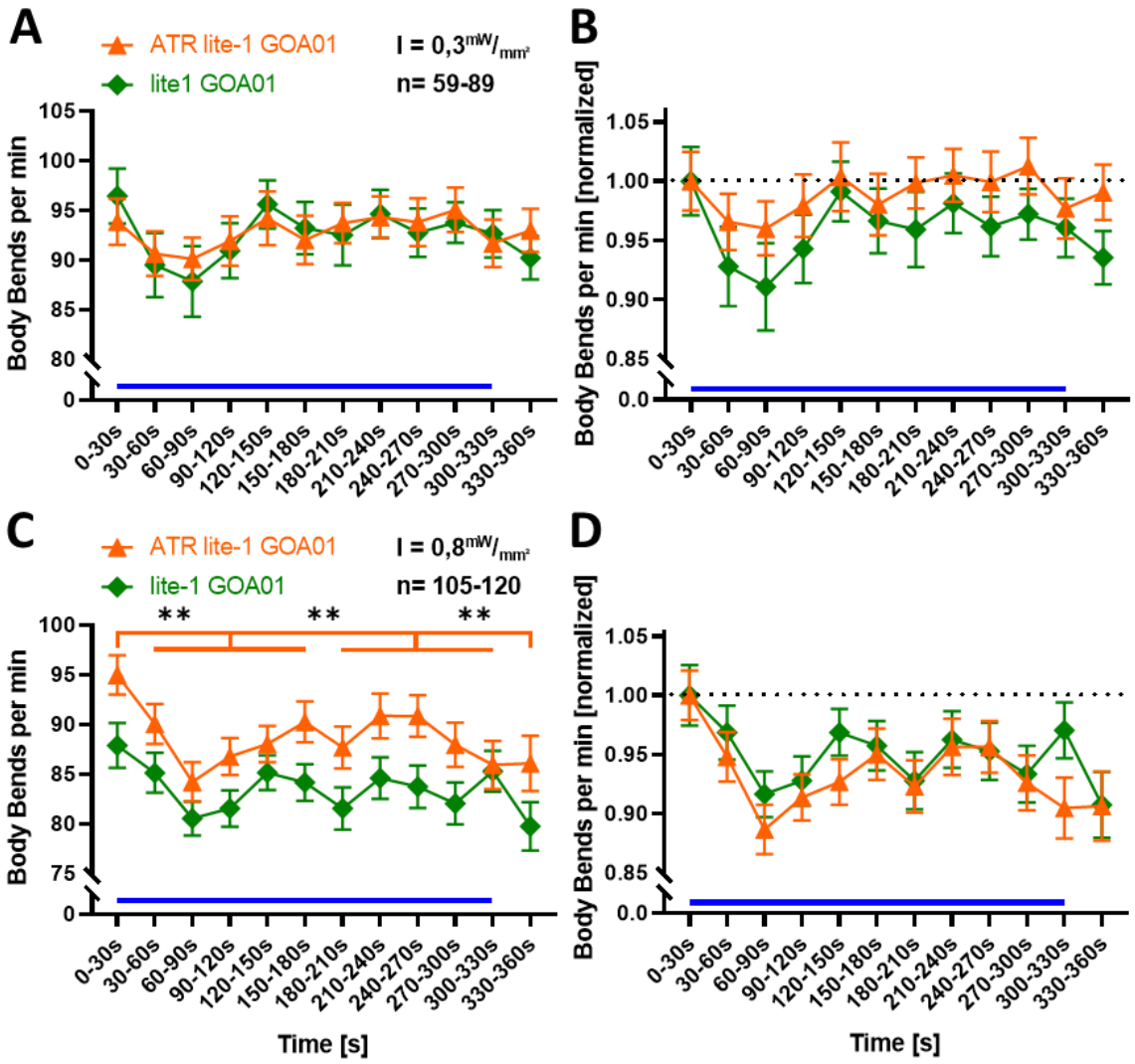

Figure 58: No difference between lite-1 GOA1 and ATR reared animals under photostimulation. A-B) 0.3mW/mm² leads to the same response in both groups. C) Notable changes of ATR lite-1 GOA01 animals were calculated for the photostimulation period and recovery phase compared to the basal swimming cycles. D) A discrepancy of both groups could not be proven in normalised data. Stimulation protocol: 30s no stimulation, 5min 470nm 0.3mW/mm² stimulation and 30s no stimulation. Blue bar on X-axis indicates time of blue light illumination. Animals were fed overnight on agar plates with ATR 0.2% in OP50. Graph with mean ± SEM, unpaired two-tailed t-test, with Welch's correction ***: $p \leq 0.001$, **: $p \leq 0.01$, *: $p \leq 0.05$.

3.4.1.4. Body wall muscle contraction is insensitive to photostimulation when ATR is administered

As the results of the previous swimming behaviour assays were inconsistent. It was now assumed that a slight contraction of the body wall muscles could be evoked by light. This might not have become apparent in the swimming behaviour, yet would be detectable when observing individual animals closely. For the strain GOA01, both reared with ATR and without, the only result that could be extracted, was the contradictory answer to low and high intensity stimulation. It can be seen that elongation occurs at an intensity of 0.3mW/mm² (A), but contraction at 0.8mW/mm² (B). However, as soon as the animals were subjected to the same experiments with a *lite-1* background, almost the same effects were seen in ATR-fed animals (C-D). Giving a contraction in both cases, 0.3mW/mm² and 0.8mW/mm². Non-supplemented animals of lite-1 GOA01, mainly followed this behaviour, with the difference of short periods of noteworthy elongation (15-20s and 25-30s) while stimulation was ongoing. As long as lite-1 GOA01 animals were fed with ATR a remarkable alteration of body length was absent in C) and D).

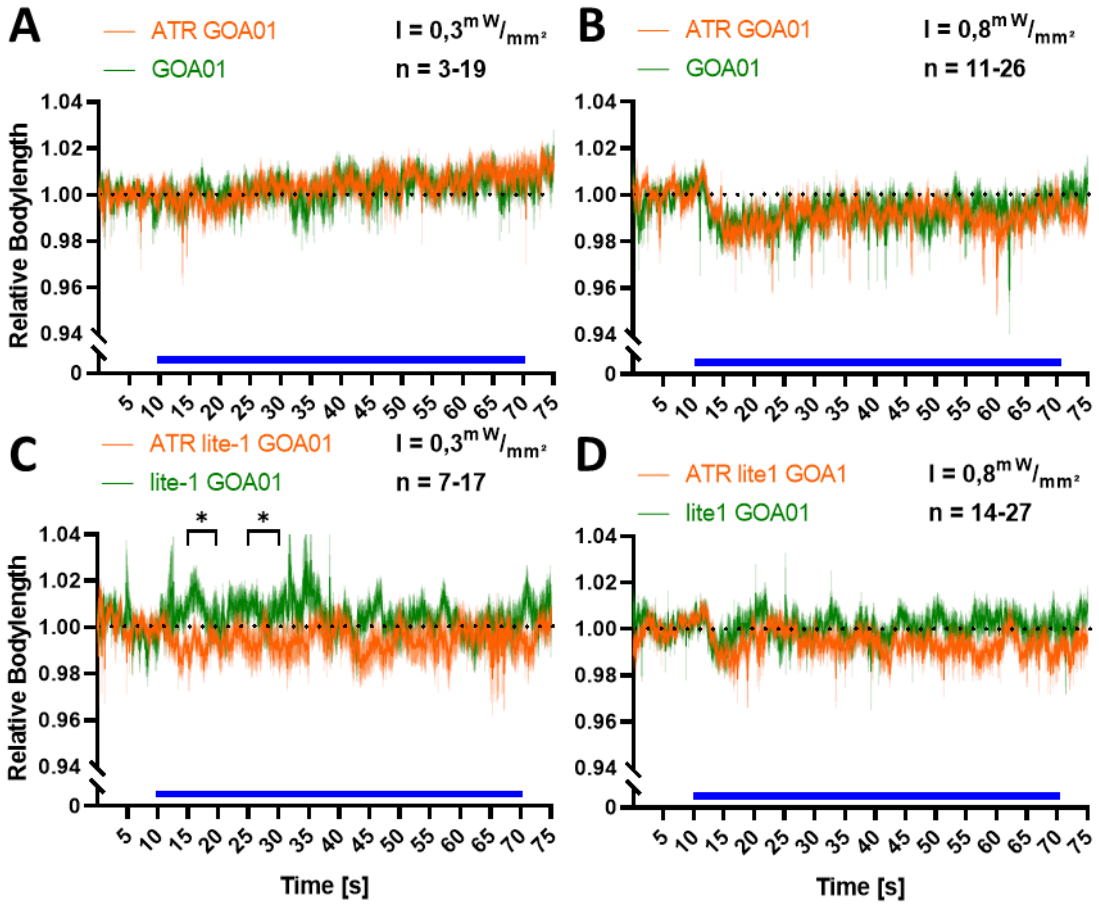

Figure 59: Short term periods of body elongation in GOA01 non-ATR supplemented animals alter body elongation. A-B) Low light stimulation intensity as well as high intensity cause the same behaviour in both groups. C) Body elongation during photostimulation of lite-1 GOA01 becomes significant in the time frames 15-20s and 25-30s, D) Enhanced intensity did not change body length. Illumination protocol: 10s no stimulus followed by 60s 470nm 0.3mW/mm² respectively 0.8mW/mm², and 5s no stimulus. Blue bar on X-axis indicates time of blue light illumination. Animals were fed overnight on agar plates with ATR 0.2% in OP50. Normalization of time frames 10-70s and 70-75s against 0-10s. Line chart with mean ± SEM, two-way ANOVA with Bonferroni correction ***: $p \leq 0.001$, **: $p \leq 0.01$, *: $p \leq 0.05$.

3.4.2. Potential expression of OptoUNC-68 in exon 1.1 and exon 1.2

When it was started to generate OptoUNC-68 by using the CRISPR/Cas9 method, it was known that there are 16 isoforms of *unc-68* expressed in *C. elegans (Figure 59)*. It has also long been proposed that diversification of their functions might be generated by different transcripts, created by alternative splicing. What was not known yet, was the fact that tissue-specific isoforms fulfil distinct functions and different isoforms may function redundantly (Marques et al. 2020). This could be a reason why effects were not emerging as expected in GOA01. To exclude a possible compensation CRISPR/Cas9 was used again, to integrate CatChUP::EYFP::CRP-1 N-terminally of exon 1.2. In this way ZX2635 wild-type exon 1.1 CatChUP:: EYFP::CRP-1::unc-68, exon 1.2 CatChUP::EYFP:: CRP-1::unc-68 was created. By that all possible isoforms should be expressed as OptoUNC-68.
However, the insertion of the CatChUP::EYFP::CRP-1 construct at the two alternative first exons apparently resulted in a disruption of the overall UNC-68 function, judged by swimming locomotion. These animals were thrashing at 4bbpm, compared to ca. 100bbpm for wild-type. *unc-68(r1162),* the null mutant, thrashed with about 10bbpm (Figure *34*). Hence, the engineered protein is unlikely to be able to fulfil its normal function. To investigate whether it is expressed at all, I imaged YFP using fluorescence microscopy. It was however not possible to observe any obvious expression. Nevertheless, the manipulated UNC-68 may only be expressed at very low levels, which could explain the apparent loss of function. Therefore, I tested if the construct could be triggered to release some Ca^{2+} from the ER, by photostimulation during swimming analysis.
Interestingly there is already a difference of 31% bbpm, which GOA14 animals exhibit when compared to ATR GOA14 (*Figure 61*, A). When supplemented with ATR, GOA14 thrashing rate is decreasing as long as photostimulation is proceeding, reaching a reduction of -37.6%, starting with 4bbpm, reducing to 2.5 in the last 30s of blue light pulse, and still going on to -40.7% when the pulse ended to a minimum of 2.4bbpm. Without any supplementation of ATR, there is a small reduction too, from 2.7bbpm to 1.96bbpm in time frame 270-300s under blue light exposure which is 28.1%. By contrast there is a recovery after stimulation in GOA14, that does not occur in ATR GOA14 animals.

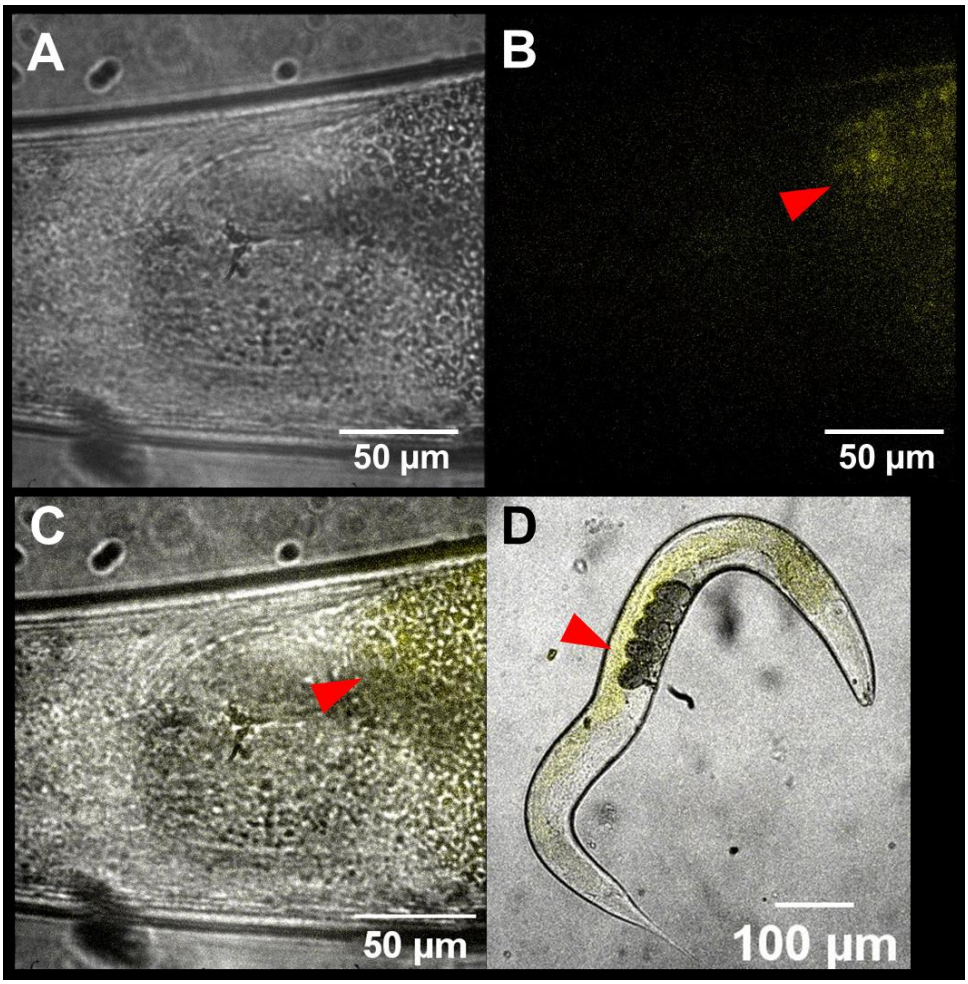

Figure 60: Fluorescence image of YFP in the head and body. A) DIC image of the grinder and intestines. B) fluorescence of intestines (red arrow head). C) Merged image of A and B. showing the fluorescence in the head region. D) Visualized auto fluorescence in the intestines, marked by red arrow head. Scale bar: A) 50µm, B) 50µm, C) 50µm, D)100µm.

3.4.2.1. Impact of OptoUNC-68 in exon 1.1 and exon 1.2 on the locomotion behaviour

An additional insertion of the "Opto" in front of exon 1.2 should omit the possible compensation by any expressed natural isoform of the intrinsic *C. elegans* RyR. Accordingly, the expectation was a change in swimming behaviour triggered by photostimulation, that may enhance over a prolonged period, as was already expected for GOA01. A swimming assay performed with an intensity of 0.3mW/mm² initially confirmed that by verifying a clear decrease of thrashes by -37.6%. ATR GOA14 animals also showed that in the late time frame 180-330s of stimulation, including a sustained decline in the recovery phase 330-360s by -40.7%. However, this must be put into perspective by the fact that even non-supplemented animals significantly reduce their swimming rate maximally by -28.1%, after long exposure to light. The difference is most evident in graph B), illustrating a clear discrepancy in the recovery phase, where non-ATR reared animals recover quickly compared to ATR supplemented. To attribute the progressive decline of swimming cycles to pure fatigue, would not explain the strong recovery after the light pulse terminated.

Under intensified stimulation of 0.8mW/mm², the response of GOA14 animals fed with ATR is conversed compared to 0.3mW/mm², as they exhibit an increase of thrashes starting with 3.4 ± 0.32bbpm and reaching a 28.3% increased maximum of 4.4 ± 0.47bbpm in time frame 90-120s. GOA14 is responding in the same way but not that prominent with a maximum raise of 13.1% after 1min

stimulation, and a drop to 2.3 ± 0.19bbpm (210-240s). Furthermore, a decrease to -31.9% can be seen, once blue light was switched off.

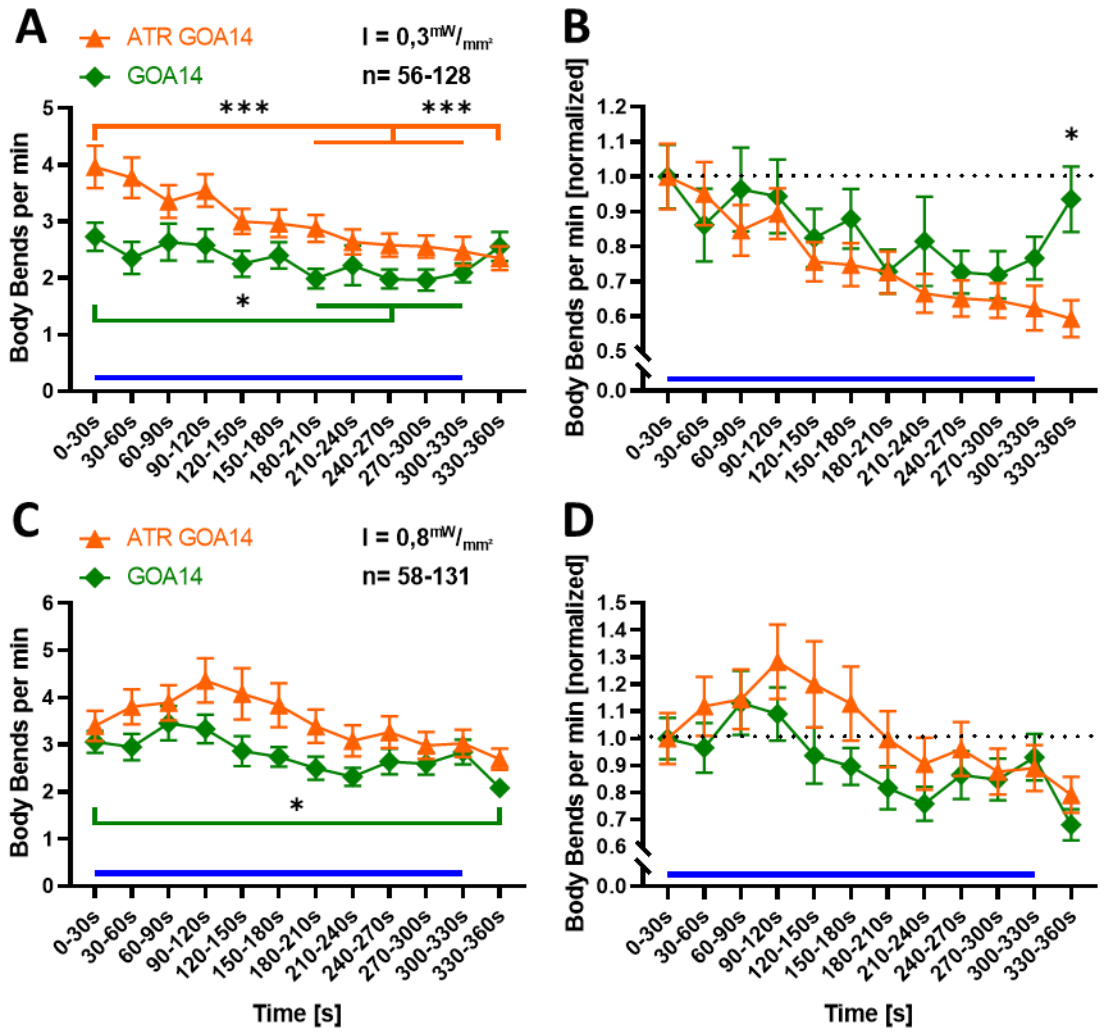

Figure 61: Intensity-dependent increase in swimming cycles was more pronounced in ATR fed animals. A-B) ATR reared animals of GOA14 are reducing thrashing rate by 37% during blue light exposure. C-D) Increased photostimulation caused a heightened thrashing rate as long as illumination persisted. Stimulation protocol: 30s no stimulation, 5min 470nm 0.3mW/mm² or 0.8mW/mm² stimulation and 30s no stimulation. Blue bar on X-axis indicates time of blue light illumination. Animals were fed overnight on agar plates with ATR 0.2% in OP50. Graph with mean ± SEM, two-way ANOVA with Bonferroni correction ***: $p \leq 0.001$, **: $p \leq 0.01$, *: $p \leq 0.05$.

The data shown in *Figure 61* indicates that, as seen in other strains (as will be demonstrated in GOA08, GOA05, GOA04), light avoiding behaviour must be taken into account when comparing blue light intensities 0.3 and 0.8mW/mm². As behaviour is changing to the opposite when light intensity is raised.

3.4.2.2. ATR supplementation leads to body wall muscle elongation under blue light stimulation

Since the swimming behaviour was clearly influenced by the intensity of the photostimulus, a comparable effect was expected for the analysis of the body length. At least an incipient increase or decrease would be detected, as was the case in the first 90s in *Figure62.* Some effect could be detected under blue light influence, albeit only in non-ATR fed animals with a maximum increase of 2.4% as seen in A) and under 0.8mw/mm² in B) 2.4%, characterised by a steady elongation throughout the assay, in low and high intensity. This ongoing increase in body length is the basis for the significant difference to ATR GOA14 in the time interval 50-55s, while low blue light was applied (A). Animals that were not influenced by ATR did not alter body length, as the data of 0.3mW/mm², Max: 1.3% and 0.8mW/mm² 0.8% proves in the time interval 10-70s. The relaxation of the non-ATR fed animals could be triggered by various mechanisms. One of them could be a conformational disturbance caused by weakened subunit-subunit interactions, which alters the stability of the RyR channel (Zhu et al. 2013), and leads to closed / dysfunctional Ca^{2+} channels. This is attributed to the concentration of Ca^{2+} ions in the cytosol falling below 10^{-5}mol/l. In this scenario, troponin I would block the binding of myosin to ATP, thereby allowing the release of the myosin head from the actin filament, causing relaxation (Behrmann et al. 2012; Block et al. 1988; Klinke et al. 2010; Sweeney and Houdusse 2010). The concentration of Ca^{2+} in the cytosol would fall below the critical level 10^{-5}mol/l as a result of the ongoing activity of SERCA. Compensation of RyR could also not be achieved by IP3Rs, as evidenced by the *unc-68* deletion mutant. In these animals only the RyR is defective, they show a relaxed posture, but much more pronounced than the relaxed GOA14 animals.

Another explanation could be the neuronal RyR activation through CatChUP upon photostimulation. This could lead to RyR-mediated Ca^{2+} up-regulation in synaptic compartments, associated with altered synaptic homeostasis and depression of the network. (Brini et al. 2014; Smith et al. 2005).
To explain the persistent body length of ATR reared GOA14, it can be hypothesised that a possible CICR induced by photostimulation of the integrated CatChUP leads to a Ca^{2+} current across the SR/ER membrane. For GOA14 (ATR), this could occur in muscle cells (BWMs: exon 1.1 and pharynx: exon 1.2), but also in neurons (exon 1.2) (Marques et al. 2020). This in turn would compensate for the relaxation of the GOA14 control, seen in *Figure 62* A and B, by sufficient Ca^{2+} in the cytosol.

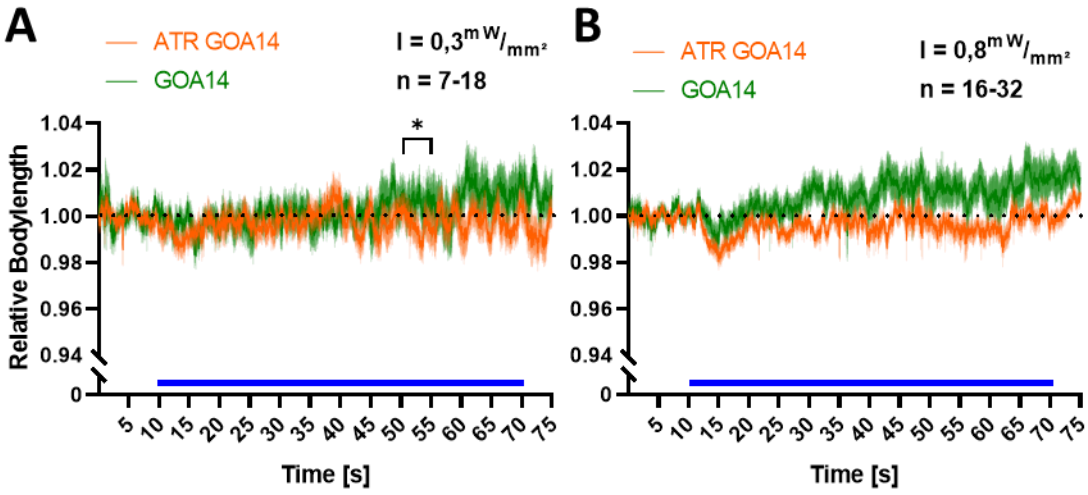

Figure 62: ATR supplementation prevents body elongation under weak and strong photostimulation. A) Reared with ATR GOA14 animals contracted notably less than ATR lacking animals (time frame 50-55s). B) GOA14 animals elongate even more under 0.8mW/mm² compared to the weak intensity. Illumination protocol: 10s no stimulus followed by 60s 470nm A) 0.3mW/mm² B) 0.8mW/mm² and 5s no stimulus. Blue bar on X-axis indicates time of blue light illumination. Animals were fed overnight on agar plates with ATR 0.2% in OP50. Normalization of time frames 10-70s and 70-75s against 0-10s. Line chart with mean ± SEM, two-way ANOVA with Bonferroni correction ***: $p \leq 0.001$, **: $p \leq 0.01$, *: $p \leq 0.05$.

3.4.2.3. Blue light stimulation leads to a varying locomotion behaviour

The positive control strain was ZX1827 (zxEX741[pmyo-3::ChR2(L132C)::YFP; pmyo-2::mCherry], that expresses ChR2 in body wall muscles, in which it leads to contraction of these upon light stimulation. It acted as predicted with a drastic reduction in swimming cycles during and after photostimulation, both in long-term assays *Figure 63* and in shortened 5min stimulations, under the influence of high and low intensities *Figure 64*.

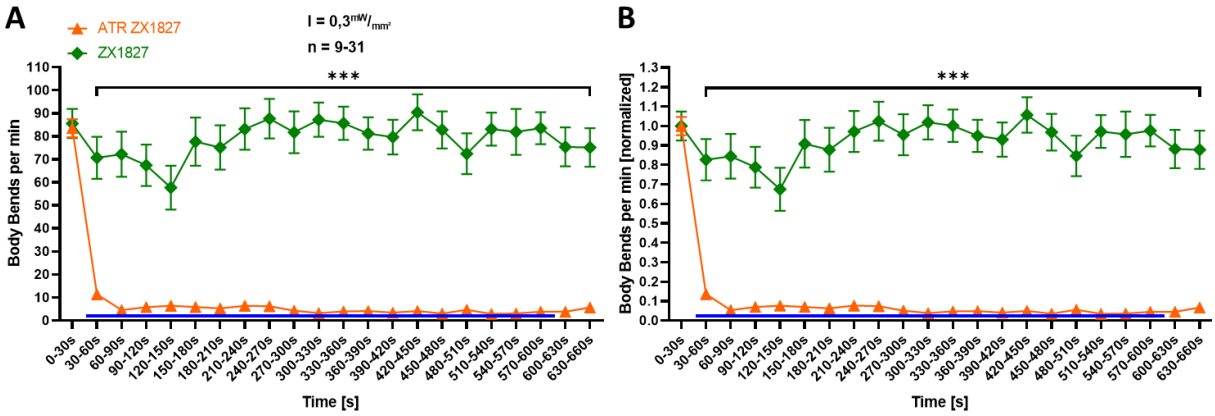

Figure 63: ZX1827 supplemented with ATR reduces body bends by -96% when exposed for 10min to 470nm light. A, B) The nearly total stop of movement is visible in both thrashes per min and normalized data. Stimulation protocol: 30s no stimulation, 10min 470nm 0.3mW/mm² stimulation and 30s no stimulation. Animals were fed overnight on agar plates with ATR 0.2% in OP50. Graph with mean ± SEM, two-way ANOVA with Bonferroni correction ***: p ≤ 0.001, **: p ≤ 0.01, *: p ≤ 0.05.

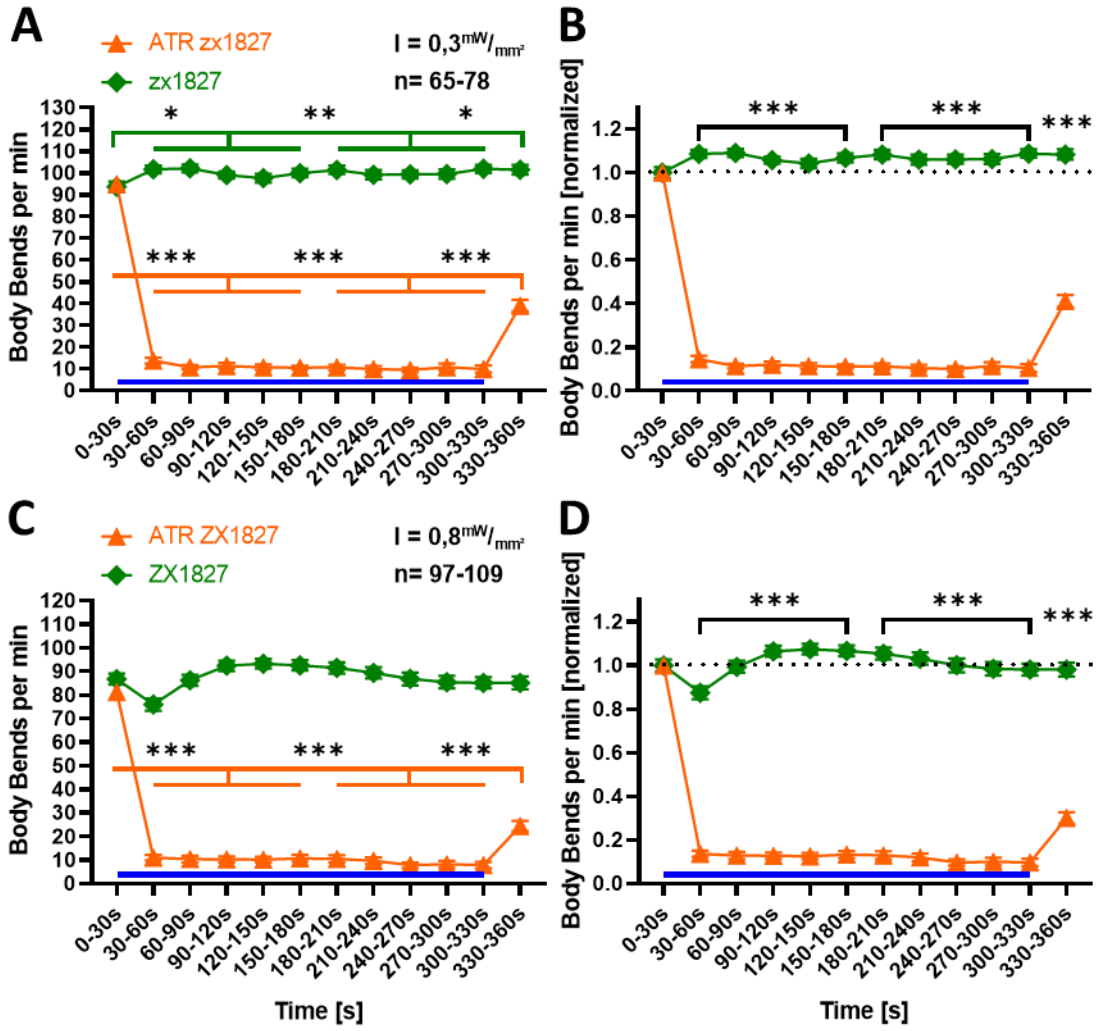

Figure 64: ZX1827 supplemented with ATR reduces body bends by 90% when exposed to 470nm light. A) low light causes a notable raise of thrashes in all periods compared to basal rate. B-D) Significant differences were detected when ATR animals were compared to non-ATR fed animals, or to their own basal thrashing rate except non-ATR animals in C). Stimulation protocol A, B: 30s no stimulation, 5min 470nm 0.3mW/mm² stimulation and 30s no stimulation, C, D: 30s no stimulation, 5min 470nm 0.3mW/mm² stimulation and 30s no stimulation. Blue bar on X-axis indicates time of blue light illumination. Animals were fed overnight on agar plates with ATR 0.2% in OP50. Graph with mean ± SEM, two-way ANOVA with Bonferroni correction ***: p ≤ 0.001, **: p ≤ 0.01, *: p ≤ 0.05.

Long exposure was accompanied by a short but drastic spike in wild-type animals when reared with ATR, after 90s stimulation.

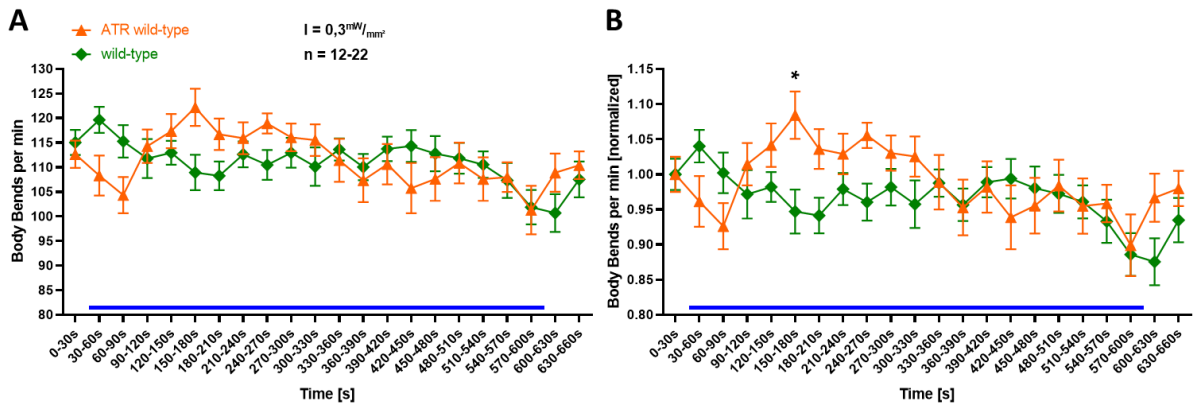

Figure 65: Long exposure leads to a short spike in wild-type animals when reared with ATR, after 90s stimulation. The comparison of bbpm of wild-type displays a response to blue light illumination. Stimulation protocol: 30s no stimulation, 10min 470nm 0.3mW/mm² stimulation and 30s no stimulation. Blue bar on X-axis indicates time of blue light illumination. Animals were fed overnight on agar plates with ATR 0.2% in OP50. Graph with mean ± SEM, two tailed T-Test with Welch's correction, two-way ANOVA with Bonferroni correction ***: p ≤ 0.001, **: p ≤ 0.01, *: p ≤ 0.05.

As long as the intensity of the stimulus was kept low, wild-type animals did not respond to blue light (A-B). It is obvious that stimulation with 0.8mW/mm² blue light led to a response, both in the analysis of basal swimming rate to stimulation phase, and recovery phase (C), as well as in the comparison of ATR animals with non-ATR animals (D). The only difference was that wild-type animals briefly but strongly increased the swimming rate immediately after the onset of the light pulse.

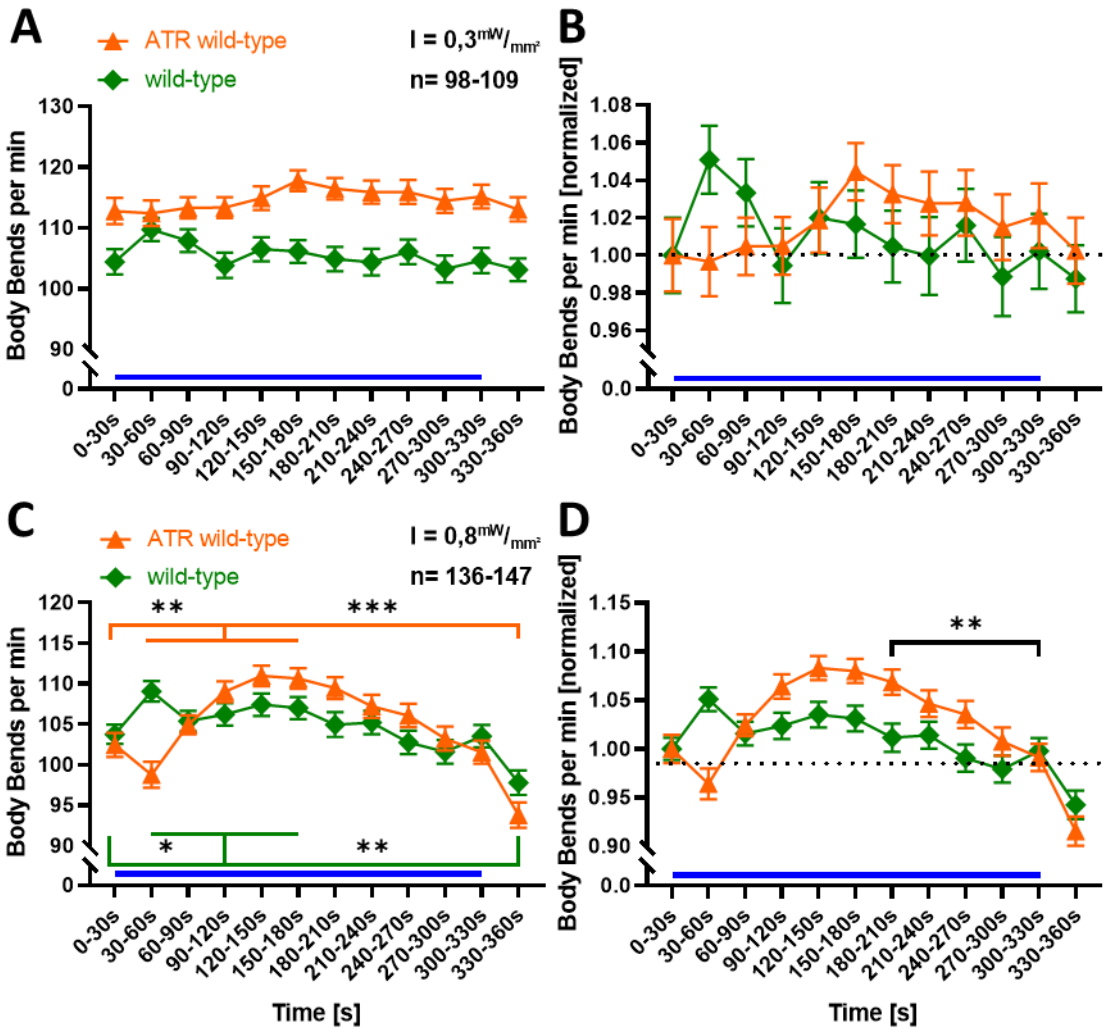

Figure 66: A high blue light stimulus caused a distinct elevation of swimming cycles, followed by a marked drop after stimulus termination. Stimulation protocol: 30s no stimulation, 5min 470nm 0.3mW/mm² / 0.8mW/mm² stimulation and 30s no stimulation. Blue bar on X-axis indicates time of blue light illumination. Animals were fed overnight on agar plates with ATR 0.2% in OP50. Graph with mean ± SEM, two tailed T-Test with Welch's correction, two-way ANOVA with Bonferroni correction ***: $p \leq 0.001$, **: $p \leq 0.01$, *: $p \leq 0.05$.

The strain *lite-1*, which should not show a light-dependent response due to its mutation, revealed clear behavioural changes in the following graphs, both during and after stimulus, even at low intensities. This should be considered when comparing strains crossed into the *lite-1* background. Due to the fact that both ATR-reared and non-ATR-fed animals react to the stimulus, ATR can be excluded as a cause. However, a conclusive explanation cannot be given here. As can be seen in *Figure 68*, this effect does not persist in contraction assays.

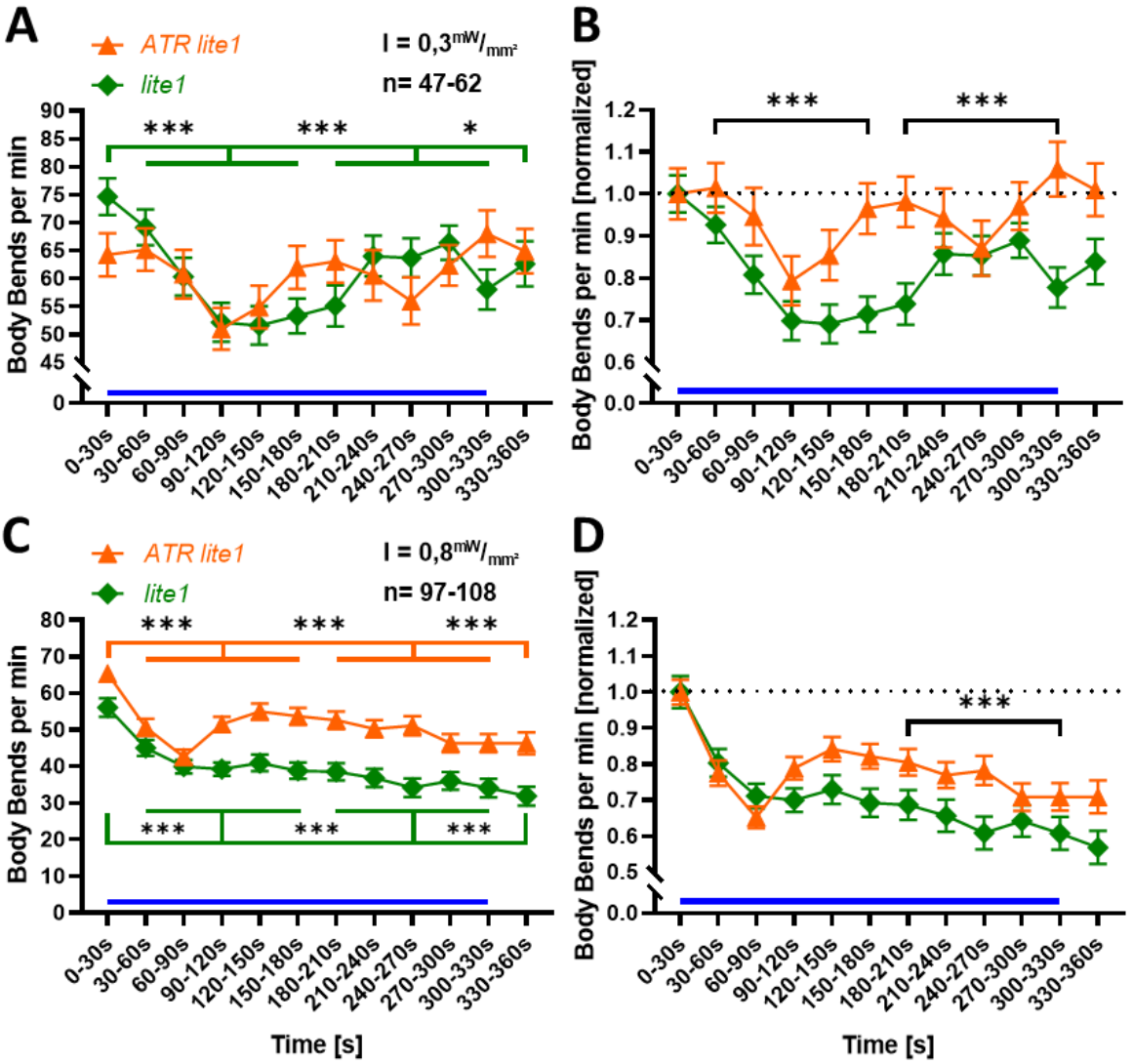

Figure 67: *lite-1* animals are not resistant to blue light exposure, neither to 0.3mW/mm² nor 0.8mW/mm². A-D) An alteration in swimming behaviour could be observed with each stimulus. Stimulation protocol: 30s no stimulation, 5min 470nm 0.3mW/mm² / 0.8mW/mm² stimulation and 30s no stimulation. Blue bar on X-axis indicates time of blue light illumination. Animals were fed overnight on agar plates with ATR 0.2% in OP50. Graph with mean ± SEM, two tailed T-Test with Welch's correction, one-way ANOVA with Bonferroni correction ***: $p \leq 0.001$, **: $p \leq 0.01$, *: $p \leq 0.05$.

3.4.2.4. The influence of blue light on the body length of the control strains

Control strains wild-type, *lite-1* and ZX1827 mainly reacted as expected under the illumination strengths 0.3mW/mm² and 0.8mW/mm². Though it should be noted that wild-type, when supplemented with ATR contracts in the time frame 15-20s 3% more than not supplemented, under 0.3mW/mm² blue light intensity. Furthermore *lite-1* is contracting before and during light under 0.3mW/mm², and under 0.8mW/mm² stimulation. Positive control ATR ZX1827 is contracting over 10%, as shown before, both during and after photostimulation, under strong and weak light intensity.

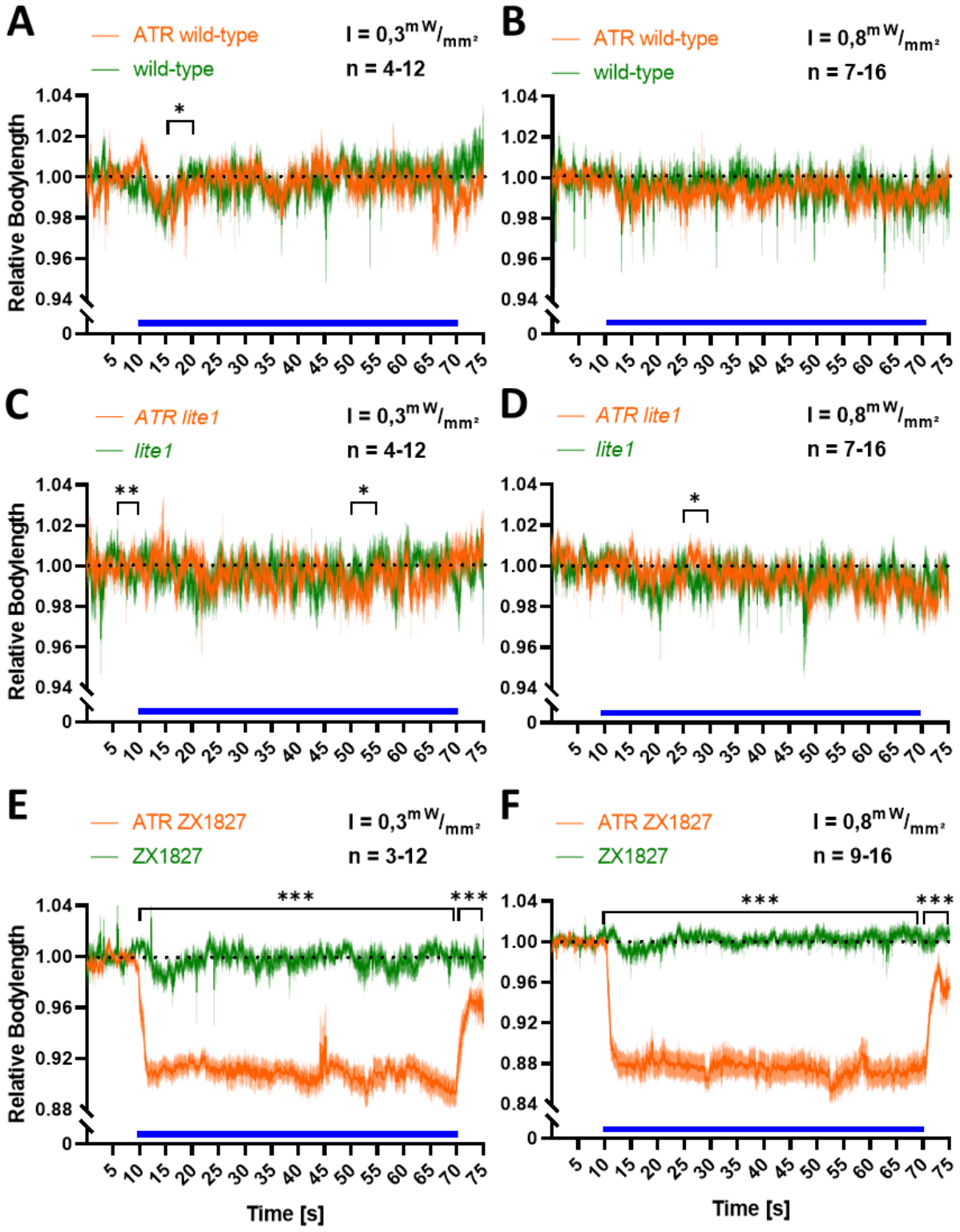

Figure 68: Control Strains react as expected in contraction assays. A) Wild-type is reacting different when ATR supplemented after start of stimulation. B) Wild-type is not reacting to blue light exposure. C) *lite-1* animals are contracting supplemented with ATR, in the time frames 5-10s and 50-55s. D) Under 0.8mW/mm² *lite-1* fed with ATR has a short elongation phase after 15s photostimulation. E-F) ZX1827 contracts as expected during and after light pulse. Illumination protocol: A, C, E: 10s no stimulus followed by 60s 470nm 0.3mW/mm² and 5s no stimulus. B, D, F: 10s no stimulus followed by 60s 470nm 0.8mW/mm² and 5s no stimulus. Blue bar on X-axis indicates time of blue light illumination. Animals were fed overnight on agar plates with ATR 0.2% in OP50. Normalization of time frames 10-70s and 70-75s against 0-10s. Line chart with mean ± SEM, one-way ANOVA with Bonferroni correction ***: $p \leq 0.001$, **: $p \leq 0.01$, *: $p \leq 0.05$.

3.5. Targeting a Ca^{2+} conductive ChR2 variant to the ER using transmembrane domains of the *C. elegans* UNC-68 ryanodine receptor

The task of manipulating the Ca^{2+} release of the SR/ER is also to limit the implementation of the tool to the sarcoplasmic membrane. Otherwise this would result in an uncontrollable influx/outflow of Ca^{2+} ions across the cell membrane, the ER membrane or any other cellular membrane that would integrate photosensitive tools. In order to exclude this, an attempt was made to restrict the light-activated tool to the SR membrane. One option was to use the transmembrane domain TM5 and TM6 of the intrinsic *C. elegans* ryanodine receptor. The plasmid comprising pmyo-3::PsCatCh::YFP::UNC-68 TM5+6 (from now on called PsCatCh UNC-68 TM5+6), exhibits a ~3-fold higher unitary conductance, greater relative permeability to Na^+ ions and faster recovery from excitation. Dr. Shiqiang Gao (Nagel lab), who kindly provided the plasmid, used PsChR and introduced the L132C mutation for increased Ca^{2+} conductivity and apparent light sensitivity (Bergs et al. 2018; Kleinlogel et al. 2011). In addition to these properties, the fluorophore EYFP and the UNC-68 sequence TM5+6 were connected C-terminally, to create a SR/ER retention of the channel protein (Bhat and Ma 2002; Meur et al. 2007). After cloning the sequence of PsChR including the mutation L132C, EYFP and UNC-68 TM5+6, it was termed "PsCatCh UNC-68 TM5+6". To adapt it to the *C. elegans* organism, this construct was transferred into a myo-3 promoter to ensure expression in muscle cells.

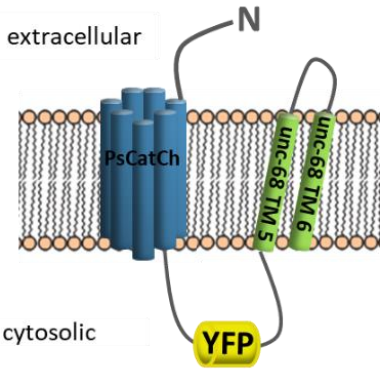

Figure 69: Graphic of the construct pmyo-3::PsCatCh::YFP::UNC-68 TM5+6. Depicted is the orientation of the SR-membrane retained channel-rhodopsin variant, cytosolic YFP and *unc-68* transmembrane helices 5 and 6.

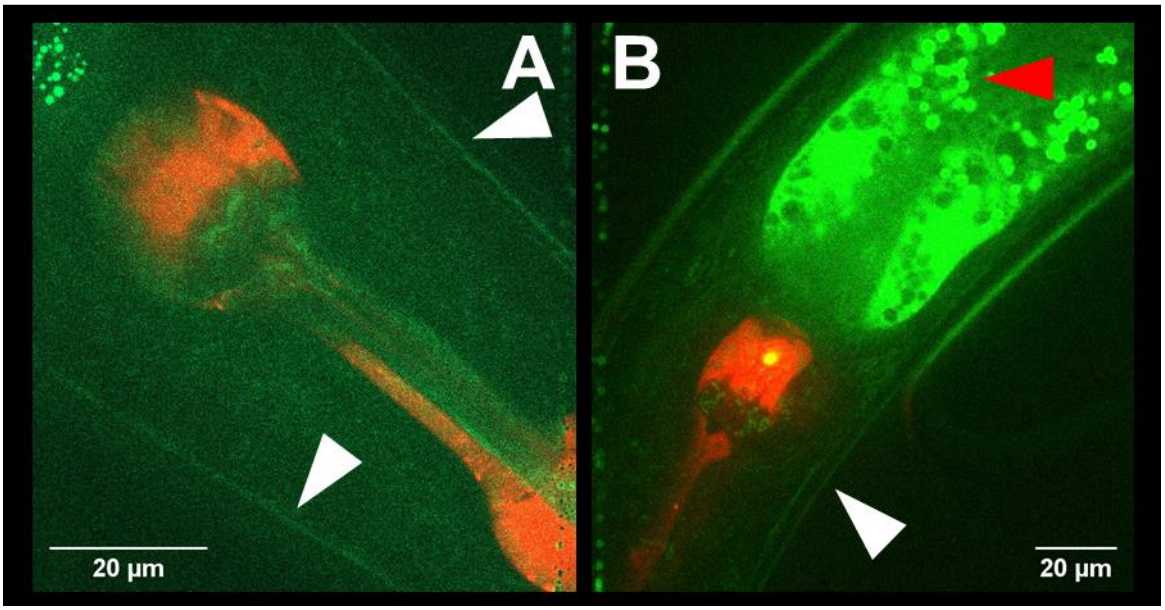

Figure 70: Fluorescence image of YFP and mCherry next to the head region. A-B) White arrow heads indicate stronger fluorescence of YFP in the cuticle. B) Also visible is the auto fluorescence in the intestine, marked by red arrow head. Scale bar, 20µm

Injection of the plasmid pmyo-3::PsCatCh::YFP::UNC-68 TM5+6 in the concentrations 30ng/µl and 300ng/µl and pmyo-2::mCherry as Co-marker, led to the strains ZX2452 and ZX2542. Expression of mCherry in the pharynx in red (*Figure 70*) verified a successful uptake of the injected DNA and

transmission to the next generation. A clear fluorescence can be seen in the body wall of the animals, indicated by white arrow heads, but also the autofluorescence of the intestine (red arrow).

3.5.1. Light-evoked effects on swimming behavior

Stimulation by 470nm was applied for 30s after a 30s period in background light. PsCatCh::YFP::UNC-68 TM5+6 (30ng/µl injected pasmid) (ZX2452 *lite-1(ce314)* [pmyo-3::PsCatCh::YFP:: UNC-68 TM5+6 (30ng/µl); pmyo-2:mCherry (3ng/µl)]) when supplemented with ATR, answered by reducing the thrashing rate from 35.2 ± 2bbpm to 28.7 ± 2bbpm during blue light stimulus. ANOVA analysis calculated a significant reduction during blue light. When PsCatCh::YFP::UNC-68 TM5+6 animals were not supplemented with ATR, reduced swimming cycles could also be observed with a mean of 37 ± 2bbpm and median 40bbpm during no stimulus period, reducing to 34 ± 2bbpm in average. Nevertheless, it was not calculated significant. *lite-1* was measured as control group as well, both supplemented with ATR and lacking ATR. These animals did not respond to 1.26mW/mm² blue light stimulation significantly, but also with decreased thrashes, wherein the mean decreased when first 30s are compared to 30-60s. *lite-1* reduced form 30.9 ± 1.8 to 28.4 ± 1.6bbpm and for ATR *lite-1* animals 36.4 ± 1.5 to 33.4 ± 1bbpm was counted. The normalized decrease in *Figure 71* B) illustrates the sharp decline even more clearly.

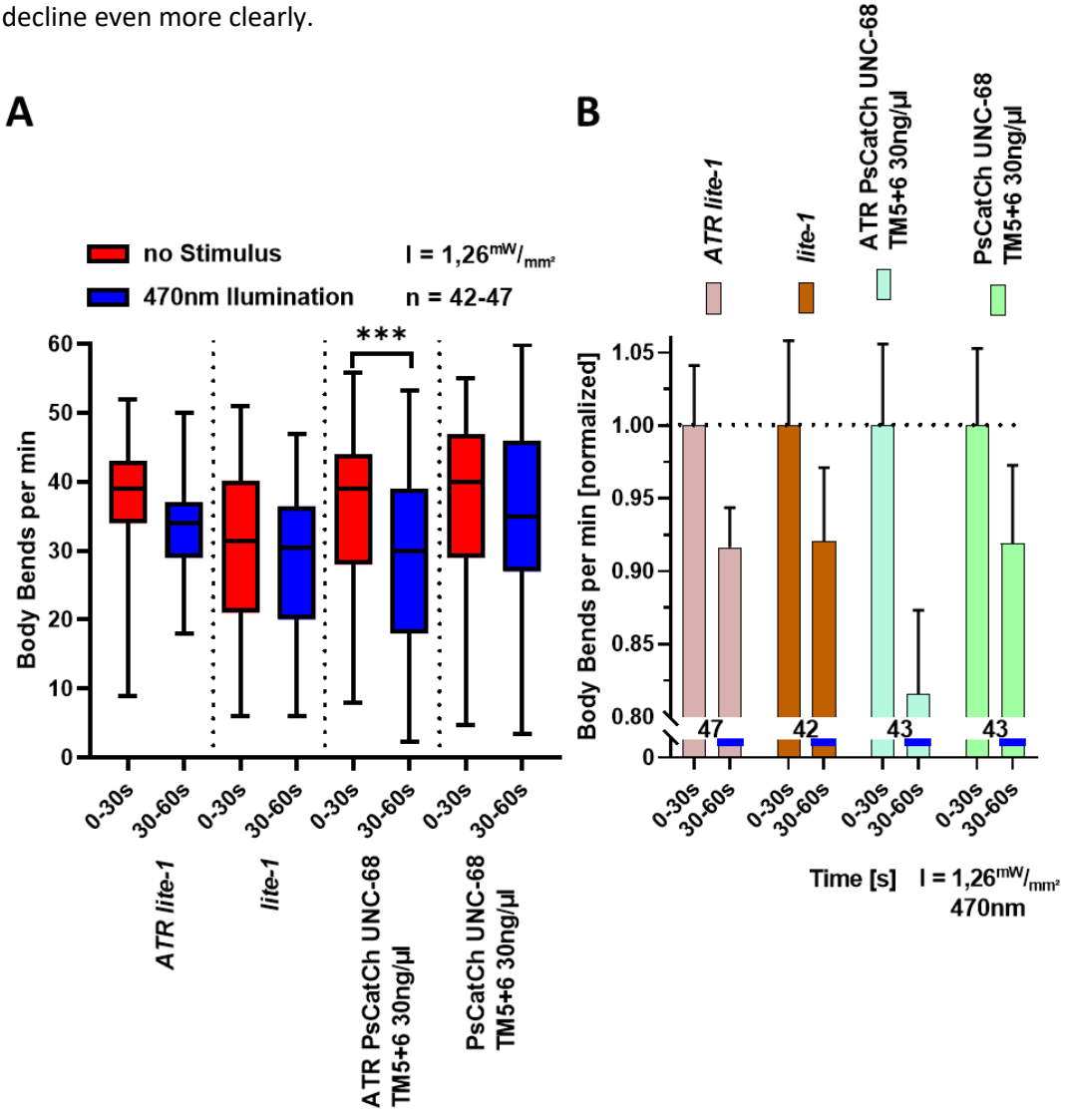

Figure 71: Photostimulation is reducing thrashing rate in ATR supplemented transgene animals. A) Strain PsCatCh::YFP::UNC-68 TM5+6 is reducing thrashes measurably during blue light illumination, when fed with ATR. Red: 30s no stimulus, blue: 30s 470nm 1.26mW/mm². Animals were fed overnight on agar plates with ATR 0.2% in OP50 and without ATR. Box plot, ANOVA with Bonferroni correction, ***: p ≤ 0.001, **: p ≤ 0.01, *: p ≤ 0.05. Median, IQR, whiskers: 2.5 to 97.5. B) Normalized data of body bends per min as seen in A). Photostimulation denoted by blue bar, n numbers for each strain are given over the X-axis. Transgenic strains were analysed by two-way ANOVA, with Bonferroni correction to the corresponding time frame of wild-type or *lite-1*, ***: p ≤ 0.001, **: p ≤ 0.01, *: p ≤ 0.05.

3.5.2. Restriction of swimming cycles through photostimulation

The assay was repeated in the Multi Worm Tracker, to obtain more data, using a lower intensity of 0.63mW/mm². Statistical tests of the data, illustrated in Figure *72*, calculated a significant drop of thrashes for ATR supplemented animals, of strain PsCatCh::YFP::UNC-68 TM5+6 30ng/µl and PsCatCh::YFP::UNC-68 TM5+6 300ng/µl (ZX2542 *lite-1(ce314)* [pmyo-3::PsCatCh::YFP::CeRyR (300ng/µl); pmyo-2:mCherry (3ng/µl)]), when comparing the stimulation period to the pre-stimulus period. PsCatCh::YFP::UNC-68 TM5+6 animals raised on ATR, lowered swimming cycles by -11.3% from 69.7 ±2.8 to 61.8 ± 2.7bbpm in mean during blue light stimulation. Lacking ATR, they exhibited a reduced thrashing rate by -2.1%. In PsCatCh::YFP::UNC-68 TM5+6 300ng/µl animals, injected with a tenfold higher dose of the plasmid, we also see a decrease when ATR was supplemented by -11.9% from 69.2 ± 2.7 to 61 ± 2.8bbpm, and for PsCatCh::YFP::UNC-68 TM5+6 300ng/µl -4.5%. A slight drop of *lite-1* and *lite-1* raised on ATR by -7%, respectively -7.2%, indicates a non-essential sensitivity to blue light. The normalized data, revealing a significant deviation between the strains PsCatCh::YFP::UNC-68 TM5+6 30ng/µl with and without ATR supplementation, indicate a blue light-dependent suppression of swimming cycles.

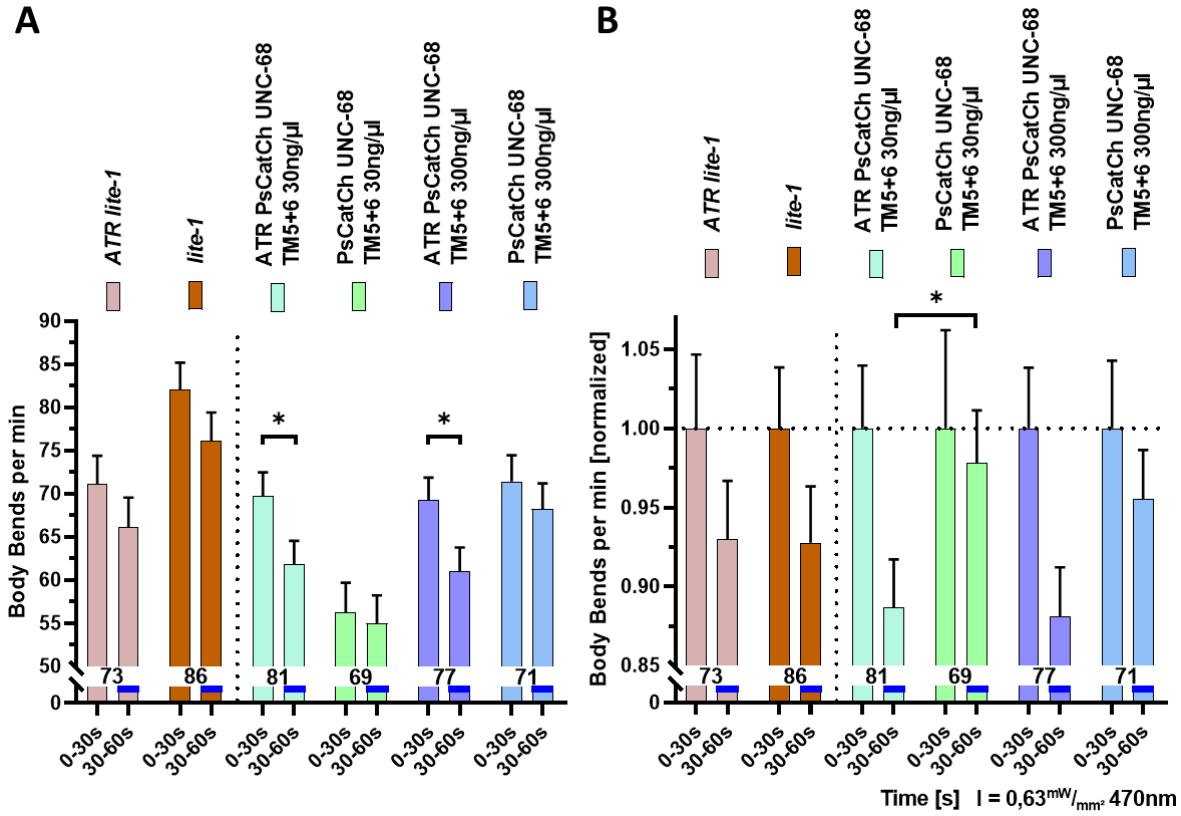

Figure 72: Swimming behaviour was restricted by photostimulation in CeRyR transgenic line strains. A) PsCatCh::YFP::UNC-68 TM5+6 inserted strains, supplemented with ATR, exhibit significantly reduced body bends, during blue light illumination. Red: 30s no stimulus, blue: 30s 470nm 0.63mW/mm². Animals were fed overnight on agar plates with ATR 0.2% in OP50 and as control without ATR. B) Normalized data of A) displays the relative deviation among the examined strains, revealing a significant divergence of stimulated animals among group ATR PsCatCh::YFP::UNC-68 TM5+6 30ng/µl and PsCatCh::YFP::UNC-

68 TM5+6 30ng/µl. Photostimulation denoted by blue bar, n numbers for each strain are given over the X-axis. Two-tailed unpaired T-test with Welch's correction, Two-way ANOVA, ***: $p \leq 0.001$, **: $p \leq 0.01$, *: $p \leq 0.05$.

3.5.3. Blue light stimulation has no UNC-68 TM5+6 induced effect on body length

The significant drop in swimming cycles raised the question of, whether this effect could also be verified by contracted body wall muscles. In order to prove this possible blue light-dependent change in the length of the BWM, a contraction assay was carried out, using the inverted microscope Zeiss Axiovert 200 (Zeiss). The protocol for this test was: 10s in dark, to have reliable data for normalization, 50s stimulation with 1.4mW/mm² 470nm blue light, terminating in 15s no stimulus to detect possible recovery or prolonged repercussions of illumination. In *Figure 73* A) we see that PsCatCh::YFP::UNC-68 TM5+6 30ng/µl contracted maximally by 3.9% in ATR supplemented, and -1.7% in mean for normal animals. Both are virtually the same, during, pre and post-stimulation, with the small difference that ATR animals approach the original body length by 2.5% in the recovery phase. In B) we have the same outcome of PsCatCh::YFP::UNC-68 TM5+6 300ng/µl animals, with the difference that ATR fed animals contract up to 4.73% and non-ATR animals contract up to 3% in body length.

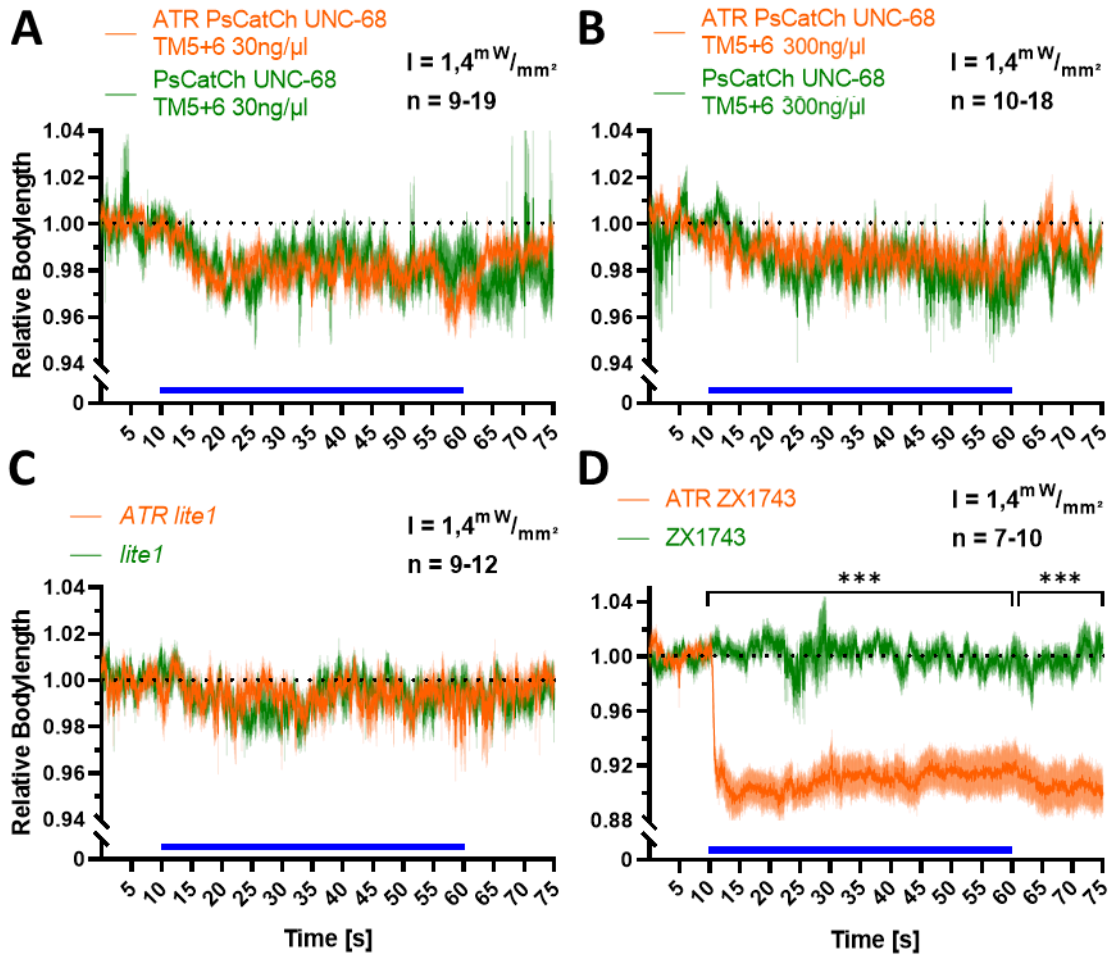

Figure 73: A strong exposure of 1.4mW/mm² blue light had no effect on body length in PsCatCh::YFP::UNC-68 TM5+6 transgenic animals. A-C) Contraction assays show no significant change in worm length during and after light illumination. D) Contraction by 9% could be detected in control strain ZX1743 supplemented with ATR. Illumination protocol: 10s no stimulus followed by 50s 470nm 1.4mW/mm² and 15s no stimulus. Blue bar on X-axis indicates time of blue light illumination. Animals were fed overnight on agar plates with ATR 0.2% in OP50. Normalization of time frames 10-60s and 60-75s against 0-10s. Line chart with mean ± SEM, two-way ANOVA with Bonferroni correction ***: $p \leq 0.001$, **: $p \leq 0.01$, *: $p \leq 0.05$.

Furthermore, the strains *lite-1* and ZX1743 (zxEx851 *lite-1 (ce315)* [pmyo-3::BeGC1::SL2::mCherry, pmyo-3::tax-2::GFP, pmyo-3::tax-4::GFP]) were measured under exactly the same conditions. Negative control is *lite-1* in C), positive control is given in D), both comprising animals reared without and with ATR. Strain *lite-1* contracted maximally by 2.4% and ATR *lite-1* in maximum 2.9%. In contrast, ATR ZX1743 contracted as expected to maximum 11.1% during the stimulus and did not recover, even after stimulus termination. Both stimulation period and recovery phase are highly significant to control animals lacking ATR.
Fluorescence of YFP could not be verified by microscopy and animals showed no discernible difference in habitus to the control group. Both, UNC-68 TM5+6 30ng/µl as well as UNC-68 TM5+6 300ng/µl responded to light stimulation in thrashing assays. In contrast, in contraction assays, ATR supplemented animals were indistinguishable from ATR deficient worms, even at higher light intensity. Further experiments with this construct, especially swimming assays, may provide better insights into its precise functionality, and perhaps answer the question why the effect is more pronounced in swimming behaviour.

3.6. Creating a Ca^{2+} leak by using the SR retention of TMH I+II of the IP_3R

In parallel to the PsCatCh::YFP::UNC-68 TM5+6 approach, another attempt was made to initiate SR-membrane retention by coupling transmembrane helices I and II (TMH I+II, aa2388-2473) of *itr-1* to psCatCh, to manipulate Ca^{2+} efflux from the SR by light stimuli. This approach was already tested by Arunas Damionaitis (Damijonaitis 2011) using TMH I and TMH II of *itr-1* for ER retention, and it was found that in rat IP_3R-1, AA E2216 to P2351 (GenBank: GQ233032), contains the TMHI and TMH II needed (Damijonaitis 2011). With this knowledge as a background, Dr. Shiqiang Gao replaced the UNC-68 TM5+6 TM5+6 in the PsCatCh construct with the IP_3R TMH I +II. In this work it was incorporated into a Vector carrying a myo-3 promoter, including an EYFP, this led to the construct PsCatCh ITR-1 TM I+II. The purpose of this plasmid was the same as PsCatCh UNC-68 TM5+6, namely retaining the light sensitive channel to the SR/ER membrane, thereby allowing a controlled Ca^{2+} efflux from the SR.

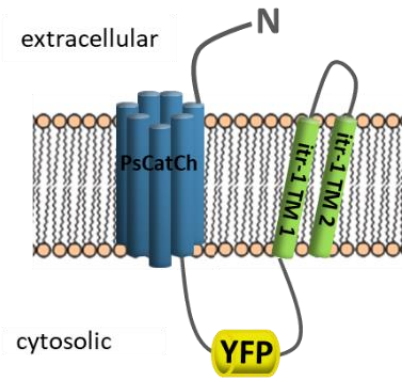

Figure 74: Schematic diagram of the PsCatCh::YFP::IP3R TMH I+II construct. It demonstrates the orientation of the SR membrane-bound PsCatCh, the cytosolic YFP and the *itr-1* transmembrane domains 1 and 2.

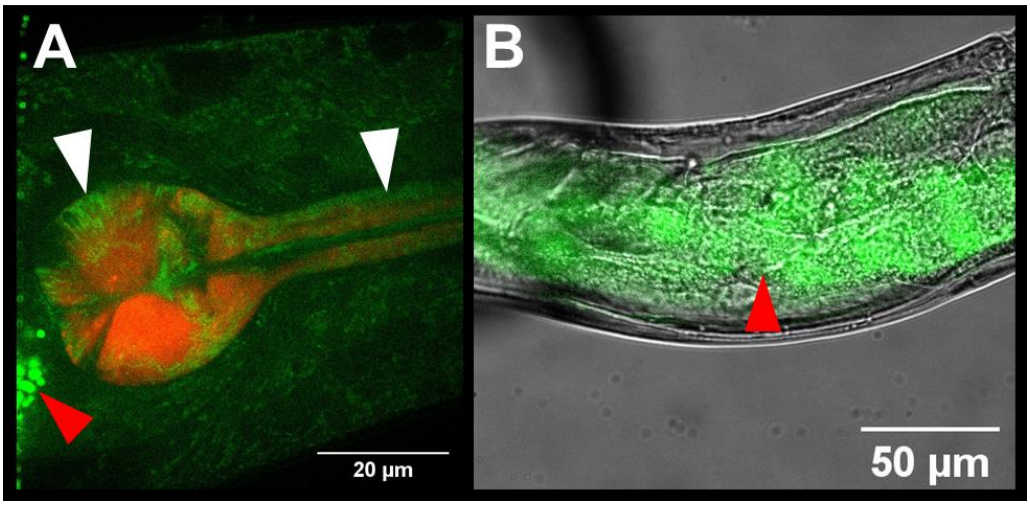

Figure 75: Fluorescence image of YFP and mCherry in the head. White arrow heads indicate auto fluorescence of the Isthmus and the Terminal bulb in A). In B) no fluorescence of body wall is visible. Auto fluorescence in the intestine, marked by red arrow head in A) and B). Scale bar, A) 20µm, B) 50µm.

Fluorescence images revealed a clear expression of the co-marker mCherry in the Terminal bulb and Isthmus in the pharynx (red coloured, in A), demonstrating successful transformation with the injected DNA. The expression in the intestines is prominent. In B) this becomes even clearer, as here no expression expected from the myo-3 promoter is visible in BWMs, instead only intestines are fluorescent (red arrow head). A correct expression of the PsCatCH::YFP::IP_3R TMH I+II construct, could therefore not be clearly confirmed by fluorescence analysis.

3.6.1. Behavioural analysis of IP3 TMH I+II transgenic animals

As in

3.5.1. swimming behaviour of ZX2539 *lite-1(ce314)* [pmyo-3::PsCatCh::YFP:: IP_3R (30ng/µl); pmyo-2:mCherry (3ng/µl)] was analysed by counting thrashes during 30s 470nm 1.26mW/mm² blue light stimulation. Outcome was a substantial decline of thrashes during light stimulation of animals reared without ATR from 26.1 ± 1.8bbpm to 22.9 ± 1.5bbpm in mean. Animals provided with ATR were thrashing without stimulus in mean with 31.1 ± 2.3bbpm and 24.6 ± 2bbpm during stimulation. Control group composed of *lite-1* was as seen in

3.5.1. The clear drop of thrashes could not be calculated significant (B), amongst the strains ATR PsCatCH::YFP::IP_3R TMH I+II 30ng/µl and PsCatCH::YFP::IP_3R TMH I+II 30ng/µl a significant deviation could not be verified in the normalised data.

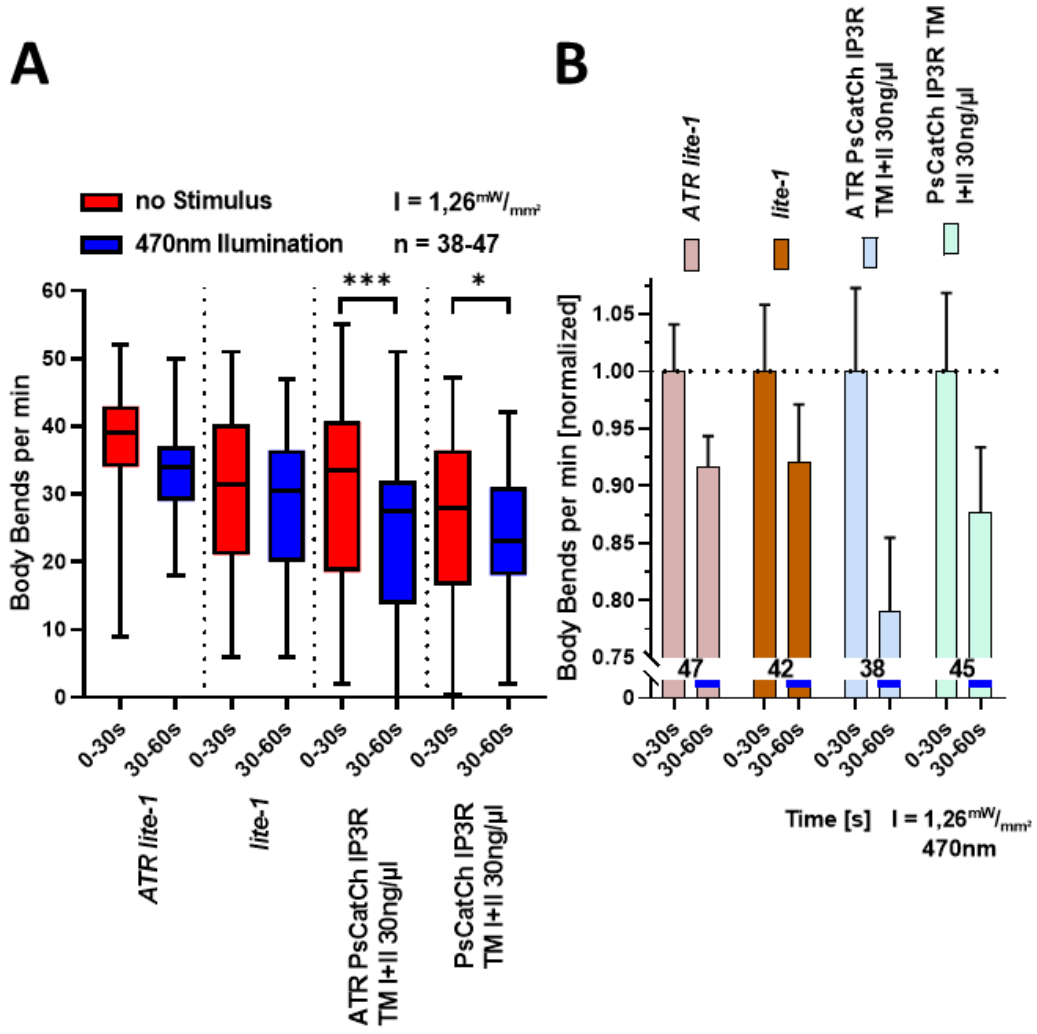

Figure 76: Strong illumination alters the swimming behaviour of transgenic animals. A) PsCatCH::YFP::IP_3R TMH I+II 30ng/µl animals significantly reduced swimming cycles during 470nm illumination. Red: 30s no stimulus, blue: 30s 470nm 1.26mW/mm². Animals were fed overnight on agar plates with ATR 0.2% in OP50 and without. B) ATR lacking animals do not clearly differ from supplemented animals in the stimulation period. Photostimulation denoted by blue bar, n numbers for each strain are given over the X-axis. Transgenic strains were analysed by two-way ANOVA, with Bonferroni correction to the corresponding time frame of wild-type or *lite-1*, ***: $p \leq 0.001$, **: $p \leq 0.01$, *: $p \leq 0.05$.

Similar, to 3.5.1. , the assays were repeated in the MWT using 0.63mw/mm². Similar to these results, we have resembling decreases in thrashes. ZX2539 and ZX2543 *lite-1(ce314)* [pmyo-

3::PsCatCh::YFP::IP3; pmyo-2:mCherry], were injected with 30ng/µl and 300ng/µl plasmid, respectively, as in 3.5. ATR PsCatCH::YFP::IP$_3$R TMH I+II 30ng/µl exhibits a 15.7% reduction starting with 68.3 ± 2.6bbpm and going down to 57.6 ± 2.8bbpm during the stimulus. PsCatCH::YFP::IP$_3$R TMH I+II 30ng/µl reduces 7.3%. Comparable data is demonstrated by ATR PsCatCH::YFP::IP$_3$R TMH I+II 300ng/µl with a 13.5% decline and PsCatCH::YFP::IP$_3$R TMH I+II 300ng/µl animals are reducing thrashes similarly by 12.6% during illumination. The animals of the strain *lite-1*, are as seen in 3.5.1. The light-induced effect observed here is much more pronounced in ATR supplemented animals (ATR Ps PsCatCH::YFP::IP$_3$R TMH I+II 30ng/µl, ATR PsCatCH::YFP::IP$_3$R TMH I+II 300ng/µl), compared to the usual response to blue light, seen in *lite-1* and in PsCatCh::YFP::UNC-68 TM5+6 animals lacking ATR. This observation is also supported by the fact that it occurs in both PsCatCH::YFP::IP$_3$R TMH I+II 30ng/µl and 300ng/µl injected animals. Retention of PsCatCh on the SR membrane may therefore have been successful, although no fluorescence could be detected by microscopic analysis.

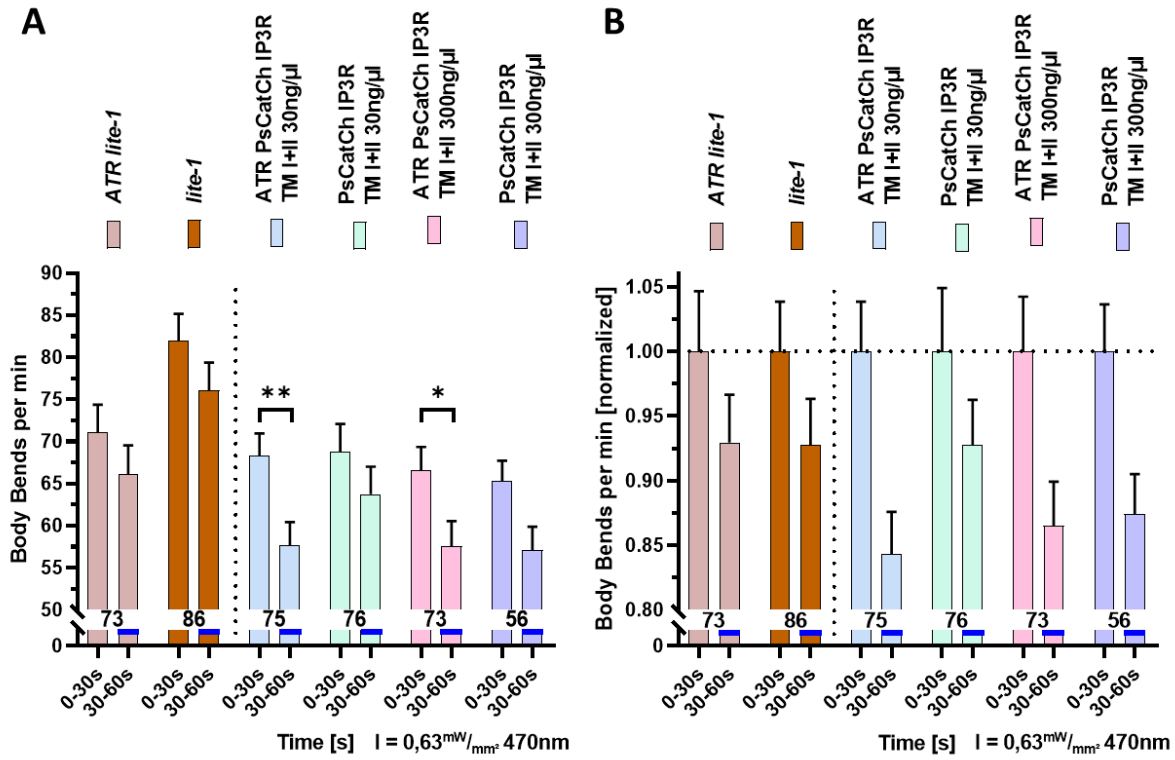

Figure 77: Swimming behaviour was restricted by photostimulation in PsCatCH::YFP::IP$_3$R TMH I+II transgenic strains Photostimulation induced inhibition of swimming cycles in ATR supplemented PsCatCH::YFP::IP$_3$R TMH I+II strains. A) PsCatCH::YFP::IP3 TMH I+II inserted strains, supplemented with ATR, exhibit significantly reduced body bends, during blue light illumination. B) Normalized data of A) displays the relative deviation among the examined strains, revealing a clear disparity of stimulated animals among PsCatCH::YFP::IP$_3$R TMH I+II ATR reared and deficient animals. Stimulation protocol: 30s no stimulus, 30s 470nm 0.63mW/mm². Animals were fed overnight on agar plates with ATR 0.2% in OP50 and as control without ATR. Photostimulation denoted by blue bar, n numbers for each strain are given over the X-axis. Two-tailed unpaired T-test with Welch's correction, Two-way ANOVA, ***: $p \leq 0.001$, **: $p \leq 0.01$, *: $p \leq 0.05$.

3.6.2. Body length under blue light stimulation

Expecting a contraction of body wall muscles, when Ca^{2+} was released from the SR (Endo 2009; Kuo and Ehrlich 2015), ATR fed animals of PsCatCH::YFP::IP_3R TMH I+II 30ng/µl contracted a maximum of 3.6% in A). Pure OP50 fed animals are 3% maximally contracted during stimulus. PsCatCH::YFP::IP_3R TMH I+II 300ng/µl and ATR PsCatCH::YFP::IP_3R TMH I+II 300ng/µl briefly contracted 4.3%, and 3.2%. In both A) and B), the different groups contracted slightly while exposed to blue light, without differing significant from their control group, except for 5s in the time frame 20-25s, which was caused by a brief re- elongation of ATR lacking animals. What all animals have in common was the slight recovery after stimulus ceased. In C), the negative control *lite-1*, and in D) the positive control, are pictured, both comprising animals reared with and in the absence of ATR. Strain *lite-1* maximally contracted by 2.4% and ATR *lite-1* by a maximum of 2.9%. ATR ZX1743 contracted by a maximum of 11.1 throughout the light pulse and did not recover, nor did it recover after stimulus termination. Both, stimulation period and recovery phase are highly significant to control animals which did not receive ATR.

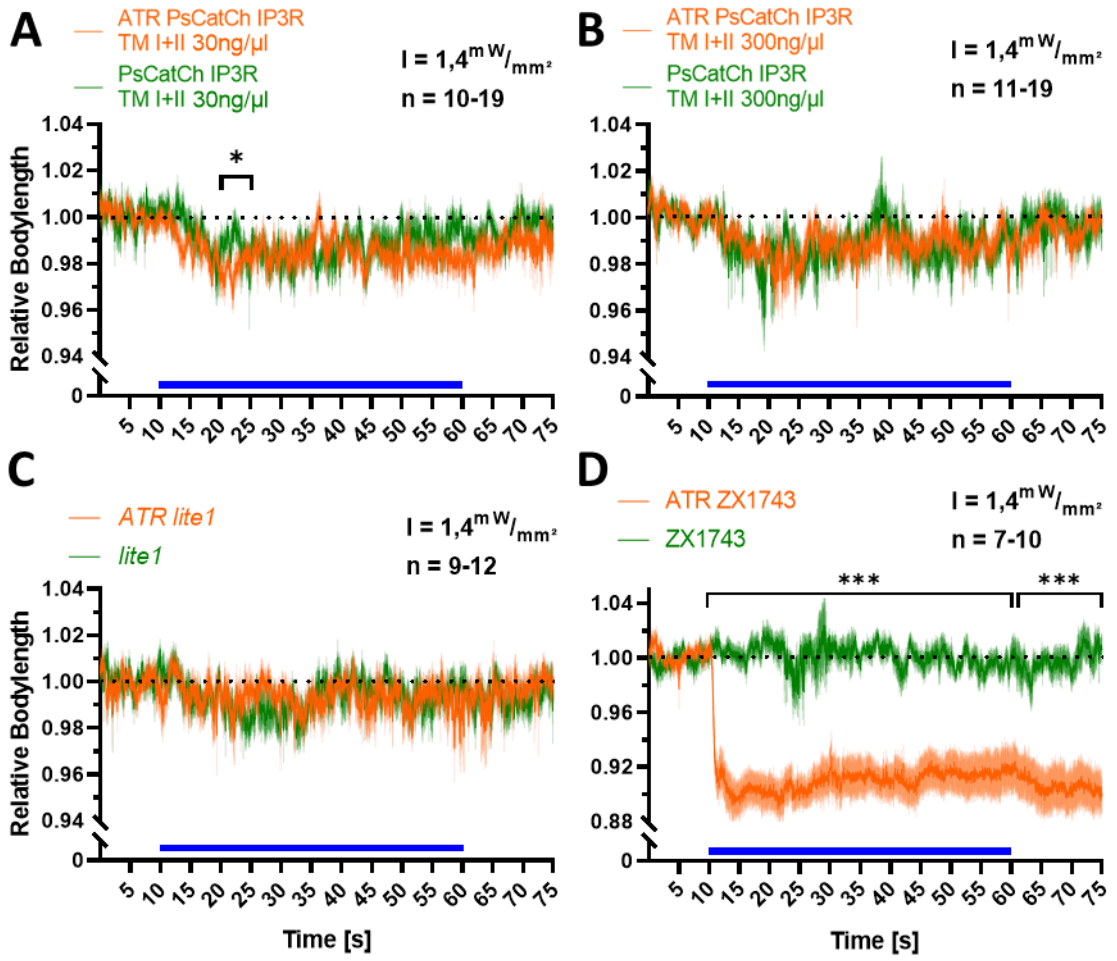

Figure 78: Strong exposure to blue light could trigger a short-term shift in the body length of ATR-reared animals. A) PsCatCH::YFP::IP_3R TMH I+II animals exhibited a stronger contraction than re-elongating ATR fed animals. B) A 10-fold higher concentration of injected plasmid did not lead to a stronger response to photostimulation, in PsCatCH::YFP::IP_3R TMH I+II 300ng/µl animals. C) Negative control *lite-1* was not influenced by the light pulse. D) The positive control of ZX1743 demonstrates the expected and prolonged contraction during and after stimulation. Illumination protocol: 10s no stimulus followed by 50s 470nm 1.4mW/mm² and 15s no stimulus. Blue bar on X-axis indicates time of blue light illumination. Animals were fed overnight on agar plates with ATR 0.2% in OP50. Normalization of time frames 10-60s and 60-75s against 0-10s. Line chart with mean ± SEM, two-way ANOVA with Bonferroni correction ***: $p \leq 0.001$, **: $p \leq 0.01$, *: $p \leq 0.05$.

Summarising the data, there is indeed a significantly stronger reduction in swimming cycles in the animals reared with ATR, however this is also evident in the control group without ATR. In addition, there is no visually detectable expression, and a non-sustained contraction during stimulation. Hence, it can be assumed, that retention of PsCatCh by ITR-1 TMH I+II is not sufficient to raise an adequate Ca^{2+} current across the SR membrane.

3.7. Light manipulation of SR Ca^{2+} dynamics with $ChRGR_{ER}$

ChRGR is a channelrhodopsin-green receiver, composing of ChR1 and ChR2, created and optimized by Wen et al. 2010 (Asano et al. 2018; Wen et al. 2010), to create the SR/ER-targeted $ChRGR_{ER}$ version. It carries the ER-retention motif Gln^{4765}-Ile^{4866} of mouse ryanodine receptor 2 and a fluorophore. Here, I availed $ChRGR_{ER}$ to directly manipulate the efflux of Ca^{2+} from the sarcoplasmic reticulum, by 450-475nm stimulation.

3.7.1. Adapting $ChRGR_{ER}$ to *C. elegans*

The first step in creating a tool suitable for *C. elegans*, was to integrate the $ChRGR_{ER}$ sequence into the myo-3 promoter. For this purpose, the original sequence was requested from Hiromu Yawo and synthesized by Eurofins. This DNA was amplified by PCR to add restriction sites, likewise the plasmid pFB14 pmyo-3::mVenus was used to integrate restriction sites. pPD96.52 was cut and all fragments were ligated with T4 DNA ligase to create pmyo-3::$ChRGR_{ER}$::mVenus. Accordingly, the plasmid pmyo-3::$ChRGR_{ER}$::mCherry was generated. This was followed by microinjection of these plasmids to generate the strains ZX2544 zxEX1191 *lite-1 (ce314)* [pmyo-3::$ChRGR_{ER}$::mCherry (0.5ng/µl); pmyo-2::CFP (2ng/µl)], ZX2545 *lite-1 (ce314)* [pmyo-3::$ChRGR_{ER}$:: mCherry (5ng/µl); pmyo-2::CFP (2ng/µl)] and ZX2546 *lite-1 (ce314)* [pmyo-3::$ChRGR_{ER}$::mVenus (2ng/µl); pmyo-2::mCherry (2ng/µl)].

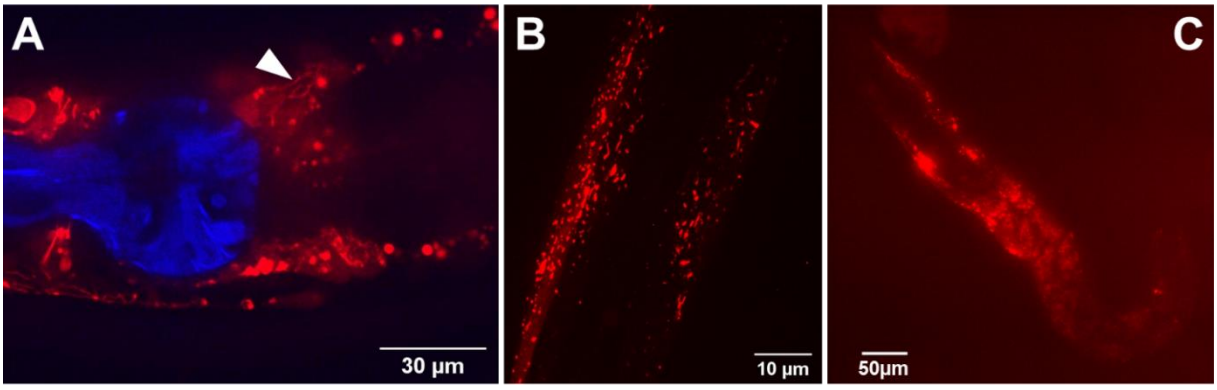

Figure 79: Fluorescence imaging of ZX2545 $ChRgR_{ER}$::mCherry (5ng/µl), using an Axiovert 200 (Zeiss). A) Merged fluorescence image of the Terminal bulb and part of the Isthmus coloured in blue by the co-marker CFP, and the expression of $ChRGR_{ER}$::mCherry, in red, in the head. B) Expression of mCherry in the mid-segment of the body, marking the BWMs that surround the body cavity. C) Image of an entire worm exhibiting fluorescence all over the body. Scale bar, A) 30µm, B) 10µm and C) 50µm.

Qualitative analysis of fluorescence was verified right after injection as seen in *Figure 79*. Co-marker expression could be detected in the pharynx, marked in blue, under the expression of the promoter myo-2. The body wall muscles were marked by the fluorescence of mCherry (B and C). In addition, the expression of $ChRGR_{ER}$::mCherry could also be verified by a 3D stack (data not shown), in which the outer layer of the worm consisting of BWMs was marked by expression, the body cavity including gonads and intestines was not affected. However, the expression pattern could also indicate that aggregated protein is present in inclusion bodies, which could explain non-functionality.

3.7.2. Swimming behaviour was not altered by photostimulation of $ChRGR_{ER}$

Body bending was quantified during 30s 60s 470nm 0.628mW/mm² and compared to a preceding 30s dark period. Swimming behaviour of transgene $ChRGR_{ER}$ animals, tended almost entirely towards a

diminished thrashing rate, with no clear change compared to ATR absent animals. ChRGR$_{ER}$ 5ng was significantly decreasing thrashes by -15.8% when comparing 0-30s and 60-90s blue light period. All transgenic strains demonstrated a lower thrashing rate than *lite-1*. Swimming behaviour of the control groups *lite-1*, ChRGR$_{ER}$ 0.5ng, ChRGR$_{ER}$ 5ng and CHRGR$_{ER}$ 2ng, should only change to the extent that it applies to *lite-1* under photostimulation. In this assay (*Figure 80*, D) *lite-1* proved to be non-sensitive to 0.63mW/mm² 470nm blue light, deprived of ATR, by thrashing with 62.4 ± 4.3bbpm; 61.2 ± 4.4bbpm and 61.9 ± 5.5bbpm, before during and after photostimulation, respectively. Supplemented with ATR, *lite-1* is reducing swimming cycles by -13.1% and -16.1% during and after light exposure.

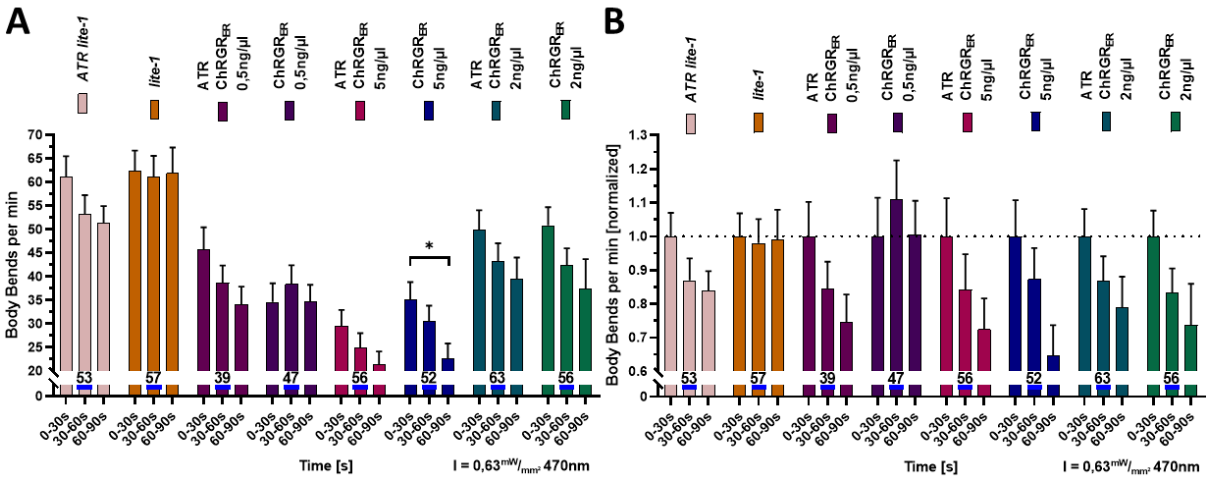

Figure 80: All ATR-supplemented animals reduced swimming cycles under the influence of blue light. A) ATR ChRGR$_{ER}$ 5ng reduced body bends during blue light illumination. B) Normalized values of body bends per min, comparing the respective time intervals of ATR-fed animals and normal animals. No definite differences could be found, the same applies to the non-supplemented animals. Stimulation protocol 30s no stimulus, blue: 60s 470nm 0.63mW/mm². Animals were fed overnight on agar plates with ATR 0.2% in OP50 and as control without ATR. Two-tailed t-test with Welch's correction, ***: $p \leq 0.001$, **: $p \leq 0.01$, *: $p \leq 0.05$.

Normalized data of the thrashing assays (*Figure 80*) underlines the figures of absolute thrashing rate. Statistical tests were performed for the time frames 0-30s compared to 30-60s and 60-90s, of ATR supplemented animals, against the corresponding ATR deficient strain, detecting no striking difference. Comparing the only significant change of swimming behaviour of ChRGR$_{ER}$ 5ng/µl in *Figure 80* A) to B) (dark green), the difference is more prominent in normalized values. However, comparing the respective time intervals of ATR-fed animals and ATR deficient animals, no definite differences could be found, the same applies to the non-supplemented animals. These results reveal that there was no blue light-dependent effect on swimming locomotion, using an intensity of 0.63mW/mm² in ATR-fed animals.

3.7.3. Elongation or contraction of body wall muscles could not be provoked by a blue light stimulus

To rule out that a small body wall muscle contraction could be overseen, a contraction assay was performed for 75s, including 10s dark video acquisition, 50s 470nm 1.4mW/mm² and recovery phase of 15s darkness. None of the tested strains showed any change in body length during or after blue light illumination, except the positive control in E), although 1.4mW/mm² should be sufficient to activate $ChRGR_{ER}$ (Asano et al. 2018).

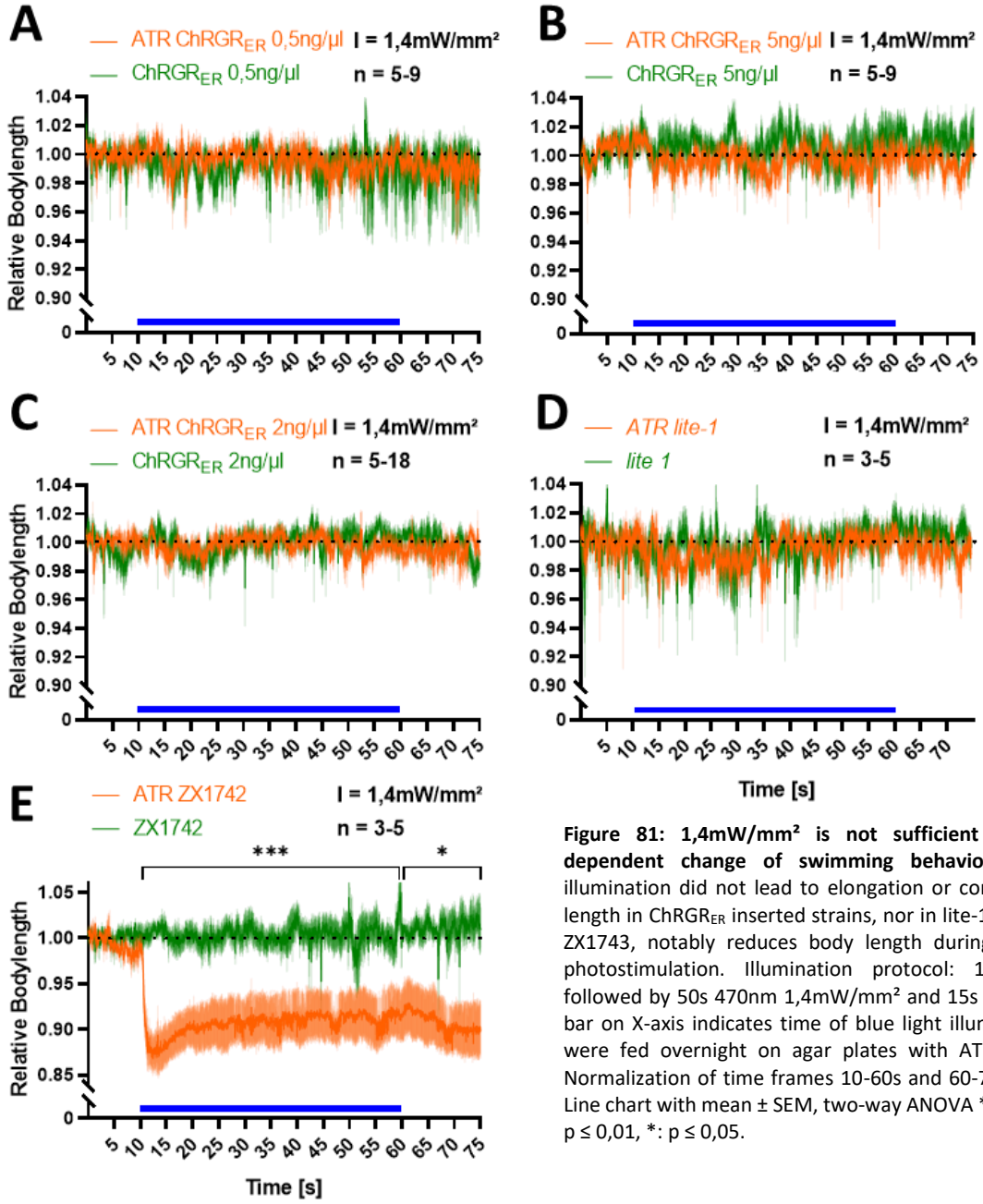

Figure 81: 1,4mW/mm² is not sufficient to evoke light dependent change of swimming behaviour. A-D) Strong illumination did not lead to elongation or contraction of body length in $ChRGR_{ER}$ inserted strains, nor in lite-1 E) Control strain ZX1743, notably reduces body length during and after light photostimulation. Illumination protocol: 10s no stimulus followed by 50s 470nm 1,4mW/mm² and 15s no stimulus. Blue bar on X-axis indicates time of blue light illumination. Animals were fed overnight on agar plates with ATR 0,2% in OP50. Normalization of time frames 10-60s and 60-75s against 0-10s. Line chart with mean ± SEM, two-way ANOVA ***: p ≤ 0,001, **: p ≤ 0,01, *: p ≤ 0,05.

Since no light-triggered response occurred during thrashing or contraction assays, despite microscopic verification of fluorophore expression, this approach was no longer pursued.

Taken together results of genetically integrating an ER retention motif of mRyR2 (*M. musculus*) and hRyR2, lead to the conclusion that 63% homology of *C. elegans* and mammalian ryanodine receptor is not sufficient, to ensure a SR retention and/or expression of RyR. Neither as truncated channel nor as working tetramer, although expression was proven by fluorescence imaging.

3.8. Enhancing Ca^{2+} conductivity with ChR-XXM

ChR-XXM (XXM), a ChR2 D156H mutant was used for testing enhanced Ca^{2+} conductivity in *C. elegans*. XXM was created as a channelrhodopsin variant, to meet the demand for higher Ca^{2+} conductance and more specific ion permeability (Duan et al. 2019). It was kindly provided by Dr. Shiqiang Gao. In order to transfect *C. elegans* with ChR-XXM, a fragment of it was amplified by PCR and digested. pDD96.52 was used as vector including the pmyo-3 promotor, additionally it was also digested for sticky ends. As fluorophore, mVenus was taken from pTH37, by PCR amplification and subsequent digestion. The three fragments were ligated to the plasmid pFB11 pmyo-3::ChR-XXM4::mVenus using T4 ligase.

Following this, a second construct was generated using ChR-XXM and the ITR-1 TMI+II, similar to the PsCatCh::IP_3R approach in

3.6. Creating a Ca^{2+} leak by using the SR retention of TMH I+II of the IP., to retain it to the SR membrane. Multiple injections of pmyo-3::ChR-XXM::eYFP::IP_3R TM I+II into *lite-1* animals, did not generate a stable viable strain.

3.8.1. Expression of ChR-XXM in body wall muscles

Injection of pFB11 into *lite-1(ce314)* animals, yielded the strain ZX2575 *lite-1* (ce314) X [pmyo-3::XXM4::mVenus (10ng/µl); pmyo-2:mCherry (2ng/µl)], named "XXM4". Expression was verified by fluorescence imaging on the Zeiss Cell Observer SD Spinning Disc Confocal microscope. In *Figure 82*, the most prominent expression was detected in the vulval muscles (arrow a). Arrowhead b indicates small granules of the intestine, composed of lipofuscin, that induce most of the background fluorescence (Forge and Macguidwin 1989; Klass 1977; Clokey and Jacobson 1986). In C) the slight expression in body wall muscles can be seen.

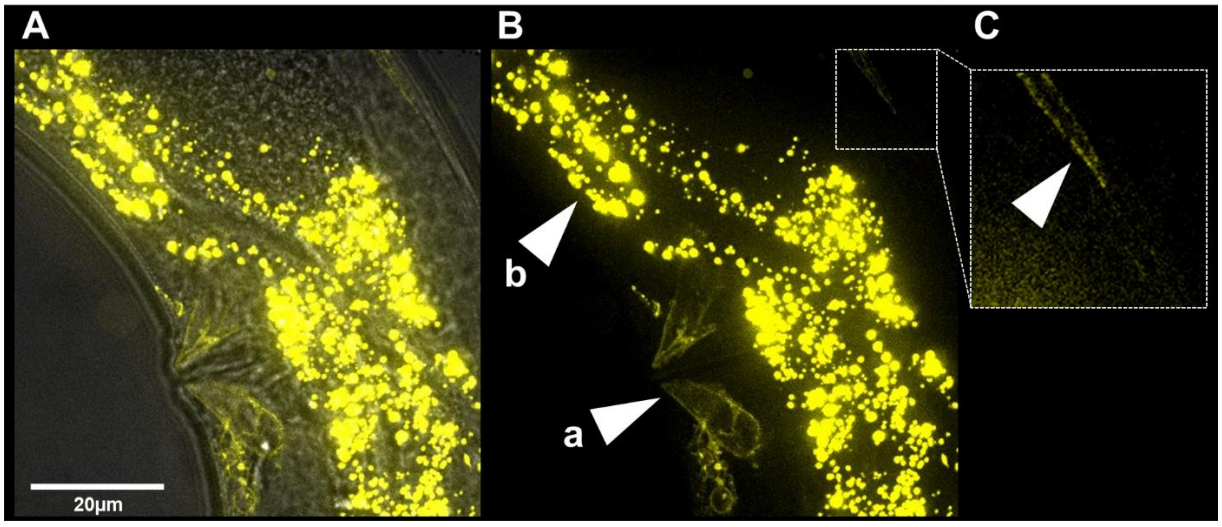

Figure 82: Confocal image of XXM4 expression in body wall and vulval muscles. A) merged image of transmission microscopy and mVenus fluorescence microscopy. B) Arrowhead a indicates the fluorescence of mVenus connected to XXM4 in the vulval muscles under the expression of the myo-3 promoter. Arrow b indicates the autofluorescence of small granules of gut tissue. C) Arrowhead indicates fainter expression in the body wall muscles. Scale bar 20µm.

3.8.2. ChR-XXM provokes body wall muscle contraction during short pulse stimulation

To investigate the effects of XXM4, which is expressed in body wall muscles devoid of retention to the SR membrane, body contraction was examined before during and after 0.8mW/mm² 470nm blue light stimulation for 2s. The maximal contraction in *Figure 83* A) in XXM4 animals without ATR supplementation is -2.6% right after the stimulus ended. This contraction is explained by reversals, which could be observed during the video recording. When XXM4 animals were raised with ATR, they contracted maximally -13.1% during photostimulation, although they reached maximum contraction with a small delay after the light was turned off at -13.4%. Contraction lasted until approximately 1s after stimulus termination until elongation reappeared but could not totally recuperate during 10s recovery phase. As control the strain ZX1743 *lite-1 (ce314)* X, zxEx851 [pmyo-3::BeGC1::SL2::mCherry, pmyo-3::tax-2::GFP, pmyo-3::tax-4::GFP] was chosen, having already demonstrated blue light dependent contraction (Nagpal 2017). In B), we see the contraction of BWMs in ZX1743 animals reached a maximum of -1.7% with. As expected, ATR fed animals maximally contracted to -8.3%, relative body length, during the light pulse and reached the maximum post-stimulus -8.5, without recovering.

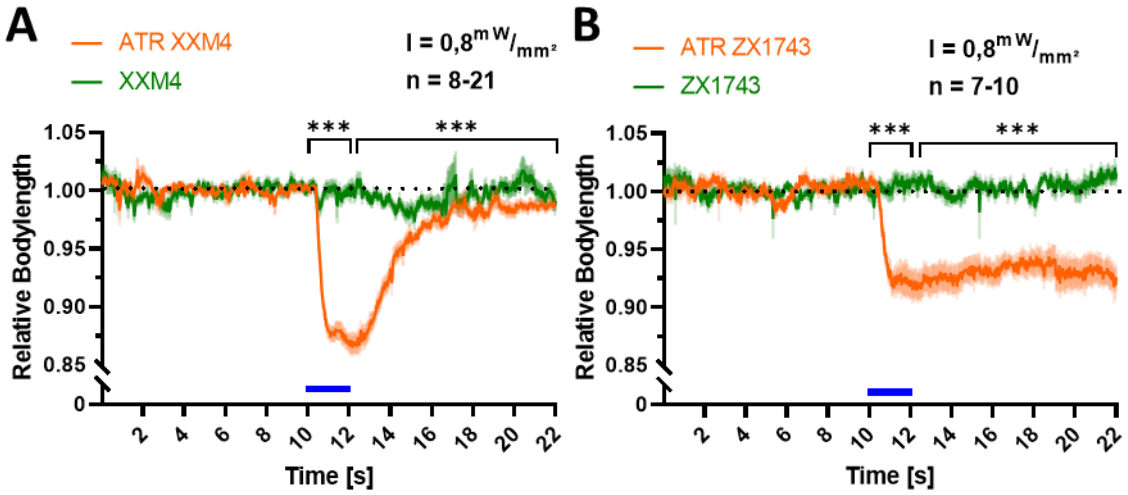

Figure 83: Blue light stimulation causes significant contraction in XXM4 animals fed with ATR. A) Contraction of XXM4 animals during light illumination of ATR reared animals. B) The positive control ZX1743 worms contracted continuously during and after light illumination. Illumination protocol: 10s no stimulus followed by 2s 470nm 0.8mW/mm² and 10s no stimulus. Blue bar on X-axis indicates time of blue light illumination. Normalization of time frames 10-12s and 12-22s against 0-10s. Line chart with mean ± SEM, two-way ANOVA with Bonferroni correction***: $p \leq 0.001$, **: $p \leq 0.01$, *: $p \leq 0.05$.

3.8.3. Strong reduction in body length during long term illumination

With a successful first test of XXM4 during a short-term low intensity blue light pulse, it was now investigated, whether an even stronger contraction could be provoked and if a full recovery of body length after stimulation would occur during a prolonged recovery phase. The adapted light protocol was set to 10s in darkness, 50s 1.4mW/mm² 470nm blue light exposure and 15s recovery in darkness. Maximal contraction of ATR fed animals in A) increased to 16%, during stimulation. XXM4 control animals contracted -1.6% in mean and elongated back to the basal length at the end of recovery period. ZX1743 worms contracted a maximum of -2.9% for short intervals, while ATR ZX1743 animals contracted -8.1% in maximum, during and -8.3% after stimulus. Furthermore, ATR-fed XXM4 animals recovered up to 93% of their natural body length very rapidly immediately after the end of stimulation, in contrast to ZX1743.

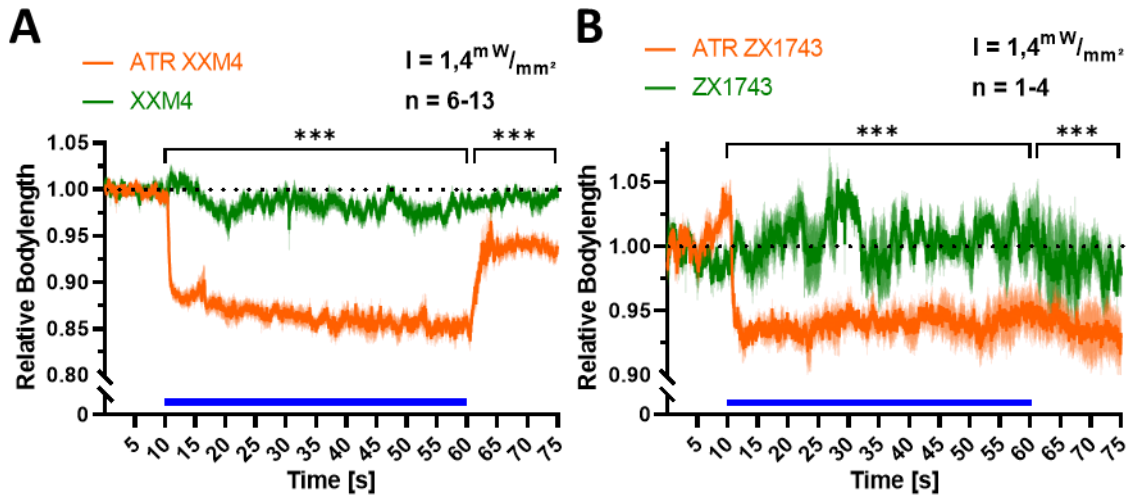

Figure 84: Contraction of XXM4 occurs during stimulus and recovers 10% afterwards. A) XXM4 shows significant change in worm length during and after light illumination, when animals fed with ATR and animals without ATR are compared. B) Contraction assay of strain ZX1743 shows significant change in worm length during and after light illumination between animals fed with ATR and without supplementation. Illumination protocol: 10s no stimulus followed by 50s 470nm

1.4mW/mm² and 15s no stimulus. Blue bar on X-axis indicates time of blue light illumination. Animals were fed overnight on agar plates with ATR 0.2% in OP50. Normalization of time frames 10-60s and 60-75s against 0-10s. Line chart with mean ± SEM, t-test with Welch's correction, two-way ANOVA with Bonferroni correction ***: $p \leq 0.001$, **: $p \leq 0.01$, *: $p \leq 0.05$.

These strong effects of the XXM4 animals reared with ATR, should be caused by the capability of ChR-XXM to depolarise the plasma membrane. Moreover, it appears that the strength of the contraction was directly related to the intensity and duration of photostimulation. These results prove that XXM is a perfect candidate to replace other ChR and maximise Ca flux on the SR/ER membrane.

3.9. Integration of the LOV2 domain into SERCA *sca-1* and RyR *unc-68* using CRISPR

As described in chapter 3.3. Attempting to achieve photo-triggering of the truncated hRyR2 through the LOV2 domain the integration of the LOV2 domains (L404-L546) into the truncated human ryanodine receptor construct did not lead to detectable expression and resulted in no significant light-triggered changes of locomotion behaviour during thrashing and contraction assays. Since it is unclear whether the human RyR2 can be functionally expressed in *C. elegans,* or if the truncated construct can function as a Ca^{2+} pore at all, the principle of LOV-domain induced conformational switching was transferred to the endogenous *C. elegans* RyR (UNC-68). To this end, the LOV2 domain was integrated directly into the genomic locus of *C. elegans* using the CRISPR/Cas9 technique. Objective of this was to minimize problems like integration of the protein at the correct location, codon consensus, or stability of mammalian DNA. In parallel the same approach was chosen for *sca-1*, encoding the sole SERCA pump in *C. elegans*. Both are located on the SR membrane, and both are essential mediators of the intracellular Ca^{2+} cycle between SR lumen and cytosol, mediating neuronal and muscular activities. To reliably integrate the LOV2 domain into the *unc-68* and *sca-1* gene the CRISPR/Cas9 method was the

preferable technique. The LOV2 sequence was inserted at distinct sites of *sca-1* and *unc-68*, replacing short loops in regions where structural disturbance would be expected to have strong effects on the protein backbone and tertiary structure, either for gating (UNC-68) or inhibition (SCA-1) (Halavaty and Moffat 2007; Dagliyan et al. 2016). Preferably the integration site was set between alpha helices or two β-sheets to provoke maximal change in the protein structure upon light activation of LOV2 (see *Figure 85*, *Figure 86* and *Figure 95).* This light induced mechanical force should lead to shift of the molecular scaffold of the RyR and SERCA and by that induce Ca^{2+} flow. In case of the ryanodine receptor, the size of the huge 2.3MDa ion channel could be a problem, if it had to be altered by one LOV2 domain, however the channel is a homotetramer (Zalk et al. 2015). Each of the monomers would be expressed with the respective inserted LOV2 domain, hence the assembled channel would be mechanically moved by four light activated domains.

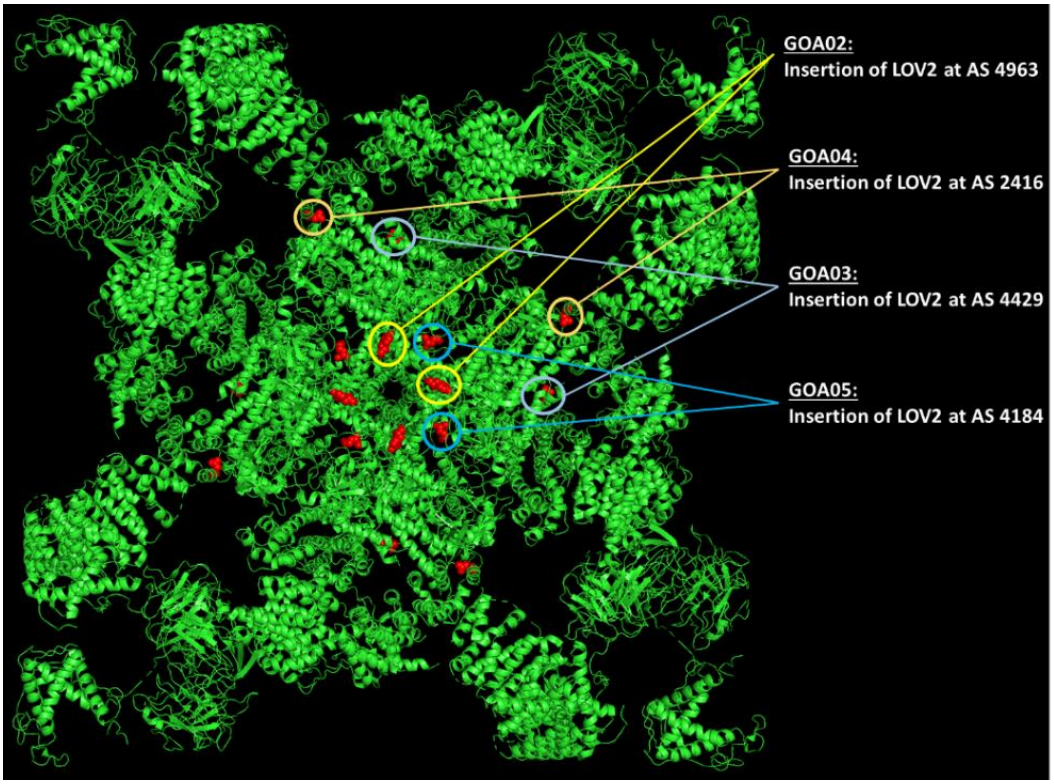

Figure 85: Insertion/replacement sites of LOV2 domains. View from above. For reasons of clarity only two of four integration sites of each LOV2 domain are marked in the molecule. This figure was generated using PyMol (PDB 6jhn).

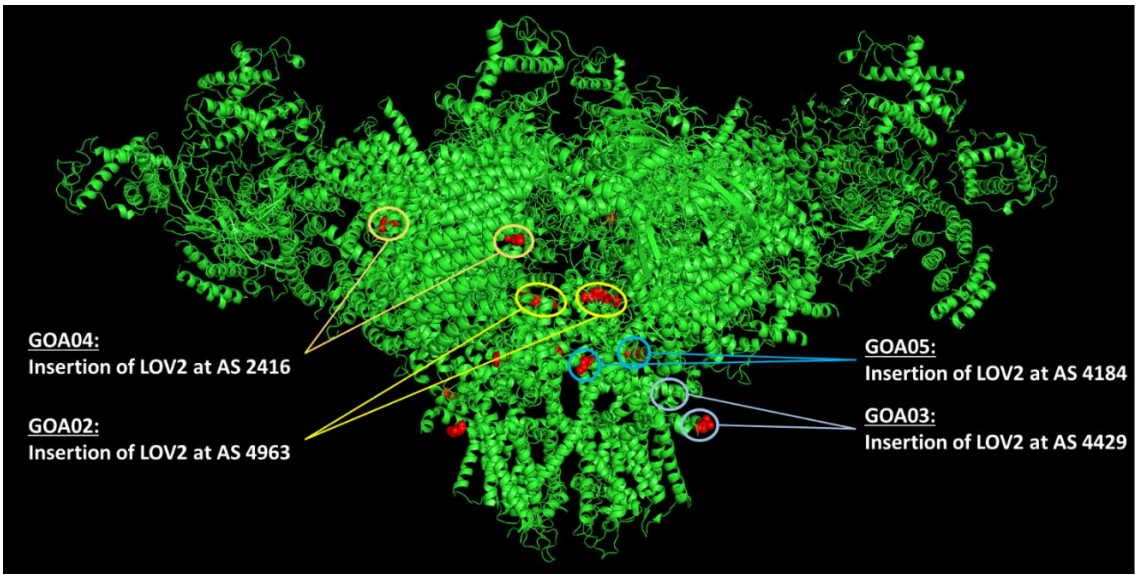

Figure 86: Insertion/replacement sites of LOV2 domains. Frontal view. For reasons of clarity only two of four integration sites of each LOV2 domain are marked in the molecule. Created with Pymol.

3.9.1. CRISPR/Cas9 based integration of LOV2 into the *unc-68 gene*

Following the same selection criteria as for optoRyR$_{Pore}$, similarly suitable sites will be chosen for insertion of the LOV2 domain in the intrinsic CeRyR (*Figure 86*). The advantage of LOV2-domain insertion by the CRISPR/Cas9 method is that the natural RyR is assumed to fulfil its function in wild-type animals with certainty, which cannot be guaranteed when replacing it by foreign proteins with high homology to the intrinsic protein. Damage, frameshift, etc. of RyR due to the insertion of the LOV2-domain would be detected similarly to an *unc-68* deletion mutant, by slow and sluggish movements, short migration distances and motor dysfunction due to flaccid paralysis (Maryon et al. 1996).
Integration of the LOV2 domain into *unc-68* was achieved by CRISPR/Cas9 mediated genome editing, by the company SUNYBiotech, creating the following transgenic strains:

Table 16: Abbreviation, ZX number of the Gottschalk lab, abbreviated strain description and integration site of LOV2 domain are listed.

Abbr.	ZX	description	Integration site
GOA02	ZX2593	UNC-68 LOV2 (1)	LOV2 inserted at AS4963 of *unc-68* Deleted sequence: TTCCTATCACCATTC Inserted sequence: TTGGCTACTACACTTGAACGTATTGAGAAGAACTTTGTCATT ACTGACCCAAGATTGCCAGATAATCCCATTATATTCGCGTCC GATAGTTTCTTGCAGTTGACAGAATATAGCCGTGAAGAAAT TTTGGGAAGAAACTGCAGGTTTCTACAAGGTCCTGAAACTG ATCGCGCGACAGTGAGAAAAATTAGAGATGCCATAGATAA CCAAACAGAGGTCACTGTTCAGCTGATTAATTATACAAAGA GTGGTAAAAAGTTCTGGAACCTCTTTCACTTGCAGCCTATGC GAGATCAGAAGGGAGATGTCCAGTACTTTATTGGGGTTCAG TTGGATGGAACTGAGCATGTCCGAGATGCTGCCGAGAGAGA GGGAGTCATGCTGATTAAGAAAACTGCAGAAAATATTGATG

			AGGCGGCAAAAGAACTT
GOA11	ZX2631	UNC-68 LOV2 (1)	LOV2 inserted at AS4963 of *unc-68*, with additional balancer Deleted sequence: TTCCTATCACCATTC Inserted sequence: TTGGCTACTACACTTGAACGTATTGAGAAGAACTTTGTCATT ACTGACCCAAGATTGCCAGATAATCCCATTATATTCGCGTCC GATAGTTTCTTGCAGTTGACAGAATATAGCCGTGAAGAAAT TTTGGGAAGAAACTGCAGGTTTCTACAAGGTCCTGAAACTG ATCGCGCGACAGTGAGAAAAATTAGAGATGCCATAGATAA CCAAACAGAGGTCACTGTTCAGCTGATTAATTATACAAAGA GTGGTAAAAAGTTCTGGAACCTCTTTCACTTGCAGCCTATGC GAGATCAGAAGGGAGATGTCCAGTACTTTATTGGGGTTCAG TTGGATGGAACTGAGCATGTCCGAGATGCTGCCGAGAGAGA GGGAGTCATGCTGATTAAGAAAACTGCAGAAAATATTGATG AGGCGGCAAAAGAACTT
GOA03	ZX2594	UNC-68 LOV2 (2)	LOV2 inserted at AS4429 of *unc-68* Deleted sequence: GGATCATCAAAGAGA Inserted sequence: TTGGCTACTACACTTGAACGTATTGAGAAGAACTTTGTCATTA CTGACCCAAGATTGCCAGATAATCCCATTATATTCGCGTCCGA TAGTTTCTTGCAGTTGACAGAATATAGCCGTGAAGAAATTTTG GGAAGAAACTGCAGGTTTCTACAAGGTCCTGAAACTGATCGC GCGACAGTGAGAAAAATTAGAGATGCCATAGATAACCAAACA GAGGTCACTGTTCAGCTGATTAATTATACAAAGAGTGGTAAAA AGTTCTGGAACCTCTTTCACTTGCAGCCTATGCGAGATCAGAA GGGAGATGTCCAGTACTTTATTGGGGTTCAGTTGGATGGAAC TGAGCATGTCCGAGATGCTGCCGAGAGAGAGGGAGTCATGC TGATTAAGAAAACTGCAGAAAATATTGATGAGGCGGCAAAAG AACTT
lite-1 GOA03	ZX2686	UNC-68 LOV2 (2), crossed into *lite-1 (ce314)*	LOV2 inserted at AS4429 of *unc-68* Deleted sequence: GGATCATCAAAGAGA Inserted sequence: TTGGCTACTACACTTGAACGTATTGAGAAGAACTTTGTCATTA CTGACCCAAGATTGCCAGATAATCCCATTATATTCGCGTCCGA TAGTTTCTTGCAGTTGACAGAATATAGCCGTGAAGAAATTTTG GGAAGAAACTGCAGGTTTCTACAAGGTCCTGAAACTGATCGC GCGACAGTGAGAAAAATTAGAGATGCCATAGATAACCAAACA GAGGTCACTGTTCAGCTGATTAATTATACAAAGAGTGGTAAAA AGTTCTGGAACCTCTTTCACTTGCAGCCTATGCGAGATCAGAA GGGAGATGTCCAGTACTTTATTGGGGTTCAGTTGGATGGAAC TGAGCATGTCCGAGATGCTGCCGAGAGAGAGGGAGTCATGC TGATTAAGAAAACTGCAGAAAATATTGATGAGGCGGCAAAAG AACTT

GOA04	ZX2595	UNC-68 LOV2 (3)	LOV2 inserted at AS2416 of *unc-68* Deleted sequence: GGATATCCAGATATTGGA Inserted sequence: TTGGCTACTACACTTGAACGTATTGAGAAGAACTTTGTCATTAC TGACCCAAGATTGCCAGATAATCCCATTATATTCGCGTCCGATA GTTTCTTGCAGTTGACAGAATATAGCCGTGAAGAAATTTTGGG AAGAAACTGCAGGTTTCTACAAGGTCCTGAAACTGATCGCGCG ACAGTGAGAAAAATTAGAGATGCCATAGATAACCAAACAGAG GTCACTGTTCAGCTGATTAATTATACAAAGAGTGGTAAAAAGT TCTGGAACCTCTTTCACTTGCAGCCTATGCGAGATCAGAAGGG AGATGTCCAGTACTTTATTGGGGTTCAGTTGGATGGAACTGAG CATGTCCGAGATGCTGCCGAGAGAGAGGGAGTCATGCTGATT AAGAAAACTGCAGAAAATATTGATGAGGCGGCAAAAGAACTT
GOA05	ZX2596	UNC-68 LOV2 (4)	LOV2 inserted at AS4184 of *unc-68* Deleted sequence: AAAGAAGTAATTGAT Inserted sequence: TTGGCTACTACACTTGAACGTATTGAGAAGAACTTTGTCATTACT GACCCAAGATTGCCAGATAATCCCATTATATTCGCGTCCGATAGT TTCTTGCAGTTGACAGAATATAGCCGTGAAGAAATTTTGGGAAG AAACTGCAGGTTTCTACAAGGTCCTGAAACTGATCGCGCGACAG TGAGAAAAATTAGAGATGCCATAGATAACCAAACAGAGGTCAC TGTTCAGCTGATTAATTATACAAAGAGTGGTAAAAAGTTCTGGA ACCTCTTTCACTTGCAGCCTATGCGAGATCAGAAGGGAGATGTC CAGTACTTTATTGGGGTTCAGTTGGATGGAACTGAGCATGTCCG AGATGCTGCCGAGAGAGAGGGAGTCATGCTGATTAAGAAAACT GCAGAAAATATTGATGAGGCGGCAAAAGAACTT

Furthermore, the strain GOA03 was crossed into *lite-1(ce314)* to exclude a light avoidance of the worms during photostimulation.

3.9.2. Potential light-evoked effects on swimming locomotion were examined in *unc-68*::LOV2 inserted strains

As a first assay to analyse light-evoked differences in the behaviour of animals bearing inserted LOV2 domains in UNC-68, thrashing assays of all *unc-68*-LOV2 strains were performed in the multi worm tracker. Data analysis is presented as body bends per min in absolute numbers and also as normalized values. The graphs depicting the bbpm are also giving the results of a two-tailed t-test including Welch's correction, in which the time frames 30-60s, 60-90s and 90-120s are matched against 0-30s. This allows a statement to be made about the influence of blue light stimulation on the respective animals.

First, we tested whether locomotion was generally impaired by the LOV2 insertion, which could indicate problems of the UNC-68 function. Strains GOA03, 4, 5 and especially GOA011 showed a significantly lower thrashing rate than wild-type animals. This suggests that the LOV2 insertions at these positions had more or less deleterious effects on UNC-68 function. Nevertheless, they did not

abrogate all UNC-68 function. The deletion mutants in this assay exhibit only about 20% of the thrashing rate of the wild-type animals. The strong effect in GOA11 probably has to do with the fact that the insertion at this position could not be homozygoused, probably because it might abolish the function of UNC-68, and that the *unc-68* locus was balanced in this strain. Thus, there is a single wild-type copy of *unc-68* and one copy with the LOV2 insertion that may not be functional. Additionally, the balancer chromosome may carry rearrangements that affect the function of several genes on this chromosome and thus may also affect normal swimming locomotion.
Next, different light intensities were used to determine a potential effect of LOV2 domain photoswitching, and to determine an optimum for these experiments. This was essential since blue light was applied in these long-term assays, which can induce photophobic responses that may interfere unspecifically with the behaviour of the LOV2 domain photoswitching. For all strains 0.3mW/mm² and 0.8mW/mm² were used, and the strains GOA04, GOA05 and GOA11 were additionally measured using 1.1mW/mm² blue light stimulation.

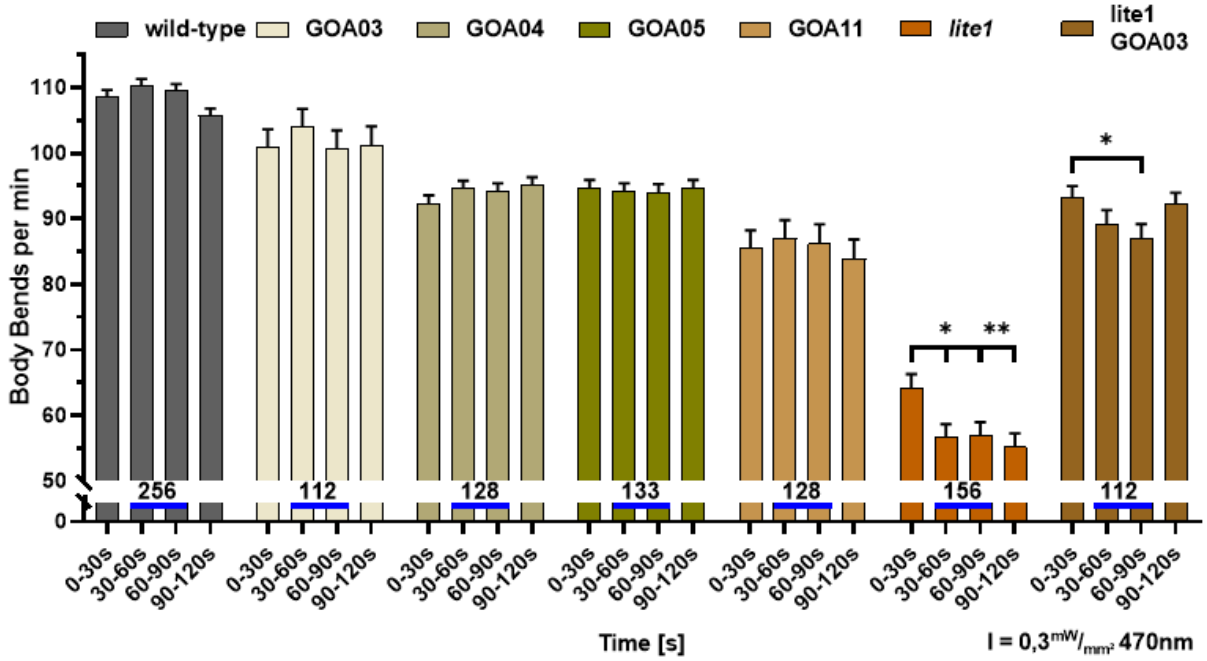

Figure 87: lite-1 GOA03 and *lite-1* shows significantly reduced thrashes during and after blue light stimulation. The strains GOA03, GOA04 and GOA11 minimally respond to photostimulation. lite-1 GOA03 and *lite-1* are reducing thrashing rate significantly during light stimulus, *lite-1* animals reduce thrashes even more after termination of blue light. Stimulation protocol: 30s no stimulation, 60s 470nm 0.3mW/mm² stimulation and 30s no stimulation. Photostimulation period is denoted by blue bars, n numbers for each strain are given above the x-axis. Time frames 30-60s, 60-90s and 90-120s of each strain were compared with the time frame 0-30s before light application, by unpaired two-tailed Student's T-Test, with Welch's correction, ***: $p \leq 0.001$, **: $p \leq 0.01$, *: $p \leq 0.05$.

During blue light stimulation, the strains GOA03, GOA04 and GOA11 follow the wild-type thrashing rate. *lite-1* animals had a significantly lower basal swimming rate, 59% of wild-type, a phenotype that has been described before (Weissenberger et al. 2011). The reason for this is unclear, but suggests that LITE-1 has positive effects on locomotion in the absence of blue light. On the other hand, despite their expected insensitivity to blue light, these animals demonstrated an unexpected and sharp drop in locomotion rate as a response to blue light. Interestingly, lite-1 GOA03 animals presented a largely restored basal swimming with an increase to 86% of wild-type. This finding is rather difficult to elucidate, as the *lite-1* mutation and the *unc-68* locus are not related and are located on different chromosomes. A functional interaction of *lite-1* and the *unc-68*, which could explain this finding, has also not been observed so far. It is also possible that the insertion of the LOV2 domain in this mutant has a general enhancing effect on UNC-68 function, counteracting the reduced swimming ability of the

lite-1 background. However, this is inconclusive as GOA03 alone had no enhancing effect on swimming in the wild-type background, rather thrashing was reduced to about 93% of wild-type, although this was not significant. Upon blue light exposure, lite-1 GOA03 showed a significant decrease of swimming locomotion after <30s photostimulation, and they showed significantly more thrashing of 12.9%, as seen in *Figure 88*, after termination of blue light, related to its control strain *lite-1*. When the relative thrashing rate of each transgenic strain in *Figure 88* is compared to wild-type, only GOA04 showed opposing swimming behaviour in the time frame 90-120s, after 470nm stimulation was turned off. GOA04 raises swimming cycles by 5.7% in relation to the respective time frame of wild-type, which dropped compared to the time of light stimulation. As mentioned above, the insertion of the LOV2 domain might have a general reinforcing influence on the UNC-68 function. However, the whole thing is put into perspective in view of the total thrashes measured, with the discrepancy being only 3bbpm *Figure 87*.

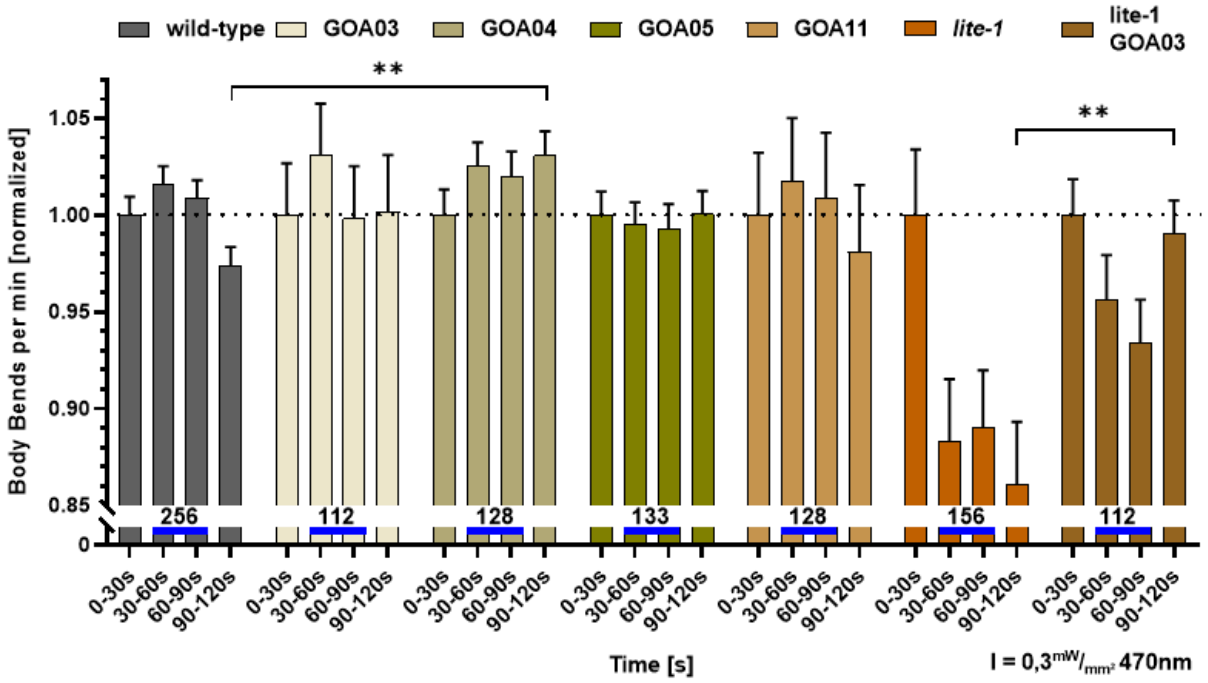

Figure 88: Comparison of LOV2 inserted strains and wild-type illustrates that 0.3mW/mm² photostimulation is insufficient to provoke altered swimming behaviour. GOA04 exhibits significant more thrashes than wild-type after stimulation terminated. lite-1 GOA03 is recovering after stimulus in contrast to *lite-1* animals. Stimulation protocol: 30s no stimulation, 60s 470nm 0.3mW/mm² stimulation and 30s no stimulation. Photostimulation denoted by blue bar, n numbers for each strain are given over the X-axis. Transgenic strains were analysed by two-way ANOVA, with Bonferroni correction to the corresponding time frame of wild-type or *lite-1*, ***: $p \leq 0.001$, **: $p \leq 0.01$, *: $p \leq 0.05$.

3.9.2.1. Moderate photostimulation induced increased swimming cycles in all strains

With an increase of light intensity to 0.8mW/mm² (*Figure 89*/*Figure 90*), the swimming performance of the animals changed to the effect that GOA11, GOA03 and GOA05 continuously increased their thrashing rate throughout the whole experiment. However, none behaved any different in relation to wild-type. Only GOA04 responded during 30-60s blue light stimulus, by diminishing the swimming cycles by -5.6%, in relation the respective time frame of wild-type. Thrashes of lite-1 GOA03 are again considerably higher than *lite-1*, whereby during and after light pulse, the progression is 16.1%, 31% and 27.2% in the corresponding time frames 30-60s, 60-90s and 90-120s of *lite-1*. Unexpectedly, the basal thrashing rate of GOA03 and lite-1 GOA03 is notably higher than its respective control wild-type and *lite-1*, throughout the entire experiment. GOA03 is thrashing faster by 9.3%. lite-1 GOA03 surprises even more with 65% increased bbpm, due to the fact that *lite-1* animals have a basal rate of 60-80bbpm. This is consistent with the previous results of 0.3mW/mm² in *Figure 87*. Importantly, in both

the 0.3 and 0.8 mW/mm² experiments, animals of the strain lite-1 GOA03 exhibited a reduced thrashing rate as response to blue light stimulation. However, the similar behaviour observed (unexpectedly) by the *lite-1* control strain, does not allow a conclusion of specific, light evoked effects in UNC-68.

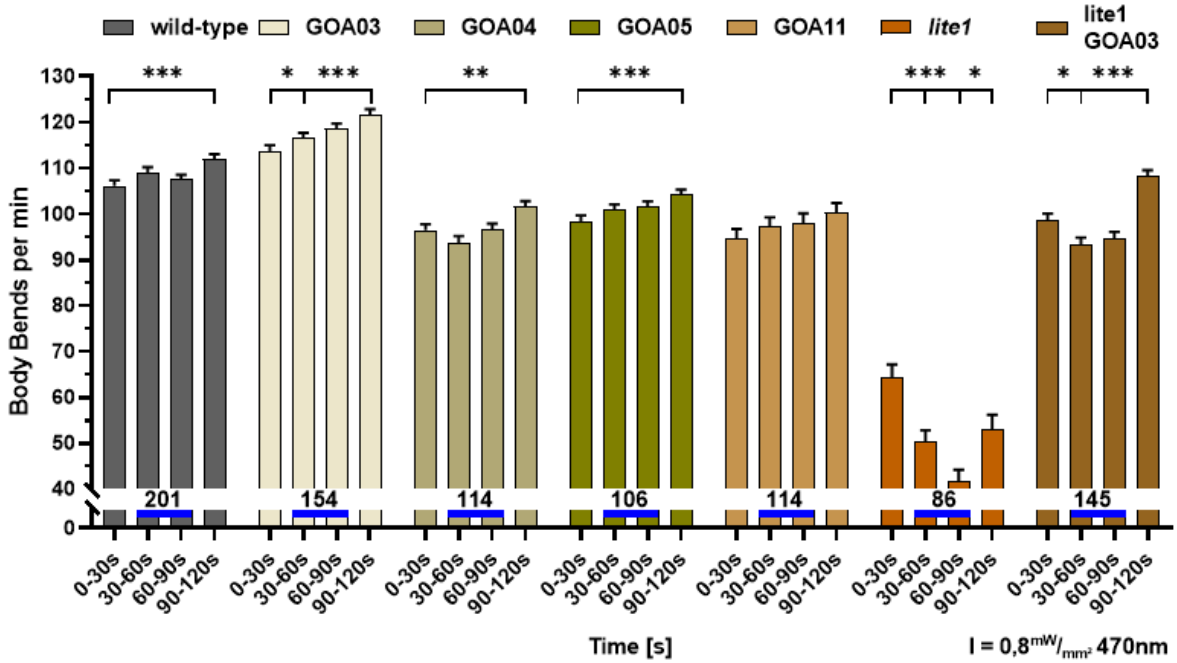

Figure 89: Illumination of transgenic strains in wild-type background causes a raise of thrashes. Significant raise of thrashes as long as illumination persists can be seen in wild-type, GOA03, GOA04 and GOA05. *lite-1* and lite-1 GOA03 react by decreasing swimming rate during 470nm stimulus. Stimulation protocol: 30s no stimulation, 60s 470nm 0.8mW/mm² stimulation and 30s no stimulation. Photostimulation denoted by blue bar, n numbers for each strain are given above the X-axis. Time frames 30-60s, 60-90s and 90-120s of each strain were compared with the time frame 0-30s before light application, by unpaired two-tailed Student's T-Test, with Welch's correction, ***: $p \leq 0.001$, **: $p \leq 0.01$, *: $p \leq 0.05$.

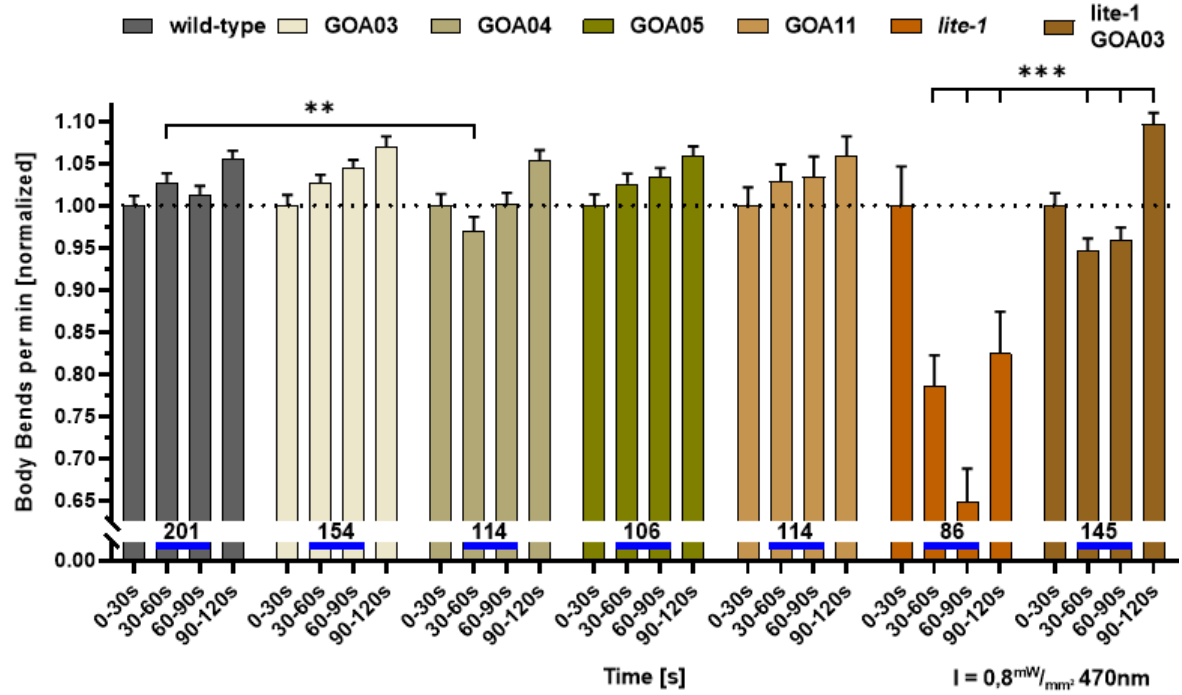

Figure 90: lite-1 GOA03 is thrashing notably more frequent than its control *lite-1* during and after photostimulation. GOA04 is reducing swimming cycles in relation to wild-type as soon as the light pulse initiates. Normalized data of body bends per min of unc-68::LOV2 integrated strains and respective control. Stimulation protocol: 30s no stimulation, 60s 470nm 0.8mW/mm² stimulation and 30s no stimulation. Photostimulation denoted by blue bar, n numbers for each strain are given

over the X-axis. Transgenic strains were analysed by two-way ANOVA, with Bonferroni correction to the corresponding time frame of wild-type or *lite-1*, ***: p ≤ 0.001, **: p ≤ 0.01, *: p ≤ 0.05.

3.9.2.2. High intensity light stimulation leads to strong reduction of swimming cycles during stimulus and to a strong increase after stimulus termination

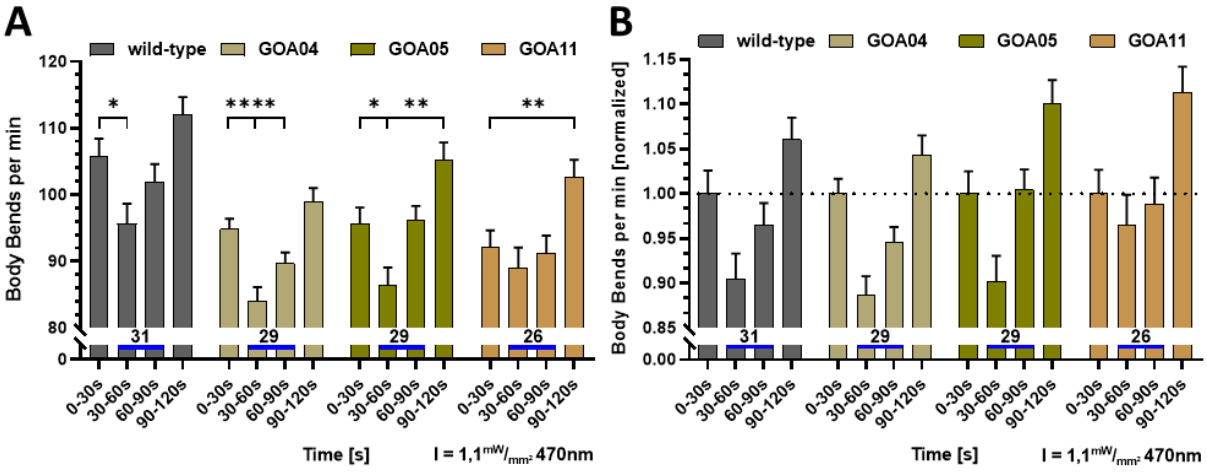

Figure 91: Strong blue light illumination leads to strong reduction of swimming cycles and a strong post-stimulus thrashing rate increase. A) Body bends per min are reduced significantly in wild-type, GOA04 and GOA05 as long as worms are illuminated with blue light. Additionally, GOA05 and GOA11 exhibit significantly increased thrashes after photostimulation ended. Transgenic strains were analysed with the corresponding time frame of wild-type, by unpaired two-tailed t-test, with Welch's correction, ***: p ≤ 0.001, **: p ≤ 0.01, *: p ≤ 0.05. B) Normalised body bends per min show no significant change when transgenic strains are compared to wild-type and its respective time frames. Stimulation protocol: 30s no stimulation, 60s 470nm 1.1mW/mm² stimulation and 30s no stimulation. Photostimulation denoted by blue bar, n numbers for each strain are given over the X-axis.

Finally, to investigate whether the response to light depends on the intensity of stimulation, a swimming assay was performed with 1.1mW/mm² 470 nm illumination for 60s. *Figure 91* A) and B), illustrate body bends per min and normalized bbpm. Here GOA05 and GOA11 are enhancing thrashing rate by 10% and 11.3% after photostimulation compared to time frame 0-30s, and by 4% and 5.3% respectively, relative to wild-type, as seen in B). This is concordant with the data shown in *Figure 88*, *Figure 89* and *Figure 90*, wherein the response was also significantly elevated after the light stimulation. GOA04 is the most regressive with -11.4% among all strains after stimulation, as demonstrated in A), besides it is the only strain that thrashes significantly less during the second period of light illumination, compared to 0-30s. Taken together, the data of *Figure 88* to *Figure 91* suggest, that the change in swimming cycles during recovery phase, is dependent on the preceding intensity of the light pulse. A rising thrash rate was observed in most strains. This would be consistent with the assumption that a stronger excitation could activate more receptors or for a longer time interval. Interestingly, the threshold at which wild-type responds to blue light by increased rather than decreased rate of swimming cycles is between 0.3mW/mm² and 0.8mW/mm². This also seems to apply to the strain *lite-1*, as we have a diminished thrashing rate at 0.3mW/mm², but an increased rate after 0.8mW/mm² blue light stimulus. Unfortunately, a measurement of *lite-1* with a photostimulation of 1.1mW/mm² was not performed.

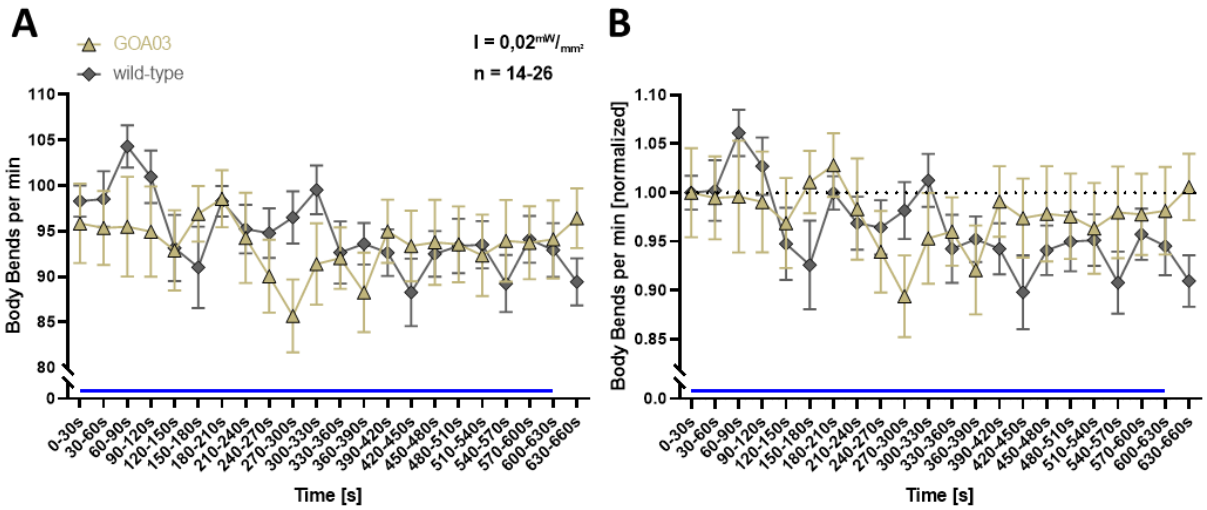

Figure 92: Very low blue light illumination leads to a reduction of swimming cycles on the long run. A) Swimming cycles of both GOA03 and wild-type animals are similarly lowered after 300s of illumination. B) Normalised data is not notably changing when GOA03 is compared to wild-type and its respective time frame. Stimulation protocol: 30s no stimulation, 600s 470nm 0.02mW/mm² stimulation and 30s no stimulation. Photostimulation denoted by blue bar.

Additional low-intensity, long-term illumination experiments with GOA03 animals, illustrate no remarkable answer compared to wild-type animals. These reach a maximum at 180-210s, which is followed by a major drop, they could not recover from. Wild-type animals on the other hand, respond to blue light after 30s of illumination by increasing thrashing frequency and dropping frequency within 120s. From time frame 330-360s onwards, the difference between the two groups was only marginal and exhibited no marked differences. Nevertheless, as soon as the light was switched off, an increase in swimming cycles in GOA03 animals could be observed, whereas wild-type animals exhibited a further reduction. With this number of animals, it was not possible to prove that long-term illumination at such low intensity levels has an effect on swimming behaviour.

3.9.3. Possible light-evoked contraction of body wall muscles was examined in unc-68::LOV2 inserted strains

3.9.3.1. Contraction of body length could be provoked in a strain by weak blue light stimulation

The change of swimming cycles in the preceding swimming assays gave a first indication, that insertion of the LOV2 domain into the *unc-68* locus could lead to a light dependent response of *C. elegans*. Hence, I continued by investigating the possible light-induced effect in 75s long contraction assays. Initial assays were performed at 470nm and an intensity of 0.3mW/mm² for 60s, with a preceding and subsequent phase of 10s and 5s, respectively, in the absence of blue light exposure. Photostimulation of strain GOA03 (*Figure 93*, A) led to a maximal body wall muscle contraction of 1.6%, in addition, a persistent contraction was observed after stimulation. When matched with the wild-type control, that maximally contracted by 1.8% during stimulation, followed by a slight contraction after the pulse, a statistical analysis revealed no noticeable difference. Animals of lite-1 GOA03 in B) contracted with a maximum of 1.8% and maximally stretched the body by 1.3%, while photostimulation was ongoing. Overall, these animals were predominantly contracted as long as blue light was shining. As soon as the blue light was switched off (70-75s) the contraction dissipated. The control for lite-1 GOA03 was the background strain *lite-1*. These animals displayed a maximal contraction by 1.2%, but also an elongation of body wall muscles by 1.1%. During relaxation period (70-75s), these animals remained slightly contracted. Altogether, the worms of strain *lite-1* did not respond at this intensity, furthermore there is also no significant difference to the strain lite-1 GOA03. When the same assay was performed

with strain GOA04, the answer to light stimulation was quite different. Graph D) illustrates that there was no response, when photostimulation was initiated, until a significant elongation in body length occurred by a maximum of 2.1% and 0.64% in Mean in the time frame 40-70s, increasing to 0.7% after termination of the light pulse. A similar response to photostimulation was found in strain GOA05, although no significance was reached. However, the first response to blue light was a contraction in time frame 10-40s by a maximum of 2.1%, followed by 1.5% elongation from 40s to 70s. Without light the recovery phase is accompanied by increased elongation. The effect of insertion of the LOV2 domain at position AS4963 of *unc-68,* including the balancer nT1[qIs51] was also investigated in contraction assays. In E) GOA11 is responding to light during a continuous stimulus after 30s of 0.3mW/mm² blue light by elongating up to a relative body length of 2.1%. After termination of photostimulation animals did not contract to normal length but remained elongated by 2.4%.

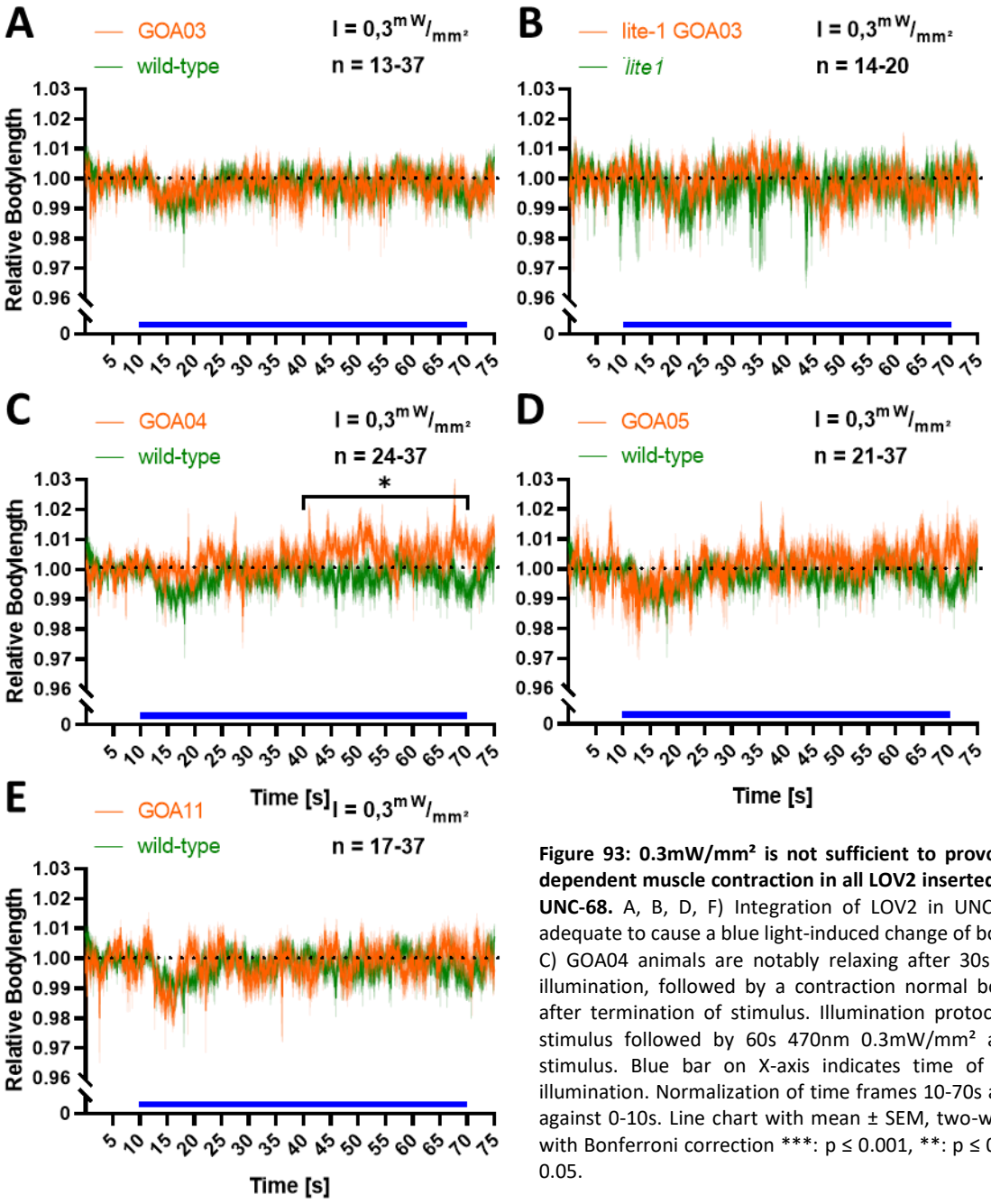

Figure 93: 0.3mW/mm² is not sufficient to provoke a light dependent muscle contraction in all LOV2 inserted strains of UNC-68. A, B, D, F) Integration of LOV2 in UNC-68 is not adequate to cause a blue light-induced change of body length. C) GOA04 animals are notably relaxing after 30s blue light illumination, followed by a contraction normal body length after termination of stimulus. Illumination protocol: 10s no stimulus followed by 60s 470nm 0.3mW/mm² and 5s no stimulus. Blue bar on X-axis indicates time of blue light illumination. Normalization of time frames 10-70s and 70-75s against 0-10s. Line chart with mean ± SEM, two-way ANOVA with Bonferroni correction ***: $p \leq 0.001$, **: $p \leq 0.01$, *: $p \leq 0.05$.

3.9.3.2. Body length measurements showed no specific effects during 0,8mW/mm² photostimulation

Increasing the intensity of blue light stimulation to 0.8mW/mm² led to no notable change of LOV2-domain inserted strains compared to their control. Yet, we see a tendency in all strains to contract as long as blue light illumination persists. In *Figure 94* A) animals of GOA03 reduced their body length to a minimum of -2.3%, shortly after the initiation of the blue light pulse. Compared to basal body length, strain GOA03 contracted as long as blue light was shining. Wild-type animals exhibited virtually identical behaviour as long as stimulation lasted. The contraction raised shortly after the onset of illumination (10-15s) to a minimum of -2.5%. Here, recovery to 0.1% and a maximal elongation of 1.1%, of wild-type animals already started at the end of photostimulation. When GOA03 was integrated in *lite-1*, the photophobic response after pulse initiation was not as pronounced, as the maximum contraction was -1.8% (10-15s), but in total it reached -2.6% during illumination.

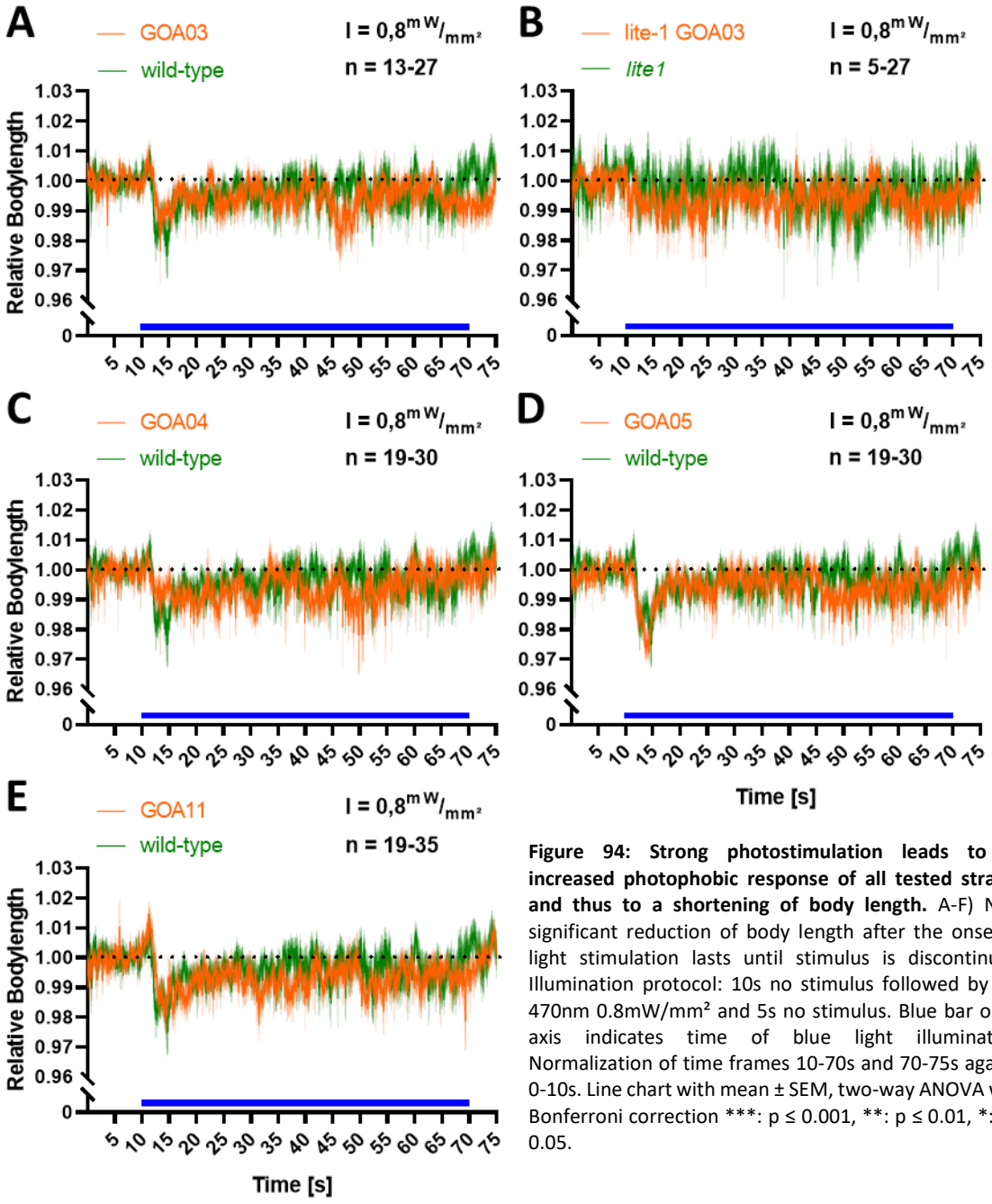

Figure 94: Strong photostimulation leads to an increased photophobic response of all tested strains, and thus to a shortening of body length. A-F) Non-significant reduction of body length after the onset of light stimulation lasts until stimulus is discontinued. Illumination protocol: 10s no stimulus followed by 60s 470nm 0.8mW/mm² and 5s no stimulus. Blue bar on X-axis indicates time of blue light illumination. Normalization of time frames 10-70s and 70-75s against 0-10s. Line chart with mean ± SEM, two-way ANOVA with Bonferroni correction ***: $p \leq 0.001$, **: $p \leq 0.01$, *: $p \leq 0.05$.

lite-1 animals revealed the most stable response to blue light initiation, however they also contracted up to -2.4% (10-70s). With quite similar responses to blue light GOA04, GOA05 and GOA11, during light stimulation, the only remarkable effect is the photophobic response shortly after photostimulation began. This side effect of the stronger intensity is visible in all strains except in *lite-1* background as seen in B). Looking at the strains GOA03, GOA04 and GOA05 in both intensities 0.3mW/mm² and 0.8mW/mm² (*Figure 93* and *Figure 94*) the difference is best visible. Collectively, the results of the contraction experiments with the two intensities, imply, that a possible light-evoked contraction of body wall muscles is not pronounced enough, to be detected by analysing the body length of individual worms.

3.10. Modulation of the SERCA pump by the light-activated LOV2 domain

In order to remove the Ca^{2+} from the cytosol and thus give a newly arriving action potential a chance to trigger a contraction of the muscle, the transporters SERCA, sarcolemmal NCX, sarcolemmal Ca^{2+}-ATPase and mitochondrial Ca^{2+} uniporter are used in the cell. The quantitatively most important transporters are SERCA and NCX (Bers 2000).
The light-controlled inhibition of SERCA should induce a noticeable change in muscle tone and thus pharyngeal pumping and/or swimming behaviour. A contraction of body length should be the outcome of a short-circuited Ca^{2+} reuptake into the SR, as long as RyRs are open. A possible relaxation caused by the simple lack of ATP in the cell would only result in a rigor mortis like contraction. Since the SERCA fulfils the essential function of transporting Ca^{2+} ions from the cytosol into the SR/ER, and it is localisation on the SR/ER membrane, it is an ideal candidate for the task this work is focussed on. SERCA, and RyR acting as counterpart by allowing rapid release of Ca^{2+} ions from the SR, both controllable by light, would allow the control of the complete cycle of Ca^{2+} import and export from the SR. Therefore, it is a concern to adapt SERCA here with the help of the LOV2 domain in such a way that a light-inhibited pump is created.

3.10.1. CRISPR based integration of LOV2 into the *sca-1 gene*

In order to create a light-inhibited SERCA pump, the LOV2 domain of *Avena sativa* was integrated by CRISPR/Cas9. Information about relevant conformational changes and the catalytic cycle was derived from the atomic structures such as PDB 3W5A, 3W5C, 3W5D, 3BA6, 1SU4 (Olesen et al. 2007; Toyoshima et al. 2013). We used this structural information to identify appropriate insertion sites. Once again, loops between α-helices or β-strands were chosen in which the LOV2 domain may influence the function of the pump when it undergoes light-induced conformational changes. To exclude that the insertion of a LOV2 domain induces steric conflicts, during the catalytic cycle with other SERCA domains, specific molecular sites had to be identified. These were found relatively peripheral to the remainder of the protein, in the ATP binding 'N' domain. It comprises several connecting loops and β-sheets and upon conformational changes it is folding away from other domains. Four loops were selected, between β-strands that are spaced ~10 Å apart, which is similar to the termini of the LOV2 domain. Due to light-induced disturbance of these β-strand domains, functional problems in SERCA are likely to occur, as the N-domain is essentially involved during the pump cycle in ATP binding and phosphorylation. Considering that complete deletion of SERCA is lethal (Zwaal et al. 2001), the sole survival of a strain would immediately prove that the insertion of LOV2 per se does not unduly impede SERCA functionality.

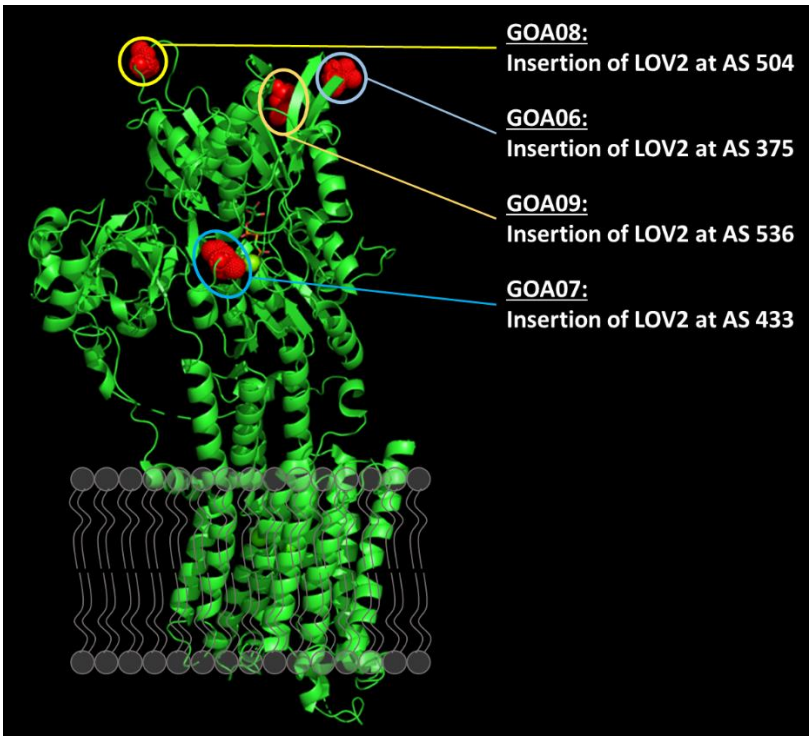

Figure 95: Illustration of the SERCA integrated in the SR-membrane. Integration sites of LOV2 domains are marked as red balls. This figure was generated using PyMol (6JJU).

The CRISPR/Cas9 method was used to generate the following transgenic strains:

Table 17: Abbreviation, ZX number of the Gottschalk lab, description integration site of LOV2 domain and SunyBiotech denotation are listed.

Abbr.	ZX	description	Integration site
GOA06	ZX2597	sca-1 LOV2 (1)	LOV2 inserted at AS375 of sca-1 Deleted sequence: TCTGGAGACAAC Inserted sequence: TTGGCTACTACACTTGAACGTATTGAGAAGAACTTTGTC ATTACTGACCCAAGATTGCCAGATAATCCCATTATATTC GCGTCCGATAGTTTCTTGCAGTTGACAGAATATAGCCG TGAAGAAATTTTGGGAAGAAACTGCAGGTTTCTACAAG GTCCTGAAACTGATCGCGCGACAGTGAGAAAAATTAG AGATGCCATAGATAACCAAACAGAGGTCACTGTTCAGC TGATTAATTATACAAAGAGTGGTAAAAAGTTCTGGAAC CTCTTTCACTTGCAGCCTATGCGAGATCAGAAGGGAGA TGTCCAGTACTTTATTGGGGTTCAGTTGGATGGAACTG AGCATGTCCGAGATGCTGCCGAGAGAGAGGGAGTCAT GCTGATTAAGAAAACTGCAGAAAATATTGATGAGGCG GCAAAAGAACTT
GOA07	ZX2598	sca-1 LOV2 (2)	LOV2 inserted at AS433 of sca-1 Deleted sequence: GAGACCAAGAAGATC Inserted sequence: TTGGCTACTACACTTGAACGTATTGAGAAGAACTTTGTC ATTACTGACCCAAGATTGCCAGATAATCCCATTATATTC

			GCGTCCGATAGTTTCTTGCAGTTGACAGAATATAGCCG TGAAGAAATTTTGGGAAGAAACTGCAGGTTTCTACAAG GTCCTGAAACTGATCGCGCGACAGTGAGAAAAATTAGA GATGCCATAGATAACCAAACAGAGGTCACTGTTCAGCT GATTAATTATACAAAGAGTGGTAAAAAGTTCTGGAACC TCTTTCACTTGCAGCCTATGCGAGATCAGAAGGGAGAT GTCCAGTACTTTATTGGGGTTCAGTTGGATGGAACTGA GCATGTCCGAGATGCTGCCGAGAGAGAGGGAGTCATG CTGATTAAGAAAACTGCAGAAAATATTGATGAGGCGGC AAAAGAACTT
GOA08	ZX2599	sca-1 LOV2 (3)	LOV2 inserted at AS504 of sca-1 <u>Deleted sequence:</u> CCAGCTTCCGGAGGATCTGGA <u>Inserted sequence:</u> TTGGCTACTACACTTGAACGTATTGAGAAGAACTTTGTCA TTACTGACCCAAGATTGCCAGATAATCCCATTATATTCGCGT CCGATAGTTTCTTGCAGTTGACAGAATATAGCCGTGAAGAA ATTTTGGGAAGAAACTGCAGGTTTCTACAAGGTCCTGAAA CTGATCGCGCGACAGTGAGAAAAATTAGAGATGCCATAGA TAACCAAACAGAGGTCACTGTTCAGCTGATTAATTATACAA AGAGTGGTAAAAAGTTCTGGAACCTCTTTCACTTGCAGCCT ATGCGAGATCAGAAGGGAGATGTCCAGTACTTTATTGGGG TTCAGTTGGATGGAACTGAGCATGTCCGAGATGCTGCCGA GAGAGAGGGAGTCATGCTGATTAAGAAAACTGCAGAAAA TATTGATGAGGCGGCAAAAGAACTT
lite-1 GOA08	ZX2633	sca-1 LOV2 (3), crossed into *lite-1 (ce314)*	LOV2 inserted at AS504 of sca-1 <u>Deleted sequence:</u> CCAGCTTCCGGAGGATCTGGA <u>Inserted sequence:</u> TTGGCTACTACACTTGAACGTATTGAGAAGAACTTTGTCA TTACTGACCCAAGATTGCCAGATAATCCCATTATATTCGCGT CCGATAGTTTCTTGCAGTTGACAGAATATAGCCGTGAAGAA ATTTTGGGAAGAAACTGCAGGTTTCTACAAGGTCCTGAAA CTGATCGCGCGACAGTGAGAAAAATTAGAGATGCCATAGA TAACCAAACAGAGGTCACTGTTCAGCTGATTAATTATACAA AGAGTGGTAAAAAGTTCTGGAACCTCTTTCACTTGCAGCCT ATGCGAGATCAGAAGGGAGATGTCCAGTACTTTATTGGGG TTCAGTTGGATGGAACTGAGCATGTCCGAGATGCTGCCGA GAGAGAGGGAGTCATGCTGATTAAGAAAACTGCAGAAAA TATTGATGAGGCGGCAAAAGAACTT
GOA09	ZX2600	sca-1 LOV2 (4)	LOV2 inserted at AS536 of sca-1 <u>Deleted sequence:</u> GTTCCACTCACC <u>Inserted sequence:</u> TTGGCTACTACACTTGAACGTATTGAGAAGAACTTTGTCATT ACTGACCCAAGATTGCCAGATAATCCCATTATATTCGCGTCC GATAGTTTCTTGCAGTTGACAGAATATAGCCGTGAAGAAAT TTTGGGAAGAAACTGCAGGTTTCTACAAGGTCCTGAAACTG ATCGCGCGACAGTGAGAAAAATTAGAGATGCCATAGATAA

	CCAAACAGAGGTCACTGTTCAGCTGATTAATTATACAAAGA GTGGTAAAAAGTTCTGGAACCTCTTTCACTTGCAGCCTATG CGAGATCAGAAGGGAGATGTCCAGTACTTTATTGGGGTTCA GTTGGATGGAACTGAGCATGTCCGAGATGCTGCCGAGAGA GAGGGAGTCATGCTGATTAAGAAAACTGCAGAAAATATTG ATGAGGCGGCAAAAGAACTT

The strains GOA07 and GOA09 were lethal and were therefore not considered any further here. Additionally, the strain GOA08 was crossed into *lite-1(ce314)* to preclude a light avoidance of the worms during photostimulation.

3.10.1.1. Swimming locomotion was investigated for possible light-evoked effects in sca-1::LOV2 inserted strains

Thrashing assays in the following chapters, that were performed with the strains GOA06 to GOA09 were measured under the intensities 0.3mW/mm², 0.8mW/mm² and GOA06, GOA07, and GOA09 also during 1.1mW/mm².

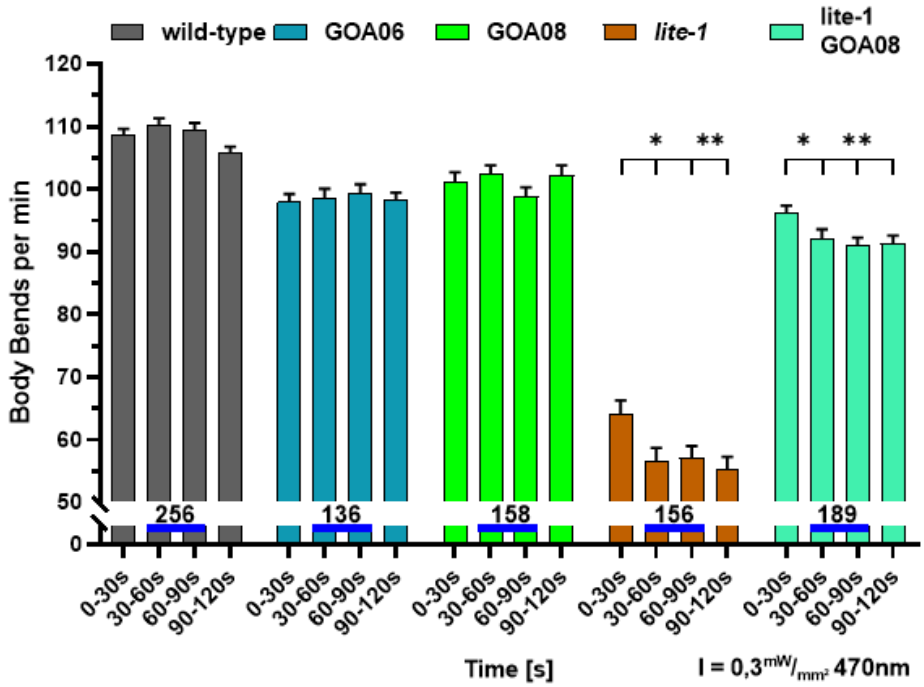

Figure 96: Low light intensity induces a substantial drop in body bends per min only in *lite-1* background. lite-1 GOA08 and *lite-1* are reducing thrashing rate significantly during light stimulus, *lite-1* animals reduce thrashes even more after termination of blue light. GOA06, and GOA08 exhibit no considerable change in thrashes. Stimulation protocol: 30s no stimulation, 60s 470nm 0.3mW/mm² stimulation and 30s no stimulation. Photostimulation denoted by blue bar, n numbers for each strain are given over the X-axis. Time frames 30-60s, 60-90s and 90-120s of each strain were compared with the time frame 0-30s before light application, by unpaired two-tailed t-test, with Welch's correction, ***: $p \leq 0.001$, **: $p \leq 0.01$, *: $p \leq 0.05$.

We first asked, whether illumination of sca-1::LOV2 inserted strains with 0.3mW/mm² blue light was sufficient to alter swimming behaviour in any way, either by increasing or decreasing the swimming cycles. We analysed this by subjecting the animals to 30s no stimulation followed by 60s 470nm photostimulation and a recovery period of 30s off stimulus. The findings can be seen in

*Figure **96*** and *Figure 97*. Wild-type animals, GOA06and GOA08 exhibit a small rise in thrashes by 1.6%, 0.6% and 1.3% respectively, during the first 30s of blue light stimulation, compared to their basal rate determined during 0-30s. In the second time frame of photostimulation (60-90s), thrashes are raising

in GOA06 animals by 1.4% compared to 0-30s. Interestingly GOA08 is dropping thrashing rate from 102.5bbpm to 98.9bbpm by 2.4%, representing the strongest decrease in wild-type background animals. During recovery phase (90-120s) we see mixed responses to the terminated light stimulus. Wild-type lowers thrashes to 105.7bbpm (-2.63%). GOA08 animals enhanced swimming cycles by 1% to 102.2bbpm, close to the maximum thrashing rate of 102.5bbpm. GOA06 animals increased thrashing rate, too, by 0.3%.

As it appeared that GOA08 performed differently from the other sca-1::LOV2 integrated strains, it was crossed into *lite-1* background, to finally rule out behaviour, that was only dependent on the avoidance of light. Fundamentally different behaviour was observed in the strains *lite-1* and lite-1 GOA08 (*Figure 97*), as long as blue light application persists.

*Figure **96*** shows the significant drop of thrashes of *lite-1* from 64.1 ± 2.2bbpm to 56.6 ± 2.1bbpm (-11.7%) during the time frame 30-60s. Subsequently a small raise to -11% after 60s in *lite-1* animals during light application is even surpassed after the stimulus ended, by diminishing swimming cycles to 55.2 ± 2.1bbpm, a reduction of 13.9%. lite-1 GOA08 followed this behaviour, in the way that animals also exhibited a notable reduction of body bends during and after photostimulation (

*Figure **96***). An initial decrease in time frame 30-60s by -4.2%, reduced thrashing rate from 96.1 ± 1.3bbpm to 92.1 ± 1.5bbpm, and further decreasing by -5.21%, in time frame 60-90s. Interestingly, the most prominent and significant change compared to *lite-1* animals occurred after termination of light stimulation (*Figure 97*). Unlike *lite-1*, the lite-1 GOA08 animals increased their thrashing rate by 0.2bbpm to 91.3 ± 1.3bbpm. Something similar, although even more pronounced, could also be observed in lite-1 GOA03 in *Figure 87*. Taken together, only the integration of LOV2 at AS504 of sca-1 in lite-1 GOA08 resp. GOA08 seems to have an effect on swimming locomotion under weak blue light stimulation.

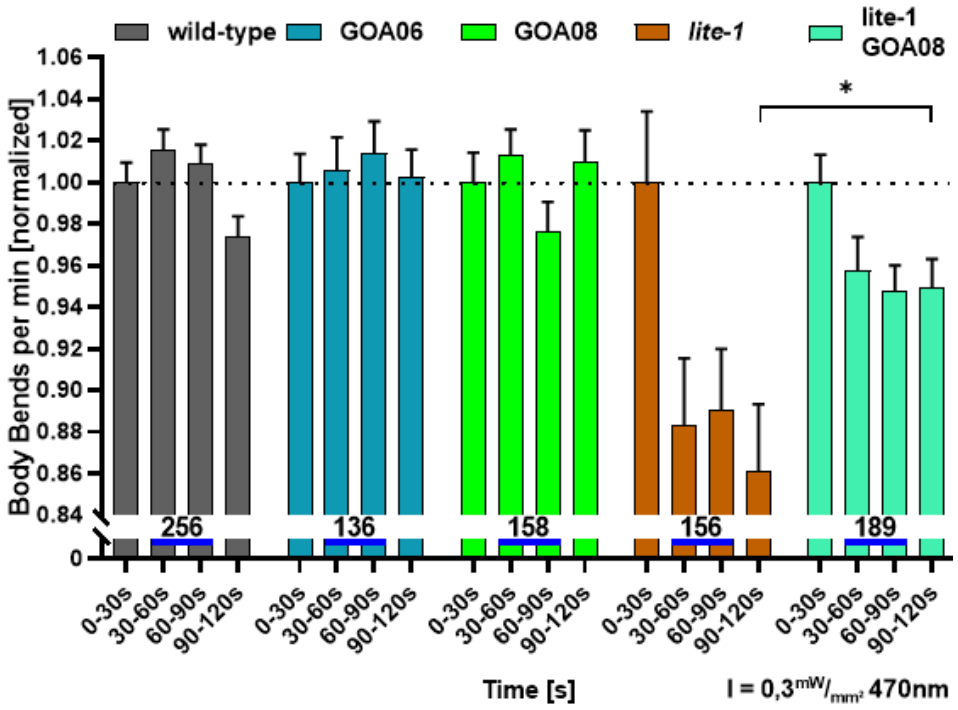

Figure 97: lite-1 GOA08 is thrashing considerably more frequent than its control *lite-1* during and after photostimulation. GOA08 animals are reducing swimming cycles in relation to wild-type as long as the light pulse persists. Normalized data of body bends per min of SCA-1::LOV2 integrated strains and respective control. Stimulation protocol: 30s no stimulation, 60s 470nm 0.3mW/mm² stimulation and 30s no stimulation. Photostimulation denoted by blue bar, n numbers for each strain are given over the X-axis. Transgenic strains were analysed by two-way ANOVA, with Bonferroni correction to the corresponding time frame of wild-type or *lite-1*, ***: $p \leq 0.001$, **: $p \leq 0.01$, *: $p \leq 0.05$.

3.10.1.2. Strong photostimulation elicits stronger changes of swimming behaviour

Variable bearings, of the individual strains to light stimulation made further tests with increased light intensity necessary, to find out whether a critical threshold has to be exceeded to detect a clear response. For this purpose, illumination with 0.8mW/mm² was used in the assay. Analysis in *Figure 98* points out that wild-type animals are raising thrashes clearly from 106.1bbpm to 112bbpm after the blue light stimulation was terminated. Animals of strain GOA06 did not noticeably change their behaviour during light stimulation at this intensity, neither compared to wild-type, nor when comparing the time frame 0-30s without stimulus with any other time frame during and after photostimulation. The only strain that stands out here is GOA08, demonstrating both, a significant decrease during light stimulation and an increase afterwards (Figure 97), by dropping the thrashing rate by -4.7% under blue light illumination. These animals exposed a distinct difference in time frame 30-60s during and in 90-120s after stimulation, compared to them self, pre-stimulated (*Figure 97*). During recovery, GOA08 animals present a raise of thrashing rate from 106.3bbpm to 113.5bbpm corresponding 5.8%. Even more interesting is the fact, that the significance in the time frame 30-60s also persists in relation to wild-type, and thus exhibits a considerable difference in behaviour to other strains (Figure 99).

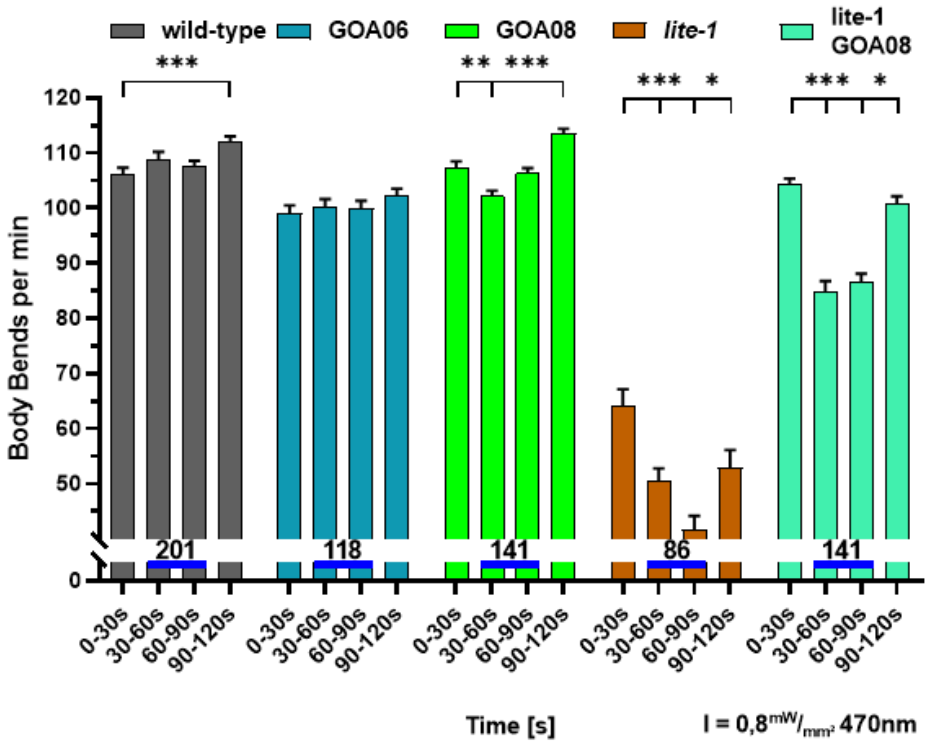

Figure 98: Strong blue light exposure of transgenic strains elicits diverse behaviour. An exception here is GOA08, which significantly decreases thrashes as soon as the blue light is switched on, and significantly increases thrashes immediately after exposure. Lite-1 GOA08 displays the same behaviour, with stronger reduction and recovery during and after photostimulation. Stimulation protocol: 30s no stimulation, 60s 470nm 0.8mW/mm² stimulation and 30s no stimulation. Photostimulation denoted by blue bar, n numbers for each strain are given over the X-axis. Time frames 30-60s, 60-90s and 90-120s of each strain were compared with the time frame 0-30s before light application, by unpaired two-tailed t-test, with Welch's correction, ***: $p \leq 0.001$, **: $p \leq 0.01$, *: $p \leq 0.05$.

In *lite-1* background we see something similar. lite-1 GOA08 displays a significant difference in *Figure 98*, when comparing photostimulation (30-90s) and recovery phase with the basal thrashing rate in the time frame 0-30s. A significant reduction in swim cycles by -18.7% in the time frame 30-60s and a sustained low thrashing rate from 60-90s by -16.9%, is followed by an almost complete recovery after photostimulation ended, in which they were thrashing with a slight reduced frequency of 100.9bbpm

(-3.3%). Intriguingly, lite-1 GOA08 animals did not exhibit a further increase of swimming cycles in time frame 60-90s, which is the basis for the significant difference to the strain *lite-1* in the respective time frame, as seen in Figure *99*. Here *lite-1* and lite-1 GOA08 differed strongly in the last period of light stimulation and in the recovery phase 90-120s. *lite-1* animals were reducing thrashing rate notably by -21.4% during the 30-60s of the assay and decreased even further to an overall drop of -35.1% in time frame 60-90s. In the recovery phase, these animals increase their swimming cycles to 52.9bbpm. Although, the control groups were responding similarly to GOA08 and lite-1 GOA08, these data suggest that there is a light-dependent effect of sca-1::LOV2 that influences swimming behaviour. Furthermore, it appears that this response is dependent on duration and intensity of blue light stimulation.

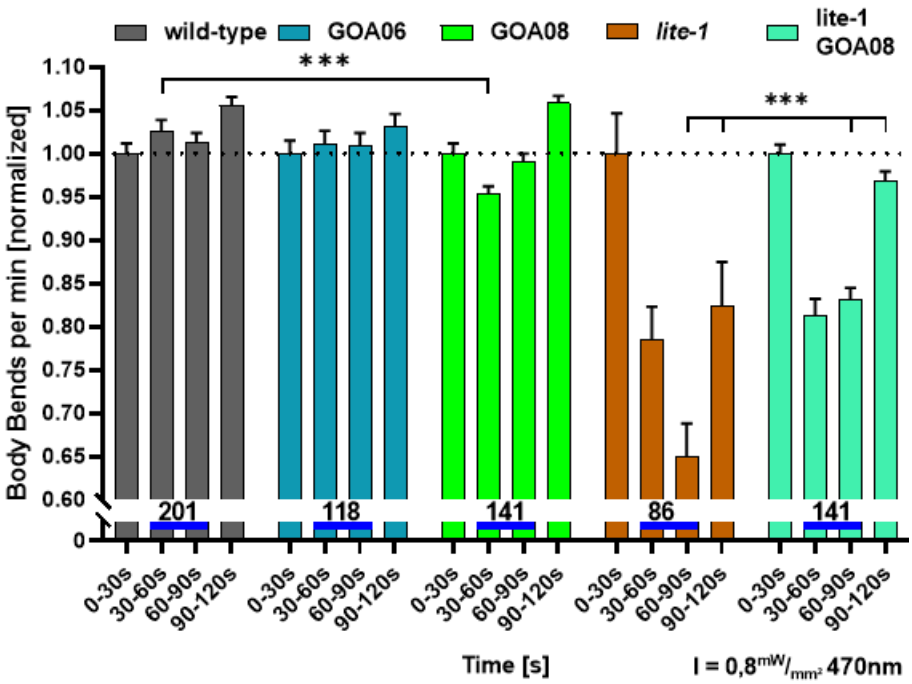

Figure 99: GOA08 displays similar behaviour in wild-type and *lite-1* background. GOA08 and lite-1 GOA08 are the only strains that show significant deviations in comparison with the respective control group. Normalized data of body bends per min of LOV2 inserted strains and respective control. Stimulation protocol: 30s no stimulation, 60s 470nm 0.8mW/mm² stimulation and 30s no stimulation. Photostimulation denoted by blue bar, n numbers for each strain are given over the X-axis. Transgenic strains were analysed by two-way ANOVA, with Bonferroni correction to the corresponding time frame of wild-type or *lite-1*, ***: $p \leq 0.001$, **: $p \leq 0.01$, *: $p \leq 0.05$.

3.10.1.3. Photophobic response masks light dependent effects of sca-1::LOV2 inserted strains

A steady rise of response to intensified photostimulation led to the assumption that stronger photostimulation would lead to a stronger response. Following that, assays were performed, in which 1.1mW/mm² strong blue light illumination was applied. Wild-type animals drastically changed their behaviour when exposed to this strong illumination. They revealed significantly decreased swimming cycles by -9.5% during the first interval of illumination. Hereafter, wild-type animals raised swimming cycles again to -3.6% compared to 0-30s, and beyond that up to 6% after photostimulation. This drastic reduction of thrashes was also observed in GOA06, displaying for the first and only time a significant change in behaviour, after the light pulse initiated in time frame 30-60s. Here the animals elevated swimming cycles by -7.2%. However, since there were no further changes deviating from wild-type animals, either under 0.3mW/mm², 0.8mW/mm² or 1.1mW/mm² blue light exposure, it can be assumed that the insertion of LOV2 at position AS375 of sca-1, is not sufficient to induce a light dependent change of swimming behaviour. Wild-type animals raised swimming cycles significantly by

11% after photostimulation terminated. Proven by statistical verification GOA06 did not exhibit a significantly different behaviour at 1.1mW/mm² compared to wild-type animals (*Figure 100*). Furthermore, a possible light-evoked effect caused by blue light stimulation of sca-1::LOV2 seems to be masked by the strong photophobic response in the first seconds after initiation of the pulse.

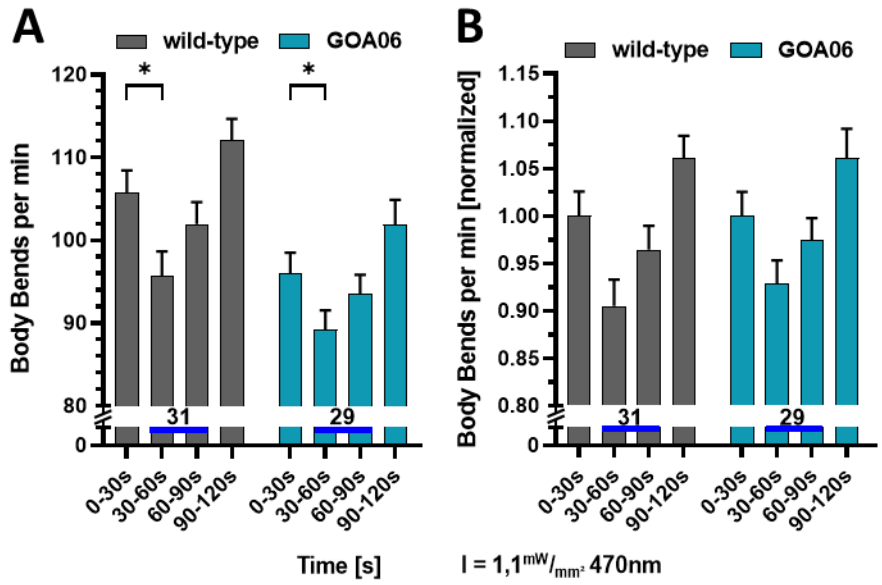

Figure 100: Strong blue light illumination leads to strong reduction of swimming cycles. A) Body bends per min are reduced significantly in wild-type and GOA06 during photostimulation with blue light. Transgenic strains were analysed with the corresponding time frame of wild-type, by unpaired two-tailed t-test, with Welch's correction, ***: p ≤ 0.001, **: p ≤ 0.01, *: p ≤ 0.05. B) Normalised body bends per min show no significant change when transgenic strains are compared to wild-type and its respective time frames. Stimulation protocol: 30s no stimulation, 60s 470nm 1.1mW/mm² stimulation and 30s no stimulation. Photostimulation denoted by blue bar, n numbers for each strain are given over the X-axis.

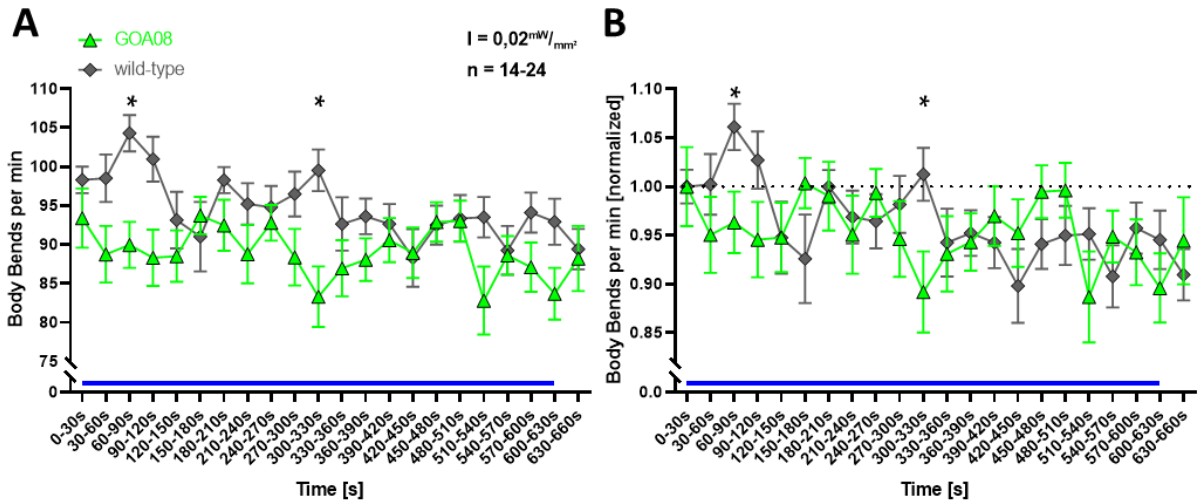

Figure 101: Long-term low-light affects the behaviour of the first 6 min of photostimulation. A) + B) Stimulation protocol: 30s no stimulation, 60s 470nm 1.1mW/mm² stimulation and 30s no stimulation. Transgenic strains were analysed with the corresponding time frame of wild-type, by unpaired two-tailed t-test, with Welch's correction, ***: p ≤ 0.001, **: p ≤ 0.01, *: p ≤ 0.05. Photostimulation denoted by blue bar, n numbers for each strain are given over the X-axis.

Additional low-intensity, long-term illumination experiments using GOA08 animals, as seen in 3.9.2.2. High intensity light stimulation leads to strong reduction of swimming cycles during stimulus and to a strong increase after stimulus, visualize a reduction of swimming cycles as soon as photostimulation was initiated (*Figure 101* A and B). Wild-type animals demonstrated the opposite behaviour, i.e. an increase in swimming cycles during the first 90 seconds of light stimulation and significantly different after 60 seconds of blue light stimulation. Intriguingly, after 150s (time frame 180-210s) of light application the response to the stimulus is roughly the same as in wild-type animals. These also respond to blue light after 30s of illumination by increasing thrashing frequency and dropping frequency within 120s. From time frame 330-360s onwards, the difference between the two groups was only marginal and exhibited no clear differences, except for the time frame 330-360s and the recovery instead of further reduction after stimulation. An increase in swimming cycles in GOA08 animals could be observed, whereas wild-type animals exhibited a further reduction. Here it is important to point out the fluctuations in the measurement values, which might be rooted in the low number of animals.

3.10.2. Light-provoked effects of body wall muscle contraction were investigated in sca-1::LOV2 inserted strains

Since a blue light dependent change in swimming behaviour was evident in most strains, the obvious consequence was to carry out contraction assays with these strains, as was done in 3.9.3.1. Contraction of body length could be provoked in a strain by weak blue light stimulation Hence, the intensities 0.3mW/mm² and 0.8mW/mm² were used again, in a 75s assay starting with 10s determination of relaxed body length, followed by 60s blue light stimulation and a recovery phase of 5s (Figure 102). In contrast to the swimming assays, a blue light induced response could already be detected at an intensity of 0.3mW/mm² in strain GOA06 A). The maximum elongation during blue light stimulation reached 1.6%, as long as the photostimulation lasted, which became clearly different to the control wild-type, in the last 5s of stimulation. Control animals of the wild-type strain maximally contracted during stimulation by 1.8%, followed by a slight contraction after stimulation. Animals of strain GOA08 (B), displayed a similar response to blue light, as did wild-type animals, except they contracted from 55s onwards, gaining significance in time frame 60-65s. Maximal contraction reached 1.9%. Furthermore, a recovery could be seen after the light was switched off. Lite-1 GOA08 (C), the partner strain of GOA08, crossed into *lite-1* background, behaved inversely, elongating to a maximum of 101.8% body length, instead of contracting. Followed by a slight contraction in time frame 70-75s. The background strain *lite-1* displayed a maximal contraction of -1.2%, as long as blue light stimulation was holding on, but also an elongation of body wall muscles by 1.1% occurred. During the relaxation period (70-75s), these animals experienced a slight contraction. In total worms of the strain *lite-1* did not change body length substantially at this intensity, moreover there is also no significant difference to the strain lite-1 GOA08.

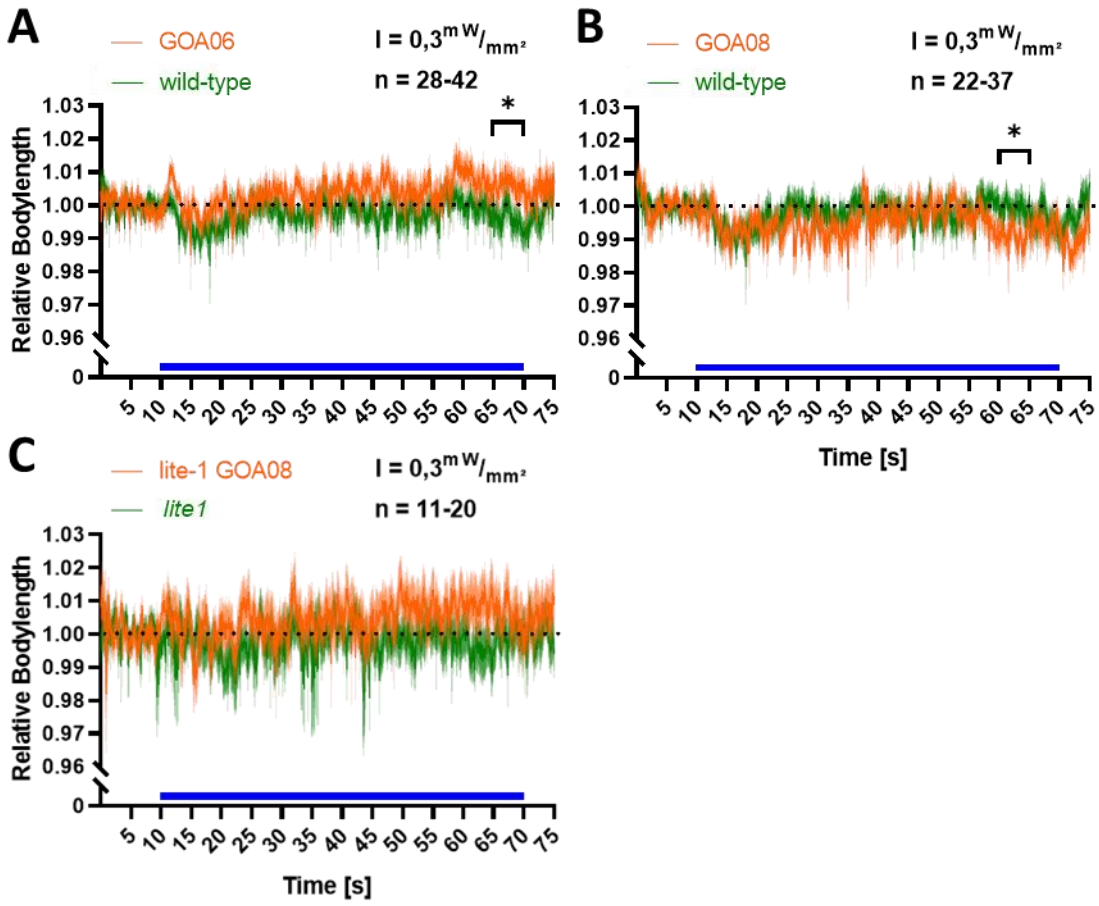

Figure 102: Only GOA06 and GOA08 react to low blue light stimulation with a change in body length. A) Elongation of body length progresses as long as the light excitation lasts, until it reaches a maximum after 49s of stimulation, but only becomes significant in time frame 65-70s. B) A light provoked effect in strain GOA08 increases with the duration of the light pulse, reaching a significant level in the time frame 60-65s, but reaching a maximum after stimulus has ended. C) Animals of the strain lite-1 GOA08 elongate increasingly as long as the light pulse lasts, but without becoming significant. Illumination protocol: 10s no stimulus followed by 60s 470nm 0.3mW/mm² and 5s no stimulus. Blue bar on X-axis indicates time of blue light illumination. Normalization of time frames 10-70s and 70-75s against 0-10s. Line chart with mean ± SEM, two-way ANOVA with Bonferroni correction ***: $p \leq 0.001$, **: $p \leq 0.01$, *: $p \leq 0.05$.

The data presented in *Figure 103* and *Figure 105* reflect the results of *Figure 102* and *Figure 104*, comparing the contraction of the body length during photostimulation with the normalised data without stimulation (0-10s). The assay was divided into time intervals, which were then used to compare wild-type (green) and transgenic strain (orange). To exclude a possible change in body length during the start of the experiment due to changing light conditions (background light), the time frame 3-9s was chosen, and to exclude a possible effect of reversals due to the start of photostimulation, the time frame 11-17s was chosen.

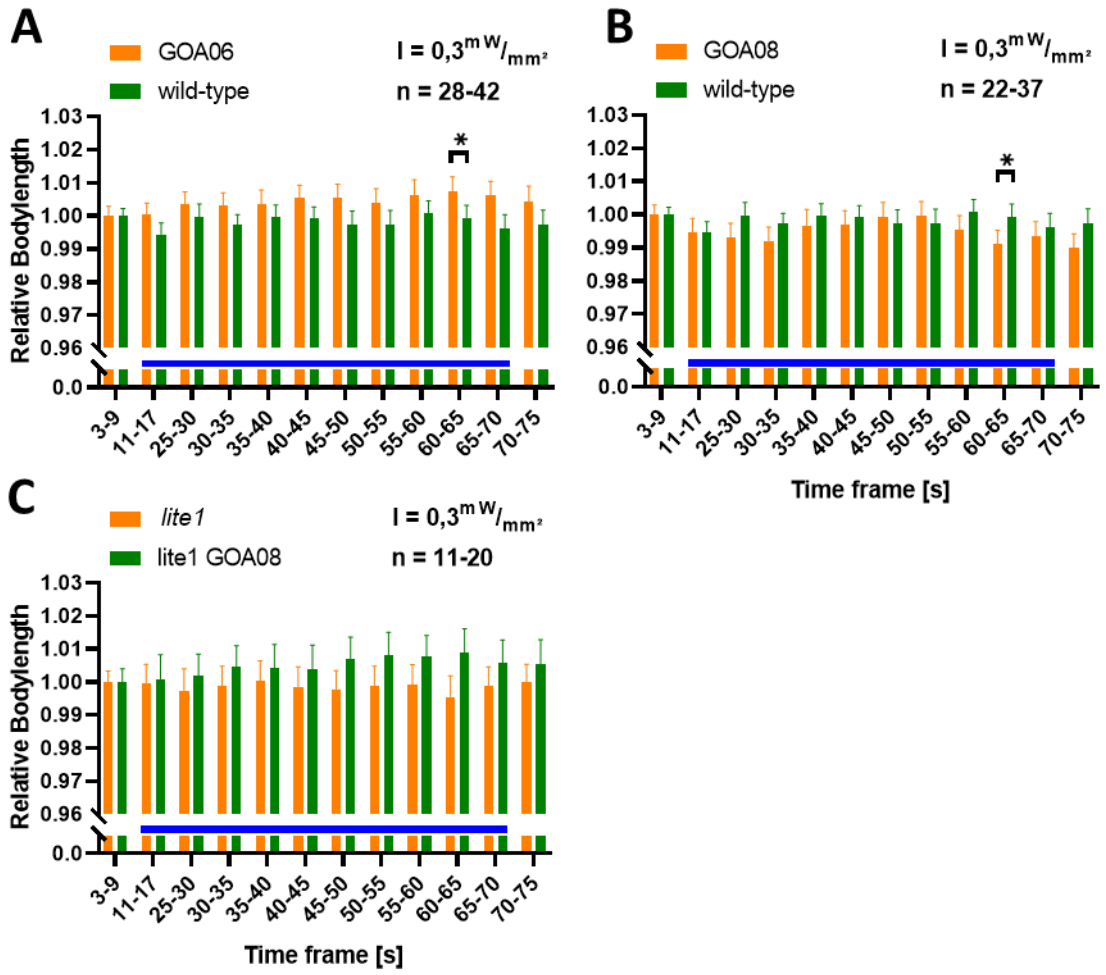

Figure 103: Blue light photostimulation leads to contraction after long exposure in wild-type background. A) Exposure to 0.3mW/mm² causes contraction in the time frame 60-65s, when compared to wild-type. B) In GOA08 in the time frame 60-65s the animals are significantly more contracted than wild-type. Photostimulation denoted by blue bar. Illumination protocol: 10s no stimulus followed by 60s 470nm 0.3mW/mm² and 5s no stimulus. Time frames of each strain were compared with the corresponding time frame of wild-type. Bar chart with mean ± SEM, two-way ANOVA with Bonferroni correction ***: p ≤ 0.001, **: p ≤ 0.01, *: p ≤ 0.05.

Significant changes of body length of some strains, as answer to low intensity photo stimulation, raised the question if a higher intensity would cause a stronger effect. I tried to answer this question by exposing the animals to 0.8mW/mm² blue light. The most pronounced contraction during strong blue light exposure could be observed in strain GOA06 (*Figure 104* A), with a maximum contraction of body length by -3.1%, on average -1.6%, representing a clear difference compared to wild-type animals. Moreover, the contraction persisted in the recovery phase, in time frame 70-75s and was clearly different from the control. This is contrary to the results of the measurement with the intensity 0.3mW/mm², in which an elongation was detected. Contraction of wild-type animals decreased shortly after the onset of illumination (10-15s) to a minimum of -2.5% (10-70s). As mentioned wild-type animals exhibit a recovery that already starts at the end of photostimulation and reaches a maximal elongation of 1.1%. Interestingly the strain GOA08 behaved differently, already in the first 10s of the assay compared to the control (B), but as seen in *Figure 102* B), a significant contraction occurs very late, by reaching a contraction of -3% and a relaxation after termination of the stimulation. It is important to mention here, that in the interval 40-70s a clearly stronger contraction could be noticed than in time frame 10-30s. Similar, but not as pronounced, a contraction could also be seen in the strain lite-1 GOA08 in C), when maximally contracted the body length was stinted by -2.8%. A quite

stable response to blue light initiation was observed by *lite-1* animals, however they also contracted up to -2.4% (10-70s) and did not alter body length significantly compared to lite-1 GOA08. The tendency to contract rather than elongate, as it appeared under 0.3mW/mm² raised the question if a photophobic response at 0.8mW/mm² is stronger than a possible light-evoked effect of SERCA.

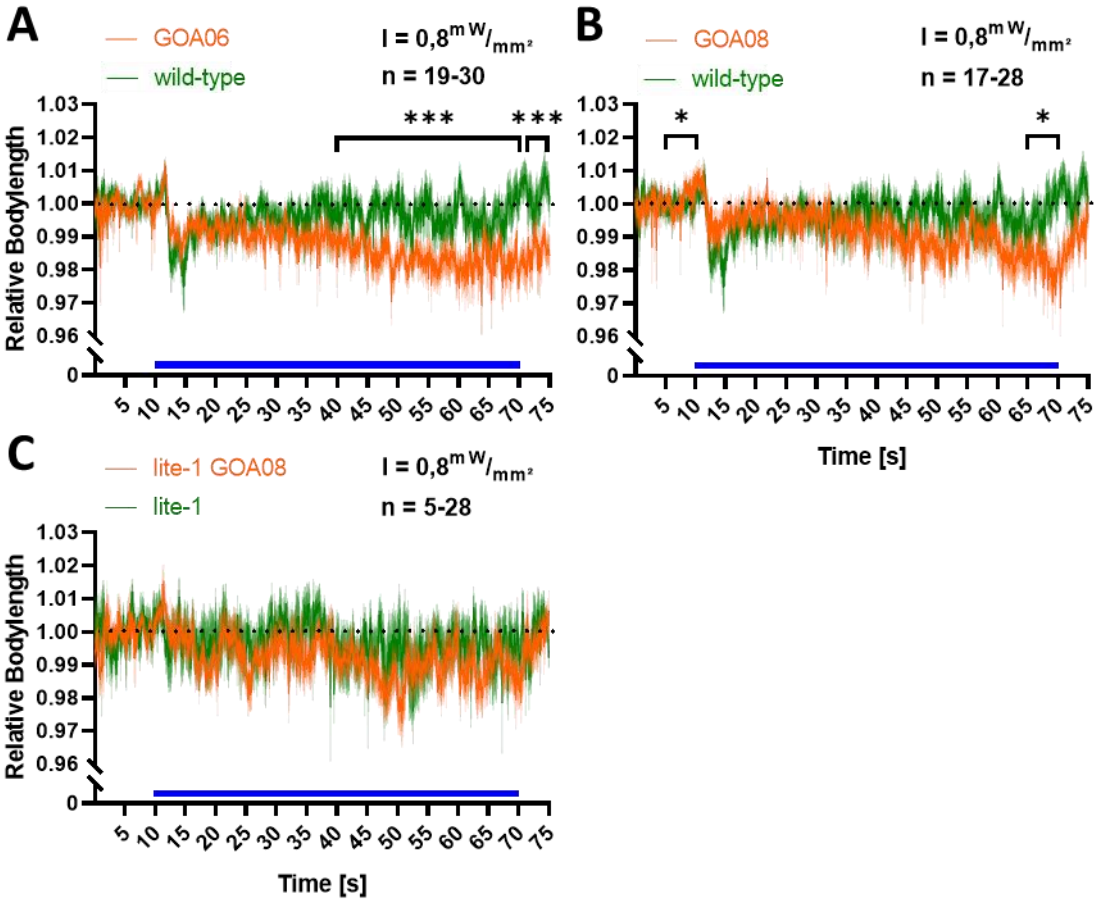

Figure 104: Photostimulation of high intensity leads to a substantial contraction of body length after prolonged exposure. A) GOA06 shows the most pronounced contraction in comparison to any other strain, during an ongoing light pulse after 30s and after stimulus has ended. B) GOA08 animals exhibit elongation shortly before photostimulation starts, but as long as light is still shining, they contract increasingly with a maximum in the time frame 65-70s. In contrast to this, lite-1 GOA08 in C) did not contract significantly compared to *lite-1*. Illumination protocol: 10s no stimulus followed by 60s 470nm 0.8mW/mm² and 5s no stimulus. Blue bar on X-axis indicates time of blue light illumination. Normalization of time frames 10-70s and 70-75s against 0-10s. Line chart with mean ± SEM, two-way ANOVA with Bonferroni correction ***: $p \leq 0.001$, **: $p \leq 0.01$, *: $p \leq 0.05$.

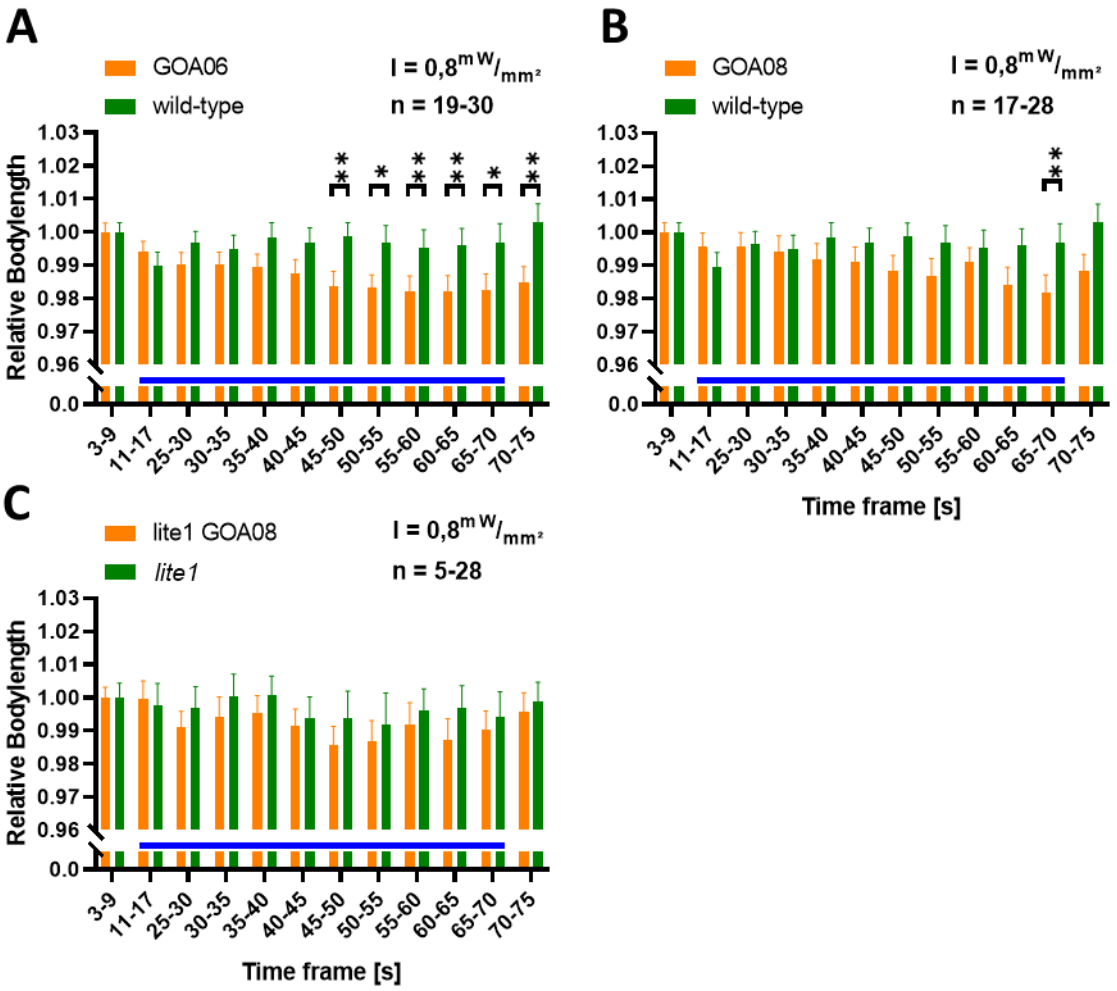

Figure 105: High intensity of blue light photostimulation leads to contraction after long exposure in GOA06. A) Exposure to 0.8mW/mm² causes contraction in the time frame 45-75s, including a persistent contraction after stimulus 70-75s, when compared to wild-type. B) In GOA08 in the time frame 65-70s the animals are significantly more contracted than wild-type. Photostimulation denoted by blue bar. Illumination protocol: 10s no stimulus followed by 60s 470nm 0.8mW/mm² and 5s no stimulus. Time frames of each strain were compared with the corresponding time frame of wild-type. Bar chart with mean ± SEM, two-way ANOVA with Bonferroni correction ***: $p \leq 0.001$, **: $p \leq 0.01$, *: $p \leq 0.05$.

3.11. Pharynx pumping

To access the pharynx as a model for the heart, it is important to be able to pace the pharynx in order to detect small aberrations during regular pumping, while optogenetically modifiable versions of SERCA or RyR are stimulated by light (Schüler et al. 2016; Fischer et al. 2017). Since these tools, as planned to be developed during this thesis, would be triggered by blue light, it would be necessary to independently trigger pharynx pumping with an optogenetic tool in the plasma membrane. To this end, C1V1 will be utilized. C1V1 is a chimera built from Chlamydomonas ChR1 and Volvox VChR1 and does not contain any ChR2 sequence. Additionally, the point mutations E122T and E162T were introduced to create C1V1 ET/ET. Both mutations jointly shorten the τ off time constant (*Figure 104* B) and the E122T/E162T mutations synergistically improved the temporal precision of the photocurrent. Robust photocurrent sizes could be obtained and additionally, the residual shorter-wavelength response could be reduced (Yizhar et al. 2011). The main advantage of C1V1 in context of this work is its red shifted action spectrum, which could still be photo stimulated in cells at low light intensities, as it was still moderately efficient in the blue range of the spectrum (Erbguth et al. 2012). Being excitable at the wavelengths 450-590nm, peaking at 520nm (Erbguth et al. 2012), it allows to achieve a dual colour excitation with a suitable partner, in muscles or neuronal cells as long as the expression is properly controlled.

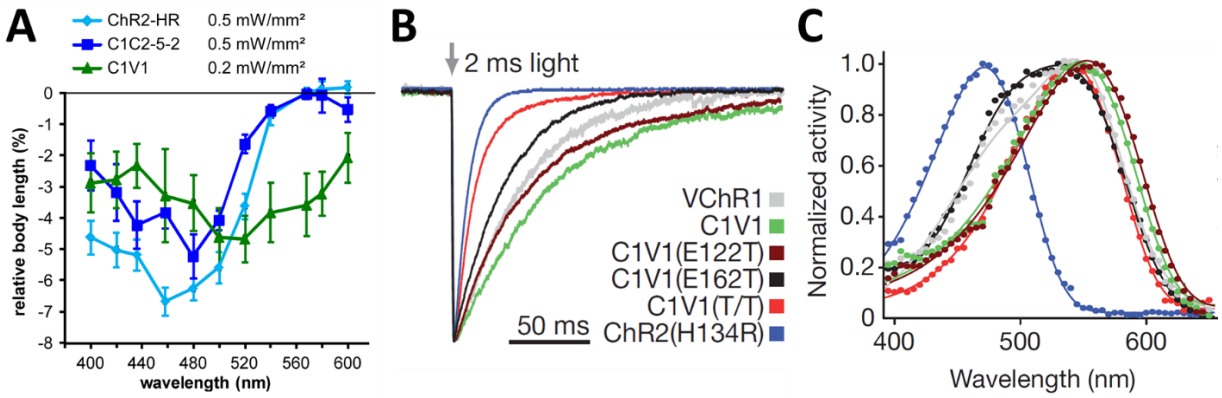

Figure 106: Excitability of the individual channelrhodopsins as a function of wavelength and channel closure time. A) Expression of ChR2-HR (light blue), C1C2 5-2::YFP (dark blue) and C1V1::YFP (green) in body wall muscle cells and photostimulation at different wavelengths with an intensity of 0.5mW/mm². Adapted from Erbguth et al. 2012. B) Summary plot graphic of τ off, the channel closing time constant, in cultured neurons, normalized to peak current. C) Action spectra collected for the in B indicated channelrhodopsins. Adapted from Yizhar et al. 2011.

A potential outcome of the interplay of C1V1 and the optoRyR is illustrated in *Figure 107* Depolarisation of the plasma membrane is triggered by the activation of C1V1 with 590nm, similar to an incoming cholinergic signal (Erbguth et al. 2012). This would be expected to trigger an action potential transmitted by the VGCCs CCA-1 and EGL-19. The Ca^{2+} influx through these channels, especially EGL-19, could then trigger the RyR and drive muscle contraction. This experimental setup will be designed mainly for the pharynx. When optoRyR is additionally triggered by blue light, it is expected that Ca^{2+} is additionally increased and, importantly, that this also occurs while the intrinsic Ca^{2+} cycle is reducing cytosolic Ca^{2+}, enabling the next pharyngeal pump cycle. As this does not happen properly, an arrhythmic situation can be expected to occur, similar to CPVT in which extra systolic Ca^{2+} drives the NCX and additional depolarisation.

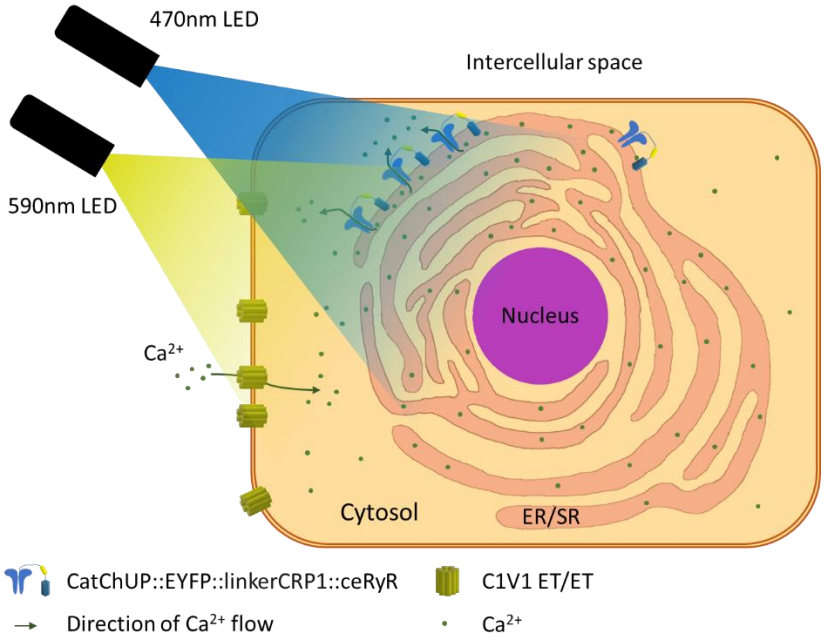

Figure 107: Blue light provoked effects during pacing by C1V1. Blue-light activated CatChUP::EYFP::linkerCRP1::UNC-68 see *1.2.1.6.1* causes light induced Ca^{2+} efflux (leak) from the SR/ER into the cytosol. Green-light activated C1V1 ET/ET (yellow channels) causes cation influx into the cytosol and enables pacing.

The pumping action of the pharynx is relatively easy to measure by eye. Though, the method used here is based on the electrophysiological measurement of the electric currents in the pharynx during a contraction. The NemaMetrix system is composed of the ScreenChip system and the software NemAquire and NemAnalysis. Experiments using serotonin to induce pharyngeal pumping were designed to determine whether pumping could be interrupted or even paced by light stimulation. The CatChUP construct in GOA01 and GOA14 is in theory be activatable by light, when ATR is supplemented, and therefore pacing by blue light should be feasible without any serotonin exposure.

3.11.1. Serotonin induced pharynx pumping in GOA01

3.11.1.1. Pharynx pumping is decreased under strong photostimulation

The strain GOA01, which was examined here, carryies the integrated CatChUP construct upstream of exon 1.1 of UNC-68. Animals were maintained overnight on ATR and incubated in 50mM serotonin in M9. Serotonin-induced pharynx pumping was recorded during a period of 30s without photo-stimulation, followed by a 1Hz stimulus of 470nm blue light with 1.4mW/mm² intensity, for 60s. Light pulses, if not stated otherwise, were set to 50ms for all subsequent pharynx pumping assays. This protocol was chosen since the results of the previous chapter 3.4. Targeting endogenous full-length UNC-68 (ceRyR) with an N-terminal, Ca^{2+}-conductive ChR2 variant (CatChUP) were not yet available at that time and the expectation was that a relatively strong but short blue light pulses would be sufficient to provoke deviant behaviour without the stimulation of C1V1. Serotonin was used, because it induces a sustained, steady pumping in the pharynx, which was eventually a major criterion for its use (Croll 1975; Horvitz et al. 1982; Avery and Horvitz 1990).

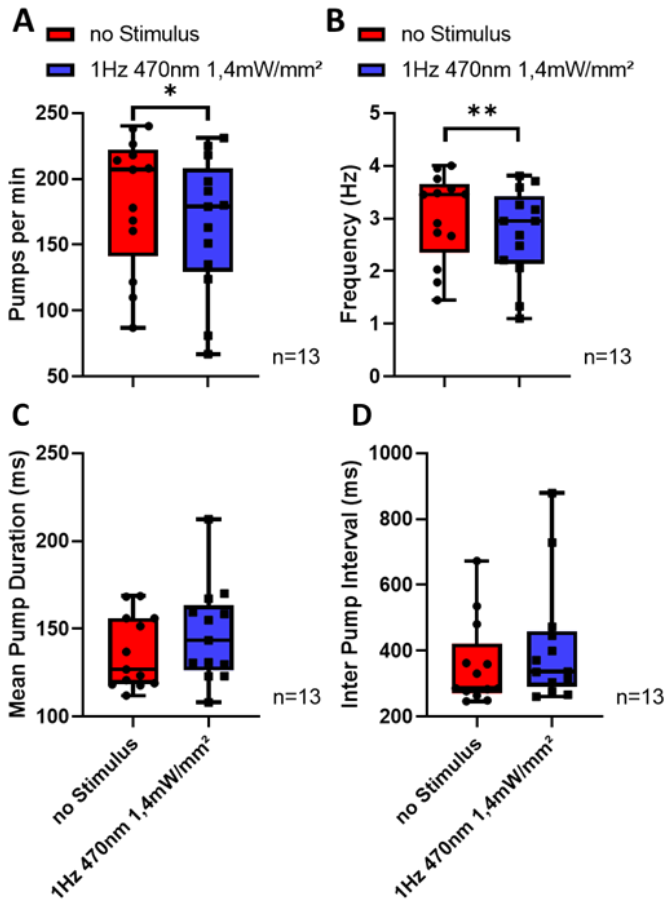

Under these conditions, without stimulation, the animals pumped on average 181 times per min, corresponding to a mean frequency of 3.02Hz (*Figure 108* A and B). While stimulating, they decreased the pumping rate to 163 pumps per min (2.72Hz), giving a significant change of pumps per min (PPM) and frequency.

Figure 108: GOA01 animals notably reduce pumping under the influence of 1Hz blue light pulses when supplemented with 50mM Serotonin. A) Pumps per min with significance. B) Frequency in Hz, significant difference of blue light illumination to no stimulus. C) Mean pump duration (average pump duration, from a pump's E-pike to the same pump's R-pike), did not alter. D) Inter pump interval (time between two spikes of two pumps) were not changed. Red: 30s no stimulus, blue: 60s 1Hz 470nm 1.4mW/mm². Animals were fed overnight on agar plates with ATR 0.2% in OP50. Incubation with 50mM Serotonin for 30min right before assay. Tracking system Nemametrix Screen Chip and software Nemaquire. Box plot with mean ± SD, two-tailed paired t-test ***: $p \leq 0.001$, **: $p \leq 0.01$, *: $p \leq 0.05$. Median, IQR, whiskers: 2.5 to 97.5.

Mean pump duration and inter pump intervals (ipi), by contrast displayed no essential changes, yet a raise of the mean pump duration from 136.6ms to 147.06ms Mean occurred, as well as a prolongation of the inter pump interval from 356.78ms to 414.80ms, when looking at the first 30s, respectively blue light stimulation.

3.11.1.2. 4Hz stimulation could not be followed by pharynx pumping of GOA01

The follow-up experiment to 1Hz stimulus was performed with a 4Hz stimulation of GOA01. ATR concentration remained constant, the no-stimulus interval was increased from 30s to 60s, which ought to have no effect on the results. Stimulus frequency was raised fourfold, to determine if more stimuli lead to a stronger response. As result, we got a raise in pumps per min and frequency. Pumps raised from 7.92 to 13.86 per min during stimulation. Frequency nearly doubled from 0.13Hz to 0.23Hz. These averages imply a drastic change, and yet the medians depicted in *Figure 109* A) resp. B), with 6.33 and 4.38 PPM, and in B) 0.11 and 0.07Hz illustrate that the change is not that pronounced. Median pump duration is raised from 112.25 to 120.5ms, congruent with their higher frequency. To the contrary, the average value decreased from 119 to 118.21ms, which is due to one animal that did not pump at all during light stimulation. Inter pump intervals (D), exhibit diminished intervals during light application, both in average and median, coincident to the higher frequency. High variance and a relatively low n number of 8 explain why no significant difference could be calculated.

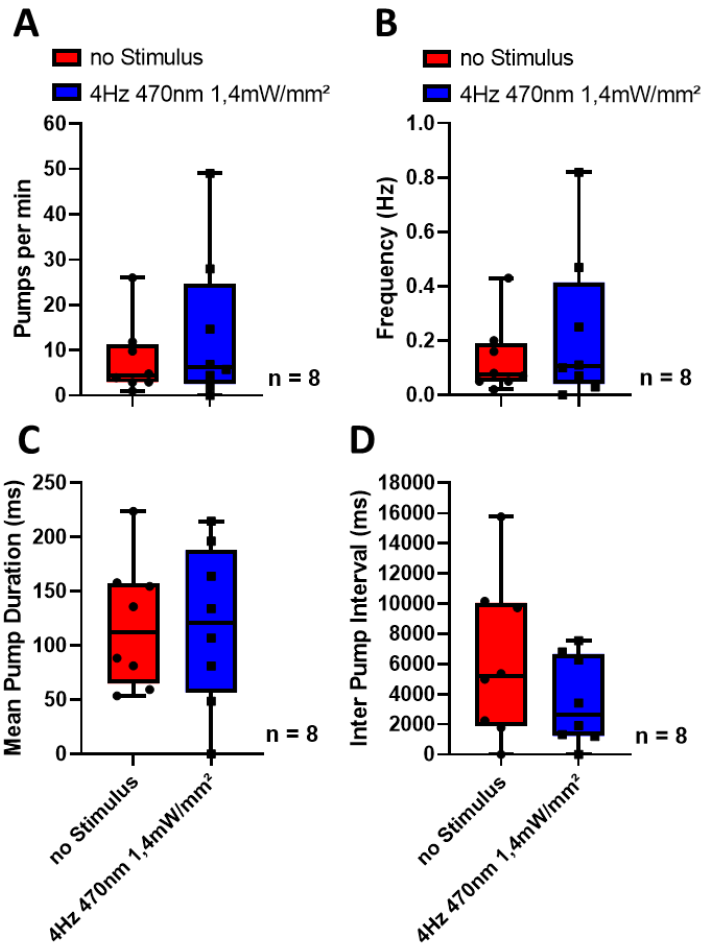

Figure 109: Pharynx pumping of ATR GOA01 could not keep pace with 4Hz blue light pulses. A) Pumps per min. B) Frequency in Hz. C) Mean pump duration (average pump duration, from a pump's E-pike to the same pump's R-pike). D) Inter pump interval (time between two spikes of two pumps). Red: 60s no stimulus, blue: 60s 4Hz 470nm 1.4mW/mm². Animals were fed overnight on agar plates with ATR 0.2% in OP50. Tracking system Nemametrix Screen Chip and software Nemaquire. Box plot with mean ± SD. Median, IQR, whiskers: 2.5 to 97.5.

3.11.1.3. Pharynx pumping under violet light

The majority of ChR variants are sensitive to blue light with a peak activation wavelength of 470nm (Beyeler et al. 2014). This also applies to ChR2, yet it can also be activated by wavelengths ranging from 410nm to 530nm (Lin 2011). The Channelrhodopsin 2 variant CatChUP, used here, carrying the mutations L134C, H134R and T159C, was modified to have high Calcium conductance (Kleinlogel et al. 2011). To test whether it is also effective in a wider range than expected, in this experiment the wavelength was lowered in the ultraviolet direction to 430nm and tested in strain GOA01 crossed into *lite-1* background, to exclude light avoidance responses specifically induced by short wavelengths (Edwards et al. 2008; Ward et al. 2008).

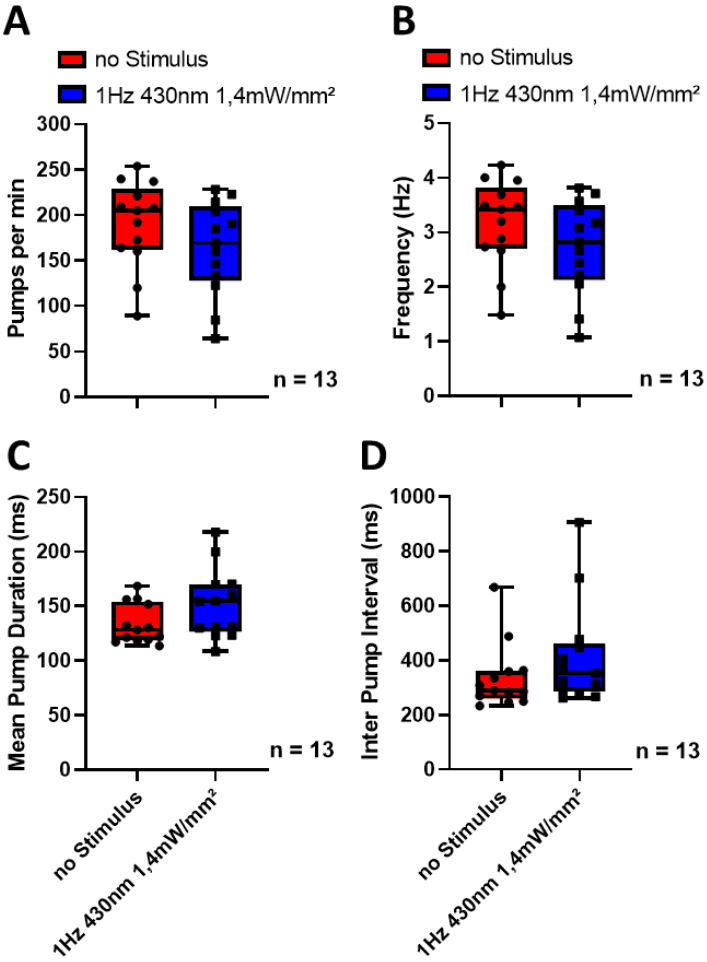

Figure 110: Violet light could not induce a change of Pharynx pumping of ATR lite-1 GOA01 during 1Hz light pulses. A) Pumps per min. B) Frequency in Hz. C) Mean pump. D) Inter pump interval. Red: 30s no stimulus, blue: 60s 1Hz 430nm 1.4mW/mm². Animals were fed overnight on agar plates with ATR 0.2% in OP50. Incubation with 50mM Serotonin for 30min right before assay. Tracking system Nemametrix Screen Chip and software Nemaquire. Box plot with mean ± SD. Median, IQR, whiskers: 2.5 to 97.5.

Animals reared with ATR and incubated in 50mM serotonin, were exposed to 60s 1Hz 430nm with an intensity of 1.4mW/mm². Statistical tests revealed no marked differences. The findings in *Figure 110* were similar compared to GOA01 (*Figure 108*). The mean value of pumps (A) decreased from 190.1PPM to 163.5PPM during stimulation, as did the median 205 to 169.2PPM. Correspondingly, the frequency also declined (B). In consequence, mean pump duration (C) and inter pump interval time (D) are raised. Inter pump interval (D) mean shifted from 336.9ms to 415ms and the median elevated from 289.3 to 352.5ms. In addition, the variance was heightened by only two extreme outliers, both in median and mean. Results of *Figure 110*, depict that a pacing with 430nm was not feasible in serotonin-exposed animals. Neither pacing with 1Hz markedly altered the frequency, nor did the animals reveal a variation in frequency, deviating from the serotonin effect during light pulses.

A comparable assay was done with the strain lite-1 GOA01 and the light protocol 30s basal pumping followed by 60s 4Hz 470nm 1.4mW/mm² (no data available). Animals were fed overnight on ATR containing OP50, but no additional serotonin was given. The intention of this experiment was to test if the naturally occurring spontaneous pumps of the pharynx were affected by blue light stimulus. This experiment was one of the prime objectives of integrating CatChUP into the RyR locus of *C. elegans*. As a successful insertion of optoRyR would also affect the pharynx muscles, by controlling the Ca^{2+}

release from the SR. Unfortunately, animals were not pumping at all, leaving this experiment not evaluable.

3.12.2. Serotonin induced pharynx pumping in GOA14

With the intention to investigate if an integration of CatChUP at both sites, exon 1.1 and exon 1.2 would be sufficient to get a reliable response during light illumination the strain GOA14 was tested under the same conditions as GOA01.

3.11.2.1. Possible effects of violet light on pharynx pumping

430nm illumination was used to check for possible sensitivity at a lower wavelength than expected (*Figure 110).* Here in *Figure 111* in A) the results indicate that both PPM and frequency are not distinctly affected during illumination periods of 60s 1Hz 430nm 0.71mW/mm². The mean decreased from 192.9PPM to 187.1PPM, on the other hand median raised from 175.7 to 187.5 PPM, as seen in A). The frequency in B) follows the same trend, whereby the mean drops from 3.2Hz to 3.1Hz whilst the median raises from 2.9Hz to 3.1Hz. The sole exception, calculated to change significantly, was the mean pump duration, wherein a rise for both mean and median occurred from 169.2ms to 182.5ms, respectively 140.9 to 164.9Hz. Following A) and B) the inter pump interval (D) rises in mean and diminishes in median. Taken together there is only a slight significance in pump duration but no consistent results in mean and median of A), B) and D), despite a relatively high n number of 20 we cannot conclude that GOA14 is sensitive to 430nm light illumination.

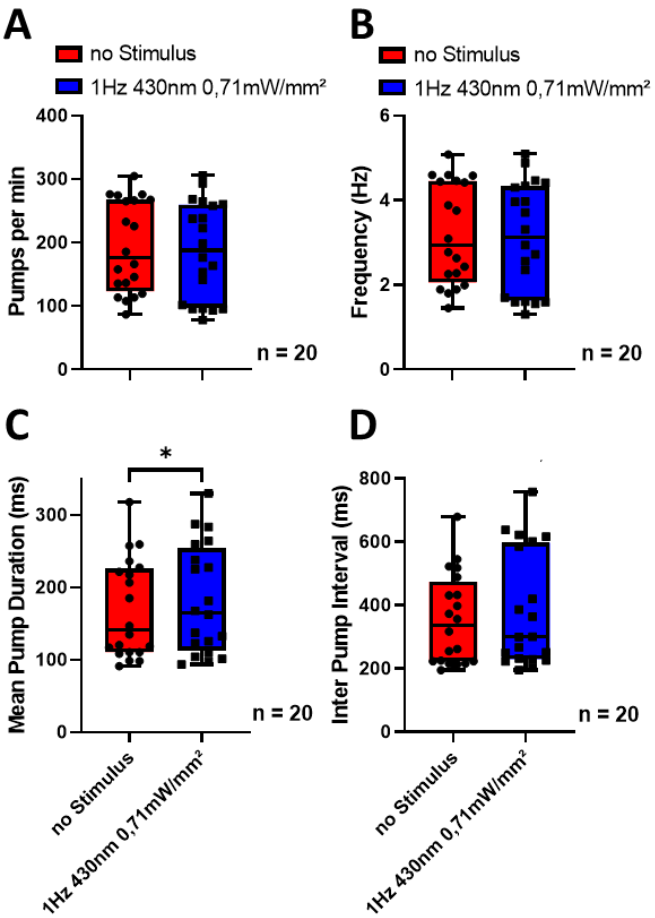

Figure 111: The effect of violet light increased the duration of the pumps notably. Pharynx pumping of GOA14 shows significant raised mean pump duration during 1Hz 430nm light pulsing on 50mM Serotonin. A) Pumps per min. B) Frequency in Hz. C) Mean pump duration significant difference of blue light illumination to no stimulus. D) Inter pump interval. Red: 30s no stimulus, blue: 60s 1Hz 430nm 0.71mW/mm². Animals were fed overnight on agar plates with ATR 0.2% in OP50. Incubation with 50mM Serotonin for 30min right before assay. Box plot with two-tailed paired t-test ***: $p \leq 0.001$, **: $p \leq 0.01$, *: $p \leq 0.05$. Median, IQR, whiskers: 2.5 to 97.5.

3.11.2.2. Stimulation with 1Hz does not affect pharynx pumping

To compare activity under strong illumination, pharyngeal pumping of GOA14 supplemented with ATR and serotonin was measured for 30s to determine basal pumps, followed by 60s 1.41mW/mm² 1Hz 470nm stimulation. We find a rise in pumps per min and frequency from 161.3PPM to 173.2PPM, respectively 2.68Hz to 2.88Hz, representing a raise of 7.4%. The median is enhanced from and frequency rose about 13.4%. In accordance with that, the mean pump duration and IPI dropped in average by 1.28% and 31.6%. Following that tendency, the mean of pump duration and IPI reveal reduction of -4.6% and -10.7%. 6 evaluable measurements reflect no discrepancy in the statistical analysis.

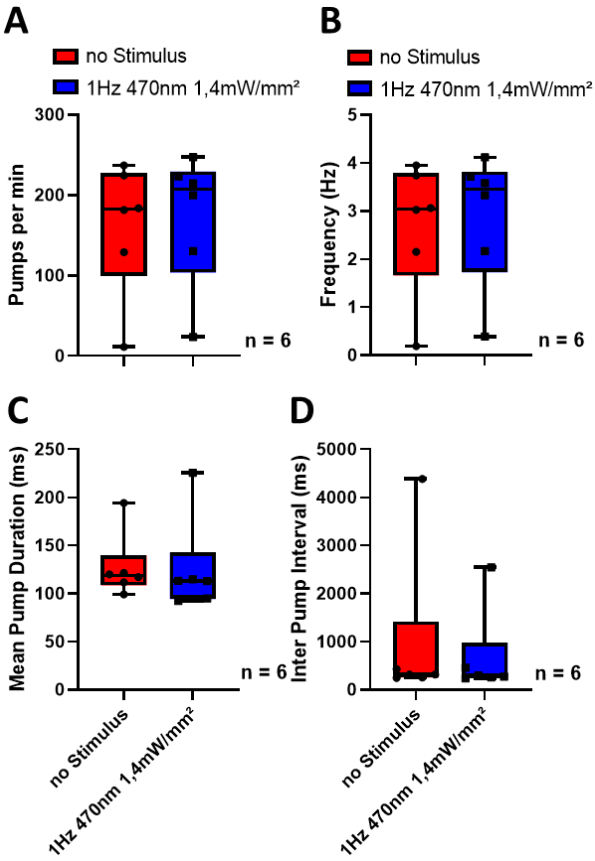

Figure 112: GOA14 is insensitive to 1Hz 470nm light pulses on 50mM Serotonin. A) Pumps per min. B) Frequency in Hz. C) Mean pump duration. D) Inter pump interval. Red: 30s no stimulus, blue: 60s 1Hz 470nm 1.4mW/mm². Animals were fed overnight on agar plates with ATR 0.2% in OP50. Incubation with 50mM Serotonin for 30min right before assay. Box plot, median, IQR, whiskers: 2.5 to 97.5.

3.11.2.3. Pharynx pumping of wildtype animals was not influenced by blue light pacing

To investigate whether there is an effect on *C. elegans* of ATR, serotonin and/or light pulses, the experiment above was repeated under the same conditions with wild-type animals. *Figure 113* represents the outcome of wild-type animals during a 30s basal pumping interval and 60s 1.4mW/mm² 1Hz 470nm stimulation, supplemented with ATR and serotonin. In A) and B), the mean value of PPM and frequency is dropping, in contrast to GOA14. The Median reduces by -31.4% in average pumps and -12.1Hz in frequency. C) illustrates a heightened mean pump duration (3.2%) and a declined median (-18.6%). Inter pump intervals on the other hand were higher in both (mean 74.6% and median 34.9%).

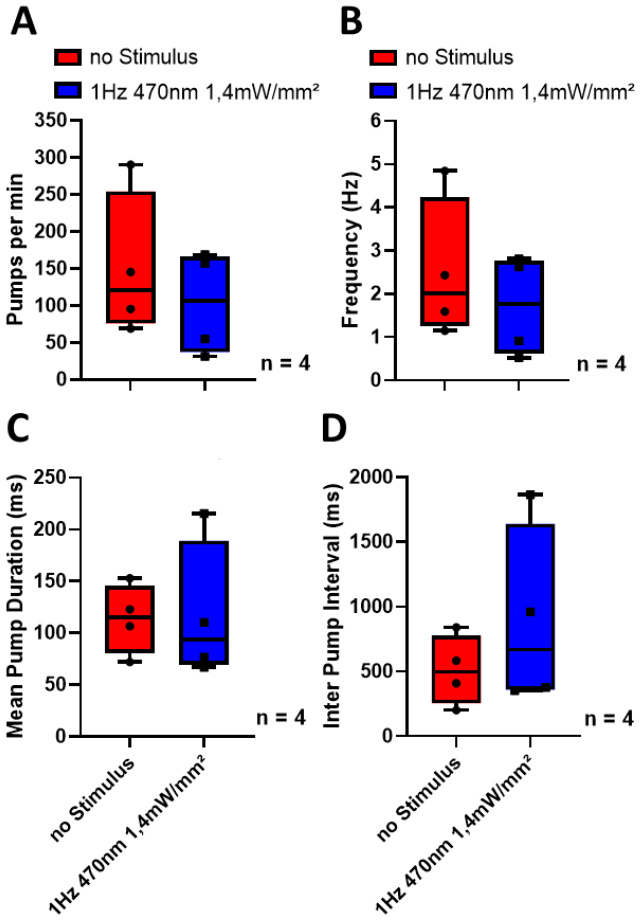

Figure 113: Strong blue light reduced pumping frequency, and raised pump duration and inter pump intervals, but the effect was not clearly pronounced. Pharynx pumping of wild-type during 1Hz 470nm light pulsing on 50mM Serotonin. A) Pumps per min. B) Frequency in Hz. C) Mean pump duration. D) Inter pump interval. Red: 30s no stimulus, blue: 60s 1Hz 470nm 1.4mW/mm². Animals were fed overnight on agar plates with ATR 0.2% in OP50. Incubation with 50mM Serotonin for 30min right before assay. Box plot, median, IQR, whiskers: 2.5 to 97.5.

3.11.2.4. Permanent stimulation of GOA14 has no influence on pharynx pumping

The following experiment tested, whether constant illumination without any pacing would have any effect on the pharynx pumping frequency. For this purpose, strain GOA14 was exposed to 470nm 1.4mW/mm² constant illumination for 60s, after a 30s period without any stimulus. Except for the change in light application the experimental setup remained constant. Results depicted in *Figure 114* lead to no statistical difference. Mean of A) and B) decreased during blue light illumination by -16.4%. Median values for A) and B) give -20.8% reduction in pumps. The average pump duration (C) rose about 17.7%. This discrepancy is put into perspective by the median, enhancing by only 1.22%. This is strongly influenced by one extreme outlier. In contradiction, the IPI given in D) displayed the contrary with a reduction of -39.1% and an increase of 11.4% for mean and median, wherein the mean is strongly shifted by one outlier. The n number here is 6, which explains why 2 outliers are having such a strong influence.

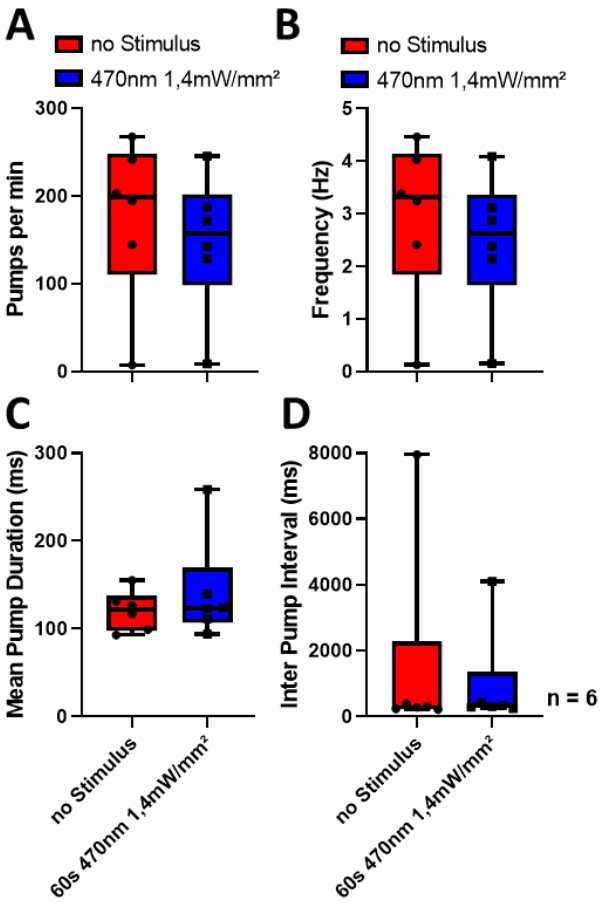

Figure 114: Pharynx pumping of GOA14 is virtually unchanged by a continuous blue light stimulus. Red: 30s no stimulus, blue: 60s 470nm 1.4mW/mm² permanent illumination. A) Pumps per min. B) Frequency in Hz. C) Mean pump duration. D) Inter pump interval. Animals were fed overnight on agar plates with ATR 0.2% in OP50. Incubation with 50mM Serotonin for 30min right before assay. Box plot, median, IQR, whiskers: 2.5 to 97.5.

3.11.2.5. Wild-type animals reduce pharyngeal pumping under the influence of permanent stimulation

Parallel to 3.11.2.4. Permanent stimulation, the assay was repeated with wild-type animals under the exact same conditions. While the animals were exposed to constant blue light, the mean of pumps per min (A: 179.5PPM to 116.7PPM) and the median (145PPM to 131.8PPM) dropped remarkably. Similarly, the frequency went down from 3Hz to 2Hz on average and the median declined from 2.4 to 2.2Hz. This led to a decline of the mean by -35% and -9.7% for the median and thus, significant p-values for pumps (0.018) and frequency (0.0177). Accordingly, the IPI is significant, too. Mean of D) was elevated by 99.2% and median by 14.8%. Only the mean pump duration was not altered by the light stimulus. Here the average changes by -8.6%, and the median by -5.2% from 110ms to 104.3ms. With a n number of 10, these results proved that pumping frequency of wild-type animal is significantly influenced by 1.4mw/mm² blue light. This in turn means that the former experiments in which light affected pumping in GOA01 and GOA014 were presumably not specifically affected, but demonstrated an intrinsic, photophobic light response. The experiments may need to be repeated with a *lite-1* or *lite-1*; gur-3 background. This would eliminate the light avoidance responses on pharynx pumping (Bhatla and Horvitz 2015).

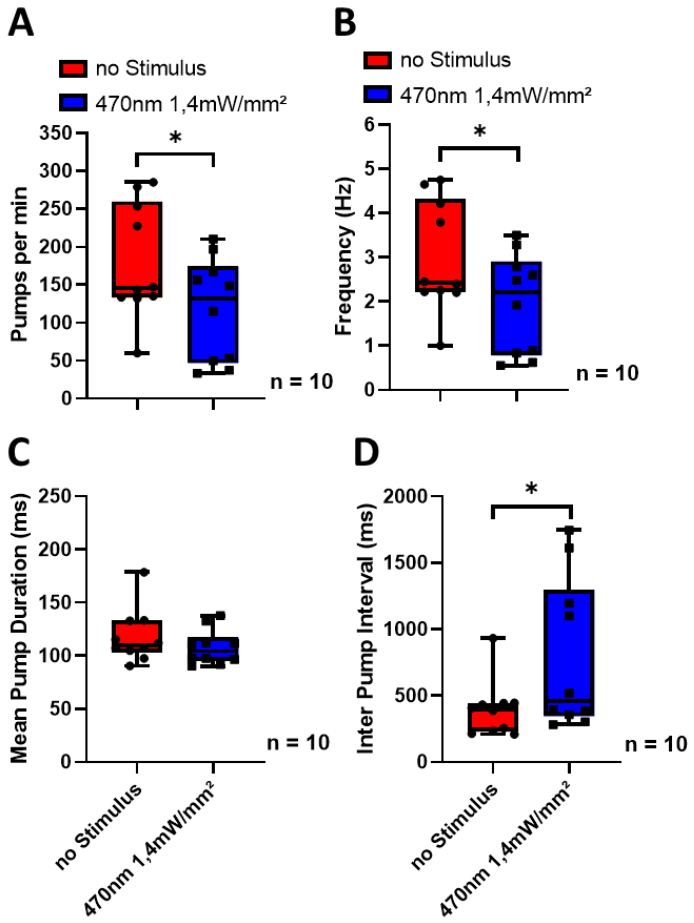

Figure 115: **Wild-type animals reduced pharynx pumping notably under the influence of permanent blue light and serotonin.** A) Pumps per min show a significance. B) Frequency in Hz is significantly different. C) Mean pump duration. D) Inter pump interval, shows significant changes. Red: 30s no stimulus, blue: 60s 470nm 1.4mW/mm² permanent illumination. Animals were fed overnight on agar plates with ATR 0.2% in OP50. Incubation with 50mM Serotonin for 30min right before assay. Box plot with two-tailed paired t-test ***: $p \leq 0.001$, **: $p \leq 0.01$, *: $p \leq 0.05$. Median, IQR, whiskers: 2.5 to 97.5.

When animals were incubated with 50mM serotonin, this induced pharyngeal pumping without any food in proximity. Under the influence of serotonin, *C. elegans* begin to pump at a rate of up to 250 pumps per min (4.16Hz) (Horvitz et al. 1982). Since we want to investigate if GOA01 and GOA14 were stronger influenced by blue light than wild-type animals, and these strains should be manipulable by blue light, inducing Ca^{2+} release through a working optoRyR construct, we tested animals without additional serotonin influence. Strain GOA01 was tested in 3.11.1.2. 4Hz stimulation could not be followed by pharynx pumping of GOA01 and GOA14 C1V1 was tested under the conditions:

60s 4Hz 590nm 1.4mW/mm²
60s 1Hz 470nm 1.4mW/mm²
60s no stimulus

In absence of serotonin no evaluable pumps of GOA14 C1V1 could be tracked. An expected pumping rate of 22per min, a range of 0.27Hz - 0.47Hz (Horvitz et al. 1982), could not be observed.

3.11.2.6. Effects of blue and yellow light on the control group

Successful pharynx pumping was tested on control strain ZX1662 under 60s 1Hz 590nm 1.4mW/mm² and partly under 60s 4Hz 470nm 1.4mW/mm². This strain contains zxIs20 [pmyo-2::ChR2(H134R)::mCherry; pges-1::nls::GFP], which leads to contraction of pharyngeal muscle cells upon blue light stimulation. It was found that during 590nm illumination the average of pumps was 70.7PPM; the frequency 1.18Hz. Medians of these were 67.1PPM; 1.18Hz. Since the animals pumped on average at 1.18Hz and this basically corresponds well with the stimulation frequency of 1Hz, this proved that there is a sensitivity to 590nm. Changing the conditions to 4Hz 470nm gave the following results: Average of pumps per min was 147.5PPM; frequency 2.46Hz. Median of these were 143.1PPM; 2.39Hz. An average frequency of 2.46Hz proved that the animals could not follow a 4Hz stimulus, however *Figure 116* A) and B) illustrate at least some approached 4Hz pacing. This proves that ZX1662 is sensitive to 590nm in addition to 470nm and that in theory a pharynx pumping assay can be performed with sensitive constructs like ChR2 (H134R) integrated into pharyngeal muscles.

Interestingly, according to (Erbguth et al. 2012), ChR2 (H134R) should not be sensitive to 590nm illumination, wherein the body length was not reduced at 580nm stimulation.

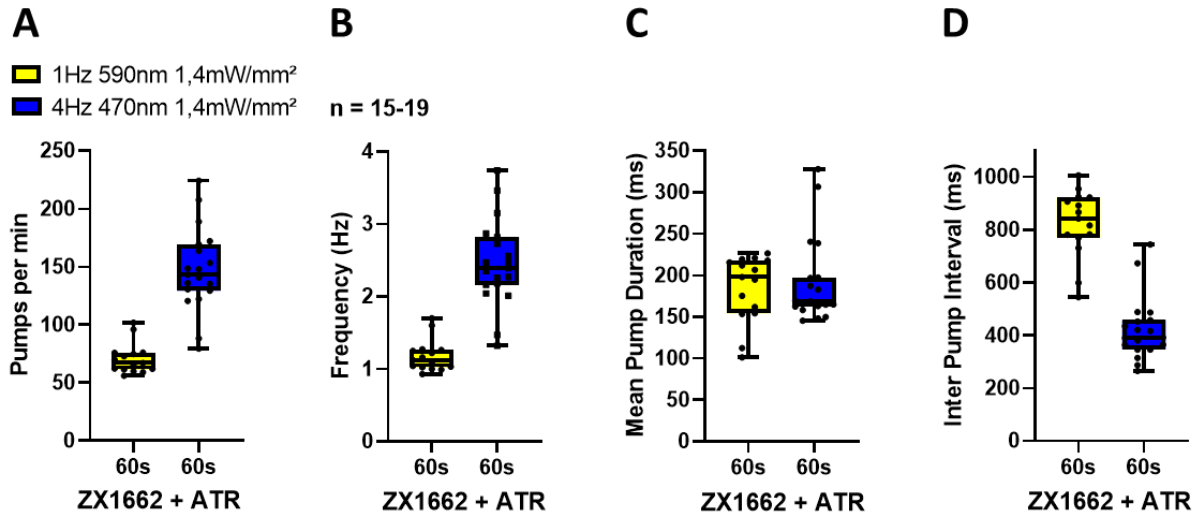

Figure 116: 1Hz pacing could be easily maintained, but 4Hz could only be reached by some animals. Pharynx pumping of ZX1662 on ATR during illumination: Yellow: 60s 1Hz 590nm 1,4mW/mm², blue: 60s 4Hz 470nm 1.4mW/mm². Animals were fed overnight on agar plates with ATR 0.2% in OP50. A) Pumps per min. B) Frequency in Hz. C) Mean pump duration. D) Inter pump interval. Box plot with Median, IQR, whiskers: 2.5 to 97.5.

In addition to strain ZX1662, which carries a ChR2, strain ZX1663 zxIs78 [pmyo-2::C1V1 ETET; pmyo3::mCherry] containing the C1V1 was also tested. Unfortunately, it was not possible to generate usable data in the short time remaining. Considering all the data from the pharyngeal assays, it is clear that there is a high standard deviation of frequency, in all strains except control ZX1662. This suggests that if the pharyngeal muscles of the transgenic strains are sensitive to pacing, this is not the case in every animal, but only in a few.

4. Discussion

Since the beginning of optogenetics, a plethora of light triggered tools have been developed in *C. elegans*. These include a variety of Ca^{2+} translocators that have different properties useful for specific applications. In this work, we attempted to develop new optogenetic tools for manipulating the release and uptake of Ca^{2+} from and into the sarcoplasmic reticulum.

I followed up on what was already known and tried to take another step towards the final goal of a spatiotemporal manipulation of the Ca^{2+} flux across the SR/ER membrane.

4.1. Channelrhodopsin based tools for Ca^{2+} flux manipulation on the SR/ER membrane

In addition to RyR as a Ca^{2+} transporter, attempts were also made to use channelrhodopsin as a trigger for CICR on the SR/ER membrane. ChRs were equipped with intrinsic or extrinsic SR retention motifs to retain them to the SR/ER membrane, by preventing their ER export.

4.1.1. SR retention using UNC-68 TM5+6 retention motif

One approach to create a light-activated tool for Ca^{2+} release in the ER was to use the recently described ChR variant from *P. subcordiformis*. The task here was to manipulate Ca^{2+} release from the SR/ER and also to confine the tool to the sarcoplasmic membrane of *C. elegans.*

By fluorescence imaging, a successful injection and transformation with the plasmid PsCatCh::YFP:: UNC-68 TM5+6 could be confirmed (*Figure 70*).

Both high and low intensity revealed a significant reduced thrashing rate under blue light stimulation, proofing an effect of the expressed plasmid. The comparison of the animals reared with ATR (30ng/µl) with the control group (B) also proves the expression of the plasmid. It is evident that ATR supplementation is necessary to activate PsCatCh and thus enable Ca^{2+} release. If we take into account that the control animals of the *lite-1* strain depict a reduction of thrashes both with and without ATR supplementation and offset this difference with the transgenic animals, we see that there is still a reduction in transgenic strains. A comparison puts the transgenic strains in a clearer relationship, but at the same time drastically mitigates the efficiency of the injected plasmid.

To confirm that the PsCatCh::YFP::UNC-68 TM5+6 construct has an effect in the muscle cells, a contraction assay was performed at an intensity of 1.4 mW/mm² (*Figure 73*). Unfortunately, with the number of animals measured here and using this light protocol, no difference between ATR reared animals and non-supplemented animals (*Figure 73* A and B) could be detected at this intensity. The control strains *lite-1* and ZX1743 were responding as expected.

Overall, the data suggest that PsCatCh::YFP::UNC-68 TM5+6 could be a useful tool for optogenetic manipulation of intracellular Ca^{2+} release from the SR/ER, as it is expressed in body wall muscle cells and affects complex coordinated swimming movements, as seen above. However, an effect is only visible when *C. elegans* has to perform a coordinated movement, such as the swimming movement in this case (Ikeda et al. 2020). This could be due to their ability to compensate during locomotion by changing the kinematics of their locomotion pattern (Hwang et al. 2016). Whereas more simple

alteration of muscle elongation or contraction of the animal could not be proven, because here a compensation by other muscles may occur, or the Ca^{2+} outflow from the SR/ER was not sufficient to trigger a contraction under these conditions. The Ca^{2+} outflow can probably be compensated by e.g. SERCA and only becomes important as soon as a movement has to be executed that has to be finely tuned, and even the smallest deviations in the interaction of the muscles become relevant (Ikeda et al. 2020; Donnelly et al. 2013; Hwang et al. 2016). In total, the results indicate that this is a photophobic response, although the experiments were carried out with *lite-1* animals. The first steps that can contribute to a useful tool in the optogenetic toolbox here should be to repeat this experiment at intensities where no photophobic response can be detected in the animals, possibly also in wild-type animals. Furthermore, it should be attempted to maximise Ca^{2+} efflux from the SR/ER and confirm SR/ER retention by fluorescence imaging, or ensure this through further modifications of PsCatCh::YFP::UNC-68 TM5+6.

4.1.2. SR retention of PsCatCh using IP_3R TMH I+II

Similar to the development of a tool to influence Ca^{2+} efflux from the SR/ER into the cytosol using the CeRyR retention motif in 4.1.1. SR retention using UNC-68 TM5+6 retention motif, TMH I+II of the Inositol 1,4,5-trisphosphate receptor are used here to generate SR/ER membrane retention of PsCatCh (*Figure 74*).

Although YFP fluorescence was faintly visible, expression of IP_3R TMH I+II in the muscles of *C. elegans* could not clearly be verified by microscopy, as it could be done by Damijonaitis 2011, in which membranous structures and not all but many muscles were fluorescent. In *Figure 75 B*, no fluorescence of body wall muscles is visible, and as indicated by red arrowheads, autofluorescence of isthmus, terminal bulb and intestines is clearly visible. Explanations for this could be that the protein is expressed but not properly inserted into the SR/ER membrane due to misfolding/maturing (reference) of TMH I+II. It is also possible that expression does not occur to a sufficient level to become visible, which could be supported by a weak or no effect during assays. The fact that this protein has not been directly adapted for expression in *C. elegans* and that additional mutations have been inserted may also play a role here.

A first assay using 1.26mW/mm² blue light stimulation as seen in *Figure 76*, illustrates a significant reduction of swimming cycles while photostimulation persists, for both ATR reared animals and not supplemented animals. Although all strains demonstrated reduced thrashing in response to photostimulation, the most pronounced response was observed in the ATR-treated animals of the transgenic strain PsCatCH::YFP::IP_3R TMH I+II injected with 30ng/µl plasmid. Since the *lite-1* control strains also demonstrated a response to photostimulation, albeit not a significant one, the experiment was repeated with only half the intensity of blue light irradiation (*Figure 77*). The fact that a significant response to the photostimulation of the animals was also measured here, and only in ATR-supplemented animals, demonstrated that the construct was working. This was true for the animals injected with 30 as well as with 300 ng/µl plasmid. Here it can also be mentioned that the n number of animals is sufficient to support the results of the swimming assay.

Supported by the positive results of the swimming tests, a contraction assay was carried out. In the contraction experiments, it was found that almost all the animals measured showed a photophobic response (Edwards et al. 2008) in the form of a reversal (Lee and Aschner 2016), as soon as the light stimulation started. However, only the ATR-supplemented animals of the PsCatCH::YFP::IP_3R TMH I+II strain 30ng/µl presented a significant difference, albeit brief, compared to the control group. The fact that this is visible in the first seconds of stimulations, while nearly all animals show reversals, can be

interpreted as an enhancement of the contraction. This occurs during the reversal due to the additionally triggered Ca^{2+} outflow, from the SR/ER. From the control group only ZX1743 did not perform reversals, due to its strong body contraction, which can only be seen in the videos (data not shown).

Since in all strains, except ZX1743 supplemented with ATR, reversals occurred as a response to photostimulation, it should be considered to reduce the intensity until reversals have decreased significantly. The thrashing assays with 0.63mW/mm² could be used as a guide for this. Since the equipment differs, direct transfer is not possible here and a separate run would have to be carried out for the appropriate intensity. By that it might be that a more pronounced difference in the transgenic lines could be detected.

Summarising the data, there is indeed a significantly stronger reduction in swimming cycles in the animals reared with ATR, however this is also evident in the control group without ATR. In addition, expression of the construct could not be clearly confirmed. Only a non-sustained contraction occurred during stimulation. The most interesting question here is if the IP_3R transmembrane helices lead to a reliable SR membrane retention. It is possible that a very short linker between PSCatCh and YFP of 12 amino acids and 9 AAs between YFP and the transmembrane helices led to a misfolding or steric hindrance of YFP, that prevented fluorescence. However, it is also possible that the protein is not well expressed in this animal. This has already been observed with other rhodopsins, indicating that not all of them are well expressed in *C. elegans*, as for example in Erbguth et al. in the case of vChR1. With these results in mind and the additional information of the outcomes of Damijonaitis 2011, in which was demonstrated that ChR2(L132C)::YFP::IP_3R-1(TMI+II) does not provoke any contraction, experiments utilizing IP_3R(TMI+II) further experiments should be done. It should be examined if the IP_3R TMH I+II retains in SR/ER membrane and if it is sufficient to generate an adequate Ca^{2+} current across the SR membrane.

4.1.3. Direct manipulation of Ca^{2+} release from the SR/ER membrane by $ChRGR_{ER}$

By equipping the Channelrhodopsin chimera $ChRGR_{ER}$ with an ER-retention motif a tool was created to manipulate the Ca^{2+} flux over the SR/ER (Asano et al. 2018). Therefore, it was used in this work to find out if it is a useful basis for a tool to control Ca^{2+} efflux from the SR/ER by photostimualtion in *C. elegans* (Figure 19).

Successful expression of the plasmid after injection was confirmed by fluorescence images (*Figure 79*). In addition, as indicated by the arrowhead in *Figure 79* A, expression can also be seen when a protein aggregates strongly and then accumulates in inclusion bodies in the intracellular membrane.

Transgenic *lite-1* strains carrying the $ChRGR_{ER}$ construct exhibited a reduced thrashing rate compared to *lite-1* control. Here thrashing assays, could not prove that a Ca^{2+} release and as result a measurable change in muscle activity (swimming cycles) could be triggered by a photostimulation of 0.63mW/mm². The only significant difference occurred in animals injected with 5ng/µl plasmid, but only in animals that had not received ATR supplementation before the assay. Animals of the strains injected with the highest amounts of plasmid displayed the same tendency during and after photostimulation (*Figure 80*), even though no ATR was added. Therefore, it cannot be assumed that this response is related to Ca^{2+} release at the SR/ER membrane, but rather to a photophobic reaction of the animals. This raises the question why a *lite-1* strain without ATR supplementation exhibits such a response. Since the ATR-supplemented *lite-1* strain reveals a visible but not significant reduction during and after light

stimulation, but the non-supplemented *lite-1* strain does not, no conclusive statement can be made here. As more than 50 animals were measured, this should provide a solid basis for statistical analysis, hence a too small sample size is not sufficient as an explanation.

Stronger photostimulation (1,4mW/mm²) used in the contraction assays underlines the previous results. Transgenic $ChRGR_{ER}$ strains did not react differently to light stimulation than the control group (*Figure 81*). The *lite-1* strains with and without ATR supplementation did not respond with a body contraction, while the control group consisting of ZX1742 fed with ATR showed a significant contraction during photostimulation and persisting afterwards. None of the strains injected with the $ChRGR_{ER}$ plasmid exhibited any change during or after photostimulation. With this information it can be concluded that a possible Ca^{2+} release could not be achieved, or the Ca^{2+} efflux from the SR/ER is not strong enough to cause a measurable change in body length or swimming behaviour under these conditions. Furthermore, the animals were found to be of sickly appearance, which is also underlined by the strongly reduced thrashing rate (*Figure 80*). One reason for this could be the muscular ER stress, which is caused by the fact that the protein is expressed but cannot be incorporated into the SR/ER without further consequences. On the one hand, the low number of animals in the contraction experiments should be seen critically here and increased. However, it should also be mentioned that the measured values in the contraction assay are not subject to a high fluctuation, and an increase in the measured animals will probably not reveal any change here. Low expression cannot be completely ruled out, but the fluorescence images (*Figure 79*) indicate that $ChRGR_{ER}$ is expressed strong enough. Nevertheless, this does not exclude the possibility of partial misfolding or aggregation (Gregoire et al. 2012). These results suggest that mere manipulation of Ca^{2+} efflux from the SR/ER in *C. elegans* cannot be achieved by only this extrinsic light-gated, through retention motif SR/ER membrane bound channel alone.

4.1.4. Enhanced Ca^{2+} conductivity with ChR-XXM

Since the amount of Ca^{2+} released from SR/ER is a critical factor, ChR-XXM was chosen as candidate for the creation of a tool for optogenetic manipulation of intracellular Ca^{2+} release from SR/ER by light stimulation, due to its increased Ca^{2+} conductivity.

Using Spinning Disc Confocal microscopy, the expression of XXM4::mVenus (ChR-XXM) could be verified in the muscle cells of *C. elegans*, as it can be seen in *Figure 82*. Fluorescence was clearly visible and most pronounced in the vulva muscle cells (*Figure 82* B, arrowhead a). Due to the high background fluorescence caused by the intestine (Klass 1977; Clokey and Jacobson 1986; Forge and Macguidwin 1989), weaker expression in the muscle cells of the body wall could only be detected after adjusting the contrast (Fig. C).

The efficiency of the new construct was proven in contraction experiments. In these, in ATR reared animals, a photostimulation of 2s with 0.8mW/mm² already led to a stronger contraction of the worms than it could be triggered in the control strain ZX1743. Here, a maximum contraction appeared after approx. 1s after exposure was stopped. When this experiment was repeated with a longer and stronger blue light pulse of 1.4mW/mm², the contraction of the ATR-fed animals increased up to 16%. The main difference between the two experiments was that a short, 0.8mW/mm² light pulse could induce a strong contraction. After 6 seconds, this value returned to the level of the animals without ATR supplementation. Furthermore, a stronger, longer lasting light pulse (1.4mW/mm²) led only to a partial recovery, which even after 10 seconds had not yet reached the level of the control group. These strong effects are presumably due to the predicted ability of ChR-XXM to depolarise the plasma membrane to a greater extent (Scholz et al. 2017). In addition, the strength of the contraction is directly related

to the intensity and duration of photostimulation, eventually leading to a sustained contraction upon strong stimulation (Figure 84, A).

Since the experiments conducted with ChR-XXM were successful, an attempt similar to experiment 3.7 was started. Here, ChR-XXM was used instead of PsCatCH and IP_3R TMH I+II was used to generate SR/ER retention. Unfortunately, multiple injections of pmyo-3::ChR-XXM::eYFP:: IP_3R TM I+II into *lite-1* animals did not yield any stable strain. No clear reason for this could be found so far. It is merely speculative that the expression of the injected plasmid already led to a lethal impairment in the early larval stages. On the one hand, ChR-XXM alone, as a substitute for another channelrhodopsin, does not provide a new tool to control Ca^{2+} flux across the SR/ER membrane. However, combined with a retention motif such as IP_3R TM I+II or UNC-68 TM5+6 and its inherent increased conductivity (Scholz et al. 2017), it can become a promising tool. Further research with these retention motifs should focus on improving expression and retention to the SR/ER, and then combine this with the increased Ca^{2+} conductance of ChR-XXM.

4.2. The human ryanodine receptor as a primary and secondary target of light-driven Ca^{2+} release

The ryanodine receptor was used here in various ways as a tool to achieve the goal of Ca^{2+} release at the SR/ER membrane. On the one hand, a truncated version was created, which should be more manageable and therefore more effective. However, experiments were also conducted with the full length human RyR. Both versions were additionally equipped with channelrhodopsin to trigger the opening of the Ca^{2+} channel. The actual target, the ryanodine receptor, is activated indirectly by a coupled ChR and its Ca^{2+} efflux. In this case, a local Ca^{2+} cloud generated by this triggers the opening of the RyR, which in turn initiates a cascade in which other RyRs are opened by the Ca^{2+} increase (CICR). The fact that RyRs are often localized in clusters, and not randomly solitarily distributed (*Figure 26*) supports this effect (Galice et al. 2018). It should be noted that at the beginning of this work it was not clear whether the human RyR could be functionally expressed in *C. elegans*.

4.2.1. The effect of an engineered photo-sensitive version of UNC-68 in deletion mutants

For strain ZX1966, no clear statement can be made about the functionality of the injected fosmid. The results presented in *Figure 34* and *Figure 35* show that the thrashing rate of ATR-supplemented ZX1966 animals is clearly increased during blue light stimulation. Compared to the control group without ATR, however, these are not significant. It also appears that animals injected with the fosmid punc-68::unc-68::mKate::ßHKATPase::ChR2(L132C_H134R_T159C), demonstrated an even lower thrashing rate than the *unc-68 (r1162)V; lite-1 (ce314)* double mutant *Figure 34*. This applies to both groups of ATR-fed and non-fed animals. However, in relative comparison (*Figure 35*), there is an effect in the ZX1966 animals that is still present after photostimulation, and this is in strong contrast to the control group unc-68 *(r1162)V; lite-1 (ce314)*, which has significantly fewer thrashes. But, it also appears in the *unc-68 (r1162)* deletion group. The strain ZX1967 did not exhibit any relevant responses to blue light, neither when 0-60s was compared to the time frames 60-120s and 120-180s, nor in comparison to the control strains wild-type and *lite-1*. Since the strain ZX1967 did not carry a deletion of RyR, the results are consistent with the hypothesis that an improvement in swimming rate can only occur, if the rescue plasmid can compensate for something that is defective or not expressed. In the *lite-1* background, no improvement in swimming rate should occur, since the ryanodine receptor is functional here. Taken together these data indicate that the fosmid punc-68::unc-68::mKate::ßHKATPase::ChR2 (L132C_H134R_T159C), could not alter the swimming behaviour in a consistent manner.

4.2.2. The human Ryanodine receptor in its truncated version

Based on the finding of Bhat et al. 1997, in which a shortened version consisting mainly of the transmembrane part of hRyR is still functional, most of the cytoplasmic "head" was cut off. The aim was to create a truncated version that is much easier to handle and can be better combined with other optogenetic tools.

Swimming experiments with deletion mutants of strain *unc-68 (r1162*) and the truncated version RyR_{pore} found no significant alteration in thrashing frequency (*Figure 43*), which would indicate a functional pore version of hRyR. Unfortunately, no expression of pmyo-3::hRyR2short::Gly-Ser

linker::mNEON could be detected by fluorescence imaging, although the Co-marker was visible. Although, this could also be due to extremely weak expression.

Based on the speculation that the N-terminal domain may be required to achieve functional or at least partial functional expression and/or assembly of the hRyR2 tetramer (Bhat et al. 1997), the $hRyR2_{pore}$ CDL was created. Here too, apart from a few exceptions of individual animals, there was no improvement in swimming behaviour. It must also be taken into account that a 67% homology of ceRyR and hRyR2 (Fischer et al. 2017), may not be sufficient to ensure reliable assembly of the tetramer. Since no expression could be detected and no improvement in swimming behaviour was observed except in individual animals, it must be assumed here that hRyR2 equipped with a long central domain cannot be truncated in this way to form a functional channel in *C. elegans*.

Due to individual *unc-68 (r1162)* animals, demonstrating a strong improvement after injection of RyR_{pore} CDL, a parallel approach was started. In this, the plasmid pFB10 (pmyo-3::CatChUP::eYFP::linker Crp1::hRyR2short CDL) was created, combining the RyR_{pore} CDL version and additionally the CatChUP::eYFP::linkerCrp1. Unfortunately, injection into *unc-68* deletion mutants and into wild-type animals both resulted in no viable transgenic offspring. No transgenic progeny was viable even when the unmodified hRyR was injected. Here, the sheer size of the plasmid is not the decisive factor (see 4.1.3), which may lead to the assumption that negative consequences due to muscle dysfunction (Forrester et al. 2017) lead to lethality in embryonic and early larval stages. But similar observations have been made in previous work in which the intentional expression of RyR led to lethality already in the larval stage (Fischer 2015).

Here, further trials with an optimised version of RyR could lead to a reliable rescue, as Bhat et al. 1997 demonstrated. Thus, the extremely large and bulky RyR could prove to be a useful tool for manipulating Ca^{2+} flux at the SR/ER membrane.

4.2.2.1. The LOV2 domain as trigger for conformational change in the truncated hRyR2

To successfully use the LOV2 domain in RyR_{pore} CDL as an optogenetic tool, the focus was on finding sites that provide enough space for LOV2 not to disturb the hRyR structure too much or lead to steric hindrances. But the need to be close enough to cause a change in the spatial structure of hRyR upon light activation of LOV2. Here, the conformational change of LOV2 should lead to an increase in the gating probability of RyR_{pore} CDL.

Injection of *C. elegans* with a plasmid containing one LOV2 domain at four different sites of the truncated hRyR resulted in the strains N2 LOV2 (1-4) and lite-1 (LOV2 (1-4)) (*Figure 46*, *Figure 47* and *Figure 48*). At a value of 0.16mW/mm², no distinction in swimming cycles between stimulation and non-stimulation could be detected in wild-type animals (*Figure 46*). To exclude a possible light avoidance reaction, transgenic strains with the background *lite-1 (r1162)* were generated. In these the contraction of body length should not be caused by the natural light avoidance behaviour of *C. elegans,* as can be observed in wild-type animals (*Figure 47*). These wild-type animals seek to flee the blue light by contracting, which is a side effect of a reversal, and changing direction (Edwards et al. 2008). In N2 LOV2(1) and N2 LOV2(3), we first get the contrary, an elongation in the first seconds after initiating blue light, followed by a contraction lasting several seconds, which could not be assigned to a reversal (*Figure 51*). Here one may speculate that upon blue light illumination a conformational change of LOV2 domains triggers an opening of the truncated hRyR2 channel resulting in a Ca^{2+} influx into the cytosol, provoking a muscle contraction.

When the lite-1 LOV2 (1-4) stains were recorded in swimming assays, a decline of thrashes was consistently observed, however this is also visible in the *lite-1* control (*Figure 49* B). Moreover, the SEM is too high to achieve any significance. Increasing the n-number could help with strains lite-1 LOV2 (1 and 2). However, based on the *lite-1* control, it cannot be concluded that the effect of reduced thrashes during stimulation is a result of LOV2 activation and thus RyR_{pore} CDL.

4.2.3. Full length RyR as optogenetic tool

Attempts to use the large full-length hRyR2 fused N-terminally with the channelrhodopsin variant CatChUP (CatChUP::eYFP::linkerCrp1::hRyR2), to adapt and express it in *C. elegans* were unfortunately not rewarded with success. Different cloning techniques had to be used to generate the plasmid. Numerous injections into wild-type and *unc-68* deletion mutant animals at different plasmid concentrations did not result in any transgenic strain. It is likely, that the 67% homology of ceRyR and hRyR2 (Fischer et al. 2017), is not sufficient for reliable expression and folding. This is further complicated by the additional CatChUP connected to eYFP and the linker Crp1. Especially, the correct assembly of the tetramer in the SR/ER membrane could be disturbed by this. Moreover, the CatChUP construct was N-terminally fused. Although the additional TM helices are functionally expressed in HEK cells, it cannot be automatically assumed that this is also the case in *C. elegans* without further adaptions to the construct. Furthermore, chaperones present in mammalian cells may have an influence on the folding of the protein, whereby it is not guaranteed that these are present in *C. elegans*. The fact that no transgenic lines could be generated may indicate that if expression did occur, a misfolding or improper assembly of the tetramers and the CatChUP construct resulted in ER stress. This could have been caused by the construct interfering with endogenous membrane proteins. If the data of the full length RyR, truncated RyR, LOV2 integrated RyR, and the punc-68::unc-68::mKate::ßHKATPase::ChR2(L132C_H134R_T159C) are combined, it must be stated that neither an expression nor a function could be unambiguously detected.

4.2.4. Genome-engineering of the endogenous *unc-68* locus to achieve Ca^{2+} flux control on the SR membrane

In addition to the insertion of $OptoRyR_{pore}$, a second experiment was conducted in which, the CRISPR/Cas9 method was used to integrate CatChUP::EYFP::CRP-1, the "Opto", directly in front of the *unc-68* locus, to create an intrinsic optpUNC-68. This allowed the creation of the strains GOA01 and GOA14, in which the Opto was integrated upstream of exon 1.1 in strain GOA01 and exon 1.1 and exon 1.2 in strain GOA14. This should avoid incompatibilities with extrinsic RyR and reduce the risk of e.g. possible steric hindrance and misfolding caused by CatChUP::EYFP::CRP-1.

4.2.4.1. The effect of photostimulation on optoUNC-68 in GOA01

After we started the project of integrating the Opto in front of the exons 1.1, Marques et al. 2020 could demonstrate, that fusion of a fluorophore with exon 1.1 (*Figure 117*) leads to fluorescence in BWMs and vulval muscles, but not in the pharynx (*Figure 118*). In contrast, if the fluorophore is integrated upstream of exon 1.2, expression occurs in the pharynx and neurons (*Figure 119*).

Here, fluorescence imaging (*Figure 53* and *Figure 54*) could not provide a clear indication whether optoUNC-68 was expressed under exon 1.1. The comparison of wild-type and transgenic animals (*Figure 54*) only revealed a difference in the tail region. This was only visible in the intestines and not in the BWMs. In this context, Marques et al. also found that the strength of expression depends on the

size of the integrated construct. This could play a decisive role here. Since the fluorescence of the BWMs depicted in *Figure 119*A, with a fluorophore of ~30 kDa that did not exhibit strong fluorescence, it has to be assumed that considerable expression losses are to be expected simply because of the almost threefold size of CatChUP::EYFP::CRP-1 with 84 kDa.

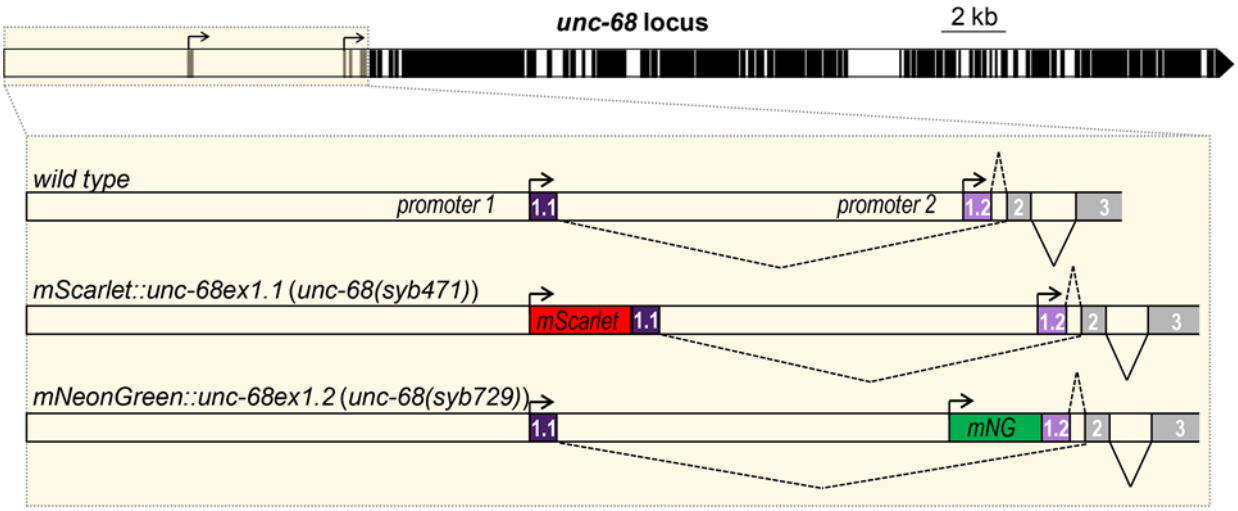

Figure 117: Schematic representation of the unc-68 locus of *C. elegans* (exons in black, introns and promoters in white). Highlighted are the alternative transcription start sites and the location of fluorescent protein sequence knock-ins produced by CRISPR/Cas9-mediated genome editing. mNG: mNeonGreen. Figure taken from Marques et al. 2020.

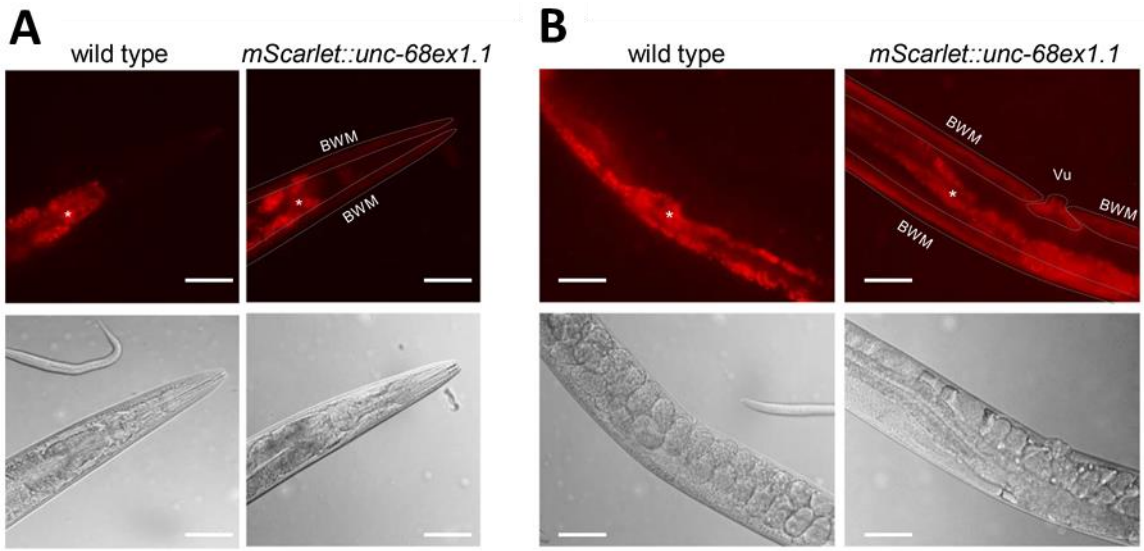

Figure 118: Alternative transcription analysis of *unc-68*. Representative fluorescence and DIC images from the head (A) and midbody (B) of wild-type and [mScarlet::unc-68ex1.1] transgenic animals. BWM: body wall muscle; Vu: vulva muscle; *, autofluorescence background in the intestine. Scale bar: 50 µm. Figure taken from Marques et al. 2020.

The first tests performed were swimming assays using a long-term illumination protocol (*Figure 55*). In these, the normalised data often calculated a significantly increased thrashing rate in ATR-reared GOA01 animals, compared to not supplemented animals during blue light stimulation. A crucial point in the calculation of the significance of the individual measurement points was the fact that ATR-supplemented animals already started with a decreased thrashing rate of ~10bbpm before photostimulation. This resulted in several time points in the normalised data with a significant difference during stimulation as seen in *Figure 55* B. However, the absolute values converge during the assay and show no particular differences during or after photostimulation (A). Here it should be discussed whether the amount of ATR fed to the animals (OP50 including 0.2% ATR) was appropriate

or even too high. To be able to compare all the data collected, the same concentration was used throughout this work. However, a lower concentration could lead to different results, especially in this strain, and could therefore be adjusted in follow-up experiments.
The following experiments conducted with an exposure time of 5 minutes revealed a similar tendency. To exclude the possibility that even very little light leads to activation of the ATR bound to CatChUP, all experiments were carried out in a dark room. The only light source, apart from blue light LEDs for stimulation, was a transmission light of 600nm necessary for the recordings, which was turned down to the minimum detectable limit of the camera. This resulted in 0.0017mW/mm² red light being transmitted to the animals.
The data of the swimming experiments with photostimulation at exposure times of 10 min and 5 min revealed that the control group without ATR and the ATR-supplemented animals basically showed no consistent differences in swimming behaviour. This applies to both GOA01 and lite-1 GOA01 animals. Thus, the swimming experiments did not provide reliable evidence that successful and sufficient expression of optoUNC-68 occurred and resulted in a Ca^{2+} current upon photostimulation.
This is also not supported by the subsequent contraction experiments. For these, a significant difference between ATR-supplemented and non-supplemented animals is evident at an intensity of 0.3mW/mm² for two 5s periods during photostimulation. However, no long-term effect can be detected as it occurred during a period of strong discontinuity. Since the remaining measurements did not differ in either GOA01 or lite-1 GOA01 animals, no effect on body length could be detected due to exposing optoUNC-68 under exon 1.1 to blue light. Taken together, the data of fluorescence imaging, the swimming experiments and the contraction experiments indicate that the expression of the CatChUP::EYFP::CRP-1 RyR linked N-terminally to exon 1.1, either did not take place at all, or if so, then in too low a quantity (Marques et al. 2020). Other constraints could also be related to steric hindrance or misfolding, which led to non-functioning (Gregoire et al. 2012). Thus, no sufficient Ca^{2+} current could be induced upon blue light stimulation on the SR/ER, to induce a clear change in swimming behaviour or body length.

4.2.4.2. The effect of photostimulation on optoUNC-68 in GOA014

Based on strain GOA01, we found that exon 1.1 as the sole target for CatChUP::EYFP::CRP-1 is not sufficient to trigger a reliable response to light. Additionally, Marques et al. found that exon 1.2 is responsible for the expression of RyR in the pharynx and neurons (*Figure 119*). These findings led to the creation of strain GOA14. In this, CatChUP::EYFP::CRP-1 was integrated N-terminally upstream of exon 1.2. and exon 1.1 to exclude that any isoforms could be expressed without CatChUP::EYFP::CRP-1, and thus outcompete the tagged version.

Fluorescence imaging of the optoUNC-68 transgenic GOA14 animals only found a background fluorescence caused by the intestine (Klass 1977; Clokey and Jacobson 1986; Forge and Macguidwin 1989), as illustrated in *Figure 60*. Comparing these images with *Figure 119*, clearly states, that no expression of the N-terminal CatChUP::EYFP::CRP-1 tag is visible, neither in the BWMs nor in the pharynx. It was also not visible in neurons, which could have been possible with a sufficiently high level of expression (Marques et al. 2020). Given that the animals also exhibited strong uncoordinated movement (see below), as is also the case with *unc-68* null mutants, the conclusion is that N-terminal tagging of UNC-68 is not tolerated, at least at the here used tag and thus the animals lost all expression of UNC-68.

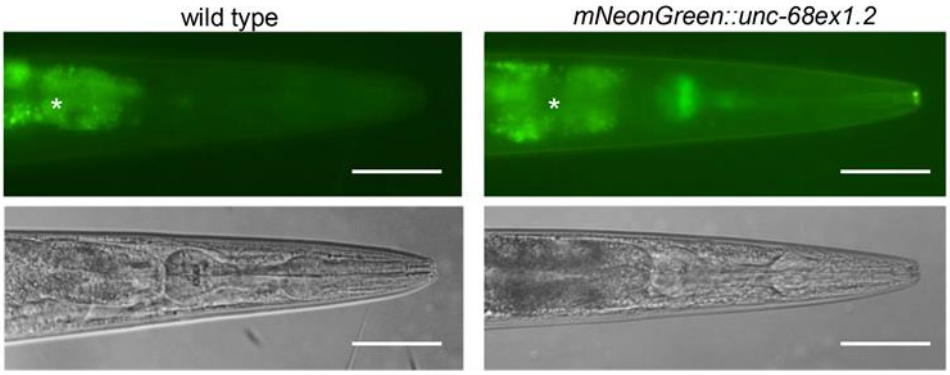

Figure 119: Representative fluorescence and DIC images of the head in wild-type and [mNeonGreen::unc-68ex1.2] transgenic animals. *, autofluorescence background in the intestine. Scale bar: 50 µm. Figure adapted from Marques et al. 2020.

Swimming experiments performed with ATR-supplemented GOA14 animals at an intensity of 0.3mW/mm² demonstrated a significant reduction in thrashes in the exposure phase from and in the recovery phase compared to the pre-stimulus period. However, this also occurred in the control group and during the 0.8mW/mm² assays (*Figure 61* A and C). Yet, the control group GOA14 was the only one to exhibit an increase in thrashing rate after exposure was stopped, but only at lower photostimulation levels. This effect was reversed under strong stimulation. A likely explanation could be the exceeding of a threshold value that generally leads to a photophobic response in GOA14 animals (Edwards et al. 2008). The data presented here do not reveal a clear trend, except for the fact that animals supplemented with ATR further decrease in swimming cycles during the recovery phase. It would have been expected that the integration of CatChUP::EYFP::CRP-1 into all expressible isoforms would have had an effect here first. This was based on the fact that both BWMs and neurons are affected by the expression of the transgenic RyR (Marques et al. 2020), and thus a possible Ca^{2+} efflux at multiple targets (BWMs and neurons, also in the pharynx, but this would not lead to changed swimming behaviour) could trigger an effect leading to alterations in swimming behaviour.
However, it is particularly clear that double-integrated animals of GOA14, in contrast to single-integrated GOA01, exhibited a drastically reduced swimming frequency of a maximum of 5bbpm (*Figure 61*). These would lead to the conclusion that if the tool worked as a light-activated channel, it would delete the *unc-68* function, rendering it useless. Although highly speculative, these severely reduced thrashes could also be related to naturally occurring mutations/integrations that weaken the normal subunit-subunit interactions and thus alter the stability of the RyR channel (Zhu et al. 2013).

In addition to the swimming assays, contraction assays were also performed. ATR supplemented GOA14 animals did not contract, except for reversals at 0.8mW/mm² immediately after the start of photostimulation. Non-supplemented animals, on the other hand, exhibit elongation at low and high exposure (*Figure 62* A and B). Considering all the results of GOA14, there is no clear evidence of successful expression, folding and assembly of the optoUNC-68. Neither could fluorescence be clearly detected, nor do the data of the swimming and contraction assays indicate that light stimulation led to successful or sufficient Ca^{2+} release at the SR/ER membrane.

Properly performed swimming and contraction assays were demonstrated by the control groups ZX1827, wild-type and *lite-1* (*Figure 63* to *Figure 68*). In line with this, these animals also demonstrated a corresponding contraction during photostimulation when fed ATR (*Figure 68*).

4.2.5. The LOV2 domain as an optical trigger of the UNC-68 RyR

To investigate whether the release of Ca^{2+} from the SR/ER could be managed by direct manipulation of a modified intrinsic UNC-68, as a model also for mammalian RyR2, the LOV2 domain was integrated at strategic locations. These were preferably situated between alpha helices or two β-sheets to provoke maximal change in the protein structure upon light stimulation of LOV2. To avoid undesired impacts on the scaffold and steric flexibility of RyR, only the minimal fragment of the LOV2 domain (L404-L546), retaining functionality, was integrated by the CRISPR/Cas9 method. Both a fluorophore and a linker were also omitted. The LOV2 domain does not require any cofactor to respond to light (Herrou and Crosson 2011; Takayama et al. 2011; Halavaty and Moffat 2007; Zayner et al. 2012; Yao et al. 2008), unlike channelrhodopsin, which requires ATR. This can be either an advantage or a disadvantage for the experimental procedure and the rearing of the animals. The disadvantage is that the animals must be raised and cared for in complete darkness to avoid unintended effects on behaviour and development. This also complicates the experimental procedure, as the animals have to be prepared for the measurements in complete darkness and the light required for the assays also has to be reduced to a minimum. This is the only way to avoid "pre-activation" of LOV2. The key advantage of LOV2 is its high sensitivity and compactness, which makes integration into such a large and complex tetramer as RyR possible in the first place, with minimal disruption to the scaffold but maximum effect through photostimulation (Zayner et al. 2012; Dagliyan et al. 2016).
By integrating the LOV2 domain into the *unc-68* locus downstream of both exons 1.1 and 1.2, the problem that occurred with the integration of CatChUP::EYFP::CRP-1 should be avoided. LOV2 should be expressed in this way by every possible isoform of *unc-68*. This includes expression in all muscle tissues, such as pharyngeal, vulval and body wall muscle cells, and also in neurons (Marques et al. 2020).
The integration of LOV2 into RyR resulted in the strains GOA03, GOA04, GOA05 and GOA11, with GOA03 additionally being crossed in *lite-1* background. When creating strain GOA11, a balancer had to be used because the insertion at this position could not be homozygoused (see 3.9.2. Potential light-evoked effects on swimming locomotion were examined in *unc-68*::LOV2 inserted strains). The data collected here can therefore not be compared with the other strains.

Strain lite-1 GOA03 presented a largely normal basal thrashing rate, in comparison to *lite-1*, with an increase to 86% of the wild-type (*Figure 87*). Since the *unc-68* locus and the *lite-1* mutation are not related and are located on different chromosomes, this is difficult to comprehend. A functional interaction between the two, which could explain this finding, has also not been observed to date. An alternative suggestion would be that LOV2 integration has an enhancing effect on UNC-68 function, but since an inverse response occurred in the GOA03 strain, this does not allow any reasonable conclusion to be drawn from the results. In total, swimming assays performed with these strains revealed significantly lower thrashing rate of strains GOA03, 04 and 05 at an intensity of 0.3 mW/mm² compared to wild-type animals. On the one hand, this indicates mainly disruptive effects on the RyR function, but also shows that the complete functionality has not been destroyed. UNC-68 deletion mutants, in comparison, only thrashed with ~11bbpm in swimming assays. Also, the fact that strain lite-1 GOA03 responded with reduced swimming cycles to photostimulation in the assays, which was also observed in *lite-1* animals in the control group, does not suggest specific light-induced effects in UNC-68.

An interesting aspect is the behaviour of GOA4 at 0.8mW/mm², which has its integrated LOV2 localised in the "head region" of RyR and thus in the cytosol. In contrast to the other strains with a wild-type background, these animals display a significant reduction in swimming cycles during the first phase of stimulation. These animals, in contrast to other strains in the wild-type background, display a

significant reduction in swimming cycles compared to wild-type animals during the first period of stimulation. Since the pH of SR/ER and Cytsol is ~7.0-7.4 (Madshus 1988), this should not affect the functionality of the LOV2 domain. Furthermore, it could be assumed that the various tissues such as BWMs and pharyngeal muscles have a different pH than neurons and thus exert an influence on LOV2. However, since neurons also have a pH of ~7.35 (Ruffin et al. 2014), this can also be ruled out. Finally, it remains to be speculated that the "head" of RyR has a stronger influence on the pore function than is the case with the integration sites of the other strains 02, 03 and 05. Nevertheless, this cannot be confirmed based on the available data.
Finally, there is a very strong photostimulation with 1.1mW/mm² (*Figure 91*) and an exposure over 10 minutes with very weak stimulation (0.02mW/mm², *Figure 92*). When stimulated very strongly, the same effect occurred in the measured strains GOA04 and 05 as in wild-type animals. A light avoidance response is therefore much more likely and stronger than any other effect triggered by an activated LOV2 (Edwards et al. 2008). Nevertheless, very weak stimulation with 0.02mW/mm² for 10 minutes also had no significant effect in GOA03 animals, compared to wild-type. This is probably due to the fact that LOV2 has not been activated here.

The results of the contraction assays with an intensity of both 0.3 and 0.8mW/mm², demonstrated that no change in body length can be detected in any strain compared to wild-type. The only exception is strain GOA04. These animals reveal a significant elongation of the body by 0.64% during the time interval 40-70s of photostimulation with 0.3mW/mm² (*Figure 89*). If this test was repeated with an intensity of 0.8mW/mm² (*Figure 90*), this effect no longer occurred. Unfortunately, this observation cannot be matched with the results of the swimming assays, as a significant effect only occurred at 0.8mW/mm² (compared to wild-type). It can be assumed that for the strain GO04 the 0.3mW/mm² light pulse, was already sufficient to trigger a conformational change of LOV2. However, the threshold that triggers reversals and a light avoidance response was possibly already exceeded at a stimulation of 0.8mW/mm² (Edwards et al. 2008). This also appeared in wild-type animals (*Figure 94* A, C, D, E) but not in the *lite-1* control (*Figure 94* B). Here, in further tests it could be tried to optimise photostimulation to a sufficient level to provoke effects but not to induce light avoidance. This can clarify whether the LOV2 domain has been integrated at a sensitive site of RyR.

The only strain that demonstrates a light-induced effect at 0.3 and 0.8 mW/mm² is lite-1 GOA03. It should be noted that a significant reduction in thrashes during photostimulation also occurs in control strain *lite-1*. This depends on the intensity, as can be seen in *Figure 87* and *Figure 89*. After stimulation, no clear tendency can be proven, since at 0.3 mW/mm² a further reduction of the thrashes takes place, whereas at 0.8 mW/mm² a clear increase is visible. The strain lite-1 GOA03 thus shows a clear light-provoked effect on its own, while the control group is not consistent with regard to the recovery phase after the stimulus. Overall, more facts suggest that a successful light-induced reduction of thrashes could be induced here by LOV2 integration, followed by a reversible increase/overcompensation of thrashes.

Looking at the results of the LOV2-integrated strains, one could speculate that the location of the integration of the LOV2 domain in RyR played a role here. Based on the data collected here, however, it is not possible to prove whether the integration of LOV2 in the "head region" of RyR (GOA04) provokes a clearer effect than integration in the "pore region" (GOA03 and 05).

It should be added that there is yet no suitable homology model of UNC-68 based on the RyR2 structure. This would have been very helpful when selecting the insertion sites, that were mainly based on the RyR2 model. Even small changes in the amino acid sequence play a decisive role here. Even small changes in the amino acid sequence play a crucial role here, as the LOV2 domain could be integrated in the middle of a β-sheet or α-helix, which would cause an impairment of the tertiary

structure. A screening approach would require the creation of a separate strain for each new amino acid position with the help of CRISPR, which would lead to enormous effort and costs.

4.2.6. Influence of optoUNC-68 on pharynx pumping

To analyse CPVT-like arrhythmias in humans that are evoked by physiological and genetic conditions, the pharynx of the model organism *C. elegans* can be analysed. Therefore the green light gated ChR variant C1V1-ETET was integrated to pace the pharynx by green light (Erbguth et al. 2012). Additionally, optoUNC-68 (GOA14) which should be activated by blue light should provoke arrythmias, while green light pacing is running. Therefore, both strains were crossed.

4.2.6.1. The effect of serotonin induced pharynx pumping in GOA01

By creating optoUNC-68, the strain GOA01 should express this not only in neurons and body wall muscles, but everywhere the RyR is naturally expressed, including the pharynx. To investigate an effect of optoUNC-68 in the pharynx, pharyngeal pumping was measured with the addition of ATR, but also with the addition of serotonin. The pumping assays performed with an intensity of 1.4mW/mm² 470nm at 1Hz showed that only ppm and thus frequency were significantly reduced (*Figure 108*). Unfortunately, this indicates a light-related influence on the animals, as it can also be seen in wild-type animals (*Figure 115*). Stimulation with 430nm, which was carried out to cover as completely as possible the spectrum causing CatChUP activation, did not lead to conclusive results. This was true for both wild-type and *lite-1 (ce314)* background animals. In a best-case scenario with the use of serotonin, these assays would have detected significantly more irregular pumping during stimulation and possibly even interruption in the event of strong effects, in case of a dysfunctional optoUNC-68. Without serotonin, though, no change at all could be observed (*Figure 109*). Since these results unfortunately correspond to those in 3.5. Targeting a Ca^{2+} conductive ChR2 variant to the ER using transmembrane domains of the *C. elegans* UNC-68 ryanodine receptor, whereby neither effects on the swimming ability nor on the body length of the animals could be clearly demonstrated, it must be assumed here and altogether that the expression of the N-terminally to exon 1.1 linked CatChUP::EYFP::CRP-1 RyR, either did not take place at all or in too low levels (Marques et al. 2020).

4.2.6.2. The effect of serotonin induced pharynx pumping in GOA14 C1V1

One of the aims of this work was to create a light-triggered paceable tool (similar to Fischer 2015 and Schüler et al. 2016). For this purpose, strain GOA14 was crossed with a transgenic strain expressing C1V1 ETET in the pharynx. In these animals (GOA14 C1V1), in theory, both optoUNC-68 with 470nm at the SR/ER and C1V1 ET/ET by 570nm at the cell membrane should be optically triggered (Figure 107). Following this, stimulation with e.g. 1Hz pulses of 590nm would be performed to activate C1V1 ET/ET. Illumination with 470 nm would then influence RyR and thus cause a change in the regular pumping frequency. Exposure to 430nm (Figure 111 C) at 0.71mW/mm² resulted in a significant prolongation of the mean pump duration, albeit only slightly. This is unfortunately not supported by either the frequency or the ipi, which is why the relevance is considerably lower. Also, at 470nm, as in wild-type animals, there was no response to stimulation with 1Hz under the influence of serotonin. A subsequent assay in which 1.4mW/mm² was applied under continuous illumination had no effect on GOA14 C1V1 (Fig. 113), but wild-type animals significantly reduced their pumps (Figure 115).
Further tests with GOA14 C1V1 under the conditions 60s 4Hz 590nm 1.4mW/mm² combined with 1Hz 470nm 1.4mW/mm² resulted in no evaluable data. The data presented in *Figure 116*, which was measured with ZX1662 showed for both 590nm and 470nm at 1Hz and 4Hz pacing of the pharynx.

Overall, it was very difficult to record data in which the worms were correctly mounted for measurement and pumped reliably without serotonin supplementation. Therefore, it must be said that an increase in the n-number would be necessary to be able to make reliable statements. Based on the data available here, it cannot be assumed, however, that GOA14 C1V1 responds sensitively to photostimulation. Unfortunately, this did not confirm that the double system of optoUNC-68 and C1V1 can trigger a paced and at the same time arrythmia-producing effect through light.

4.3. SERCA – manipulating the Ca^{2+} uptake into the SR/ER

SERCA is localised on the SR/ER membrane and it is the Ca^{2+} translocator that quantitatively transports most Ca^{2+} ions into the SR. This made it an ideal candidate to create a modified version that affects the reuptake of Ca^{2+} from the cytosol into the SR under blue light activation.
The light-controlled inhibition of SERCA should induce a noticeable change in muscle tone and thus pharyngeal pumping and/or swimming behaviour. This would be caused by an incoming action potential from an adjacent cell that opens voltage-gated Ca^{2+} channels, enabling Calcium to enter the cells and provoke CICR via the RyR. This local Ca^{2+} release forms a Ca^{2+} spark that adds to other sparks to initiate a Ca^{2+} signal by binding calcium to troponin I in the contractile unit of the muscle. Troponin I, a protein building block of the actin filament, is capable of binding four Ca^{2+} ions. When it is fully occupied by Ca^{2+} ions, two are bound with high affinity of 10^{-7}mol/l and two with low affinity of 10^{-5}mol/l, wherein the low affinity binding triggers muscle contraction (Johnson et al. 1979; Johnson et al. 1994; Schober et al. 2012). Once troponin I, the subunit that inhibits the Mg^{2+}-activated ATPase of actomyosin, changes its conformation, myosin can bind to the actin filament (Herzberg et al. 1987). Upon Ca^{2+} activation, myosin will convert ATP to ADP and Pi, catalysed by Mg^{2+}, and cause the snap off of the myosin head. By that, the myosin filaments will slide along the actin filament, resulting in a muscle contraction. Once new ATP has bound to myosin, the cycle can start again. As soon as the Ca^{2+} ion concentration in the cytosol falls below 10^{-5}mol/l, troponin I again blocks the binding of myosin, thereby allowing the detachment of the myosin head from the actin filament, which leads to relaxation (Block et al. 1988; Klinke et al. 2010; Behrmann et al. 2012; Sweeney and Houdusse 2010). This Ca^{2+} drop is mainly caused by the SERCA, and other Ca^{2+} transporters, which is responsible for the reuptake of Ca^{2+} into the SR. Bypassing the Ca^{2+} reuptake by open RyRs, leads to contraction of all myosin heads as long as there is ATP available. While Ca^{2+} is bound to troponin I, relaxation is not possible due to the fact that myosin heads will recontract, even if single heads are unbound to actin temporarily. Hence, a contraction of body length should be the outcome of a short-circuited Ca^{2+} reuptake into the SR, as long as RyRs are open. A possible relaxation caused by the simple lack of ATP in the cell would only result in a rigor mortis like contraction.

The importance of SERCA is also demonstrated by the fact that manipulation by CRISPR/CAS9 led to lethality in two strains (GOA07 and GOA09). In these, the insertion of the LOV2 domain probably led to the SERCA function being restricted or even completely destroyed to such an extent that the animals did not survive.

As can be seen in *Figure 103* and 105and 122, the data for both strains GOA06 and GOA08 reveal a significant contraction of body length, commencing at the earliest after 25s of strong photostimulation (0.8mW/mm²).

Swimming and contraction experiments were performed with strains GOA06 and GOA08, in which the LOV2 domain was integrated at different sites of the SERCA (see 3.10. Modulation of the SERCA pump by the light-activated LOV2 domain As can be seen in *Figure 96* and *Figure 97*, swimming behaviour was not affected by 0.3mW/mm² photostimulation, except for the *lite-1* background strains. Looking at strain GOA08 and comparing no stimulation and the first time interval while photostimulation of 0.8mW/mm² was applied, it is evident that there is a significant decrease in thrashes in the first time-interval of stimulation compared to no stimulation (*Figure 98*). This decrease is also significant compared to the wild-type animals (*Figure 99*). However, all strains present an increase in thrashing rate after photostimulation. Nevertheless, during the application of 0. 8mW/mm², the *lite-1* control is also significant, which leaves the result of lite-1 GOA08 inconclusive. It can be assumed that a non-significant reduction of bbpm in the second time frame of the 0.3mW/mm² stimulation is directly dependent on the photostimulus, but the relevance of this finding is diminished by the fact that the wild-type animals also reduce thrashes, albeit not as pronounced. For strain GOA08, it can be concluded that its integrated LOV2 domain has no reliable effect on swimming behaviour at low stimulation (0.3mW/mm²), but at 0.8mW/mm² a drop, in contrast to wild-type animals could indicate a functional LOV2 domain blockade of SERCA upon photostimulation.

Strain GOA06 did only respond to stimulation with 1.1mW/mm². For this stimulus, it should be noted that due to the fact that GOA06 and also wild-type animals significantly reduce the thrashing rate in the first time-interval of stimulation (*Figure 100*), an effect in GOA06 animals of blue light on complex movement as swimming cannot be assumed. The same applies to low-dose long-term photostimulation, as depicted in *Figure 101*.

A different picture emerges, however, when looking at the body length and the influence of photostimulation. A significant change in body length can be observed in both strains in the wild-type background, as can be seen in *Figure 102*, 103, 104 and 105. Animals of strain GOA08 reveal a contraction of body length at the intensities 0.3 and 0.8mW/mm². This is particularly pronounced at 0.8mW/mm² moments after the onset of photostimulation, but only becomes significant in the final time intervals, as can be clearly seen in *Figure 102*, 103, 104 and 105. Elongation as a contrary reaction at 0.3 and 0.8mW/mm², as is visible for the strain lite-1 GOA08, does not display any significance. In summary, the results of the contraction and swimming experiments of strain lite-1 GOA08 do not conclusively prove that a light-stimulated LOV2 domain in SERCA provokes an effect on swimming behaviour or mere length of body wall muscles.

Animals of GOA06, on the other hand, demonstrated contraction of up to ~2% as long as the stimulus was applied, especially in the contraction assays at 0.8mW/mm² (Figure 104 A and Figure 105 A). This was followed in accordance by a slight elongation in the recovery phase without stimulus. A significant elongation of the GOA03 animals during the 0.3mW/mm² stimulus (*Figure 102* A and *Figure 105* A) contradicts the result of the 0.8mW/mm² assay.

Here one could speculate that by inhibiting SERCA, less Ca^{2+} is pumped back into the SR/ER, which runs empty since all Ca^{2+} exporters (e.g. RyR, IP_3R) are still working. Since Ca^{2+} can also leave the cytosol via the NCX, the cytosol and the SR/ER are drained over time, leading to a decrease of the excitability of the cells. This could therefore also reduce the activity of the neurons and muscle cells, which would lead to a relaxation and by that elongation of the BWMs and the worm. However, it is unknown whether the effects of SERCA inhibition are first and or mainly noticeable in neurons or muscles.

Also the question is raised of whether 0.3mW/mm² was already sufficient to trigger a LOV2 conformational change; the high intensity of blue light that is required to activate the LOV2 (Pudasaini et al. 2015), would suggest 0.3mW/mm² was not enough to lead to full conformational change of LOV2. Another important aspect is that the LOV2 domain is now located in a somewhat transparent worm,

which complicates the determination of the sensitivity of the LOV2. The contraction of GOA06 and GOA08 at 0.8mW/mm², which becomes stronger with time and is most pronounced in late time intervals, could also be attributed to an accumulation of Ca^{2+} in the cytosol. This could be triggered by a conformational change of the LOV2 domain and an associated impairment of SERCA activity. As a result, SERCA would not be able to translocate sufficient Ca^{2+} back into the SR, leading to prolonged contraction, as outlined above. Based on this, we can assume there is a light-triggered effect of the LOV2 domain on SERCA in GOA06 and GOA08. This effect is not manifested in more complex movement patterns such as three-dimensional swimming cycles, but is sufficiently strong in two-dimensional crawling movements. Further experiments with enhanced photostimulation could provide clarity here and shed more light on the question of whether sufficient blue light stimulation has taken place. In addition, with more recent findings on the tertiary structure of SERCA, a new attempt can be made to integrate the LOV2 domain at more suitable, more sensitive sites. In this way, an even stronger effect could be provoked upon photostimulation to possibly achieve precise spatiotemporal control of SERCA.

5. Outlook

A project like this is not a sprint but a marathon and it takes long time investments and a lot of mistakes to make it work. Nonetheless its final aim is a unique opportunity to control the heart optogenetically and thereby cure or at least ease the pain of people suffering heart arrythmias or a higher heart attack risk. The optical control of a muscle in a transparent organism like *C. elegans*, or a heart beat is only one step towards an optical cardiac pacemaker, replacing electric currents by less invasive, and better controllable light pulses. In addition to that, a system is needed that can distribute spatiotemporal cardiac stimulation across the entire epicardium. Such a system could be the multifunctional integumentary membrane shown by Xu et al. 2014. In which light emitting diodes are integrated in a glove like membrane surrounding the whole heart, and thereby giving the possibility of precise spatiotemporal light application.

5.1. Manipulation of Ca^{2+} flux by various optogenetic tools

In this work, different ChR variants were considered as possible candidates for manipulating Ca^{2+} flux. Unfortunately, with the exception of two variants, none of the candidates could generate promising results that could significantly affect Ca^{2+} flux in *C. elegans* at the SR/ER membrane. In some cases, the failure of individual tools such as $ChRGR_{ER}$ can probably be attributed to, for example, insufficient sequence homology between mammalian and *C. elegans* RyR. In this case, a retention sequence of *M. musculus* should lead to retention of the ChR1 and ChR2 chimera $ChRGR_{ER}$ in the SR/ER membrane. Adapting this chimera and the retention sequence specifically to *C. elegans* would likely be promising in follow-up experiments.

One of the best working experiments here was the ChR-XXM, an optimised channelrhodopsin variant with increased Ca^{2+} conductivity. In this case, this could be a good substitute for the CatChUP used in RyR, as the expression could be reliably and strongly detected, especially in the muscle cells of the body wall. It could therefore be part of a tool that can be used to manipulate Ca^{2+} flux at the SR/ER membrane. In the following experiments, CatChUP could be replaced by ChR-XXM to achieve better results in *C. elegans* by photostimulation due to increased Ca^{2+} conductance and better expression.

The inherent SR membrane retention motif of UNC-68 TM5+6 also appears to be a promising candidate for the development of an optical tool for the same reason, namely homology. In further attempts, a ChR variant with maximum Ca^{2+} conductivity, such as ChR-XXM, could be combined with UNC-68 TM5+6 to significantly increase efficacy. In this way, precise localisation of the construct at the SR/ER membrane in the muscle cells could be ensured and a significant effect achieved by light stimulation.

5.2. Manipulating the Rynodine receptor 2

Mixed results can be summarised here for manipulation of Ca^{2+} efflux from the SR/ER via the ryanodine receptor. On the one hand, no positive results could be achieved with the CatChUP construct and extrinsic hRyR in both its natural and truncated form. This can probably be attributed to too low sequence homology between CeRyR and hRyR. This was also confirmed with the variants of optoUNC-68 integrated in LOV2. When CRISPR/Cas9 was used to connect CatChUP to the natural RyR of *C. elegans*, the problem of receptor homology could be solved. However, the N-terminal coupling of CatChUP::EYFP::CRP-1 to RyR, neither upstream of exon 1.1 nor exon 1.2, gave meaningful results. Similar results were obtained for the LOV2 strains integrated into RyR using CRISPR. Here, future experiments based on new insights into the spatial structure would have to search for promising insertion sites to maximise the conformational change and influence on the pore region of RyR so that light stimulation would induce a significant effect in the animal. At the same time, the handling of pharynx pumping would also be optimised.

In particular, in GOA14 C1V1 and the underlying principle of a dual integration of manipulable RyR and C1V1 to be stimulated simultaneously with different wavelengths, and thus both, paced and arrhythmicity, would benefit from improved optoUNC-68. If we want to focus specifically on muscle cells, we need to ensure in future experiments that the different isoforms and their site of expression (e.g. in neurons or muscle cells) and time of expression (L1-L4 or adult) also play a huge role in integration by CRISPR. Therefore, isoforms should be chosen that only express in muscle cells to avoid the influence of neuronal stimulation. In this way, it would be easier to obtain and evaluate clear results.

5.3. Manipulation of the SERCA

When LOV2 was integrated into SERCA with CRISPR, relatively positive results were obtained in 2 out of 4 strains. This especially manifested itself in simple contractions of the body wall muscles. As with the insertion sites for RyR, significant improvement could be achieved in follow-up experiments by using the recent studies on the three-dimensional structure of SERCA to select new insertion sites that maximise the impact of the conformational change of LOV2 upon photostimulation on the SERCA scaffold. Multiple integration of LOV2 into SERCA is also a possible approach to efficiently disturb SERCA in the translocation of Ca^{2+} ions by light stimulation.

Considering the positive results of the integrated strains GOA06 and GOA08, it can be assumed that in this work the development of a tool for optogenetic manipulation of intracellular Ca^{2+} uptake from the SR/ER was partly successful. However, this achievement is only a first step on the way to a spatially and temporally precise light-controlled tool. It could be demonstrated that the basic idea works and that the translocation of Ca^{2+} ions through SERCA into the SR/ER can be suppressed or at least restricted in a light-controlled manner. However, taking all the information gathered here together, it might be necessary to focus not only on one part of the SR/ER-cytosol Ca^{2+}-cycle, but on both at once. Because either SERCA compensates for open RyR channels or vice versa. Further experiments should include the approach of combining a CRISPR manipulation of the SERCA and the RyR at the same time in the same animal.

Publication bibliography

A. Chu; M. Díaz-Muñoz; M. Hawkes; K. Brush; S. Hamilton (1990): Ryanodine as a probe for the functional state of the skeletal muscle sarcoplasmic reticulum calcium release channel. In *Molecular Pharmacology*. Available online at https://www.semanticscholar.org/paper/78f4c3a8904afdf63a0ada0420eeec024c05d9ad.

A.H.J. Burr; A. Forest Robinson (2004): Locomotion behaviour. In *Nematode Behavior (ed. A. L. Bilgrami and R. Gaugler), pp. 25-62. Oxford: CAB International.*

Aaij, C.; Borst, P. (1972): The gel electrophoresis of DNA. In *Biochimica et biophysica acta* 269 (2), pp. 192–200. DOI: 10.1016/0005-2787(72)90426-1.

Ahringer, Julie (2006): Reverse genetics: WormBook.

Akbar, S.; Gaidenko, T. A.; Kang, C. M.; O'Reilly, M.; Devine, K. M.; Price, C. W. (2001): New family of regulators in the environmental signaling pathway which activates the general stress transcription factor sigma(B) of Bacillus subtilis. In *Journal of Bacteriology* 183 (4), pp. 1329–1338. DOI: 10.1128/JB.183.4.1329-1338.2001.

Akerström, Göran; Hellman, Per; Hessman, Ola; Segersten, Ulrika; Westin, Gunnar (2005): Parathyroid glands in calcium regulation and human disease. In *Annals of the New York Academy of Sciences* 1040, pp. 53–58. DOI: 10.1196/annals.1327.005.

Albertson, D. G.; Thomson, J. N. (1976): The pharynx of Caenorhabditis elegans. In *Philosophical transactions of the Royal Society of London. Series B, Biological sciences* 275 (938), pp. 299–325. DOI: 10.1098/RSTB.1976.0085.

Altun; Hall (2009a): Alimentary system, intestine. WormAtlas.

Altun, Z. F.; Hall, D. H. (2009b): Handbook - Muscle System Introduction. With assistance of Altun, Z.F. and Hall, D.H. 2009. Muscle system, introduction. In WormAtlas. Edited by Wormatlas. Available online at https://www.wormatlas.org/hermaphrodite/muscleintro/mainframe.htm#Jospin2002, updated on 1/31/2018, checked on 3/1/2021.

Altun, Z. F.; Hall, D. H. (2009c): Hermaphrodite - Muscle System - Somatic Muscle. With assistance of Z. F. Altun, D. H. Hall. Cold Spring Harbor Laboratory Press. WormAtlas. Available online at https://www.wormatlas.org/hermaphrodite/musclesomatic/MusSomaticframeset.html, updated on 3/11/2016, checked on 2/17/2021.

Andersson, Julia; Hauser, Karin; Karjalainen, Eeva-Liisa; Barth, Andreas (2008): Protonation and hydrogen bonding of Ca2+ site residues in the E2P phosphoenzyme intermediate of sarcoplasmic reticulum Ca2+-ATPase studied by a combination of infrared spectroscopy and electrostatic calculations. In *Biophysical Journal* 94 (2), pp. 600–611. DOI: 10.1529/biophysj.107.114033.

Ardiel, Evan L.; Rankin, Catharine H. (2010): An elegant mind: learning and memory in Caenorhabditis elegans. In *Learning & Memory* 17 (4), pp. 191–201. DOI: 10.1101/lm.960510.

Arenkiel, Benjamin R.; Peca, Joao; Davison, Ian G.; Feliciano, Catia; Deisseroth, Karl; Augustine, George J. et al. (2007): In vivo light-induced activation of neural circuitry in transgenic mice expressing channelrhodopsin-2. In *Neuron* 54 (2), pp. 205–218. DOI: 10.1016/j.neuron.2007.03.005.

Asano, Toshifumi; Igarashi, Hiroyuki; Ishizuka, Toru; Yawo, Hiromu (2018): Organelle Optogenetics: Direct Manipulation of Intracellular Ca2+ Dynamics by Light. In *Frontiers in neuroscience* 12, p. 561. DOI: 10.3389/fnins.2018.00561.

Asano, Toshifumi; Ishizuka, Toru; Morishima, Keisuke; Yawo, Hiromu (2015): Optogenetic induction of contractile ability in immature C2C12 myotubes. In *Scientific reports* 5, p. 8317. DOI: 10.1038/srep08317.

Avery, L.; Horvitz, H. R. (1990): Effects of starvation and neuroactive drugs on feeding in Caenorhabditis elegans. In *The Journal of experimental zoology* 253 (3), pp. 263–270. DOI: 10.1002/jez.1402530305.

Avery, Leon; Horvitz, H.Robert (1987): A cell that dies during wild-type C. elegans development can function as a neuron in a ced-3 mutant. In *Cell* 51 (6), pp. 1071–1078. DOI: 10.1016/0092-8674(87)90593-9.

Avery, Leon; Horvitzt, H.Robert (1989): Pharyngeal pumping continues after laser killing of the pharyngeal nervous system of C. elegans. In *Neuron* 3 (4), pp. 473–485. DOI: 10.1016/0896-6273(89)90206-7.

Avery, Leon; You, Young-jai (2012): C. elegans feeding. In *Wormbook*, pp. 1–23. DOI: 10.1895/wormbook.1.150.1.

Avila-Pérez, Marcela; Hellingwerf, Klaas J.; Kort, Remco (2006): Blue light activates the sigmaB-dependent stress response of Bacillus subtilis via YtvA. In *Journal of Bacteriology* 188 (17), pp. 6411–6414. DOI: 10.1128/JB.00716-06.

Badhwar, Rahul; Bagler, Ganesh (2015): Control of Neuronal Network in Caenorhabditis elegans. In *PLoS ONE* 10 (9), e0139204. DOI: 10.1371/journal.pone.0139204.

Bai, Xiao-chen; Yan, Zhen; Wu, Jianping; Li, Zhangqiang; Yan, Nieng (2016): The Central domain of RyR1 is the transducer for long-range allosteric gating of channel opening. In *Cell research* 26 (9), pp. 995–1006. DOI: 10.1038/cr.2016.89.

Ballario, P.; Talora, C.; Galli, D.; Linden, H.; Macino, G. (1998): Roles in dimerization and blue light photoresponse of the PAS and LOV domains of Neurospora crassa white collar proteins. In *Molecular Microbiology* 29 (3), pp. 719–729. DOI: 10.1046/j.1365-2958.1998.00955.x.

Balshaw, D.; Gao, L.; Meissner, G. (1999): Luminal loop of the ryanodine receptor: a pore-forming segment? In *Proceedings of the National Academy of Sciences of the United States of America* 96 (7), pp. 3345–3347. DOI: 10.1073/PNAS.96.7.3345.

Beard, N. A.; Laver, D. R.; Dulhunty, A. F. (2004): Calsequestrin and the calcium release channel of skeletal and cardiac muscle. In *Progress in Biophysics and Molecular Biology* 85 (1), pp. 33–69. DOI: 10.1016/j.pbiomolbio.2003.07.001.

Behrmann, Elmar; Müller, Mirco; Penczek, Pawel A.; Mannherz, Hans Georg; Manstein, Dietmar J.; Raunser, Stefan (2012): Structure of the rigor actin-tropomyosin-myosin complex. In *Cell* 150 (2), pp. 327–338. DOI: 10.1016/j.cell.2012.05.037.

Bellinger, Andrew M.; Reiken, Steven; Carlson, Christian; Mongillo, Marco; Liu, Xiaoping; Rothman, Lisa et al. (2009): Hypernitrosylated ryanodine receptor calcium release channels are leaky in dystrophic muscle. In *Nature medicine* 15 (3), pp. 325–330. DOI: 10.1038/nm.1916.

Bellinger, Andrew M.; Reiken, Steven; Dura, Miroslav; Murphy, Peter W.; Deng, Shi-Xian; Landry, Donald W. et al. (2008): Remodeling of ryanodine receptor complex causes "leaky" channels: a molecular mechanism for decreased exercise capacity. In *PNAS* 105 (6), pp. 2198–2202. DOI: 10.1073/pnas.0711074105.

Benchling (2020): Cloud-Based Informatics Platform for Life Sciences R&D | Benchling. Available online at https://www.benchling.com/, updated on 12/7/2020, checked on 1/22/2021.

Bergs, Amelie; Schultheis, Christian; Fischer, Elisabeth; Tsunoda, Satoshi P.; Erbguth, Karen; Husson, Steven J. et al. (2018): Rhodopsin optogenetic toolbox v2.0 for light-sensitive excitation and inhibition in Caenorhabditis elegans. In *PLoS ONE* 13 (2), e0191802. DOI: 10.1371/journal.pone.0191802.

Berndt, André; Schoenenberger, Philipp; Mattis, Joanna; Tye, Kay M.; Deisseroth, Karl; Hegemann, Peter; Oertner, Thomas G. (2011): High-efficiency channelrhodopsins for fast neuronal stimulation at low light levels. In *PNAS* 108 (18), pp. 7595–7600. DOI: 10.1073/pnas.1017210108.

Bernstein, Scott A.; Morley, Gregory E. (2006): Gap junctions and propagation of the cardiac action potential. In *Advances in cardiology* 42, pp. 71–85. DOI: 10.1159/000092563.

Berridge, Michael J. (2009): Inositol trisphosphate and calcium signalling mechanisms. In *Biochimica et biophysica acta* 1793 (6), pp. 933–940. DOI: 10.1016/j.bbamcr.2008.10.005.

Bers, D. M. (2000): Calcium fluxes involved in control of cardiac myocyte contraction. In *Circulation research* 87 (4), pp. 275–281. DOI: 10.1161/01.res.87.4.275.

Beyeler, Anna; Eckhardt, Christine A.; Tye, Kay M. (2014): Chapter Twelve - Deciphering Memory Function with Optogenetics. In Zafar U. Khan, E. Chris Muly (Eds.): Progress in Molecular Biology and Translational Science : Molecular Basis of Memory, vol. 122: Academic Press, pp. 341–390. Available online at http://www.sciencedirect.com/science/article/pii/B978012420170500012X.

Bezprozvanny, I.; Watras, J.; Ehrlich, B. E. (1991): Bell-shaped calcium-response curves of Ins(1,4,5)P3- and calcium-gated channels from endoplasmic reticulum of cerebellum. In *Nature* 351 (6329), pp. 751–754. DOI: 10.1038/351751a0.

Bhat, M. B.; Zhao, J.; Takeshima, H.; Ma, J. (1997): Functional calcium release channel formed by the carboxyl-terminal portion of ryanodine receptor. In *Biophysical Journal* 73 (3), pp. 1329–1336.

Bhat, Manjunatha B.; Ma, Jianjie (2002): The transmembrane segment of ryanodine receptor contains an intracellular membrane retention signal for Ca(2+) release channel. In *The Journal of biological chemistry* 277 (10), pp. 8597–8601. DOI: 10.1074/jbc.M107609200.

Bhatla, Nikhil; Horvitz, H. Robert (2015): Light and hydrogen peroxide inhibit C. elegans Feeding through gustatory receptor orthologs and pharyngeal neurons. In *Neuron* 85 (4), pp. 804–818. DOI: 10.1016/j.neuron.2014.12.061.

Bi, Anding; Cui, Jinjuan; Ma, Yu-Ping; Olshevskaya, Elena; Pu, Mingliang; Dizhoor, Alexander M.; Pan, Zhuo-Hua (2006): Ectopic expression of a microbial-type rhodopsin restores visual responses in mice with photoreceptor degeneration. In *Neuron* 50 (1), pp. 23–33. DOI: 10.1016/j.neuron.2006.02.026.

Bidwell, Philip; Blackwell, Daniel J.; Hou, Zhanjia; Zima, Aleksey V.; Robia, Seth L. (2011): Phospholamban binds with differential affinity to calcium pump conformers. In *Journal of Biological Chemistry* 286 (40), pp. 35044–35050. DOI: 10.1074/jbc.M111.266759.

Block, B. A.; Imagawa, T.; Campbell, K. P.; Franzini-Armstrong, C. (1988): Structural evidence for direct interaction between the molecular components of the transverse tubule/sarcoplasmic reticulum junction in skeletal muscle. In *The Journal of Cell Biology* 107 (6 Pt 2), pp. 2587–2600. DOI: 10.1083/jcb.107.6.2587.

Block, Dena H. S.; Twumasi-Boateng, Kwame; Kang, Hae Sung; Carlisle, Jolie A.; Hanganu, Alexandru; Lai, Ty Yu-Jen; Shapira, Michael (2015): The Developmental Intestinal Regulator ELT-2 Controls p38-Dependent Immune Responses in Adult C. elegans. In *PLoS genetics* 11 (5), e1005265. DOI: 10.1371/journal.pgen.1005265.

Bootman, Martin D.; Berridge, Michael J. (1995): The elemental principles of calcium signaling. In *Cell* 83 (5), pp. 675–678. DOI: 10.1016/0092-8674(95)90179-5.

Boyden, Edward S. (2011): A history of optogenetics: the development of tools for controlling brain circuits with light. In *F1000 biology reports* 3, p. 11. DOI: 10.3410/B3-11.

Boyden, Edward S.; Zhang, Feng; Bamberg, Ernst; Nagel, Georg; Deisseroth, Karl (2005): Millisecond-timescale, genetically targeted optical control of neural activity. In *Nature neuroscience* 8 (9), pp. 1263–1268. DOI: 10.1038/nn1525.

Breimann, Laura; Preusser, Friedrich; Preibisch, Stephan (2019): Light-microscopy methods in C. elegans research. In *Current Opinion in Systems Biology* 13, pp. 82–92. DOI: 10.1016/j.coisb.2018.11.004.

Brenner, Sydney (2001): A life in science. As told to Lewis Wolpert ; edited interview with additional material. Edited by Errol C. Friedberg, Eleanor Lawrence. London: BioMed Central.

Briggs, Winslow R. (2007): The LOV domain: a chromophore module servicing multiple photoreceptors. In *Journal of Biomedical Science* 14 (4), pp. 499–504. DOI: 10.1007/s11373-007-9162-6.

Brillantes, Anne-Marie B.; Ondrias, Karol; Scott, Andrew; Kobrinsky, Evgeny; Ondriašová, Elena; Moschella, Maria C. et al. (1994): Stabilization of calcium release channel (ryanodine receptor) function by FK506-binding protein. In *Cell* 77 (4), pp. 513–523. DOI: 10.1016/0092-8674(94)90214-3.

Brini, Marisa; Calì, Tito; Ottolini, Denis; Carafoli, Ernesto (2014): Neuronal calcium signaling: function and dysfunction. In *Cellular and molecular life sciences : CMLS* 71 (15), pp. 2787–2814. DOI: 10.1007/s00018-013-1550-7.

Britzolaki, Aikaterini; Saurine, Joseph; Klocke, Benjamin; Pitychoutis, Pothitos M. (2020): A Role for SERCA Pumps in the Neurobiology of Neuropsychiatric and Neurodegenerative Disorders. In *Advances in experimental medicine and biology* 1131, pp. 131–161. DOI: 10.1007/978-3-030-12457-1_6.

Bronner, F. (2001): Extracellular and intracellular regulation of calcium homeostasis. In *TheScientificWorldJournal* 1, pp. 919–925. DOI: 10.1100/tsw.2001.489.

Brown, Leonid S. (2004): Fungal rhodopsins and opsin-related proteins: eukaryotic homologues of bacteriorhodopsin with unknown functions. In *Photochemical & photobiological sciences : Official journal of the European Photochemistry Association and the European Society for Photobiology* 3 (6), pp. 555–565. DOI: 10.1039/b315527g.

Bruckert, Eric; Parhofer, Klaus Georg; Gonzalez-Juanatey, Jose Ramon; Nordestgaard, Børge; Arca, Marcello; Giovas, Periklis; Ray, Kausik (2020): Proportion of High-Risk/Very High-Risk Patients in Europe with Low-Density Lipoprotein Cholesterol at Target According to European Guidelines: A Systematic Review. In *Advances in therapy* 37 (5), pp. 1724–1736. DOI: 10.1007/s12325-020-01285-2.

Bruegmann, Tobias; van Bremen, Tobias; Vogt, Christoph C.; Send, Thorsten; Fleischmann, Bernd K.; Sasse, Philipp (2015): Optogenetic control of contractile function in skeletal muscle. In *Nature Communications* 6, p. 7153. DOI: 10.1038/ncomms8153.

Bubeck, Felix; Hoffmann, Mareike D.; Harteveld, Zander; Aschenbrenner, Sabine; Bietz, Andreas; Waldhauer, Max C. et al. (2018): Engineered anti-CRISPR proteins for optogenetic control of CRISPR-Cas9. In *Nat Methods* 15 (11), pp. 924–927. DOI: 10.1038/s41592-018-0178-9.

Bublitz, Maike; Poulsen, Hanne; Morth, J. Preben; Nissen, Poul (2010): In and out of the cation pumps: P-type ATPase structure revisited. In *Current Opinion in Structural Biology* 20 (4), pp. 431–439. DOI: 10.1016/j.sbi.2010.06.007.

Cassada, Randall C.; Russell, Richard L. (1975): The dauerlarva, a post-embryonic developmental variant of the nematode Caenorhabditis elegans. In *Developmental Biology* 46 (2), pp. 326–342. DOI: 10.1016/0012-1606(75)90109-8.

Catterall, William A. (2011): Voltage-gated calcium channels. In *Cold Spring Harbor perspectives in biology* 3 (8), a003947. DOI: 10.1101/cshperspect.a003947.

Chasnov, J. R.; Chow, King L. (2002): Why are there males in the hermaphroditic species Caenorhabditis elegans? In *Genetics* 160 (3), pp. 983–994.

Chen; MacLennan DH. (1994): Identification of calmodulin-, Ca2þ-, and ruthenium red-binding domains in the Ca2þ release channel (ryanodine receptor) of rabbit skeletal muscle sarcoplasmic reticulum. In *J Biol Chem 269: 22698–22704*.

Chen, S. R.; Ebisawa, K.; Li, X.; Zhang, L. (1998): Molecular identification of the ryanodine receptor Ca2+ sensor. In *The Journal of biological chemistry* 273 (24), pp. 14675–14678. DOI: 10.1074/jbc.273.24.14675.

Chi, Ximin; Gong, Deshun; Ren, Kang; Zhou, Gewei; Huang, Gaoxingyu; Lei, Jianlin et al. (2019): Molecular basis for allosteric regulation of the type 2 ryanodine receptor channel gating by key modulators. In *PNAS* 116 (51), pp. 25575–25582. DOI: 10.1073/pnas.1914451116.

Cho, Jeong Hoon; Ko, Kyung Min; Singaruvelu, Gunasekaran; Lee, Wonhae; Kang, Gil Bu; Rho, Seong-Hwan et al. (2007): Functional importance of polymerization and localization of calsequestrin in C. elegans. In *Journal of Cell Science* 120 (Pt 9), pp. 1551–1558. DOI: 10.1242/jcs.001016.

Christie, J. M.; Reymond, P.; Powell, G. K.; Bernasconi, P.; Raibekas, A. A.; Liscum, E.; Briggs, W. R. (1998): Arabidopsis NPH1: a flavoprotein with the properties of a photoreceptor for phototropism. In *Science (New York, N.Y.)* 282 (5394), pp. 1698–1701. DOI: 10.1126/science.282.5394.1698.

Christie, J. M.; Salomon, M.; Nozue, K.; Wada, M.; Briggs, W. R. (1999): LOV (light, oxygen, or voltage) domains of the blue-light photoreceptor phototropin (nph1): binding sites for the chromophore flavin mononucleotide. In *Proceedings of the National Academy of Sciences of the United States of America* 96 (15), pp. 8779–8783. DOI: 10.1073/pnas.96.15.8779.

Clokey, George V.; Jacobson, Lewis A. (1986): The autofluorescent “lipofuscin granules” in the intestinal cells of Caenorhabditis elegans are secondary lysosomes. In *Mechanisms of Ageing and Development* 35 (1), pp. 79–94. DOI: 10.1016/0047-6374(86)90068-0.

Cook, S.J., Crouse, C.M., Yemini, E., Hall, D.H., Emmons, S.W., Hobert, O., 2020. The connectome of the Caenorhabditis elegans pharynx. J. Comp. Neurol. 528, 2767–2784. https://doi.org/10.1002/cne.24932

Coronado, R.; Morrissette, J.; Sukhareva, M.; Vaughan, D. M. (1994): Structure and function of ryanodine receptors. In *The American journal of physiology* 266 (6 Pt 1), C1485-504. DOI: 10.1152/ajpcell.1994.266.6.C1485.

Corsi, Ann K.; Wightman, Bruce; Chalfie, Martin (2015): A Transparent Window into Biology: A Primer on Caenorhabditis elegans. In *Genetics* 200 (2), pp. 387–407. DOI: 10.1534/genetics.115.176099.

Cox, Elisabeth A.; Hardin, Jeff (2004): Sticky worms: adhesion complexes in C. elegans. In *Journal of Cell Science* 117 (Pt 10), pp. 1885–1897. DOI: 10.1242/jcs.01176.

Croll, N. A. (1975): Indolealkylamines in the coordination of nematode behavioral activities. In *Canadian journal of zoology* 53 (7), pp. 894–903. DOI: 10.1139/z75-103.

Crosson, Sean; Moffat, Keith (2002): Photoexcited structure of a plant photoreceptor domain reveals a light-driven molecular switch. In *The Plant Cell* 14 (5), pp. 1067–1075. DOI: 10.1105/tpc.010475.

Crosson, Sean; Rajagopal, Sudarshan; Moffat, Keith (2003): The LOV domain family: photoresponsive signaling modules coupled to diverse output domains. In *Biochemistry* 42 (1), pp. 2–10. DOI: 10.1021/bi026978l.

D. Raizen; R. Lee; L. Avery (1995): Interacting genes required for pharyngeal excitation by motor neuron MC in Caenorhabditis elegans. In *Genetics*. Available online at https://www.semanticscholar.org/paper/8c6ed1c2a95fbd7e8a77d525afccd36e750bc5dd.

Dagliyan, Onur; Dokholyan, Nikolay V.; Hahn, Klaus M. (2019): Engineering proteins for allosteric control by light or ligands. In *Nature protocols* 14 (6), pp. 1863–1883. DOI: 10.1038/s41596-019-0165-3.

Dagliyan, Onur; Tarnawski, Miroslaw; Chu, Pei-Hsuan; Shirvanyants, David; Schlichting, Ilme; Dokholyan, Nikolay V.; Hahn, Klaus M. (2016): Engineering extrinsic disorder to control protein activity in living cells. In *Science (New York, N.Y.)* 354 (6318), pp. 1441–1444. DOI: 10.1126/science.aah3404.

Dahl, Russell (2017): A new target for Parkinson's disease: Small molecule SERCA activator CDN1163 ameliorates dyskinesia in 6-OHDA-lesioned rats. In *Bioorganic & medicinal chemistry* 25 (1), pp. 53–57. DOI: 10.1016/j.bmc.2016.10.008.

Damijonaitis, Arunas (2011): Modifikationen an Channelrhodopsin-2 für neue optogenetische Anwendungen in Caenorhabditis elegans.

Davis, M. W.; Fleischhauer, R.; Dent, J. A.; Joho, R. H.; Avery, L. (1999): A mutation in the C. elegans EXP-2 potassium channel that alters feeding behavior. In *Science (New York, N.Y.)* 286 (5449), pp. 2501–2504. DOI: 10.1126/science.286.5449.2501.

Deisseroth, Karl; Hegemann, Peter (2017): The form and function of channelrhodopsin. In *Science (New York, N.Y.)* 357 (6356). DOI: 10.1126/science.aan5544.

Dellis, Olivier; Dedos, Skarlatos G.; Tovey, Stephen C.; Taufiq-Ur-Rahman; Dubel, Stefan J.; Taylor, Colin W. (2006): Ca2+ entry through plasma membrane IP3 receptors. In *Science* 313 (5784), pp. 229–233. DOI: 10.1126/science.1125203.

Denborough, Michael (1998): Malignant hyperthermia. In *The Lancet* 352 (9134), pp. 1131–1136. DOI: 10.1016/S0140-6736(98)03078-5.

Des Georges, Amédée; Clarke, Oliver B.; Zalk, Ran; Yuan, Qi; Condon, Kendall J.; Grassucci, Robert A. et al. (2016): Structural Basis for Gating and Activation of RyR1. In *Cell* 167 (1), 145-157.e17. DOI: 10.1016/j.cell.2016.08.075.

Dickinson, Daniel J.; Pani, Ariel M.; Heppert, Jennifer K.; Higgins, Christopher D.; Goldstein, Bob (2015): Streamlined Genome Engineering with a Self-Excising Drug Selection Cassette. In *Genetics* 200 (4), pp. 1035–1049. DOI: 10.1534/genetics.115.178335.

Dimov, Ivan; Maduro, Morris F. (2019): The C. elegans intestine: organogenesis, digestion, and physiology. In *Cell & tissue research* 377 (3), pp. 383–396. DOI: 10.1007/s00441-019-03036-4.

Ding, Mei; Woo, Wei-Meng; Chisholm, Andrew D. (2004): The cytoskeleton and epidermal morphogenesis in C. elegans. In *Experimental Cell Research* 301 (1), pp. 84–90. DOI: 10.1016/j.yexcr.2004.08.017.

Donnelly, Jamie L.; Clark, Christopher M.; Leifer, Andrew M.; Pirri, Jennifer K.; Haburcak, Marian; Francis, Michael M. et al. (2013): Monoaminergic orchestration of motor programs in a complex C. elegans behavior. In *PLoS biology* 11 (4), e1001529. DOI: 10.1371/journal.pbio.1001529.

Douglass, Adam D.; Kraves, Sebastian; Deisseroth, Karl; Schier, Alexander F.; Engert, Florian (2008): Escape behavior elicited by single, channelrhodopsin-2-evoked spikes in zebrafish somatosensory neurons. In *Current biology : CB* 18 (15), pp. 1133–1137. DOI: 10.1016/j.cub.2008.06.077.

Duan, Xiaodong; Nagel, Georg; Gao, Shiqiang (2019): Mutated Channelrhodopsins with Increased Sodium and Calcium Permeability. In *Applied Sciences* 9 (4), p. 664. DOI: 10.3390/app9040664.

Durham, William J.; Aracena-Parks, Paula; Long, Cheng; Rossi, Ann E.; Goonasekera, Sanjeewa A.; Boncompagni, Simona et al. (2008): RyR1 S-nitrosylation underlies environmental heat stroke and sudden death in Y522S RyR1 knockin mice. In *Cell* 133 (1), pp. 53–65. DOI: 10.1016/j.cell.2008.02.042.

EB Maryon (1998): Maryon, E. B., Saari, B. & Anderson, P. Muscle-specific functions of ryanodine receptor channels in Caenorhabditis elegans. J Cell Sci 111, 2885–2895 (1998). In *J Cell Sci* 111, p. 2885.

Edwards, Stacey L.; Charlie, Nicole K.; Milfort, Marie C.; Brown, Brandon S.; Gravlin, Christen N.; Knecht, Jamie E.; Miller, Kenneth G. (2008): A novel molecular solution for ultraviolet light detection in Caenorhabditis elegans. In *PLoS biology* 6 (8), e198. DOI: 10.1371/journal.pbio.0060198.

Efremov, Rouslan G.; Leitner, Alexander; Aebersold, Ruedi; Raunser, Stefan (2015): Architecture and conformational switch mechanism of the ryanodine receptor. In *Nature* 517 (7532), pp. 39–43. DOI: 10.1038/nature13916.

El-Brolosy, Mohamed A.; Kontarakis, Zacharias; Rossi, Andrea; Kuenne, Carsten; Günther, Stefan; Fukuda, Nana et al. (2019): Genetic compensation triggered by mutant mRNA degradation. In *Nature* 568 (7751), pp. 193–197. DOI: 10.1038/s41586-019-1064-z.

El-Brolosy, Mohamed A.; Stainier, Didier Y. R. (2017): Genetic compensation: A phenomenon in search of mechanisms. In *PLoS genetics* 13 (7), e1006780. DOI: 10.1371/journal.pgen.1006780.

Endo, Makoto (2006): Calcium ion as a second messenger with special reference to excitation-contraction coupling. In *Journal of pharmacological sciences* 100 (5), pp. 519–524. DOI: 10.1254/jphs.cpj06004x.

Endo, Makoto (2009): Calcium-induced calcium release in skeletal muscle. In *Physiological reviews* 89 (4), pp. 1153–1176. DOI: 10.1152/physrev.00040.2008.

Erbguth, Karen; Prigge, Matthias; Schneider, Franziska; Hegemann, Peter; Gottschalk, Alexander (2012): Bimodal activation of different neuron classes with the spectrally red-shifted channelrhodopsin chimera C1V1 in Caenorhabditis elegans. In *PLoS ONE* 7 (10), e46827. DOI: 10.1371/journal.pone.0046827.

Erkasap, Nilüfer (2007): SERCA in genesis of arrhythmias: what we already know and what is new? In *Anadolu kardiyoloji dergisi : AKD = the Anatolian journal of cardiology* 7 Suppl 1, pp. 43–46.

Erkut, Cihan; Vasilj, Andrej; Boland, Sebastian; Habermann, Bianca; Shevchenko, Andrej; Kurzchalia, Teymuras V. (2013): Molecular strategies of the Caenorhabditis elegans dauer larva to survive extreme desiccation. In *PLoS ONE* 8 (12), e82473. DOI: 10.1371/journal.pone.0082473.

Evans, T. C. (2021): Transformation and microinjection. Edited by WormBook, ed. The C. elegans Research Community, WormBook, doi/10.1895/wormbook.1.108.1. Available online at http://www.wormbook.org/chapters/www_transformationmicroinjection/transformationmicroinjection.html, updated on 1/5/2021, checked on 1/5/2021.

Ezcurra, Marina; Benedetto, Alexandre; Sornda, Thanet; Gilliat, Ann F.; Au, Catherine; Zhang, Qifeng et al. (2018): C. elegans Eats Its Own Intestine to Make Yolk Leading to Multiple Senescent Pathologies. In *Current Biology* 28 (20), p. 3352. DOI: 10.1016/j.cub.2018.10.003.

Fang-Yen, Christopher; Avery, Leon; Samuel, Aravinthan D. T. (2009): Two size-selective mechanisms specifically trap bacteria-sized food particles in Caenorhabditis elegans. In *PNAS* 106 (47), pp. 20093–20096. DOI: 10.1073/pnas.0904036106.

Fessenden, J. D.; Chen, L.; Wang, Y.; Paolini, C.; Franzini-Armstrong, C.; Allen, P. D.; Pessah, I. N. (2001): Ryanodine receptor point mutant E4032A reveals an allosteric interaction with ryanodine. In *Proceedings of the National Academy of Sciences of the United States of America* 98 (5), pp. 2865–2870. DOI: 10.1073/pnas.041608898.

Fill, Michael; Copello, Julio A. (2002): Ryanodine receptor calcium release channels. In *Physiological reviews* 82 (4), pp. 893–922. DOI: 10.1152/PHYSREV.00013.2002.

Fill, Michael; Gillespie, Dirk (2018): Ryanodine Receptor Open Times Are Determined in the Closed State. In *Biophysical Journal* 115 (7), pp. 1160–1165. DOI: 10.1016/j.bpj.2018.08.025.

Fire, A.; Waterston, R. H. (1989): Proper expression of myosin genes in transgenic nematodes. In *The EMBO Journal* 8 (11), pp. 3419–3428.

Fire, Andrew; Harrison, Susan White; Dixon, Dennis (1990): A modular set of lacZ fusion vectors for studying gene expression in Caenorhabditis elegans. In *Gene* 93 (2), pp. 189–198. DOI: 10.1016/0378-1119(90)90224-F.

Fischer, Elisabeth (2015): Etablierung eines Arrhythmiemodells im Pharynx des Nematoden Caenorhabditis elegans unter Verwendung optogenetischer Methoden. Dissertation. Johann Wolfgang Goethe-Universität, Frankfurt am Main.

Fischer, Elisabeth; Gottschalk, Alexander; Schüler, Christina (2017): An optogenetic arrhythmia model to study catecholaminergic polymorphic ventricular tachycardia mutations. In *Sci Rep* 7 (1), p. 17514. DOI: 10.1038/s41598-017-17819-8.

Flucher, B. E.; Andrews, S. B.; Daniels, M. P. (1994): Molecular organization of transverse tubule/sarcoplasmic reticulum junctions during development of excitation-contraction coupling in skeletal muscle. In *Molecular Biology of the Cell* 5 (10), pp. 1105–1118. DOI: 10.1091/mbc.5.10.1105.

Forge, T. A.; Macguidwin, A. E. (1989): Nematode autofluorescence and its use as an indicator of viability. In *Journal of nematology* 21 (3), pp. 399–403.

Forrester, Frances M.; Umanskaya, Alisa; Xie, Wenjun; Reiken, Steven; Yuan, Qi; Lacampagne, Alain; Marks, Andrew (2017): The Role of Calcium Leak in Age-Dependent Loss of C. Elegans Muscle Function. In *Biophysical Journal* 112 (3), 232a. DOI: 10.1016/j.bpj.2016.11.1274.

Francis, G. R.; Waterston, R. H. (1985): Muscle organization in Caenorhabditis elegans: localization of proteins implicated in thin filament attachment and I-band organization. In *The Journal of Cell Biology* 101 (4), pp. 1532–1549. DOI: 10.1083/jcb.101.4.1532.

Francis, R.; Waterston, R. H. (1991): Muscle cell attachment in Caenorhabditis elegans. In *The Journal of Cell Biology* 114 (3), pp. 465–479. DOI: 10.1083/jcb.114.3.465.

Franks, Christopher J.; Holden-Dye, Lindy; Bull, Kathryn; Luedtke, Sarah; Walker, Robert J. (2006): Anatomy, physiology and pharmacology of Caenorhabditis elegans pharynx: a model to define gene function in a simple neural system. In *Invertebrate neuroscience : IN* 6 (3), pp. 105–122. DOI: 10.1007/s10158-006-0023-1.

Franzini-Armstrong, C.; Protasi, F. (1997): Ryanodine receptors of striated muscles: a complex channel capable of multiple interactions. In *Physiological reviews* 77 (3), pp. 699–729. DOI: 10.1152/physrev.1997.77.3.699.

Froehlich, Allan C.; Liu, Yi; Loros, Jennifer J.; Dunlap, Jay C. (2002): White Collar-1, a circadian blue light photoreceptor, binding to the frequency promoter. In *Science* 297 (5582), pp. 815–819. DOI: 10.1126/science.1073681.

Gagliano, Maria Cristina; Sudmalis, Dainis; Temmink, Hardy; Plugge, Caroline M. (2020): Calcium effect on microbial activity and biomass aggregation during anaerobic digestion at high salinity. In *New biotechnology* 56, pp. 114–122. DOI: 10.1016/j.nbt.2020.01.001.

Galice, Samuel; Xie, Yuanfang; Yang, Yi; Sato, Daisuke; Bers, Donald M. (2018): Size Matters: Ryanodine Receptor Cluster Size Affects Arrhythmogenic Sarcoplasmic Reticulum Calcium Release. In *Journal of the American Heart Association* 7 (13). DOI: 10.1161/JAHA.118.008724.

García-Casas, Paloma; Arias-Del-Val, Jessica; Alvarez-Illera, Pilar; Fonteriz, Rosalba I.; Montero, Mayte; Alvarez, Javier (2018): Inhibition of Sarco-Endoplasmic Reticulum Ca2+ ATPase Extends the Lifespan in C. elegans Worms. In *Frontiers in pharmacology* 9, p. 669. DOI: 10.3389/fphar.2018.00669.

Ghosh, Rajarshi; Emmons, Scott W. (2008): Episodic swimming behavior in the nematode C. elegans. In *The Journal of experimental biology* 211 (Pt 23), pp. 3703–3711. DOI: 10.1242/jeb.023606.

Gilbert, Scott F. (Ed.) (2000): Developmental Biology. 6th edition: Sinauer Associates.

Golden, James W.; Riddle, Donald L. (1984): The Caenorhabditis elegans dauer larva: Developmental effects of pheromone, food, and temperature. In *Developmental Biology* 102 (2), pp. 368–378. DOI: 10.1016/0012-1606(84)90201-X.

Golec, Piotr; Karczewska-Golec, Joanna; Łoś, Marcin; Węgrzyn, Grzegorz (2014): Bacteriophage T4 can produce progeny virions in extremely slowly growing Escherichia coli host: comparison of a mathematical model with the experimental data. In *FEMS microbiology letters* 351 (2), pp. 156–161. DOI: 10.1111/1574-6968.12372.

Gong, Jianke; Yuan, Yiyuan; Ward, Alex; Kang, Lijun; Zhang, Bi; Wu, Zhiping et al. (2016): The C. elegans Taste Receptor Homolog LITE-1 Is a Photoreceptor. In *Cell* 167 (5), 1252-1263.e10. DOI: 10.1016/j.cell.2016.10.053.

Gottschalk, Alexander (2020): Optogenetic analyses of neuronal networks that generate behavior in Caenorhabditis elegans. In *Neuroforum* 0 (0). DOI: 10.1515/nf-2020-0022.

Govorunova, Elena G.; Sineshchekov, Oleg A.; Li, Hai; Janz, Roger; Spudich, John L. (2013): Characterization of a highly efficient blue-shifted channelrhodopsin from the marine alga Platymonas subcordiformis. In *Journal of Biological Chemistry* 288 (41), pp. 29911–29922. DOI: 10.1074/jbc.M113.505495.

Grabner, M.; Dirksen, R. T.; Beam, K. G. (1998): Tagging with green fluorescent protein reveals a distinct subcellular distribution of L-type and non-L-type Ca2+ channels expressed in dysgenic myotubes. In *Proceedings of the National Academy of Sciences of the United States of America* 95 (4), pp. 1903–1908. DOI: 10.1073/pnas.95.4.1903.

Grabner, Manfred; Dayal, Anamika (2010): Crosstalk via the Sarcoplasmic Gap. In Irina Serysheva (Ed.): Structure and Function of Calcium Release Channels, vol. 66. 1. Aufl. s.l.: Elsevier textbooks (Current Topics in Membranes, 66), pp. 115–138.

Gradinaru, Viviana; Mogri, Murtaza; Thompson, Kimberly R.; Henderson, Jaimie M.; Deisseroth, Karl (2009): Optical deconstruction of parkinsonian neural circuitry. In *Science* 324 (5925), pp. 354–359. DOI: 10.1126/science.1167093.

Grant, B.; Hirsh, D. (1999): Receptor-mediated endocytosis in the Caenorhabditis elegans oocyte. In *Molecular Biology of the Cell* 10 (12), pp. 4311–4326. DOI: 10.1091/mbc.10.12.4311.

Green, Kim N.; Demuro, Angelo; Akbari, Yama; Hitt, Brian D.; Smith, Ian F.; Parker, Ian; LaFerla, Frank M. (2008a): SERCA pump activity is physiologically regulated by presenilin and regulates amyloid beta production. In *Journal of Cell Biology* 181 (7), pp. 1107–1116. DOI: 10.1083/jcb.200706171.

Green, Rebecca A.; Audhya, Anjon; Pozniakovsky, Andrei; Dammermann, Alexander; Pemble, Hayley; Monen, Joost et al. (2008b): Expression and Imaging of Fluorescent Proteins in the C. elegans Gonad and Early Embryo. In : Methods in Cell Biology : Fluorescent Proteins, vol. 85: Academic Press, pp. 179–218. Available online at http://www.sciencedirect.com/science/article/pii/S0091679X08850091.

Gregoire, Simpson; Irwin, Jacob; Kwon, Inchan (2012): Techniques for Monitoring Protein Misfolding and Aggregation in Vitro and in Living Cells. In *The Korean journal of chemical engineering* 29 (6), pp. 693–702. DOI: 10.1007/s11814-012-0060-x.

Hahn, Bum-Soo; Labouesse, Michel (2001): Tissue integrity: Hemidesmosomes and resistance to stress. In *Current biology : CB* 11 (21), R858-R861. DOI: 10.1016/S0960-9822(01)00516-4.

Halavaty, Andrei S.; Moffat, Keith (2007): N- and C-terminal flanking regions modulate light-induced signal transduction in the LOV2 domain of the blue light sensor phototropin 1 from Avena sativa. In *Biochemistry* 46 (49), pp. 14001–14009. DOI: 10.1021/bi701543e.

Hamada, Tomoyo; Sakube, Yasuji; Ahnn, Joohong; Kim, Do Han; Kagawa, Hiroaki (2002): Molecular Dissection, Tissue Localization and Ca2+ Binding of the Ryanodine Receptor of Caenorhabditis elegans. In *Journal of molecular biology* 324 (1), pp. 123–135. DOI: 10.1016/S0022-2836(02)01032-X.

Han, Xue (2012): Optogenetics in the nonhuman primate. In *Progress in brain research* 196, pp. 215–233. DOI: 10.1016/B978-0-444-59426-6.00011-2.

Hardie, R. C.; Raghu, P. (2001): Visual transduction in Drosophila. In *Nature* 413 (6852), pp. 186–193. DOI: 10.1038/35093002.

Haun, C.; Alexander, J.; Stainier, D. Y.; Okkema, P. G. (1998): Rescue of Caenorhabditis elegans pharyngeal development by a vertebrate heart specification gene. In *Proceedings of the National Academy of Sciences of the United States of America* 95 (9), pp. 5072–5075. DOI: 10.1073/PNAS.95.9.5072.

Hauser, K.; Barth, A. (2007): Side-chain protonation and mobility in the sarcoplasmic reticulum Ca2+-ATPase: implications for proton countertransport and Ca2+ release. In *Biophysical Journal* 93 (9), pp. 3259–3270. DOI: 10.1529/biophysj.107.109363.

Hegemann, Peter; Ehlenbeck, Sabine; Gradmann, Dietrich (2005): Multiple photocycles of channelrhodopsin. In *Biophysical Journal* 89 (6), pp. 3911–3918. DOI: 10.1529/BIOPHYSJ.105.069716.

Heintzen, Christian; Loros, Jennifer J.; Dunlap, Jay C. (2001): The PAS Protein VIVID Defines a Clock-Associated Feedback Loop that Represses Light Input, Modulates Gating, and Regulates Clock Resetting. In *Cell* 104 (3), pp. 453–464. DOI: 10.1016/S0092-8674(01)00232-X.

Herrou, Julien; Crosson, Sean (2011): Function, structure and mechanism of bacterial photosensory LOV proteins. In *Nature reviews. Microbiology* 9 (10), pp. 713–723. DOI: 10.1038/nrmicro2622.

Herzberg, Osnat; Moult, John; James, Michael N.G. (1987): [46] molecular structure of troponin C and its implications for the Ca2+ triggering of muscle contraction. In : Methods in Enzymology : Cellular Regulators Part A: Calcium- and Calmodulin-Binding Proteins, vol. 139: Academic Press, pp. 610–632. Available online at http://www.sciencedirect.com/science/article/pii/0076687987391153.

Hillier, Ladeana W.; Coulson, Alan; Murray, John I.; Bao, Zhirong; Sulston, John E.; Waterston, Robert H. (2005): Genomics in C. elegans: so many genes, such a little worm. In *Genome research* 15 (12), pp. 1651–1660. DOI: 10.1101/gr.3729105.

Hobson, Robert J.; Geng, Jinming; Gray, Anjali D.; Komuniecki, Richard W. (2003): SER-7b, a constitutively active Galphas coupled 5-HT7-like receptor expressed in the Caenorhabditis elegans M4 pharyngeal motorneuron. In *Journal of neurochemistry* 87 (1), pp. 22–29. DOI: 10.1046/J.1471-4159.2003.01967.X.

Hochbaum, Daniel; Ferguson, Annabel A.; Fisher, Alfred L. (2010): Generation of transgenic C. elegans by biolistic transformation. In *Journal of visualized experiments : JoVE* (42). DOI: 10.3791/2090.

Hoon Cho, Jeong; Bandyopadhyay, Jaya; Lee, Jiyeon; Park, Chul-Seung; Ahnn, Joohong (2000): Two isoforms of sarco/endoplasmic reticulum calcium ATPase (SERCA) are essential in Caenorhabditis elegans. In *Gene* 261 (2), pp. 211–219. DOI: 10.1016/S0378-1119(00)00536-9.

Hope, Ian A. (Ed.) (2005): C. elegans. A practical approach. Repr. Oxford: Oxford Univ. Press (The practical approach series, 213).

Horner, M. A.; Quintin, S.; Domeier, M. E.; Kimble, J.; Labouesse, M.; Mango, S. E. (1998): pha-4, an HNF-3 homolog, specifies pharyngeal organ identity in Caenorhabditis elegans. In *Genes & Development* 12 (13), pp. 1947–1952. DOI: 10.1101/GAD.12.13.1947.

Horvitz, H. R.; Chalfie, M.; Trent, C.; Sulston, J. E.; Evans, P. D. (1982): Serotonin and octopamine in the nematode Caenorhabditis elegans. In *Science (New York, N.Y.)* 216 (4549), pp. 1012–1014. DOI: 10.1126/science.6805073.

Hovnanian, A. (2007): SERCA pumps and human diseases. In *Sub-cellular biochemistry* 45, pp. 337–363. DOI: 10.1007/978-1-4020-6191-2_12.

Hresko, M. C.; Schriefer, L. A.; Shrimankar, P.; Waterston, R. H. (1999): Myotactin, a novel hypodermal protein involved in muscle-cell adhesion in Caenorhabditis elegans. In *The Journal of Cell Biology* 146 (3), pp. 659–672. DOI: 10.1083/jcb.146.3.659.

Huala, E.; Oeller, P. W.; Liscum, E.; Han, I. S.; Larsen, E.; Briggs, W. R. (1997): Arabidopsis NPH1: a protein kinase with a putative redox-sensing domain. In *Science (New York, N.Y.)* 278 (5346), pp. 2120–2123. DOI: 10.1126/science.278.5346.2120.

Hwang, Hyundoo; Barnes, Dawn E.; Matsunaga, Yohei; Benian, Guy M.; Ono, Shoichiro; Lu, Hang (2016): Muscle contraction phenotypic analysis enabled by optogenetics reveals functional relationships of sarcomere components in Caenorhabditis elegans. In *Scientific reports* 6, p. 19900. DOI: 10.1038/srep19900.

Idnurm, Alexander; Heitman, Joseph (2005): Light controls growth and development via a conserved pathway in the fungal kingdom. In *PLoS biology* 3 (4), e95. DOI: 10.1371/journal.pbio.0030095.

Ikeda, Yusaku; Jurica, Peter; Kimura, Hiroshi; Takagi, Hiroaki; Struzik, Zbigniew R.; Kiyono, Ken et al. (2020): C. elegans episodic swimming is driven by multifractal kinetics. In *Scientific reports* 10 (1), p. 14775. DOI: 10.1038/s41598-020-70319-0.

Ikemoto, N.; Antoniu, B.; Kang, J. J.; Mészáros, L. G.; Ronjat, M. (1991): Intravesicular calcium transient during calcium release from sarcoplasmic reticulum. In *Biochemistry* 30 (21), pp. 5230–5237. DOI: 10.1021/BI00235A017.

Imagawa, T.; Smith, J. S.; Coronado, R.; Campbell, K. P. (1987): Purified ryanodine receptor from skeletal muscle sarcoplasmic reticulum is the Ca2+-permeable pore of the calcium release channel. In *The Journal of biological chemistry* 262 (34), pp. 16636–16643. DOI: 10.1016/s0021-9258(18)49303-9.

Inesi, Giuseppe; Lewis, David; Toyoshima, Chikashi; Hirata, Ayami; Meis, Leopoldo de (2008): Conformational fluctuations of the Ca2+-ATPase in the native membrane environment. Effects of pH, temperature, catalytic substrates, and thapsigargin. In *The Journal of biological chemistry* 283 (2), pp. 1189–1196. DOI: 10.1074/jbc.M707189200.

Inui, M.; Saito, A.; Fleischer, S. (1987): Purification of the ryanodine receptor and identity with feet structures of junctional terminal cisternae of sarcoplasmic reticulum from fast skeletal muscle. In *The Journal of biological chemistry* 262 (4), pp. 1740–1747. DOI: 10.1016/s0021-9258(19)75701-9.

Ishizuka, Toru; Kakuda, Masaaki; Araki, Rikita; Yawo, Hiromu (2006): Kinetic evaluation of photosensitivity in genetically engineered neurons expressing green algae light-gated channels. In *Neuroscience Research* 54 (2), pp. 85–94. DOI: 10.1016/j.neures.2005.10.009.

J. Chen; M. Fishman (1996): Zebrafish tinman homolog demarcates the heart field and initiates myocardial differentiation. In *Development*. Available online at https://www.semanticscholar.org/paper/bb6f48650e5ce475faa06ba41bebbeddefc7947d.

J. Gray; H. W. Lissmann (1964): THE LOCOMOTION OF NEMATODES. In *The Journal of experimental biology*. Available online at https://www.semanticscholar.org/paper/aa1eac47a1c0528bf50ef12b05706cfeffe30e1f.

JH Cho (1999): Cho, J. H., Eom, S. H. & Ahnn, J. Analysis of calsequestrin gene expression using green fluorescent protein in Caenorhabditis elegans. Mol Cells 9, 230–234 (1999). In *Mol Cells* 9, p. 230.

Johnson, J. D.; Charlton, S. C.; Potter, J. D. (1979): A fluorescence stopped flow analysis of Ca2+ exchange with troponin C. In *The Journal of biological chemistry* 254 (9), pp. 3497–3502. DOI: 10.1016/S0021-9258(18)50787-0.

Johnson, J. D.; Nakkula, R. J.; Vasulka, C.; Smillie, L. B. (1994): Modulation of Ca2+ exchange with the Ca(2+)-specific regulatory sites of troponin C. In *The Journal of biological chemistry* 269 (12), pp. 8919–8923. DOI: 10.1016/S0021-9258(17)37055-2.

Johnson, Thomas E.; Mitchell, David H.; Kline, Susan; Kemal, Rebecca; Foy, John (1984): Arresting development arrests aging in the nematode Caenorhabditis elegans. In *Mechanisms of Ageing and Development* 28 (1), pp. 23–40. DOI: 10.1016/0047-6374(84)90150-7.

Jorgensen, A. O.; Shen, A. C.; Arnold, W.; Leung, A. T.; Campbell, K. P. (1989): Subcellular distribution of the 1,4-dihydropyridine receptor in rabbit skeletal muscle in situ: an immunofluorescence and immunocolloidal gold-labeling study. In *The Journal of Cell Biology* 109 (1), pp. 135–147. DOI: 10.1083/jcb.109.1.135.

Jospin, Maëlle; Jacquemond, Vincent; Mariol, Marie-Christine; Ségalat, Laurent; Allard, Bruno (2002): The L-type voltage-dependent Ca2+ channel EGL-19 controls body wall muscle function in Caenorhabditis elegans. In *The Journal of Cell Biology* 159 (2), pp. 337–348. DOI: 10.1083/jcb.200203055.

Kato, Hideaki E.; Zhang, Feng; Yizhar, Ofer; Ramakrishnan, Charu; Nishizawa, Tomohiro; Hirata, Kunio et al. (2012): Crystal structure of the channelrhodopsin light-gated cation channel. In *Nature* 482 (7385), pp. 369–374. DOI: 10.1038/nature10870.

Kellerman, S. (1992): Nuclear DNA content and nucleation patterns in rat cardiac myocytes from different models of cardiac hypertrophy. In *Journal of Molecular and Cellular Cardiology* 24 (5), pp. 497–505. DOI: 10.1016/0022-2828(92)91839-W.

Kiefer, Julie C.; Smith, Pliny A.; Mango, Susan E. (2007): PHA-4/FoxA cooperates with TAM-1/TRIM to regulate cell fate restriction in the C. elegans foregut. In *Developmental Biology* 303 (2), pp. 611–624. DOI: 10.1016/J.YDBIO.2006.11.042.

Kimble, Judith; Hirsh, David (1979): The postembryonic cell lineages of the hermaphrodite and male gonads in Caenorhabditis elegans. In *Developmental Biology* 70 (2), pp. 396–417. DOI: 10.1016/0012-1606(79)90035-6.

Kimble, Judith; Sharrock, William J. (1983): Tissue-specific synthesis of yolk proteins in Caenorhabditis elegans. In *Developmental Biology* 96 (1), pp. 189–196. DOI: 10.1016/0012-1606(83)90322-6.

Kimble, J. and S. Ward (1988): Germ-line development and fertilization. In *The nematode Caenorhabditis elegans*, pp. 191–213. Available online at https://biochem.wisc.edu/sites/default/files/people/judith-kimble/pdfs/1980s/22_kimble_ward_1988.pdf, checked on 2/19/2021.

Kimlicka, Lynn; Lau, Kelvin; Tung, Ching-Chieh; van Petegem, Filip (2013): Disease mutations in the ryanodine receptor N-terminal region couple to a mobile intersubunit interface. In *Nat Commun* 4 (1), p. 1506. DOI: 10.1038/ncomms2501.

Kishore; Arnaboldi (2021): sca-1 (gene). WormBase : Nematode Information Resource. Available online at https://wormbase.org/species/c_elegans/gene/WBGene00004736#0-9f-10, updated on 1/27/2021, checked on 1/27/2021.

Klapoetke, Nathan C.; Murata, Yasunobu; Kim, Sung Soo; Pulver, Stefan R.; Birdsey-Benson, Amanda; Cho, Yong Ku et al. (2014): Independent optical excitation of distinct neural populations. In *Nat Methods* 11 (3), pp. 338–346. DOI: 10.1038/nmeth.2836.

Klass, Michael R. (1977): Aging in the nematode Caenorhabditis elegans: Major biological and environmental factors influencing life span. In *Mechanisms of Ageing and Development* 6, pp. 413–429. DOI: 10.1016/0047-6374(77)90043-4.

Kleinlogel, Sonja; Feldbauer, Katrin; Dempski, Robert E.; Fotis, Heike; Wood, Phillip G.; Bamann, Christian; Bamberg, Ernst (2011): Ultra light-sensitive and fast neuronal activation with the Ca^{2+}-permeable channelrhodopsin CatCh. In *Nature neuroscience* 14 (4), pp. 513–518. DOI: 10.1038/nn.2776.

Klinke, Rainer; Pape, Hans-Christian; Kurtz, Armin; Silbernagl, Stefan; Baumann, Rosemarie; Brenner, Bernhard et al. (2010): Physiologie. 6., vollständig überarb. Aufl. Stuttgart: Thieme. Available online at http://ebooks.thieme.de/9783137960065.

Kloss, Loreen; Meyer, Julia Dawn; Graeve, Lutz; Vetter, Walter (2015): Sodium intake and its reduction by food reformulation in the European Union — A review. In *NFS Journal* 1, pp. 9–19. DOI: 10.1016/j.nfs.2015.03.001.

Kobayashi, Y. M.; Alseikhan, B. A.; Jones, L. R. (2000): Localization and characterization of the calsequestrin-binding domain of triadin 1. Evidence for a charged beta-strand in mediating the

protein-protein interaction. In *The Journal of biological chemistry* 275 (23), pp. 17639–17646. DOI: 10.1074/jbc.M002091200.

Kon, Naohiro; Fukada, Yoshitaka (2015): Cognitive Function and Calcium. Ca2+-dependent regulatory mechanism of circadian clock oscillation and its relevance to neuronal function. In *Clinical calcium* 25 (2), pp. 201–208.

Korta, Jeremie; Clark, Damon A.; Gabel, Christopher V.; Mahadevan, L.; Samuel, Aravinthan D. T. (2007): Mechanosensation and mechanical load modulate the locomotory gait of swimming C. elegans. In *The Journal of experimental biology* 210 (Pt 13), pp. 2383–2389. DOI: 10.1242/jeb.004572.

Kuo, Ivana Y.; Ehrlich, Barbara E. (2015): Signaling in muscle contraction. In *Cold Spring Harbor perspectives in biology* 7 (2), a006023. DOI: 10.1101/cshperspect.a006023.

Lai, F. A.; Erickson, H. P.; Rousseau, E.; Liu, Q. Y.; Meissner, G. (1988): Purification and reconstitution of the calcium release channel from skeletal muscle. In *Nature* 331 (6154), pp. 315–319. DOI: 10.1038/331315A0.

Lanner, Johanna T.; Georgiou, Dimitra K.; Joshi, Aditya D.; Hamilton, Susan L. (2010): Ryanodine receptors: structure, expression, molecular details, and function in calcium release. In *Cold Spring Harbor perspectives in biology* 2 (11), a003996. DOI: 10.1101/cshperspect.a003996.

Lee, Kun He; Aschner, Michael (2016): A Simple Light Stimulation of Caenorhabditis elegans. In *Current protocols in toxicology* 67, 11.21.1-11.21.5. DOI: 10.1002/0471140856.tx1121s67.

Lee, R. Y.; Lobel, L.; Hengartner, M.; Horvitz, H. R.; Avery, L. (1997): Mutations in the alpha1 subunit of an L-type voltage-activated Ca2+ channel cause myotonia in Caenorhabditis elegans. In *The EMBO Journal* 16 (20), pp. 6066–6076. DOI: 10.1093/emboj/16.20.6066.

Lefebvre, Christophe; Largeau, Céline; Michelet, Xavier; Fourrage, Cécile; Maniere, Xavier; Matic, Ivan et al. (2016): The ESCRT-II proteins are involved in shaping the sarcoplasmic reticulum in C. elegans. In *Journal of Cell Science* 129 (7), pp. 1490–1499. DOI: 10.1242/jcs.178467.

Lewis, R. S. (2001): Calcium signaling mechanisms in T lymphocytes. In *Annual review of immunology* 19, pp. 497–521. DOI: 10.1146/annurev.immunol.19.1.497.

L'Hernault, Steven W. (2006): Spermatogenesis. In *Wormbook*, pp. 1–14. DOI: 10.1895/wormbook.1.85.1.

Li, Chris; Kim, Kyuhyung (2008): Neuropeptides. In *Wormbook*, pp. 1–36. DOI: 10.1895/wormbook.1.142.1.

Liao, R.; Helm, P. A.; Hajjar, R. J.; Saha, C.; Gwathmey, J. K. (1994): Ca2+i in human heart failure: a review and discussion of current areas of controversy. In *The Yale Journal of Biology and Medicine* 67 (5-6), pp. 247–264.

Lin, John Y. (2011): A user's guide to channelrhodopsin variants: features, limitations and future developments. In *Experimental physiology* 96 (1), pp. 19–25. DOI: 10.1113/expphysiol.2009.051961.

Lints, Robyn; Hall, David H. (2004): WormAtlas Male Handbook - Introduction. In *WormAtlas*. DOI: 10.3908/wormatlas.2.1.

Lints, R. and Hall, D.H. (2009): Male Neuronal Support Cells - Overview. Edited by Wormatlas. Available online at https://www.wormatlas.org/male/neuronalsupport/Neuroframeset.html, updated on 11/17/2015, checked on 2/24/2021.

Losi, Aba (2004): The bacterial counterparts of plant phototropins. In *Photochemical & photobiological sciences : Official journal of the European Photochemistry Association and the European Society for Photobiology* 3 (6), pp. 566–574. DOI: 10.1039/b400728j.

Losi, Aba; Polverini, Eugenia; Quest, Benjamin; Gärtner, Wolfgang (2002): First Evidence for Phototropin-Related Blue-Light Receptors in Prokaryotes. In *Biophysical Journal* 82 (5), pp. 2627–2634. DOI: 10.1016/S0006-3495(02)75604-X.

Lovelock J. E.; Porterfield, B. M. (1952): Blood clotting; the function of electrolytes and of calcium. In *The Biochemical journal* 50 (3), pp. 415–420. DOI: 10.1042/bj0500415.

Ma, J.; Bhat, M. B.; Zhao, J. (1995): Rectification of skeletal muscle ryanodine receptor mediated by FK506 binding protein. In *Biophysical Journal* 69 (6), pp. 2398–2404. DOI: 10.1016/S0006-3495(95)80109-8.

Madshus, I. H. (1988): Regulation of intracellular pH in eukaryotic cells. In *Biochemical Journal* 250 (1), pp. 1–8. DOI: 10.1042/bj2500001.

Malcuit, Christopher; Kurokawa, Manabu; Fissore, Rafael A. (2006): Calcium oscillations and mammalian egg activation. In *Journal of cellular physiology* 206 (3), pp. 565–573. DOI: 10.1002/jcp.20471.

Mango, Susan E. (2007): The C. elegans pharynx: a model for organogenesis. In *Wormbook*, pp. 1–26. DOI: 10.1895/wormbook.1.129.1.

Mango, Susan E. (2009): The molecular basis of organ formation: insights from the C. elegans foregut. In *Annual Review of Cell and Developmental Biology* 25 (1), pp. 597–628. DOI: 10.1146/annurev.cellbio.24.110707.175411.

Marques, Filipe; Thapliyal, Saurabh; Javer, Avelino; Shrestha, Priyanka; Brown, André E. X.; Glauser, Dominique A. (2020): Tissue-specific isoforms of the single C. elegans Ryanodine receptor gene unc-68 control specific functions. In *PLoS genetics* 16 (10), e1009102. DOI: 10.1371/journal.pgen.1009102.

Marsman, Roos F.; Tan, Hanno L.; Bezzina, Connie R. (2014): Genetics of sudden cardiac death caused by ventricular arrhythmias. In *Nature Reviews Cardiology* 11 (2), pp. 96–111. DOI: 10.1038/nrcardio.2013.186.

Maryon, E. B.; Coronado, R.; Anderson, P. (1996): unc-68 encodes a ryanodine receptor involved in regulating C. elegans body-wall muscle contraction. In *The Journal of Cell Biology* 134 (4), pp. 885–893. DOI: 10.1083/jcb.134.4.885.

Maryon, E. B.; Saari, B.; Anderson, P. (1998): Muscle-specific functions of ryanodine receptor channels in Caenorhabditis elegans. In *Journal of Cell Science* 111 (Pt 19), pp. 2885–2895.

Maures, Travis J.; Booth, Lauren N.; Benayoun, Bérénice A.; Izrayelit, Yevgeniy; Schroeder, Frank C.; Brunet, Anne (2014): Males shorten the life span of C. elegans hermaphrodites via secreted compounds. In *Science (New York, N.Y.)* 343 (6170), pp. 541–544. DOI: 10.1126/science.1244160.

Mayrleitner, M.; Chandler, R.; Schindler, H.; Fleischer, S. (1995): Phosphorylation with protein kinases modulates calcium loading of terminal cisternae of sarcoplasmic reticulum from skeletal muscle. In *Cell Calcium* 18 (3), pp. 197–206. DOI: 10.1016/0143-4160(95)90064-0.

McKay, James P.; Raizen, David M.; Gottschalk, Alexander; Schafer, William R.; Avery, Leon (2004): eat-2 and eat-18 are required for nicotinic neurotransmission in the Caenorhabditis elegans pharynx. In *Genetics* 166 (1), pp. 161–169. DOI: 10.1534/genetics.166.1.161.

Meissner, G. (1994): Ryanodine receptor/Ca2+ release channels and their regulation by endogenous effectors. In *Annual review of physiology* 56 (1), pp. 485–508. DOI: 10.1146/ANNUREV.PH.56.030194.002413.

Mello, C. C.; Kramer, J. M.; Stinchcomb, D.; Ambros, V. (1991): Efficient gene transfer in C.elegans: extrachromosomal maintenance and integration of transforming sequences. In *The EMBO Journal* 10 (12), pp. 3959–3970.

Meulenaere, Evelien de; Nguyen Bich, Ngan; Wergifosse, Marc de; van Hecke, Kristof; van Meervelt, Luc; Vanderleyden, Jozef et al. (2013): Improving the second-order nonlinear optical response of fluorescent proteins: the symmetry argument. In *Journal of the American Chemical Society* 135 (10), pp. 4061–4069. DOI: 10.1021/ja400098b.

Meur, Gargi; Parker, Andrew K. T.; Gergely, Fanni V.; Taylor, Colin W. (2007): Targeting and retention of type 1 ryanodine receptors to the endoplasmic reticulum. In *The Journal of biological chemistry* 282 (32), pp. 23096–23103. DOI: 10.1074/jbc.M702457200.

Mikoshiba, Katsuhiko (2007): IP3 receptor/Ca2+ channel: from discovery to new signaling concepts. In *Journal of neurochemistry* 102 (5), pp. 1426–1446. DOI: 10.1111/j.1471-4159.2007.04825.x.

Miyazaki, S. I.; Takahashi, K.; Tsuda, K. (1974): Electrical excitability in the egg cell membrane of the tunicate. In *The Journal of Physiology* 238 (1), pp. 37–54. DOI: 10.1113/jphysiol.1974.sp010509.

Mollard, Patrice; Schlegel, Werner (1996): Why are endocrine pituitary cells excitable? In *Trends in Endocrinology & Metabolism* 7 (10), pp. 361–365. DOI: 10.1016/S1043-2760(96)00186-5.

Moorman, A. F.; Jong, F. de; Lamers, W. H. (1997): Development of the conduction system of the heart. In *Pacing and clinical electrophysiology : PACE* 20 (8 Pt 2), pp. 2087–2092. DOI: 10.1111/j.1540-8159.1997.tb03634.x.

Murshed, Monzur (2018): Mechanism of Bone Mineralization. In *Cold Spring Harbor perspectives in medicine* 8 (12). DOI: 10.1101/cshperspect.a031229.

Musgaard, Maria; Thøgersen, Lea; Schiøtt, Birgit (2011): Protonation states of important acidic residues in the central Ca^{2+} ion binding sites of the Ca^{2+}-ATPase: a molecular modeling study. In *Biochemistry* 50 (51), pp. 11109–11120. DOI: 10.1021/bi201164b.

Nagasaki, Kazuo; Fleischer, Sidney (1988): Ryanodine sensitivity of the calcium release channel of sarcoplasmic reticulum. In *Cell Calcium* 9 (1), pp. 1–7. DOI: 10.1016/0143-4160(88)90032-2.

Nagel; Szellas; Huhn; Kateriya; Adeishvili; Berthold et al. (2003a): Channelrhodopsin-2, a directly light gated cation-selective membrane channel. In *Current biology : CB* 15 (24), pp. 2279–2284. DOI: 10.1016/j.cub.2005.11.032.

Nagel, Georg; Brauner, Martin; Liewald, Jana F.; Adeishvili, Nona; Bamberg, Ernst; Gottschalk, Alexander (2005): Light activation of channelrhodopsin-2 in excitable cells of Caenorhabditis elegans triggers rapid behavioral responses. In *Current biology : CB* 15 (24), pp. 2279–2284. DOI: 10.1016/j.cub.2005.11.032.

Nagel, Georg; Ollig, Doris; Fuhrmann, Markus; Kateriya, Suneel; Musti, Anna Maria; Bamberg, Ernst; Hegemann, Peter (2002): Channelrhodopsin-1: a light-gated proton channel in green algae. In *Science* 296 (5577), pp. 2395–2398. DOI: 10.1126/SCIENCE.1072068.

Nagel, Georg; Szellas, Tanjef; Huhn, Wolfram; Kateriya, Suneel; Adeishvili, Nona; Berthold, Peter et al. (2003b): Channelrhodopsin-2, a directly light-gated cation-selective membrane channel. In *Proceedings of the National Academy of Sciences of the United States of America* 100 (24), pp. 13940–13945. DOI: 10.1073/pnas.1936192100.

Nagpal, Jatin (2017): Development and implementation of novel optogenetic tools in the nematode Caenorhabditis elegans. Dissertation. Universitätsbibliothek Johann Christian Senckenberg, Frankfurt am Main.

Nakai, J.; Sekiguchi, N.; Rando, T. A.; Allen, P. D.; Beam, K. G. (1998): Two regions of the ryanodine receptor involved in coupling with L-type Ca2+ channels. In *The Journal of biological chemistry* 273 (22), pp. 13403–13406. DOI: 10.1074/jbc.273.22.13403.

NEBcloner (2020). Available online at http://nebcloner.neb.com/#!/redigest, updated on 7/25/2020, checked on 11/13/2020.

NEBcutter V2.0 (2020). Available online at http://nc2.neb.com/NEBcutter2/, updated on 11/13/2020, checked on 11/13/2020.

Nelson, David C.; Lasswell, Jamie; Rogg, Luise E.; Cohen, Mindy A.; Bartel, Bonnie (2000): FKF1, a Clock-Controlled Gene that Regulates the Transition to Flowering in Arabidopsis. In *Cell* 101 (3), pp. 331–340. DOI: 10.1016/S0092-8674(00)80842-9.

Nigon, Victor Marc; Félix, Marie-Anne (Eds.) (2018): WormBook: The Online Review of C. elegans Biology [Internet]: WormBook.

Nixon, G. F.; Mignery, G. A.; Somlyo, A. V. (1994): Immunogold localization of inositol 1,4,5-trisphosphate receptors and characterization of ultrastructural features of the sarcoplasmic reticulum in phasic and tonic smooth muscle. In *Journal of Muscle Research and Cell Motility* 15 (6), pp. 682–700. DOI: 10.1007/BF00121075.

Nowycky, Martha C.; Thomas, Andrew P. (2002): Intracellular calcium signaling. In *Journal of Cell Science* 115 (Pt 19), pp. 3715–3716. DOI: 10.1242/jcs.00078.

Obara, Koji; Miyashita, Naoyuki; Xu, Cheng; Toyoshima, Itaru; Sugita, Yuji; Inesi, Giuseppe; Toyoshima, Chikashi (2005): Structural role of countertransport revealed in Ca(2+) pump crystal structure in the absence of Ca(2+). In *Proceedings of the National Academy of Sciences of the United States of America* 102 (41), pp. 14489–14496. DOI: 10.1073/pnas.0506222102.

Okamoto, O. Keith; Hastings, J. Woodland (2003): NOVEL DINOFLAGELLATE CLOCK-RELATED GENES IDENTIFIED THROUGH MICROARRAY ANALYSIS1. In *J Phycol* 39 (3), pp. 519–526. DOI: 10.1046/j.1529-8817.2003.02170.x.

Olesen, Claus; Picard, Martin; Winther, Anne-Marie Lund; Gyrup, Claus; Morth, J. Preben; Oxvig, Claus et al. (2007): The structural basis of calcium transport by the calcium pump. In *Nature* 450 (7172), pp. 1036–1042. DOI: 10.1038/nature06418.

Olesen, Claus; Sørensen, Thomas Lykke-Møller; Nielsen, Rikke Christina; Møller, Jesper Vuust; Nissen, Poul (2004): Dephosphorylation of the calcium pump coupled to counterion occlusion. In *Science* 306 (5705), pp. 2251–2255. DOI: 10.1126/science.1106289.

Olsen, Anders; Vantipalli, Maithili C.; Lithgow, Gordon J. (2006): Using Caenorhabditis elegans as a model for aging and age-related diseases. In *Annals of the New York Academy of Sciences* 1067, pp. 120–128. DOI: 10.1196/annals.1354.015.

Otsu, K.; Willard, H. F.; Khanna, V. K.; Zorzato, F.; Green, N. M.; MacLennan, D. H. (1990): Molecular cloning of cDNA encoding the Ca2+ release channel (ryanodine receptor) of rabbit cardiac muscle sarcoplasmic reticulum. In *The Journal of biological chemistry* 265 (23), pp. 13472–13483. DOI: 10.1016/s0021-9258(18)77371-7.

Oulès, Bénédicte; Del Prete, Dolores; Greco, Barbara; Zhang, Xuexin; Lauritzen, Inger; Sevalle, Jean et al. (2012): Ryanodine receptor blockade reduces amyloid-β load and memory impairments in Tg2576

mouse model of Alzheimer disease. In *J. Neurosci.* 32 (34), pp. 11820–11834. DOI: 10.1523/JNEUROSCI.0875-12.2012.

P. Okkema; A. Fire (1994): The Caenorhabditis elegans NK-2 class homeoprotein CEH-22 is involved in combinatorial activation of gene expression in pharyngeal muscle. In *Development*. Available online at https://www.semanticscholar.org/paper/fab249f50786c9ffa399aa10e518ef27503306ba.

P. Okkema; E. Ha; C. Haun; W. Chen; A. Fire (1997): The Caenorhabditis elegans NK-2 homeobox gene ceh-22 activates pharyngeal muscle gene expression in combination with pha-1 and is required for normal pharyngeal development. In *Development*. Available online at https://www.semanticscholar.org/paper/0b7ac452b4087dad17d6d476a770de2ff3315945.

Pantazaka, Evangelia; Taylor, Colin W. (2009): Targeting of inositol 1,4,5-trisphosphate receptor to the endoplasmic reticulum by its first transmembrane domain. In *The Biochemical journal* 425 (1), pp. 61–69. DOI: 10.1042/BJ20091051.

Park, M.; Lewis, C.; Turbay, D.; Chung, A.; Chen, J. N.; Evans, S. et al. (1998): Differential rescue of visceral and cardiac defects in Drosophila by vertebrate tinman-related genes. In *Proceedings of the National Academy of Sciences of the United States of America* 95 (16), pp. 9366–9371. DOI: 10.1073/PNAS.95.16.9366.

Parker, Andrew K. T.; Gergely, Fanni V.; Taylor, Colin W. (2004): Targeting of inositol 1,4,5-trisphosphate receptors to the endoplasmic reticulum by multiple signals within their transmembrane domains. In *The Journal of biological chemistry* 279 (22), pp. 23797–23805. DOI: 10.1074/jbc.M402098200.

Pásti, Gabriella; Labouesse, Michel (Eds.) (2018): WormBook: The Online Review of C. elegans Biology [Internet]: WormBook.

Patrick J. Hu (2018): Dauer. In Patrick J. Hu (Ed.): WormBook: The Online Review of C. elegans Biology [Internet]: WormBook. Available online at https://www.ncbi.nlm.nih.gov/books/NBK116082/.

Penela, Petronila; Murga, Cristina; Ribas, Catalina; Tutor, Antonio S.; Peregrín, Sandra; Mayor, Federico (2006): Mechanisms of regulation of G protein-coupled receptor kinases (GRKs) and cardiovascular disease. In *Cardiovascular research* 69 (1), pp. 46–56. DOI: 10.1016/J.CARDIORES.2005.09.011.

Peng, Wei; Shen, Huaizong; Wu, Jianping; Guo, Wenting; Pan, Xiaojing; Wang, Ruiwu et al. (2016): Structural basis for the gating mechanism of the type 2 ryanodine receptor RyR2. In *Science (New York, N.Y.)* 354 (6310). DOI: 10.1126/science.aah5324.

Peres, Tanara V.; Arantes, Leticia P.; Miah, Mahfuzur R.; Bornhorst, Julia; Schwerdtle, Tanja; Bowman, Aaron B. et al. (2018): Role of Caenorhabditis elegans AKT-1/2 and SGK-1 in Manganese Toxicity. In *Neurotoxicity Research* 34 (3), pp. 584–596. DOI: 10.1007/s12640-018-9915-1.

Periasamy, Muthu; Kalyanasundaram, Anuradha (2007): SERCA pump isoforms: their role in calcium transport and disease. In *Muscle & nerve* 35 (4), pp. 430–442. DOI: 10.1002/mus.20745.

Petersen, Ole H.; Tepikin, Alexei V. (2008): Polarized calcium signaling in exocrine gland cells. In *Annual review of physiology* 70, pp. 273–299. DOI: 10.1146/annurev.physiol.70.113006.100618.

Porter Moore, C.; Zhang, J. Z.; Hamilton, S. L. (1999): A role for cysteine 3635 of RYR1 in redox modulation and calmodulin binding. In *The Journal of biological chemistry* 274 (52), pp. 36831–36834. DOI: 10.1074/jbc.274.52.36831.

Portereiko, M. F.; Mango, S. E. (2001): Early morphogenesis of the Caenorhabditis elegans pharynx. In *Developmental Biology* 233 (2), pp. 482–494. DOI: 10.1006/DBIO.2001.0235.

Primer designing tool (2021). Available online at https://www.ncbi.nlm.nih.gov/tools/primer-blast/, updated on 1/22/2021, checked on 1/22/2021.

Pudasaini, Ashutosh; El-Arab, Kaley K.; Zoltowski, Brian D. (2015): LOV-based optogenetic devices: light-driven modules to impart photoregulated control of cellular signaling. In *Frontiers in molecular biosciences* 2, p. 18. DOI: 10.3389/fmolb.2015.00018.

Pukkila-Worley, Read; Ausubel, Frederick M. (2012): Immune defense mechanisms in the Caenorhabditis elegans intestinal epithelium. In *Current Opinion in Immunology* 24 (1), pp. 3–9. DOI: 10.1016/j.coi.2011.10.004.

Purcell, Erin B.; Siegal-Gaskins, Dan; Rawling, David C.; Fiebig, Aretha; Crosson, Sean (2007): A photosensory two-component system regulates bacterial cell attachment. In *PNAS* 104 (46), pp. 18241–18246. DOI: 10.1073/pnas.0705887104.

R. Bodmer (1993): The gene tinman is required for specification of the heart and visceral muscles in Drosophila. In *Development*. Available online at https://www.semanticscholar.org/paper/4b5822f94788e9b20c7802a0e82d9fc35b674ad3.

Raizen, David M.; Avery, Leon (1994): Electrical activity and behavior in the pharynx of caenorhabditis elegans. In *Neuron* 12 (3), pp. 483–495. DOI: 10.1016/0896-6273(94)90207-0.

Raizen, David M.; Zimmerman, John E.; Maycock, Matthew H.; Ta, Uyen D.; You, Young-jai; Sundaram, Meera V.; Pack, Allan I. (2008): Lethargus is a Caenorhabditis elegans sleep-like state. In *Nature* 451 (7178), pp. 569–572. DOI: 10.1038/nature06535.

Ramos-Franco, J.; Galvan, D.; Mignery, G. A.; Fill, M. (1999): Location of the permeation pathway in the recombinant type 1 inositol 1,4,5-trisphosphate receptor. In *Journal of General Physiology* 114 (2), pp. 243–250. DOI: 10.1085/jgp.114.2.243.

Richmond, J. E.; Jorgensen, E. M. (1999): One GABA and two acetylcholine receptors function at the C. elegans neuromuscular junction. In *Nature neuroscience* 2 (9), pp. 791–797. DOI: 10.1038/12160.

Silke Rickert-Sperling, Robert G. Kelly, David J. Driscoll (2016): Congenital Heart Diseases: The Broken Heart | ISBN 978-3-7091-1882-5.

Riddle, Donald L. (1997a): C. elegans II. Genetic and Environmental Regulation of Dauer Larva Development. 2nd. Edited by Donald L. Riddle, Thomas Blumenthal, Barbara J. Meyer, James R. Priess. Cold Spring Harbor NY: Cold Spring Harbor Laboratory Press (Cold Spring Harbor monograph series).

Riddle, Donald L. (1997b): C. elegans II. Muscle: Structure, Function, and Development. 2nd. Edited by Donald L. Riddle, Thomas Blumenthal, Barbara J. Meyer, James R. Priess. Cold Spring Harbor NY: Cold Spring Harbor Laboratory Press (Cold Spring Harbor monograph series).

Ritter, Eglof; Stehfest, Katja; Berndt, Andre; Hegemann, Peter; Bartl, Franz J. (2008): Monitoring light-induced structural changes of Channelrhodopsin-2 by UV-visible and Fourier transform infrared spectroscopy. In *The Journal of biological chemistry* 283 (50), pp. 35033–35041. DOI: 10.1074/jbc.M806353200.

Robert H. Waterston (1988): 10 Muscle | Waterston | Cold Spring Harbor Monograph Archive. Cold Spring Harbor Monograph Archive. Available online at http://cshmonographs.org/index.php/monographs/article/view/5025, updated on 3/1/2021, checked on 3/1/2021.

Roderick, H.Llewelyn; Berridge, Michael J.; Bootman, Martin D. (2003): Calcium-induced calcium release. In *Current biology : CB* 13 (11), R425. DOI: 10.1016/S0960-9822(03)00358-0.

Rodney, G. G.; Williams, B. Y.; Strasburg, G. M.; Beckingham, K.; Hamilton, S. L. (2000): Regulation of RYR1 activity by Ca(2+) and calmodulin. In *Biochemistry* 39 (26), pp. 7807–7812. DOI: 10.1021/BI0005660.

Ruffin, Vernon A.; Salameh, Ahlam I.; Boron, Walter F.; Parker, Mark D. (2014): Intracellular pH regulation by acid-base transporters in mammalian neurons. In *Frontiers in physiology* 5, p. 43. DOI: 10.3389/fphys.2014.00043.

Sabbadini, R. A.; Betto, R.; Teresi, A.; Fachechi-Cassano, G.; Salviati, G. (1992): The effects of sphingosine on sarcoplasmic reticulum membrane calcium release. In *The Journal of biological chemistry* 267 (22), pp. 15475–15484. DOI: 10.1016/s0021-9258(19)49559-8.

Salkoff, L.; Wei, A. D.; Baban, B.; Butler, A.; Fawcett, G.; Ferreira, G.; Santi, C. M. (2005): Potassium channels in C. elegans. In *Wormbook*, pp. 1–15. DOI: 10.1895/WORMBOOK.1.42.1.

Salomon, M.; Christie, J. M.; Knieb, E.; Lempert, U.; Briggs, W. R. (2000): Photochemical and mutational analysis of the FMN-binding domains of the plant blue light receptor, phototropin. In *Biochemistry* 39 (31), pp. 9401–9410. DOI: 10.1021/bi000585.

Samsó, Montserrat; Feng, Wei; Pessah, Isaac N.; Allen, P. D. (2009): Coordinated movement of cytoplasmic and transmembrane domains of RyR1 upon gating. In *PLoS biology* 7 (4), e85. DOI: 10.1371/journal.pbio.1000085.

Samsó, Montserrat; Wagenknecht, Terence; Allen, P. D. (2005): Internal structure and visualization of transmembrane domains of the RyR1 calcium release channel by cryo-EM. In *Nature Structural & Molecular Biology* 12 (6), pp. 539–544. DOI: 10.1038/nsmb938.

Sanderson, Michael J.; Delmotte, Philippe; Bai, Yan; Perez-Zogbhi, Jose F. (2008): Regulation of airway smooth muscle cell contractility by Ca2+ signaling and sensitivity. In *Proceedings of the American Thoracic Society* 5 (1), pp. 23–31. DOI: 10.1513/pats.200704-050VS.

Sayers, L. G.; Miyawaki, A.; Muto, A.; Takeshita, H.; Yamamoto, A.; Michikawa, T. et al. (1997): Intracellular targeting and homotetramer formation of a truncated inositol 1,4,5-trisphosphate receptor-green fluorescent protein chimera in Xenopus laevis oocytes: evidence for the involvement of the transmembrane spanning domain in endoplasmic reticulum targeting and homotetramer complex formation. In *The Biochemical journal* 323 (Pt 1), pp. 273–280. DOI: 10.1042/bj3230273.

Schafer, William R. (2002): Genetic analysis of nicotinic signaling in worms and flies. In *Journal of Neurobiology* 53 (4), pp. 535–541. DOI: 10.1002/neu.10154.

Scheuner, M. T. (2001): Genetic predisposition to coronary artery disease. In *Current opinion in cardiology* 16 (4), pp. 251–260. DOI: 10.1097/00001573-200107000-00006.

Schneider, Franziska; Gradmann, Dietrich; Hegemann, Peter (2013): Ion selectivity and competition in channelrhodopsins. In *Biophysical Journal* 105 (1), pp. 91–100. DOI: 10.1016/j.bpj.2013.05.042.

Schneider, Franziska; Grimm, Christiane; Hegemann, Peter (2015): Biophysics of Channelrhodopsin. In *Annual review of biophysics* 44, pp. 167–186. DOI: 10.1146/annurev-biophys-060414-034014.

Schober, Tilmann; Huke, Sabine; Venkataraman, Raghav; Gryshchenko, Oleksiy; Kryshtal, Dmytro; Hwang, Hyun Seok et al. (2012): Myofilament Ca sensitization increases cytosolic Ca binding affinity, alters intracellular Ca homeostasis, and causes pause-dependent Ca-triggered arrhythmia. In *Circulation research* 111 (2), pp. 170–179. DOI: 10.1161/CIRCRESAHA.112.270041.

Scholz, Nicole; Guan, Chonglin; Nieberler, Matthias; Grotemeyer, Alexander; Maiellaro, Isabella; Gao, Shiqiang et al. (2017): Mechano-dependent signaling by Latrophilin/CIRL quenches cAMP in proprioceptive neurons. In *eLife* 6. DOI: 10.7554/eLife.28360.

Schüler, Christina; Fischer, Elisabeth; Shaltiel, Lior; Steuer Costa, Wagner; Gottschalk, Alexander (2016): Arrhythmogenic effects of mutated L-type Ca 2+-channels on an optogenetically paced muscular pump in Caenorhabditis elegans. Frankfurt am Main: Universitätsbibliothek Johann Christian Senckenberg.

Schwerdtfeger, C.; Linden, H. (2001): Blue light adaptation and desensitization of light signal transduction in Neurospora crassa. In *Molecular Microbiology* 39 (4), pp. 1080–1087. DOI: 10.1046/j.1365-2958.2001.02306.x.

SE Lehnart (2008): Lehnart, S. E. et al. Leaky Ca2+release channel/ryanodine receptor 2 causes seizures and sudden cardiac death in mice. J. Clin. Invest. 118, 2230–2245 (2008). In *J. Clin. Invest.* 118, p. 2230.

Sedej, Simon; Heinzel, Frank R.; Walther, Stefanie; Dybkova, Nataliya; Wakula, Paulina; Groborz, Jan et al. (2010): Na+-dependent SR Ca2+ overload induces arrhythmogenic events in mouse cardiomyocytes with a human CPVT mutation. In *Cardiovascular research* 87 (1), pp. 50–59. DOI: 10.1093/cvr/cvq007.

Serobyan, Vahan; Kontarakis, Zacharias; El-Brolosy, Mohamed A.; Welker, Jordan M.; Tolstenkov, Oleg; Saadeldein, Amr M. et al. (2020): Transcriptional adaptation in Caenorhabditis elegans. In *eLife* 9. DOI: 10.7554/eLife.50014.

Sham, J. S.; Song, L. S.; Chen, Y.; Deng, L. H.; Stern, M. D.; Lakatta, E. G.; Cheng, H. (1998): Termination of Ca2+ release by a local inactivation of ryanodine receptors in cardiac myocytes. In *Proceedings of the National Academy of Sciences of the United States of America* 95 (25), pp. 15096–15101. DOI: 10.1073/pnas.95.25.15096.

Sharma, Adrian K.; Spudich, John L.; Doolittle, W. Ford (2006): Microbial rhodopsins: functional versatility and genetic mobility. In *Trends in Microbiology* 14 (11), pp. 463–469. DOI: 10.1016/j.tim.2006.09.006.

Shimano, T.; Fyk-Kolodziej, B.; Mirza, N.; Asako, M.; Tomoda, K.; Bledsoe, S. et al. (2013): Assessment of the AAV-mediated expression of channelrhodopsin-2 and halorhodopsin in brainstem neurons mediating auditory signaling. In *Brain Research* 1511, pp. 138–152. DOI: 10.1016/j.brainres.2012.10.030.

Shtonda, Boris; Avery, Leon (2005): CCA-1, EGL-19 and EXP-2 currents shape action potentials in the Caenorhabditis elegans pharynx. In *The Journal of experimental biology* 208 (Pt 11), pp. 2177–2190. DOI: 10.1242/jeb.01615.

Shyr, Zeenat A.; Wang, Zhiyu; York, Nathaniel W.; Nichols, Colin G.; Remedi, Maria S. (2019): The role of membrane excitability in pancreatic β-cell glucotoxicity. In *Sci Rep* 9 (1), p. 6952. DOI: 10.1038/s41598-019-43452-8.

Simpson, Peter B.; John Challiss, R. A.; Nahorski, Stefan R. (1995): Neuronal Ca2+ stores: activation and function. In *Trends in Neurosciences* 18 (7), pp. 299–306. DOI: 10.1016/0166-2236(95)93919-O.

Sineshchekov, Oleg A.; Govorunova, Elena G.; Jung, Kwang-Hwan; Zauner, Stefan; Maier, Uwe-G; Spudich, John L. (2005): Rhodopsin-mediated photoreception in cryptophyte flagellates. In *Biophysical Journal* 89 (6), pp. 4310–4319. DOI: 10.1529/biophysj.105.070920.

Sineshchekov, Oleg A.; Govorunova, Elena G.; Wang, Jihong; Li, Hai; Spudich, John L. (2013): Intramolecular proton transfer in channelrhodopsins. In *Biophysical Journal* 104 (4), pp. 807–817. DOI: 10.1016/j.bpj.2013.01.002.

Sineshchekov, Oleg A.; Jung, Kwang-Hwan; Spudich, John L. (2002): Two rhodopsins mediate phototaxis to low- and high-intensity light in Chlamydomonas reinhardtii. In *Proceedings of the National Academy of Sciences of the United States of America* 99 (13), pp. 8689–8694. DOI: 10.1073/pnas.122243399.

Smith, Ian F.; Hitt, Brian; Green, Kim N.; Oddo, Salvatore; LaFerla, Frank M. (2005): Enhanced caffeine-induced Ca2+ release in the 3xTg-AD mouse model of Alzheimer's disease. In *Journal of neurochemistry* 94 (6), pp. 1711–1718. DOI: 10.1111/j.1471-4159.2005.03332.x.

Smith, J. S.; Coronado, R.; Meissner, G. (1986): Single channel measurements of the calcium release channel from skeletal muscle sarcoplasmic reticulum. Activation by Ca2+ and ATP and modulation by Mg2+. In *Journal of General Physiology* 88 (5), pp. 573–588. DOI: 10.1085/JGP.88.5.573.

Somers, David E.; Schultz, Thomas F.; Milnamow, Maureen; Kay, Steve A. (2000): ZEITLUPE Encodes a Novel Clock-Associated PAS Protein from Arabidopsis. In *Cell* 101 (3), pp. 319–329. DOI: 10.1016/S0092-8674(00)80841-7.

Song, Bo-mi; Avery, Leon (2012): Serotonin activates overall feeding by activating two separate neural pathways in Caenorhabditis elegans. In *J. Neurosci.* 32 (6), pp. 1920–1931. DOI: 10.1523/JNEUROSCI.2064-11.2012.

Song, Bo-mi; Avery, Leon (2013): The pharynx of the nematode C. elegans: A model system for the study of motor control. In *Worm* 2 (1), e21833. DOI: 10.4161/worm.21833.

Song, Ziguo; Wang, Yu; Zhang, Fei; Yao, Fangyao; Sun, Chao (2019): Calcium Signaling Pathways: Key Pathways in the Regulation of Obesity. In *International Journal of Molecular Sciences* 20 (11). DOI: 10.3390/ijms20112768.

Starich, T. A.; Lee, R. Y.; Panzarella, C.; Avery, L.; Shaw, J. E. (1996): eat-5 and unc-7 represent a multigene family in Caenorhabditis elegans involved in cell-cell coupling. In *The Journal of Cell Biology* 134 (2), pp. 537–548. DOI: 10.1083/JCB.134.2.537.

Starich, Todd A.; Miller, Agnes; Nguyen, Rachel L.; Hall, David H.; Shaw, Jocelyn E. (2003): The caenorhabditis elegans innexin INX-3 is localized to gap junctions and is essential for embryonic development. In *Developmental Biology* 256 (2), pp. 403–417. DOI: 10.1016/S0012-1606(02)00116-1.

Steger, Katherine A.; Avery, Leon (2004): The GAR-3 muscarinic receptor cooperates with calcium signals to regulate muscle contraction in the Caenorhabditis elegans pharynx. In *Genetics* 167 (2), pp. 633–643. DOI: 10.1534/GENETICS.103.020230.

Stetina, Stephen E. von; Treinin, Millet; Miller, David M. (2005): The Motor Circuit: Elsevier (International Review of Neurobiology, 69), pp. 125–167.

Steuer Costa, Wagner (2016): Neuropeptidergic control of synaptic vesicle filling and behavior in the nematode "Caenorhabditis elegans". Available online at http://publikationen.ub.uni-frankfurt.de/frontdoor/index/index/year/2017/docId/44507.

Stewart, Andrew D.; Phillips, Patrick C. (2002): Selection and maintenance of androdioecy in Caenorhabditis elegans. In *Genetics* 160 (3), pp. 975–982.

Stinchcomb, D. T.; Shaw, J. E.; Carr, S. H.; Hirsh, D. (1985): Extrachromosomal DNA transformation of Caenorhabditis elegans. In *Molecular and Cellular Biology* 5 (12), pp. 3484–3496. DOI: 10.1128/mcb.5.12.3484.

Sulston, J. E.; Albertson, D. G.; Thomson, J. N. (1980): The Caenorhabditis elegans male: Postembryonic development of nongonadal structures. In *Developmental Biology* 78 (2), pp. 542–576. DOI: 10.1016/0012-1606(80)90352-8.

Sulston, J. E.; Horvitz, H. R. (1977): Post-embryonic cell lineages of the nematode, Caenorhabditis elegans. In *Developmental Biology* 56 (1), pp. 110–156. DOI: 10.1016/0012-1606(77)90158-0.

Sulston, J. E.; Schierenberg, E.; White, J. G.; Thomson, J. N. (1983): The embryonic cell lineage of the nematode Caenorhabditis elegans. In *Developmental Biology* 100 (1), pp. 64–119. DOI: 10.1016/0012-1606(83)90201-4.

Suzuki, Takeshi; Yamasaki, Kenta; Fujita, Satoshi; Oda, Kazushi; Iseki, Mineo; Yoshida, Kazuichi et al. (2003): Archaeal-type rhodopsins in Chlamydomonas: model structure and intracellular localization. In *Biochemical and biophysical research communications* 301 (3), pp. 711–717. DOI: 10.1016/S0006-291X(02)03079-6.

Swartz, T. E.; Corchnoy, S. B.; Christie, J. M.; Lewis, J. W.; Szundi, I.; Briggs, W. R.; Bogomolni, R. A. (2001): The photocycle of a flavin-binding domain of the blue light photoreceptor phototropin. In *The Journal of biological chemistry* 276 (39), pp. 36493–36500. DOI: 10.1074/jbc.M103114200.

Swartz, Trevor E.; Tseng, Tong-Seung; Frederickson, Marcus A.; Paris, Gastón; Comerci, Diego J.; Rajashekara, Gireesh et al. (2007): Blue-light-activated histidine kinases: two-component sensors in bacteria. In *Science* 317 (5841), pp. 1090–1093. DOI: 10.1126/science.1144306.

Sweeney, H. Lee; Houdusse, Anne (2010): Structural and functional insights into the Myosin motor mechanism. In *Annual review of biophysics* 39, pp. 539–557. DOI: 10.1146/annurev.biophys.050708.133751.

Takahashi, Fumio; Yamagata, Daisuke; Ishikawa, Mié; Fukamatsu, Yosuke; Ogura, Yasunobu; Kasahara, Masahiro et al. (2007): AUREOCHROME, a photoreceptor required for photomorphogenesis in stramenopiles. In *PNAS* 104 (49), pp. 19625–19630. DOI: 10.1073/pnas.0707692104.

Takayama, Yuki; Nakasako, Masayoshi; Okajima, Koji; Iwata, Aya; Kashojiya, Sachiko; Matsui, Yuka; Tokutomi, Satoru (2011): Light-induced movement of the LOV2 domain in an Asp720Asn mutant LOV2-kinase fragment of Arabidopsis phototropin 2. In *Biochemistry* 50 (7), pp. 1174–1183. DOI: 10.1021/bi101689b.

Tanabe, T.; Beam, K. G.; Adams, B. A.; Niidome, T.; Numa, S. (1990): Regions of the skeletal muscle dihydropyridine receptor critical for excitation-contraction coupling. In *Nature* 346 (6284), pp. 567–569. DOI: 10.1038/346567A0.

Tanimoto, Yuki; Yamazoe-Umemoto, Akiko; Fujita, Kosuke; Kawazoe, Yuya; Miyanishi, Yosuke; Yamazaki, Shuhei J. et al. (2017): Calcium dynamics regulating the timing of decision-making in C. elegans. In *eLife* 6. DOI: 10.7554/eLife.21629.

Taylor, Barry L.; Zhulin, Igor B. (1999): PAS Domains: Internal Sensors of Oxygen, Redox Potential, and Light. In *Microbiol. Mol. Biol. Rev.* 63 (2), pp. 479–506. DOI: 10.1128/MMBR.63.2.479-506.1999.

Taylor, C. W.; Genazzani, A. A.; Morris, S. A. (1999): Expression of inositol trisphosphate receptors. In *Cell Calcium* 26 (6), pp. 237–251. DOI: 10.1054/ceca.1999.0090.

Teotónio, Henrique; Manoel, Diogo; Phillips, Patrick C. (2006): Genetic variation for outcrossing among Caenorhabditis elegans isolates. In *Evolution; international journal of organic evolution* 60 (6), pp. 1300–1305.

Terentyev, Dmitry; Cala, Steven E.; Houle, Timothy D.; Viatchenko-Karpinski, Serge; Gyorke, Inna; Terentyeva, Radmila et al. (2005): Triadin overexpression stimulates excitation-contraction coupling and increases predisposition to cellular arrhythmia in cardiac myocytes. In *Circulation research* 96 (6), pp. 651–658. DOI: 10.1161/01.RES.0000160609.98948.25.

The C. elegans Sequencing Consortium (1998): Genome sequence of the nematode C. elegans: a platform for investigating biology. In *Science (New York, N.Y.)* 282 (5396), pp. 2012–2018. DOI: 10.1126/science.282.5396.2012.

Timerman, A. P.; Onoue, H.; Xin, H. B.; Barg, S.; Copello, J.; Wiederrecht, G.; Fleischer, S. (1996): Selective binding of FKBP12.6 by the cardiac ryanodine receptor. In *The Journal of biological chemistry* 271 (34), pp. 20385–20391. DOI: 10.1074/jbc.271.34.20385.

Towers, Paula R.; Edwards, Ben; Richmond, Janet E.; Sattelle, David B. (2005): The Caenorhabditis elegans lev-8 gene encodes a novel type of nicotinic acetylcholine receptor alpha subunit. In *Journal of neurochemistry* 93 (1), pp. 1–9. DOI: 10.1111/j.1471-4159.2004.02951.x.

Toyoshima, C.; Iwasawa, S.; Ogawa, H.; Hirata, A.; Tsueda, J.; Inesi, G. (2013): Crystal structure of the calcium pump and sarcolipin from rabbit fast twitch skeletal muscle in the E1.Mg2+ state.

Toyoshima, Chikashi (2009): How Ca2+-ATPase pumps ions across the sarcoplasmic reticulum membrane. In *Biochimica et biophysica acta* 1793 (6), pp. 941–946. DOI: 10.1016/j.bbamcr.2008.10.008.

Toyoshima, Chikashi; Cornelius, Flemming (2013): New crystal structures of PII-type ATPases: excitement continues. In *Current Opinion in Structural Biology* 23 (4), pp. 507–514. DOI: 10.1016/j.sbi.2013.06.005.

Toyoshima, Chikashi; Mizutani, Tatsuaki (2004): Crystal structure of the calcium pump with a bound ATP analogue. In *Nature* 430 (6999), pp. 529–535. DOI: 10.1038/nature02680.

Toyoshima, Chikashi; Nomura, Hiromi (2002): Structural changes in the calcium pump accompanying the dissociation of calcium. In *Nature* 418 (6898), pp. 605–611. DOI: 10.1038/nature00944.

Tripathy, A.; Xu, L.; Mann, G.; Meissner, G. (1995): Calmodulin activation and inhibition of skeletal muscle Ca2+ release channel (ryanodine receptor). In *Biophysical Journal* 69 (1), pp. 106–119. DOI: 10.1016/S0006-3495(95)79880-0.

Troemel, Emily R.; Félix, Marie-Anne; Whiteman, Noah K.; Barrière, Antoine; Ausubel, Frederick M. (2008): Microsporidia are natural intracellular parasites of the nematode Caenorhabditis elegans. In *PLoS biology* 6 (12), pp. 2736–2752. DOI: 10.1371/journal.pbio.0060309.

Trojanowski, Nicholas F.; Fang-Yen, Christopher (2015): Simultaneous Optogenetic Stimulation of Individual Pharyngeal Neurons and Monitoring of Feeding Behavior in Intact C. elegans. In *Methods in molecular biology (Clifton, N.J.)* 1327, pp. 105–119. DOI: 10.1007/978-1-4939-2842-2_9.

Tsechpenakis, Gabriel; Bianchi, Laura; Metaxas, Dimitris; Driscoll, Monica (2008): A novel computational approach for simultaneous tracking and feature extraction of C. elegans populations in fluid environments. In *IEEE transactions on bio-medical engineering* 55 (5), pp. 1539–1549. DOI: 10.1109/TBME.2008.918582.

van Petegem, Filip (2016): How to open a Ryanodine Receptor. In *Cell research* 26 (10), pp. 1073–1074. DOI: 10.1038/cr.2016.106.

Vandecaetsbeek, Ilse; Vangheluwe, Peter; Raeymaekers, Luc; Wuytack, Frank; Vanoevelen, Jo (2011): The Ca2+ pumps of the endoplasmic reticulum and Golgi apparatus. In *Cold Spring Harbor perspectives in biology* 3 (5). DOI: 10.1101/cshperspect.a004184.

Venetucci, Luigi; Denegri, Marco; Napolitano, Carlo; Priori, Silvia G. (2012): Inherited calcium channelopathies in the pathophysiology of arrhythmias. In *Nature Reviews Cardiology* 9 (10), pp. 561–575. DOI: 10.1038/nrcardio.2012.93.

Verboomen, H.; Wuytack, F.; Smedt, H. de; Himpens, B.; Casteels, R. (1992): Functional difference between SERCA2a and SERCA2b Ca2+ pumps and their modulation by phospholamban. In *The Biochemical journal* 286 (Pt 2) (2), pp. 591–595. DOI: 10.1042/bj2860591.

Voermans, N. C.; Laan, A. E.; Oosterhof, A.; van Kuppevelt, T. H.; Drost, G.; Lammens, M. et al. (2012): Brody syndrome: a clinically heterogeneous entity distinct from Brody disease: a review of literature and a cross-sectional clinical study in 17 patients. In *Neuromuscular disorders : NMD* 22 (11), pp. 944–954. DOI: 10.1016/j.nmd.2012.03.012.

W. Wood (1988): The Nematode Caenorhabditis elegans. Available online at https://www.semanticscholar.org/paper/2003f25a0e33e4f575d899d41078218fa3c6416a.

Wang, Hongxia; Sugiyama, Yuka; Hikima, Takuya; Sugano, Eriko; Tomita, Hiroshi; Takahashi, Tetsuo et al. (2009): Molecular determinants differentiating photocurrent properties of two channelrhodopsins from chlamydomonas. In *The Journal of biological chemistry* 284 (9), pp. 5685–5696. DOI: 10.1074/jbc.M807632200.

Wang, J.; Best, P. M. (1992): Inactivation of the sarcoplasmic reticulum calcium channel by protein kinase. In *Nature* 359 (6397), pp. 739–741. DOI: 10.1038/359739A0.

Ward, Alex; Liu, Jie; Feng, Zhaoyang; Xu, X. Z. Shawn (2008): Light-sensitive neurons and channels mediate phototaxis in C. elegans. In *Nature neuroscience* 11 (8), pp. 916–922. DOI: 10.1038/nn.2155.

Watson, H., 2015. Biological membranes. Essays Biochem. 59, 43–69. https://doi.org/10.1042/bse0590043

Wayne, Randy (1993): Excitability in Plant Cells. In *American Scientist* 81 (2), pp. 140–149.

Wei, Risheng; Wang, Xue; Zhang, Yan; Mukherjee, Saptarshi; Zhang, Lei; Chen, Qiang et al. (2016): Structural insights into Ca(2+)-activated long-range allosteric channel gating of RyR1. In *Cell research* 26 (9), pp. 977–994. DOI: 10.1038/cr.2016.99.

Weissenberger, Simone; Schultheis, Christian; Liewald, Jana Fiona; Erbguth, Karen; Nagel, Georg; Gottschalk, Alexander (2011): PACalpha--an optogenetic tool for in vivo manipulation of cellular cAMP levels, neurotransmitter release, and behavior in Caenorhabditis elegans. In *Journal of neurochemistry* 116 (4), pp. 616–625. DOI: 10.1111/j.1471-4159.2010.07148.x.

Wen, Lei; Wang, Hongxia; Tanimoto, Saki; Egawa, Ryo; Matsuzaka, Yoshiya; Mushiake, Hajime et al. (2010): Opto-current-clamp actuation of cortical neurons using a strategically designed channelrhodopsin. In *PLoS ONE* 5 (9), e12893. DOI: 10.1371/journal.pone.0012893.

White (1986): The structure of the nervous system of the nematode Caenorhabditis elegans. In *Phil Trans Roy Soc Lond* 314, p. 1.

White, J. G.; Southgate, E.; Thomson, J. N.; Brenner, S. (1976): The structure of the ventral nerve cord of Caenorhabditis elegans. In *Philosophical transactions of the Royal Society of London. Series B, Biological sciences* 275 (938), pp. 327–348. DOI: 10.1098/rstb.1976.0086.

White, J. G.; Southgate, E.; Thomson, J. N.; Brenner, S. (1986): The structure of the nervous system of the nematode Caenorhabditis elegans. In *Philosophical transactions of the Royal Society of London. Series B, Biological sciences* 314 (1165), pp. 1–340. DOI: 10.1098/RSTB.1986.0056.

Williams, A. J.; West, D. J.; Sitsapesan, R. (2001): Light at the end of the Ca(2+)-release channel tunnel: structures and mechanisms involved in ion translocation in ryanodine receptor channels. In *Quarterly reviews of biophysics* 34 (1), pp. 61–104. DOI: 10.1017/s0033583501003675.

Wu, K. D.; Lee, W. S.; Wey, J.; Bungard, D.; Lytton, J. (1995): Localization and quantification of endoplasmic reticulum Ca(2+)-ATPase isoform transcripts. In *The American journal of physiology* 269 (3 Pt 1), C775-84. DOI: 10.1152/ajpcell.1995.269.3.C775.

Wu, Xu; Bers, Donald M. (2006): Sarcoplasmic reticulum and nuclear envelope are one highly interconnected Ca2+ store throughout cardiac myocyte. In *Circulation research* 99 (3), pp. 283–291. DOI: 10.1161/01.RES.0000233386.02708.72.

Xiao, Bailong; Masumiya, Haruko; Jiang, Dawei; Wang, Ruiwu; Sei, Yoshitatsu; Zhang, Lin et al. (2002): Isoform-dependent formation of heteromeric Ca2+ release channels (ryanodine receptors). In *The Journal of biological chemistry* 277 (44), pp. 41778–41785. DOI: 10.1074/jbc.M208210200.

Xu, Lizhi; Gutbrod, Sarah R.; Bonifas, Andrew P.; Su, Yewang; Sulkin, Matthew S.; Lu, Nanshu et al. (2014): 3D multifunctional integumentary membranes for spatiotemporal cardiac measurements and stimulation across the entire epicardium. In *Nat Commun* 5 (1), p. 3329. DOI: 10.1038/ncomms4329.

Yan, Zhen; Bai, Xiaochen; Yan, Chuangye; Wu, Jianping; Li, Zhangqiang; Xie, Tian et al. (2015): Structure of the rabbit ryanodine receptor RyR1 at near-atomic resolution. In *Nature* 517 (7532), pp. 50–55. DOI: 10.1038/nature14063.

Yang, H. C.; Reedy, M. M.; Burke, C. L.; Strasburg, G. M. (1994): Calmodulin interaction with the skeletal muscle sarcoplasmic reticulum calcium channel protein. In *Biochemistry* 33 (2), pp. 518–525. DOI: 10.1021/BI00168A017.

Yao, X.; Pérez-Alvarado, G. C.; Louis, H. A.; Pomiès, P.; Hatt, C.; Summers, M. F.; Beckerle, M. C. (1999): Solution structure of the chicken cysteine-rich protein, CRP1, a double-LIM protein implicated in muscle differentiation. In *Biochemistry* 38 (18), pp. 5701–5713. DOI: 10.1021/bi982036y.

Yao, Xiaolan; Rosen, Michael K.; Gardner, Kevin H. (2008): Estimation of the available free energy in a LOV2-J alpha photoswitch. In *Nature chemical biology* 4 (8), pp. 491–497. DOI: 10.1038/nchembio.99.

Yizhar, Ofer; Fenno, Lief E.; Prigge, Matthias; Schneider, Franziska; Davidson, Thomas J.; O'Shea, Daniel J. et al. (2011): Neocortical excitation/inhibition balance in information processing and social dysfunction. In *Nature* 477 (7363), pp. 171–178. DOI: 10.1038/nature10360.

Young, E. F.; McKee, M. J.; Ferguson, D. G.; Kranias, E. G. (1989): Structural characterization of phospholamban in cardiac sarcoplasmic reticulum membranes by cross-linking. In *Membrane biochemistry* 8 (2), pp. 95–106. DOI: 10.3109/09687688909082263.

Yu, X.; Carroll, S.; Rigaud, J. L.; Inesi, G. (1993): H+ countertransport and electrogenicity of the sarcoplasmic reticulum Ca2+ pump in reconstituted proteoliposomes. In *Biophysical Journal* 64 (4), pp. 1232–1242. DOI: 10.1016/S0006-3495(93)81489-9.

Yue, Xiaomin; Zhao, Jian; Li, Xiao; Fan, Yuedan; Duan, Duo; Zhang, Xiaoyan et al. (2018): TMC Proteins Modulate Egg Laying and Membrane Excitability through a Background Leak Conductance in C. elegans. In *Neuron* 97 (3), 571-585.e5. DOI: 10.1016/j.neuron.2017.12.041.

Zafar, Sufi; Hussain, Arif; Liu, Yueyong; Lewis, David; Inesi, G. (2008): Specificity of ligand binding to transport sites: Ca2+ binding to the Ca2+ transport ATPase and its dependence on H+ and Mg2+. In *Archives of Biochemistry and Biophysics* 476 (1), pp. 87–94. DOI: 10.1016/j.abb.2008.04.035.

Zalk, Ran; Clarke, Oliver B.; Des Georges, Amédée; Grassucci, Robert A.; Reiken, Steven; Mancia, Filippo et al. (2015): Structure of a mammalian ryanodine receptor. In *Nature* 517 (7532), pp. 44–49. DOI: 10.1038/nature13950.

Zalk, Ran; Lehnart, Stephan E.; Marks, Andrew R. (2007): Modulation of the ryanodine receptor and intracellular calcium. In *Annual review of biochemistry* 76, pp. 367–385. DOI: 10.1146/annurev.biochem.76.053105.094237.

Zalk, Ran; Marks, Andrew R. (2017): Ca2+ Release Channels Join the 'Resolution Revolution'. In *Trends in biochemical sciences* 42 (7), pp. 543–555. DOI: 10.1016/j.tibs.2017.04.005.

Zayner, Josiah P.; Antoniou, Chloe; Sosnick, Tobin R. (2012): The amino-terminal helix modulates light-activated conformational changes in AsLOV2. In *Journal of molecular biology* 419 (1-2), pp. 61–74. DOI: 10.1016/j.jmb.2012.02.037.

Zayner, Josiah P.; Sosnick, Tobin R. (2014): Factors that control the chemistry of the LOV domain photocycle. In *PLoS ONE* 9 (1), e87074. DOI: 10.1371/journal.pone.0087074.

Zhang, Feng; Vierock, Johannes; Yizhar, Ofer; Fenno, Lief E.; Tsunoda, Satoshi; Kianianmomeni, Arash et al. (2011): The microbial opsin family of optogenetic tools. In *Cell* 147 (7), pp. 1446–1457. DOI: 10.1016/j.cell.2011.12.004.

Zhang, Wei; Ge, Wooping; Wang, Zuoren (2007): A toolbox for light control of Drosophila behaviors through Channelrhodopsin 2-mediated photoactivation of targeted neurons. In *The European journal of neuroscience* 26 (9), pp. 2405–2416. DOI: 10.1111/j.1460-9568.2007.05862.x.

Zhao, M.; Li, P.; Li, X.; Zhang, L.; Winkfein, R. J.; Chen, S. R. (1999): Molecular identification of the ryanodine receptor pore-forming segment. In *The Journal of biological chemistry* 274 (37), pp. 25971–25974. DOI: 10.1074/jbc.274.37.25971.

Zhu, Li; Zhong, Xiaowei; Chen, S. R. Wayne; Banavali, Nilesh; Liu, Zheng (2013): Modeling a ryanodine receptor N-terminal domain connecting the central vestibule and the corner clamp region. In *The Journal of biological chemistry* 288 (2), pp. 903–914. DOI: 10.1074/jbc.M112.429670.

Zuker, C. S. (1996): The biology of vision of Drosophila. In *Proceedings of the National Academy of Sciences of the United States of America* 93 (2), pp. 571–576. DOI: 10.1073/pnas.93.2.571.

Zwaal, R. R.; van Baelen, K.; Groenen, J. T.; van Geel, A.; Rottiers, V.; Kaletta, T. et al. (2001): The sarco-endoplasmic reticulum Ca2+ ATPase is required for development and muscle function in Caenorhabditis elegans. In *The Journal of biological chemistry* 276 (47), pp. 43557–43563. DOI: 10.1074/jbc.M104693200.

Appendix

A. Acronyms

Acronym	Name
A	anterior
ACh	acetylcholine
AChE	acetylcholinesterase
AChT	acetylcholine transporter
ACR	anion channelrhodopsin
AMP	adenosine-monophosphate
ATP	adenosine-5‘-triphosphate
ATR	all-trans retinal
bbpm	body bends per min
BLAST	basic local alignment search
BLUF	blue light using FAD
BSA	Bovine Serum Albumin
C. elegans	*Caenorhabditis elegans*
Ca^{2+}	calcium
CAPS	calcium-activated protein for secretion
CatCh	calcium translocating ChR2
CatChUP	calcium translocating ChR2 UP
CDL	long, original central domain
CeRyR	Caenorhabditis elegans Rynodine receptor
CFP	cyan fluorescent proteins
ChloC	chloride conducting ChR
ChR	channelrhodopsin
ChRGR	Channel rhodopsin green receiver
ChRGR(ER)	Channel rhodopsin green receiver in the endoplasmatic reticulum
CRISPR/Cas9	Clustered Regularly Interspaced Short Palindromic Repeats / cas-Operon
D	dorsal
ddH_2O	double deionized water
DMSO	dimethyl-sulfoxide
DNA	deoxyribonucleic acid
DNase	deoxyribonuclease
dNTP	deoxy-nucleotide-triphosphate
E. coli	*Escherichia coli*
EDTA	ethylene-diamine-tetra-aceticacid
ER	endoplasmatic reticulum
EtBr	ethidium bromide
EYFP	enhanced yellow fluorescent protein
FAD	falvin-adenin-denucleotide
FLP	FMRFamide-like proteins
FMN	flavin-mononucleotide
FRET	Förster resonance energy transfer

GDP	guanosine-diphosphate
GEF	nucleotide exchange factor
GFP	green fluorescent protein
GMP	guanosine-monophosphate
GPCR	G protein-coupled receptor
GRK	GPCR kinase
GTP	guanosine-triphosphate
H^+	proton
HisCl	histamine-gated chloride channel
hRyR	human Rynodine rezeptor
RyRpore	human Rynodine rezeptor reduced to the pore region
IP_3R	inositol-1,4,5-triphosphate receptor
ITR1	inositol-1,4,5-triphosphate receptor
K^+	potassium
L	lateral
LB	Lysogeny Broth
LOV	light-oxygen-voltage-sensing domain
LOV2	Light-oxygen-voltage-sensing domain 2
mCherry	red fluorescent protein
mNEON	green/yellow fluorescent protein
mRNA	messenger ribonucleic acid
mVenus	yellow fluorescent protein
MWT	Multi Worm Tracker
Na^+	sodium
NEB	New England Biolabs
NGM	Nematode Growth Medium
NMJ	neuromuscular junction
NTD	N-terminal domain
optoUNC-68	CatChUP:: EYFP::CRP-1::unc-68
P	posterior
PAM	peptidylglycine-a-amidating monooxygenase
PCA	phenol chloroform isoamyl alcohol
PCR	polymerase chain reaction
PEG	polyethylene glycol
PKA	protein kinase A
RNA	ribonucleic acid
RNAse	ribonuclease
ROI	regions of interest
RT	room temperature
RyR	Rynodine receptor
SEM	standard error of the mean
SERCA	Sarcoplasmic/endoplasmic reticulum calcium ATPase
SEWLB	Single Egg Worm Lysis Buffer
SR	Sarcoplasmic reticulum

TAE	TRIS acetate EDTA
TM	trans membrane
TRIS	tris-(hydroxymethyl)aminomethane
TRP	transient receptor (TRP)
UTR	untranslated region
UV	ultraviolet
V	ventral
v/v	volume per volume
w/v	weight per volume
XXM	ChR2 D156H mutant
YFP	yellow fluorescent protein

B. Units and prefixes

Unit	Name	Unit	Name
°C	degree Celsius	**M**	molar
c	centi	**min**	minute
g	gram	**n**	nano
h	hour	**s**	second
Hz	hertz	**U**	Unit
l	liter	**V**	Volt
µ	micro	**W**	Watt
m	milli/meter		

D. List of Figures

E. List of Tables

F. Figure and table contribution

If not stated otherwise the contribution of the author consists only in the image that has been adapted.

Figure/Name	Page	Author
Figure 1: Overview of the intracellular calcium signalling.	1	Nowycky, Martha C.; Thomas, Andrew P. (2002): Intracellular calcium signaling. In Journal of Cell Science 115 (Pt 19), pp. 3715–3716. DOI: 10.1242/jcs.00078
Figure 2: Leading causes of lost years of life in 2013.	2	Global burden of disease study & the Lancet, 2014. Matthews 2015; Global, regional, and national age–sex specific all-cause and cause-specific mortality for 240 causes of death, 1990–2013: a systematic analysis for the Global Burden of Disease Study 2013-2015. Max Roser, Hannah Ritchie and Fiona Spooner (2021) - "Burden of disease". Published online at OurWorldInData.org. Retrieved from: 'https://ourworldindata.org/burden-of-disease' [Online Resource]
Figure 3: Total burden of disease in Germany 2017, measured in Disability-Adjusted Life Years (DALYs) by sub-category of disease or injury.	2	Global Burden of Disease Collaborative Network. Global Burden of Disease Study 2019 (GBD 2019) Results. Seattle, United States: Institute for Health Metrics and Evaluation (IHME), 2021. Max Roser, Hannah Ritchie and Fiona Spooner (2021) - "Burden of disease". Published online at OurWorldInData.org. Retrieved from: 'https://ourworldindata.org/burden-of-disease' [Online Resource]
Figure 4: Adult male and life cycle of hermaphroditic C. elegans.	4	Altun, Z. F.; Hall, D. H. (2009c): Hermaphrodite - Muscle System - Somatic Muscle. With assistance of Z. F. Altun, D. H. Hall. Cold Spring Harbor Laboratory Press. WormAtlas. Available online at https://www.wormatlas.org/hermaphrodite/musclesomatic/MusSomaticframeset.html, updated on 3/11/2016, checked on 2/17/2021
Figure 5: Major anatomical features of C. elegans anatomy.	5	Corsi, Ann K.; Wightman, Bruce; Chalfie, Martin (2015): A Transparent Window into Biology: A Primer on Caenorhabditis elegans. In *Genetics* 200 (2), pp. 387–407. DOI: 10.1534/genetics.115.176099
Figure 6: Graphic of C. elegans nervous system.	6	Badhwar, Rahul; Bagler, Ganesh (2015): Control of Neuronal Network in Caenorhabditis elegans. In *PLoS ONE* 10 (9), e0139204. DOI: 10.1371/journal.pone.0139204
Figure 7: Cross section of the contractile apparatus in a body wall muscle and organization of the myofilament lattice including localisation of RyR and SERCA. .	7	Altun, Z. F.; Hall, D. H. (2009b): Handbook - Muscle System Introduction. With assistance of Altun, Z.F. and Hall, D.H. 2009. Muscle system, introduction. In WormAtlas. Edited by Wormatlas. Available online at https://www.wormatlas.org/hermaphrodite/muscleintro/mainframe.htm#Jospin2002, updated on 1/31/2018, checked on 3/1/2021

Figure/Name	Page	Author
Figure 8: Body wall muscle development.	8	Altun, Z. F.; Hall, D. H. (2009b): Handbook - Muscle System Introduction. With assistance of Altun, Z.F. and Hall, D.H. 2009. Muscle system, introduction. In WormAtlas. Edited by Wormatlas. Available online at https://www.wormatlas.org/hermaphrodite/muscleintro/mainframe.htm#Jospin2002, updated on 1/31/2018, checked on 3/1/2021
Figure 9: Body wall muscle structure.	9	Altun, Z. F.; Hall, D. H. (2009c): Hermaphrodite - Muscle System - Somatic Muscle. With assistance of Z. F. Altun, D. H. Hall. Cold Spring Harbor Laboratory Press. WormAtlas. Available online at https://www.wormatlas.org/hermaphrodite/musclesomatic/MusSomaticframeset.html, updated on 3/11/2016, checked on 2/17/2021
Figure 10: Head and pharynx of C. elegans.	10	Shtonda, Boris; Avery, Leon (2005): CCA-1, EGL-19 and EXP-2 currents shape action potentials in the Caenorhabditis elegans pharynx. In The Journal of experimental biology 208 (Pt 11), pp. 2177–2190. DOI: 10.1242/jeb.01615
Figure 11: Comparison of fluidflow of C. elegans pharynx and human heart	11	Cook, S.J., Crouse, C.M., Yemini, E., Hall, D.H., Emmons, S.W., Hobert, O., 2020. The connectome of the Caenorhabditis elegans pharynx. J. Comp. Neurol. 528, 2767–2784. https://doi.org/10.1002/cne.24932 Silke Rickert-Sperling, Robert G. Kelly, David J. Driscoll (2016): Congenital Heart Diseases: The Broken Heart | ISBN 978-3-7091-1882-5
Figure 12: Top view of the ryanodine receptor 2 (RyR2).	12	Frank Becker, Software PyMol
Figure 13: Structural transitions of the selectivity filter.	12	Wei, Risheng; Wang, Xue; Zhang, Yan; Mukherjee, Saptarshi; Zhang, Lei; Chen, Qiang et al. (2016): Structural insights into Ca(2+)-activated long-range allosteric channel gating of RyR1. In *Cell research* 26 (9), pp. 977–994. DOI: 10.1038/cr.2016.99.
Figure 14: Moving parts of ryanodine receptor 1..	13	Zalk, Ran; Marks, Andrew R. (2017): Ca2+ Release Channels Join the 'Resolution Revolution'. In Trends in biochemical sciences 42 (7), pp. 543–555. DOI: 10.1016/j.tibs.2017.04.005
Figure 15: Course of opening of the RyR.	14	Des Georges, Amédée; Clarke, Oliver B.; Zalk, Ran; Yuan, Qi; Condon, Kendall J.; Grassucci, Robert A. et al. (2016): Structural Basis for Gating and Activation of RyR1. In *Cell* 167 (1), 145-157.e17. DOI: 10.1016/j.cell.2016.08.075.
Figure 16: Crystal structure of SERCA localised in the SR-membrane.	15	Adapted from Watson, H., 2015. Biological membranes. Essays Biochem. 59, 43–69. https://doi.org/10.1042/bse0590043, edited by Frank Becker

Figure/Name	Page	Author
Figure 17: Schematic representation of the Post-Albers pumping cycle of SERCA.	16	Aguayo-Ortiz, R., Espinoza-Fonseca, L.M., 2020. Linking Biochemical and Structural States of SERCA: Achievements, Challenges, and New Opportunities. Int. J. Mol. Sci. 21, 4146. https://doi.org/10.3390/ijms21114146
Figure 18: Full intracellular Ca2+ cycle between SER/ESR and cytosol.	17	Frank Becker, Software PyMol;
Figure 19: Optogenetics of ChRGRER, RyR, IP3R and SERCA on the SR/ER-membrane.	18	Asano, Toshifumi; Igarashi, Hiroyuki; Ishizuka, Toru; Yawo, Hiromu (2018): Organelle Optogenetics: Direct Manipulation of Intracellular Ca2+ Dynamics by Light. In *Frontiers in neuroscience* 12, p. 561. DOI: 10.3389/fnins.2018.00561
Figure 20: Structure of ChR showing the 7-TM helices.	19	Zhang, Feng; Vierock, Johannes; Yizhar, Ofer; Fenno, Lief E.; Tsunoda, Satoshi; Kianianmomeni, Arash et al. (2011): The microbial opsin family of optogenetic tools. In *Cell* 147 (7), pp. 1446–1457. DOI: 10.1016/j.cell.2011.12.004
Figure 21: Light induced ChR2 pore formation.	20	Schneider, Franziska; Grimm, Christiane; Hegemann, Peter (2015): Biophysics of Channelrhodopsin. In *Annual review of biophysics* 44, pp. 167–186. DOI: 10.1146/annurev-biophys-060414-034014
Figure 22: Photocycle model of ChR2.	20	Ritter, Eglof; Stehfest, Katja; Berndt, Andre; Hegemann, Peter; Bartl, Franz J. (2008): Monitoring light-induced structural changes of Channelrhodopsin-2 by UV-visible and Fourier transform infrared spectroscopy. In *The Journal of biological chemistry* 283 (50), pp. 35033–35041. DOI: 10.1074/jbc.M806353200
Figure 23: Expression of ChR2-WT::YFP and ChR2-XXM::YFP in Xenopus oocytes and photocurrents.	21	Scholz, Nicole; Guan, Chonglin; Nieberler, Matthias; Grotemeyer, Alexander; Maiellaro, Isabella; Gao, Shiqiang et al. (2017): Mechano-dependent signaling by Latrophilin/CIRL quenches cAMP in proprioceptive neurons. In *eLife* 6. DOI: 10.7554/eLife.28360.
Figure 24: Cellular expression of ChRGRER.	22	Asano, Toshifumi; Igarashi, Hiroyuki; Ishizuka, Toru; Yawo, Hiromu (2018): Organelle Optogenetics: Direct Manipulation of Intracellular Ca2+ Dynamics by Light. In *Frontiers in neuroscience* 12, p. 561. DOI: 10.3389/fnins.2018.00561
Figure 25: Spectra of channel currents generated by PsChR	23	Govorunova, Elena G.; Sineshchekov, Oleg A.; Li, Hai; Janz, Roger; Spudich, John L. (2013): Characterization of a highly efficient blue-shifted channelrhodopsin from the marine alga Platymonas subcordiformis. In *Journal of Biological Chemistry* 288 (41), pp. 29911–29922. DOI: 10.1074/jbc.M113.505495.
Figure 26: Clusters of DHPR-RyR in cardiac muscle membranes.	24	Grabner, Manfred; Dayal, Anamika (2010): Crosstalk via the Sarcoplasmic Gap. In Irina Serysheva (Ed.): Structure and Function of Calcium Release Channels, vol. 66. 1. Aufl. s.l.: Elsevier textbooks (Current Topics in Membranes, 66), pp. 115–138

Figure/Name	Page	Author
Figure 27: AsLOV2 photocycle chemistry.	25	Zayner, Josiah P.; Sosnick, Tobin R. (2014): Factors that control the chemistry of the LOV domain photocycle. In *PLoS ONE* 9 (1), e87074. DOI: 10.1371/journal.pone.0087074
Figure 28: AsLOV2 structure and signalling.	26	Zayner, Josiah P.; Antoniou, Chloe; Sosnick, Tobin R. (2012): The amino-terminal helix modulates light-activated conformational changes in AsLOV2. In *Journal of molecular biology* 419 (1-2), pp. 61–74. DOI: 10.1016/j.jmb.2012.02.037 Herrou, Julien; Crosson, Sean (2011): Function, structure and mechanism of bacterial photosensory LOV proteins. In Nature reviews. Microbiology 9 (10), pp. 713–723. DOI: 10.1038/nrmicro2622
Figure 29: Insertion sites of LOV2 in hRyR2 pore.	27	Frank Becker, Software PyMol;
Figure 30: Plasmid map of pFB02 (pmyo3::hRyR2 short) shows the remaining domains of the truncated version of hRyR2 .	38	Frank Becker, Software SnapGene Viewer
Figure 31: Plasmid map of pFB04 (pmyo3::mNEON::hRyR2 short CDL) depicts the remaining domains of RyRpore with a long central domain.	38	Frank Becker, Software SnapGene Viewer
Figure 32: Plasmid chart of hRyR2 cDNA	39	Frank Becker, Software SnapGene Viewer
Figure 33: Top view of the chimeric RyR channels.	61	Frank Becker
Figure 34: The rescue plasmid enhances thrashing rate in deletion mutants.	61	Frank Becker, Software GraphPad Prism
Figure 35: Light stimulation increased thrashing rate of ATR supplemented transgenic animals, in relation to no stimulation.	62	Frank Becker, Software GraphPad Prism
Figure 36: ZX1967 displays simmilar swimming behaviour as lite-1 (ce314).	63	Frank Becker, Software GraphPad Prism
Figure 37: The rescue plasmid has no notable effect in lite-1 background.	63	Frank Becker, Software GraphPad Prism

Figure/Name	Page	Author
Figure 51: Blue light exposure led to contraction of all LOV2 inserted strains.	75	Frank Becker, Software GraphPad Prism
Figure 52: Localization of alternative exons in the current unc-68 gene model.	76	Wormbase ID WBGene00006801 (Dec 2020)
Figure 53: Possible expression of GOA01 in BWM and pharynx.	78	Frank Becker
Figure 54: Comparing the fluorescence of transgenic and wild type animals.	78	Frank Becker
Figure 55: Long term illumination does not reveal exceptional swimming behaviour after prolonged blue light stimulus.	79	Frank Becker, Software GraphPad Prism
Figure 56: Low light induced effects, are stronger in ATR lacking animals, and high intensity reveals a stronger effect on ATR reared animals	80	Frank Becker, Software GraphPad Prism
Figure 57: Long term illumination of lite-1 GOA01 displays a reduction of swimming cycles during photostimulation, and a further drop of thrashes after light pulse.	81	Frank Becker, Software GraphPad Prism
Figure 58: No difference between lite-1 GOA1 and ATR reared animals under photostimulation.	82	Frank Becker, Software GraphPad Prism
Figure 59: Short term periods of body elongation in GOA01 non-ATR supplemented animals alter body elongation.	83	Frank Becker, Software GraphPad Prism
Figure 60: Fluorescence image of YFP in the head and body. A) DIC image of the grinder and intestines.	85	Frank Becker
Figure 61: Intensity-dependent increase in swimming cycles was more pronounced in ATR fed animals.	86	Frank Becker, Software GraphPad Prism

Figure/Name	Page	Author
all LOV2 inserted strains of UNC-68.		
Figure 94: Strong photostimulation leads to an increased photophobic response of all tested strains, and thus to a shortening of body length.	119	Frank Becker, Software GraphPad Prism
Figure 95: Illustration of the SERCA integrated in the SR-membrane.	122	Frank Becker, Software PyMol
Figure 96: Low light intensity induces a substantial drop in body bends per min only in lite-1 background.	124	Frank Becker, Software GraphPad Prism
Figure 97: lite-1 GOA08 is thrashing considerably more frequent than its control lite-1 during and after photostimulation.	125	Frank Becker, Software GraphPad Prism
Figure 98: Strong blue light exposure of transgenic strains elicits diverse behaviour.	126	Frank Becker, Software GraphPad Prism
Figure 99: GOA08 displays similar behaviour in wild-type and lite-1 background.	127	Frank Becker, Software GraphPad Prism
Figure 100: Strong blue light illumination leads to strong reduction of swimming cycles.	128	Frank Becker, Software GraphPad Prism
Figure 101: Long-term low-light affects the behaviour of the first 6min of photostimulation.	128	Frank Becker, Software GraphPad Prism
Figure 102: Only GOA06 and GOA08 react to low blue light stimulation with a change in body length.	130	Frank Becker, Software GraphPad Prism
Figure 103: Blue light photostimulation leads to contraction after long exposure in wild type background.	131	Frank Becker, Software GraphPad Prism
Figure 104: Photostimulation of high intensity leads to a	132	Frank Becker, Software GraphPad Prism

Figure/Name	Page	Author
substantial contraction of body length after prolonged exposure.		
Figure 105: High intensity of blue light photostimulation leads to contraction after long exposure in GOA06.	133	Frank Becker, Software GraphPad Prism
Figure 106: Excitability of the individual channelrhodopsins as a function of wavelength and channel closure time.	134	Yizhar, Ofer; Fenno, Lief E.; Prigge, Matthias; Schneider, Franziska; Davidson, Thomas J.; O'Shea, Daniel J. et al. (2011): Neocortical excitation/inhibition balance in information processing and social dysfunction. In *Nature* 477 (7363), pp. 171–178. DOI: 10.1038/nature10360.
Figure 107: Blue light provoked effects during pacing by C1V1.	135	Frank Becker
Figure 108: GOA01 animals notably reduce pumping under the influence of 1Hz blue light pulses when supplemented with 50mM Serotonin.	136	Frank Becker, Software GraphPad Prism
Figure 109: Pharynx pumping of ATR GOA01 could not keep pace with 4Hz blue light pulses.	137	Frank Becker, Software GraphPad Prism
Figure 110: Violet light could not induce a change of Pharynx pumping of ATR lite-1 GOA01 during 1Hz light pulses.	138	Frank Becker, Software GraphPad Prism
Figure 111: The effect of violet light increased the duration of the pumps notably.	139	Frank Becker, Software GraphPad Prism
Figure 112: GOA14 is insensitive to 1Hz 470nm light pulses on 50mM Serotonin.	140	Frank Becker, Software GraphPad Prism
Figure 113: Strong blue light reduced pumping frequency, and raised pump duration and inter pump intervals, but the effect was not clearly pronounced.	141	Frank Becker, Software GraphPad Prism
Figure 114: Pharynx pumping of GOA14 is virtually unchanged by a continous blue light stimulus.	142	Frank Becker, Software GraphPad Prism
Figure 115: Wild-type animals reduced pharynx pumping notably	143	Frank Becker, Software GraphPad Prism

Figure/Name	Page	Author
under the influence of permanent blue light and serotonin.		
Figure 116: 1Hz pacing could be easily maintained, but 4Hz could only be reached by some animals.	144	Frank Becker, Software GraphPad Prism
Figure 117: Schematic representation of the unc-68 locus of C. elegans (exons in black, introns and promoters in white).	153	Marques, Filipe; Thapliyal, Saurabh; Javer, Avelino; Shrestha, Priyanka; Brown, André E. X.; Glauser, Dominique A. (2020): Tissue-specific isoforms of the single C. elegans Ryanodine receptor gene unc-68 control specific functions. In *PLoS genetics* 16 (10), e1009102. DOI: 10.1371/journal.pgen.1009102
Figure 118: Alternative transcription analysis of unc-68.	153	Marques, Filipe; Thapliyal, Saurabh; Javer, Avelino; Shrestha, Priyanka; Brown, André E. X.; Glauser, Dominique A. (2020): Tissue-specific isoforms of the single C. elegans Ryanodine receptor gene unc-68 control specific functions. In *PLoS genetics* 16 (10), e1009102. DOI: 10.1371/journal.pgen.1009102
Figure 119: Representative fluorescence and DIC images.	155	Marques, Filipe; Thapliyal, Saurabh; Javer, Avelino; Shrestha, Priyanka; Brown, André E. X.; Glauser, Dominique A. (2020): Tissue-specific isoforms of the single C. elegans Ryanodine receptor gene unc-68 control specific functions. In *PLoS genetics* 16 (10), e1009102. DOI: 10.1371/journal.pgen.1009102

List of tables and author: